SHORT PAPERS IN—

Analytical techniques

Economic geology

Engineering geology

Geochemical exploration

Geochemistry

Geomorphology

Geophysics

Glacial geology

Ground water

Mineralogy

Ore deposits

Paleontology

Petrology

Quality of water

Sedimentation

Stratigraphy

Structural geology

Surface water

Theoretical hydrology

GEOLOGICAL SURVEY RESEARCH 1964

Chapter B

GEOLOGICAL SURVEY PROFESSIONAL PAPER 501

GEOLOGICAL SURVEY RESEARCH 1964

Chapter B

GEOLOGICAL SURVEY PROFESSIONAL PAPER 501

Scientific notes and summaries of investigations prepared by members of the Geologic and Water Resources Divisions in the fields of geology, hydrology, and related sciences

UNITED STATES GOVERNMENT PRINTING OFFICE, WASHINGTON: 1964

UNITED STATES DEPARTMENT OF THE INTERIOR

STEWART L. UDALL, Secretary

GEOLOGICAL SURVEY

Thomas B. Nolan, Director

For sale by the Superintendent of Documents, U.S. Government Printing Office,
Washington, D. C., 20402

FOREWORD

This collection of 46 short papers is one of a series to be released as chapters of Geological Survey Research 1964. The papers report on scientific and economic results of current work by members of the Geologic and Water Resources Divisions of the U.S. Geological Survey. Some of the papers present results of completed parts of continuing investigations; others announce new discoveries or preliminary results of investigations that will be discussed in greater detail in reports to be published in the future. Still others are scientific notes of limited scope, and short papers on techniques and instrumentation.

Chapter A of this series will be published later in the year, and will present a summary of results of work done during the present fiscal year.

Thomas B. Nolan,
Director.

CONTENTS

Geomorphology and glacial geology

Sedimentation

Analytical techniques

HYDROLOGIC STUDIES

Surface water

Ground water

Quality of water

Theoretical hydrology

INDEXES

INTERPRETATION OF THE GARDEN SPRINGS AREA, TEXAS, BY THE "DOWN-STRUCTURE" METHOD OF TECTONIC ANALYSIS

By PHILIP B. KING, Menlo Park, Calif.

Abstract.—Complex structures in Paleozoic rocks of the Garden Springs area, west Texas, plunge to the southwest and are capable of interpretation by the "down-structure" method of tectonic analysis. When the map is oriented so that the geologist views it in the direction of plunge, the outcrop pattern becomes a structure section, but in a near-horizontal plane rather than the vertical plane of conventional structure sections. This analysis demonstrates that the Garden Springs area contains what was originally a low-angle thrust fault that was subsequently steeply folded.

In 1937 Bailey and Mackin (1937, p. 189) called attention to several "self-evident propositions in geologic map reading, some of which are not found in ordinary text books," including:

> If two boundaries of a formation, under the influence of pitch, follow one another with rough parallelism across the regional strike of fold axes, then the one boundary is (structurally) at the top, and the other is (structurally) at the bottom of the formation. . . .
>
> If the observer orients the map so as to look along it in the direction of pitch, he will see the formations disposed on the flat surface of the map in much the same attitude as they would present in a vertical cross-section, though, of course, with different proportions.

Mackin (1950) later termed the use of these propositions in tectonic analysis "the down-structure method of viewing geologic maps." Knopf (1962, p. 42–45) and Christensen (1963, p. 97–102) recently summarized the use which has been made of this method in the analysis of structures in metamorphic terranes in the Alps (where Lugeon applied it as early as 1901), the Scottish Highlands, and elsewhere,[1] and they themselves used it to interpret relations of the metamorphic rocks of the Stissing Mountain area, New York, and the Hoosac Mountain area, Massachusetts.

[1] The reference list by Christensen (1963, p. 107) provides the best summary of previous uses of the "down-structure" method.

The Garden Springs area in western Texas provides an excellent example of the application of the "down-structure" method to tectonic analysis. The area was described about 25 years ago (King, 1937, p. 124–128, pl. 19B), but in a report that dealt so extensively with other matters that the example has largely escaped the notice of tectonic geologists. The features of the Garden Springs area are here illustrated by a geologic map (fig. 1), which is based on field surveys made in 1929 and 1930 and which presents more data than were included in the small-scale map of the original report, and by an aerial photograph of the area taken in 1954 (fig. 2). Use of the "down-structure" method to interpret the relations shown on the map is demonstrated by structure sections (fig. 1) and by the tectonic diagrams (fig. 4).

The Garden Springs area lies in the Marathon Basin about 10 miles south of the town of Marathon, Brewster County. The Marathon Basin exposes a sequence of Paleozoic rocks of Cambrian to Pennsylvanian age, which were deformed during late Pennsylvanian and early Permian orogenies that produced structures of the Appalachian type. The Paleozoic rocks are virtually unmetamorphosed, but their structural complexity equals that of many metamorphic terranes. General features of the Marathon Basin have been described by King (1937), and the results of later investigations have been summarized by Flawn (1961, p. 49–61).

The Garden Springs area lies on the northwest flank of the Dagger Flat anticlinorium, which is one of the large uplifts of the Marathon Basin where older rocks come to the surface. The anticlinorium as a whole has many complex structures; the particular significance of the Garden Springs area is that it contains a representative sample of these structures within a relatively

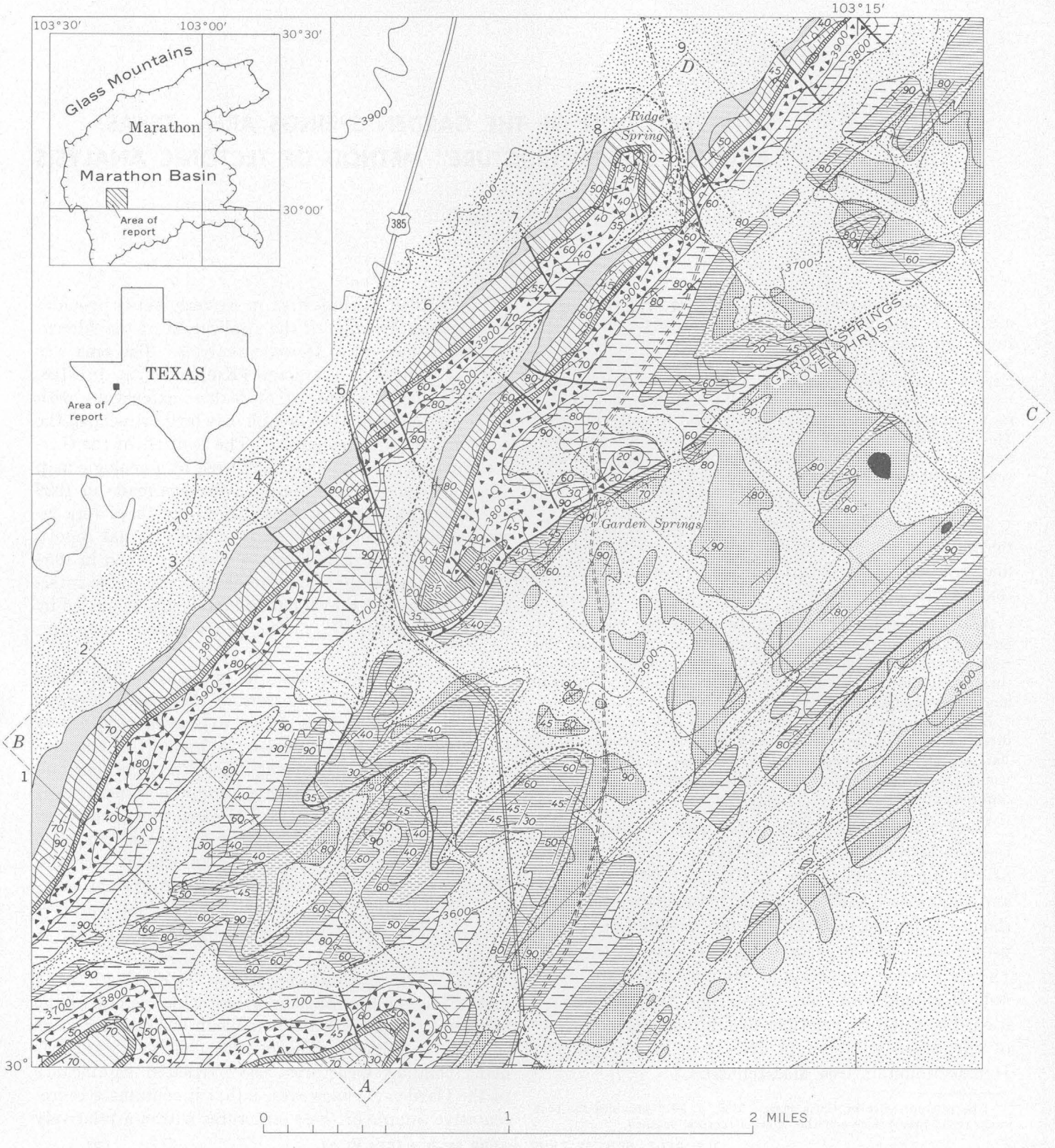
103°30′
103°00′
30°30′
30°00′
Glass Mountains
Marathon
Marathon Basin
Area of report
TEXAS
Area of report
103°15′
30°
Ridge Spring
Garden Springs
GARDEN SPRINGS OVERTHRUST
385
A
B
C
D
1
2
3
4
5
6
7
8
9
0
1
2 MILES

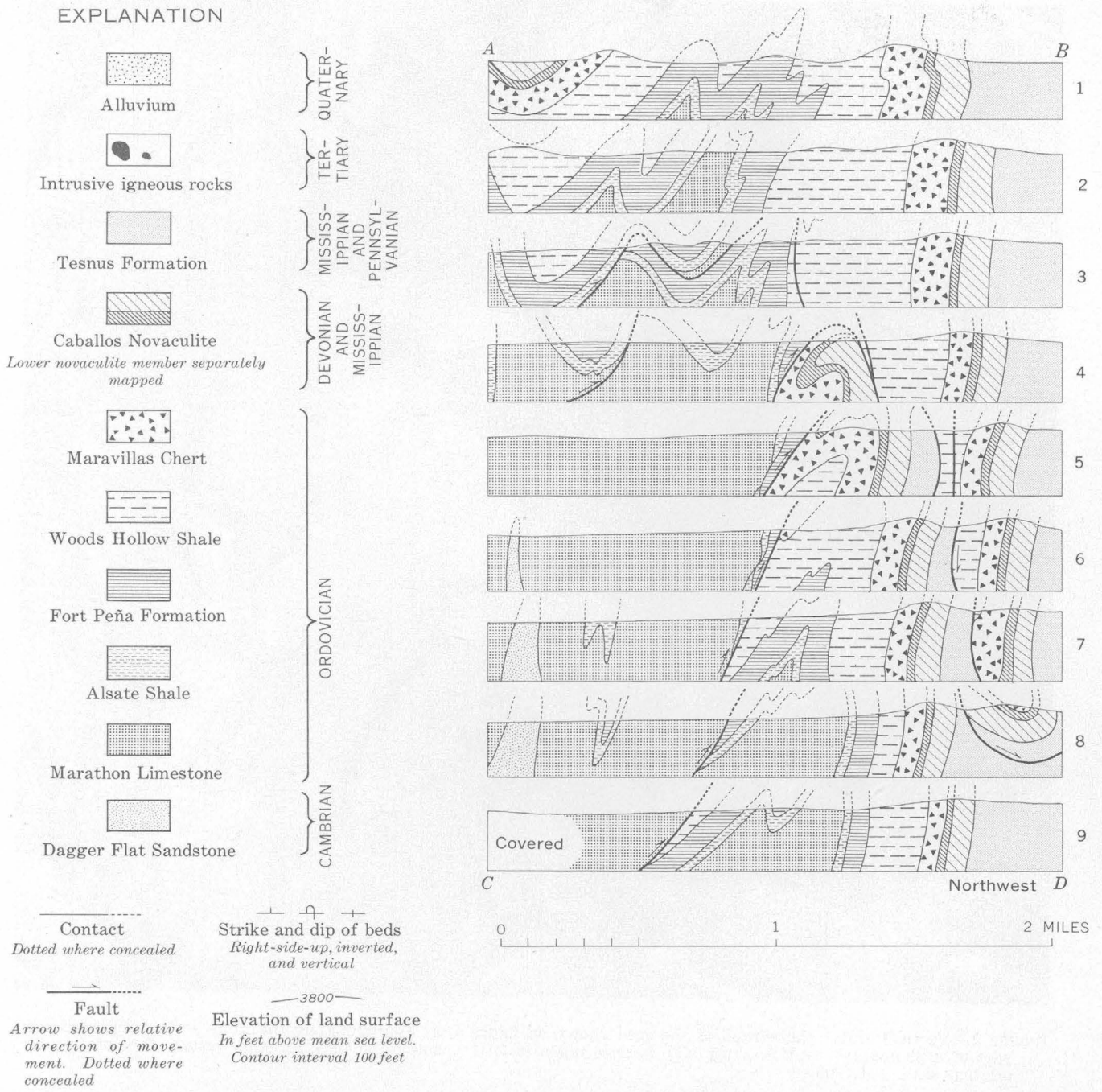

FIGURE 1.—Geologic map and structure sections of the Garden Springs area. Geology mapped by P. B. King in 1929 and 1930; geologic mapping has not been adjusted to agree with the aerial photograph taken later (fig. 2). Inset maps show location of area in the Marathon Basin, and in the State of Texas. Rectangle *ABCD* outlines the area shown in the structure sections on the opposite page, and projected in the tectonic diagrams of figure 4 as rectangles *ABC'D'* and *ABC''D''*. Sections are drawn at half-mile intervals and are oriented as though the geologist were looking southwestward down the plunge of the folds. Consequently, sections are seen in an order opposite to that indicated on the map. Alluvial cover is thin in the area and is omitted in sections.

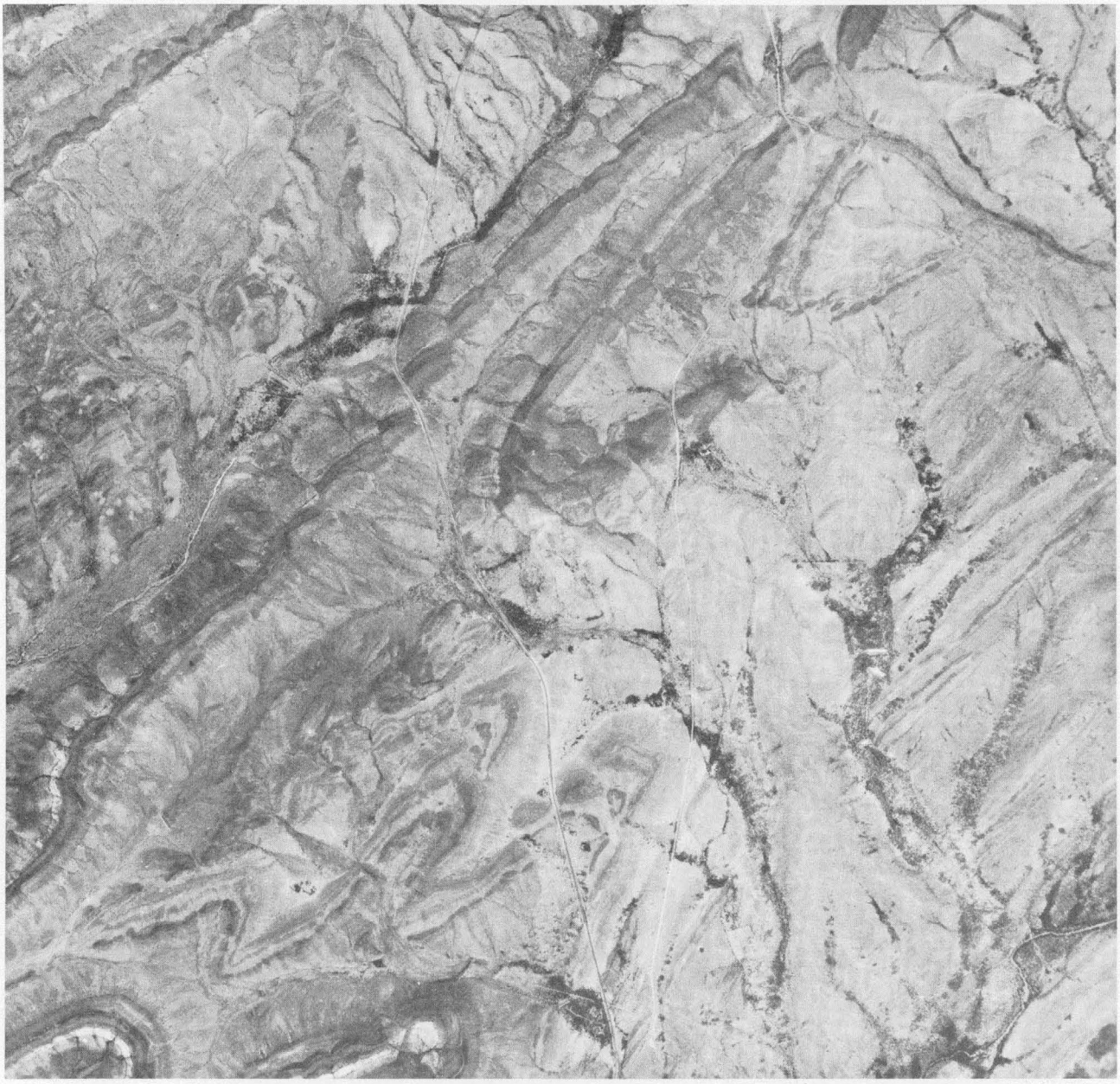

FIGURE 2.—Vertical aerial photograph of the area shown on figure 1, at approximately the same scale. Enlarged from part of a photograph by U.S. Army Map Service taken in 1954 (photograph 2854, lot AM, western U.S. project 138; original scale 1:63,000).

small compass. As elsewhere in the Marathon Basin, the sequence in the Garden Springs area consists of alternating "hard" and "soft" units, each a few hundred to more than a thousand feet thick; the "hard" and "soft" units show contrasting competency under deformation, and contrasting resistance to erosion. Within the area, the most conspicuous "hard" unit is formed by the Caballos Novaculite (Devonian and Mississippian) and the Maravillas Chert (Upper Ordovician), which together produced prominent ridges and outcrops; a lesser "hard" unit lower in the sequence is the Fort Peña Formation (Middle Ordovician), which forms lower narrower ridges.

The map and photograph of the area (figs. 1 and 2) indicate anomalous features. The ridge-making Caballos Novaculite and Maravillas Chert form two belts of outcrop which end in hooks that face in opposite directions, one at Ridge Spring on the north, the other west of Garden Springs on the south. The hook on the south defines an anticline, but the Caballos extends

only a little past its crest, where it is bent back on itself. The anticline is bordered on the southeast by a fault, termed the Garden Springs overthrust in the original report, which brings older Ordovician formations against the Maravillas Chert on the anticlinal flank. The northwestern flank of the anticline is also bordered by a fault, which likewise brings older Ordovician formations against the rocks of the anticline. Although the connection between the two faults is partly concealed by alluvium, they evidently join, as the older Ordovician formations outside the two faults are continuous southwestward around the nose of the anticline.

These relations are especially baffling because, whereas the component formations are distinctive and easily recognizable, lie in a known stratigraphic sequence, and have a well-defined structure at any individual exposure, these local structures cannot be rationalized into any larger structure made up of the usual kinds of folds and faults.

The essential clue to interpretation of the Garden Springs area is the plunge of its structures. The outcrop pattern of the anticline west of Garden Springs suggests a plunge to the southwest, which is confirmed by the dips of its component beds. The pattern of the hook-shaped outcrop at Ridge Spring suggests an anticline that plunges to the northeast, but the dip of its component beds indicates that it, too, plunges to the southwest—hence, that it is a synform, rather than an anticline in the usual sense.

More specific data as to the plunge of the structures can be obtained by plotting the poles of the 111 observed strikes and dips on the lower hemisphere of an equal-area projection (figs. 3 *A*, *B*, and *C*). This plotting indicates a well-defined girdle that closely follows a great circle whose plane dips 60° northeast (fig. 3*D*). A line normal to this plane, with a dip of 30° southwest, is approximately parallel to the plunge of the folds.[2]

Tectonic analysis can now proceed by means of the "down-structure" method. If the geologist turns the map so that he faces southwestward down the plunge of the folds, he will see that the map itself provides a sort of structure section. In the present example, as the topographic relief is slight, this section is in a nearly horizontal plane, rather than in the vertical plane of conventional structure sections, and hence is much distorted in one dimension. The gross structure thus perceived can be verified by preparation of sections showing the structure of the near-surface rocks along closely spaced, parallel lines. No single section affords much of an idea of the gross structure, yet if the sections are arranged in geographic order, with those down the plunge above those up the plunge, a blurred picture is produced that closely resembles the map pattern (fig. 1).

Even more illuminating than the structure sections is a tectonic diagram, in which the map pattern is projected down the plunge into a vertical plane, the plane conventionally used in structure sections (fig. 4*A*). This projection can be made easily,[3] by compressing the map pattern by the desired amount in a northeast-southwest direction. If all the structures exposed at the surface were cylindrically persistent throughout the area, such a diagram would perfectly express the gross structure, which, at localities up the plunge is now largely removed by erosion, and at localities down the plunge lies beneath the surface. But complete persistence of structures is unlikely in nature; therefore, the tectonic diagram merely provides the geologist with a picture of the style of the gross structure with which he is dealing.

Although a tectonic diagram projected into a vertical plane provides a picture of the gross structure as it would appear in a conventional structure section, it is nevertheless not a true representation of the deformation. A true representation in an area of plunging folds is in a plane normal to the plunge, and this will differ more or less from representation in a vertical plane, depending on the steepness of the plunge. In the present example, where the folds plunge 30° southwest, true representation of the deformation is in a plane dipping 60° northeast (fig. 4*B*); even in this example where the plunge is low, note that representation is perceptibly less distorted in a plane normal to the folds than in a vertical plane.

Interpretation of the features which are revealed by the "down-structure" method in the Garden Springs area, and elsewhere in the Dagger Flat anticlinorium, have been set forth elsewhere (King, 1937, p. 124–128). Suffice it to say that the Garden Springs area must contain what was originally a low-angle thrust fault, the

[2] Mackin (1950, p. 62–65) and other authors have shown that in asymmetrical plunging folds it is geometrically necessary that the direction of the plunge of the folds should diverge down the plunge from the surface traces of the folds. A disconcerting result of the present analysis is that the direction of the plunge obtained from it is nearly the same as the direction of the surface traces on the geologic map (fig. 1). However, the margin of error in determining the strike of the plane of the great circle is probably somewhat greater than 10°, and the divergence must lie within these limits.

[3] To prepare a tectonic diagram in the desired plane: Trace the generalized map pattern onto a rectangle made up of a grid of squares; the rectangle is so oriented that one dimension is parallel to, and the other dimension at right angles to, the plunge of the folds. By means of a grid of rectangular coordinates, transfer the pattern points onto a second rectangle oriented similarly to the first. The sides of this second rectangle and of the smaller rectangles subdividing it that lie at right angles to the plunge have the same lengths as the similar elements in the first rectangle. However, the sides parallel to the plunge have the lengths to which the similar elements in the first rectangle would be reduced if projected onto the desired plane.

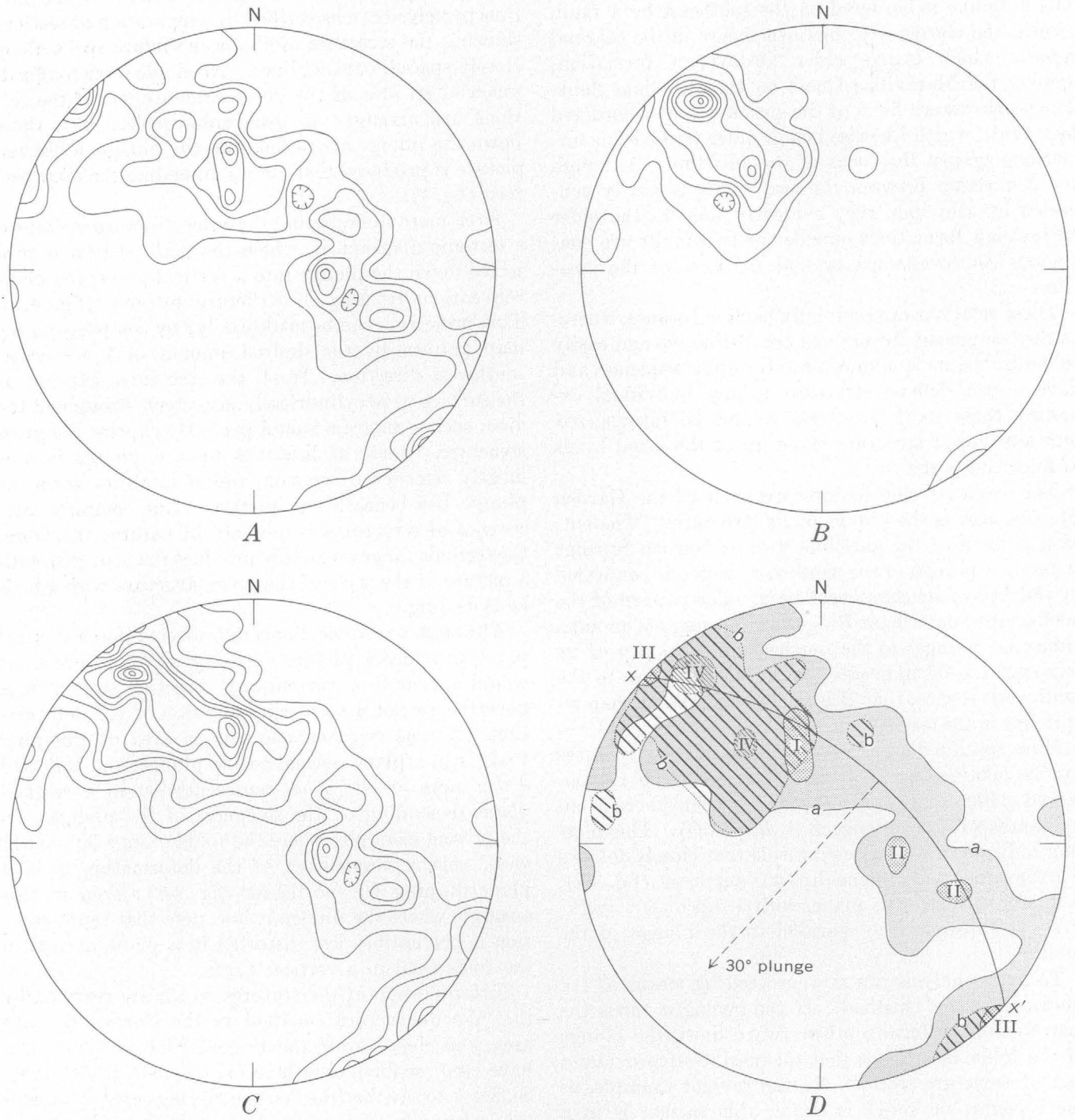

FIGURE 3.—Diagrams prepared to calculate plunge of folds in Garden Springs area, showing poles of observed strikes and dips of bedding, plotted and contoured on lower hemisphere of an equal-area projection.

A. Right-side-up beds and vertical beds; poles of 69 observations, including 6 observations on inverted beds in synform at Ridge Spring; contour interval 9 percent of 1 percent of area.

B. Inverted beds; poles of 42 observations; contour interval 20 percent of 1 percent of area.

C. All observations on bedding; poles of 111 observations; contour interval 10 percent of 1 percent of area.

D. Summary diagram: *a*, outer contour on right-side-up beds; *b*, outer contour on inverted beds. I, maximum of poles of right-side-up beds on southeast flanks of folds; II, maxima of poles of right-side-up beds on northwest flanks of folds; III, maximum of poles of vertical beds; IV, maxima of poles of inverted beds on northwest flanks of folds. *x*–*x*′, great circle which approximates the girdle shown by the contours, whose plane dips 60° northeast. A line normal to this plane dips 30° southwest, and is approximately parallel to the plunge of the folds.

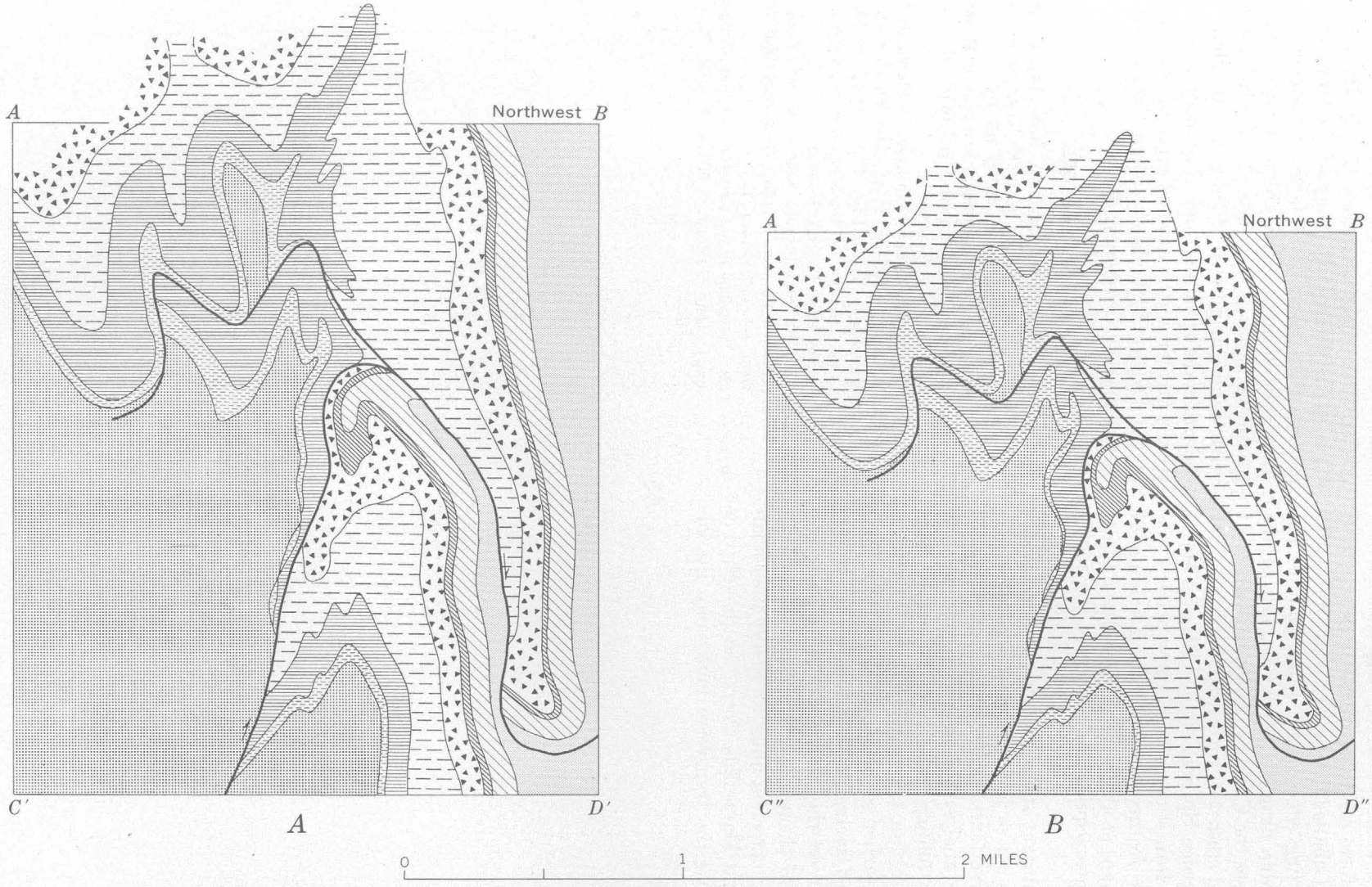

FIGURE 4.—Tectonic diagrams that summarize the structure of the Garden Springs area. *A*, surface outcrop pattern of area *ABCD* of figure 1 projected into a vertical plane, *ABC′D′*, the plane used in conventional structure sections; vertical transverse faults are omitted from outcrop pattern used. *B*, a similar projection into a plane normal to the plunge of the folds, *ABC″D″*, or with a dip of 60° northeast (fig. 3*D*); note the lesser vertical distortion than in *A*. Diagrams are oriented in the same manner as the structure sections of figure 1.

Garden Springs overthrust, which was subsequently folded. The synform at Ridge Spring was produced by drag of the Caballos Novaculite and Maravillas Chert on the leading edge of the upper plate of the thrust. Comparable drag on the lower plate of the thrust occurs where the Caballos is bent back on itself near the anticlinal crest west of Garden Springs. The anticline near Garden Springs in the Caballos, Maravillas, and older formations of the lower plate is evidently a younger feature, formed during folding of the thrust. Perhaps at about the time of this folding, the whole structure acquired its plunge to the southwest.

One other significant structural item in the Garden Springs area has not so far been mentioned—the host of minor transverse faults. These were not considered in the preceding analysis because they are probably younger than the folding and thrust faulting, and because they merely blur, but do not obliterate the map pattern of the earlier structures. Many transverse faults were located during the field survey (fig. 1), and more are evident on the aerial photograph (fig. 2). As mapped, all of them are of short length, and all lie in the "hard," competent units, especially the Caballos Novaculite and Maravillas Chert. Although it is impossible to trace the transverse faults into the adjacent "soft," incompetent units, the presumption is great that they die out there. Gently dipping slickensides on the surfaces of many of the transverse faults indicate that they have a large component of strike-slip displacement; in the Garden Springs area this displacement is mainly left-lateral. Probably the transverse faults originated during a late phase of the Paleozoic deformation, and they may have resulted from a greater northwestward surge of the central part of the Dagger Flat anticlinorium than of its northeastern and southwestern ends.

REFERENCES

Bailey, E. B., and Mackin, J. H., 1937, Recumbent folding in the Pennsylvania Piedmont; a preliminary statement: Am. Jour. Sci., 5th ser., v. 33, no. 195, p. 187–190.

Christensen, M. N., 1963, Structural analysis of Hoosac nappe of northwestern Massachusetts: Am. Jour. Sci., v. 261, no. 2, p. 97–107.

Flawn, P. T., 1961, The Marathon area, *in* Flawn, P. T., Goldstein, August, Jr., King, P. B., and Weaver, C. E., The Ouachita system: Texas Univ. Pub. 6120, p. 49–58.

King, P. B., 1937, Geology of the Marathon region, Texas: U.S. Geol. Survey Prof. Paper 187, 148 p.

Knopf, E. B., 1962, Stratigraphy and structure of the Stissing Mountain area, Dutchess County, New York: Stanford Univ. Pubs. Geol. Sci., v. 7, no. 1, p. 1–55.

Mackin, J. H., 1950, The down-structure-method of viewing geologic maps: Jour. Geology, v. 58, no. 1, p. 55–72.

CRYPTOEXPLOSIVE STRUCTURE NEAR VERSAILLES, KENTUCKY

By DOUGLAS F. B. BLACK, Lexington, Ky.

Work done in cooperation with the Kentucky Geological Survey

Abstract.—A circular structure nearly a mile in diameter was mapped 3½ miles northeast of Versailles, Ky. This structure, of undetermined origin, consists of a brecciated central dome, a marginal structural depression partly bounded by normal faults, and, on the east, an outer semicircular anticline of low amplitude.

A previously unreported cryptoexplosive structure approximately 5,000 feet in diameter was discovered by E. R. Cressman and the author 3½ miles northeast of Versailles, Woodford County, Ky. (fig. 1), in October 1962 and has since been mapped by the author at a scale of 1:24,000. A. M. Miller (1924) mapped an elongate graben that in part coincides with the arcuate graben on the north side of the cryptoexplosive structure, though his map does not show the circular nature of this structure or its extent. The term "cryptoexplosive" (Dietz, 1946) is used because it has little genetic implication.

Versailles is in the central Blue Grass region of Kentucky. Topographic relief is gentle, soils are deep, and outcrops generally sparse. The geologic map (fig. 2) is based on about 100 outcrops within and adjacent to the structure. The nearly circular feature is expressed physiographically by an almost continuous ring of small sinkholes.

Rocks exposed in the structure are Middle and Upper Ordovician carbonates with some beds of shale and comprise the upper part of the Lexington Limestone, the Cynthiana Formation, and the basal part of the Million Shale of Nickles (1905).

The cryptoexplosive structure consists of a central uplift, a nearly circular marginal structural depression bounded by arcuate normal faults, and on the east an outer rim of gentle anticlinal folds which flank the marginal depression.

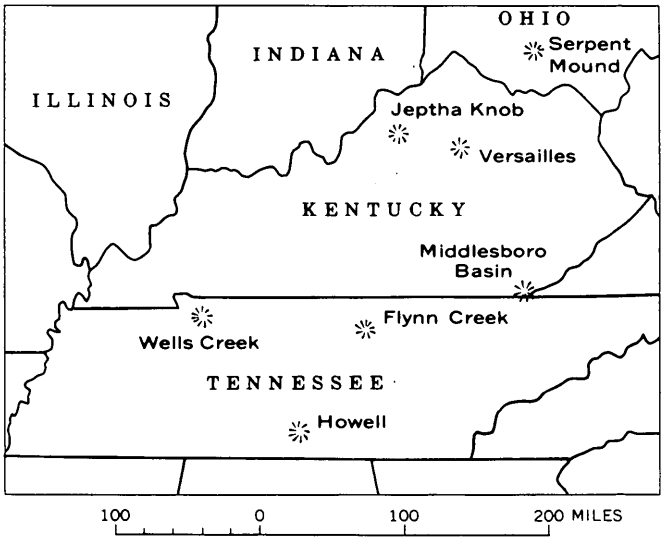

FIGURE 1.—Location of the Versailles cryptoexplosive structure and similar structures in Kentucky and the surrounding States.

The central uplift of the structure is shown as an asymmetrical dome. This interpretation is borne out by all observed outcrops, though much of the central area is concealed. Numerous outcrops of coarsely brecciated limestone containing large blocks derived from beds of the Lexington Limestone and the lower part of the Cynthiana Formation are exposed near the center of the central uplift. This area, shown on the map as undifferentiated Cynthiana Formation and Lexington Limestone, may be intricately crosscut by faults or possibly underlain by a lens of limestone breccia. The crest of the dome is uplifted relative to the marginal depression, but the rocks in the central uplift have little stratigraphic throw compared with undisturbed beds surrounding the structure.

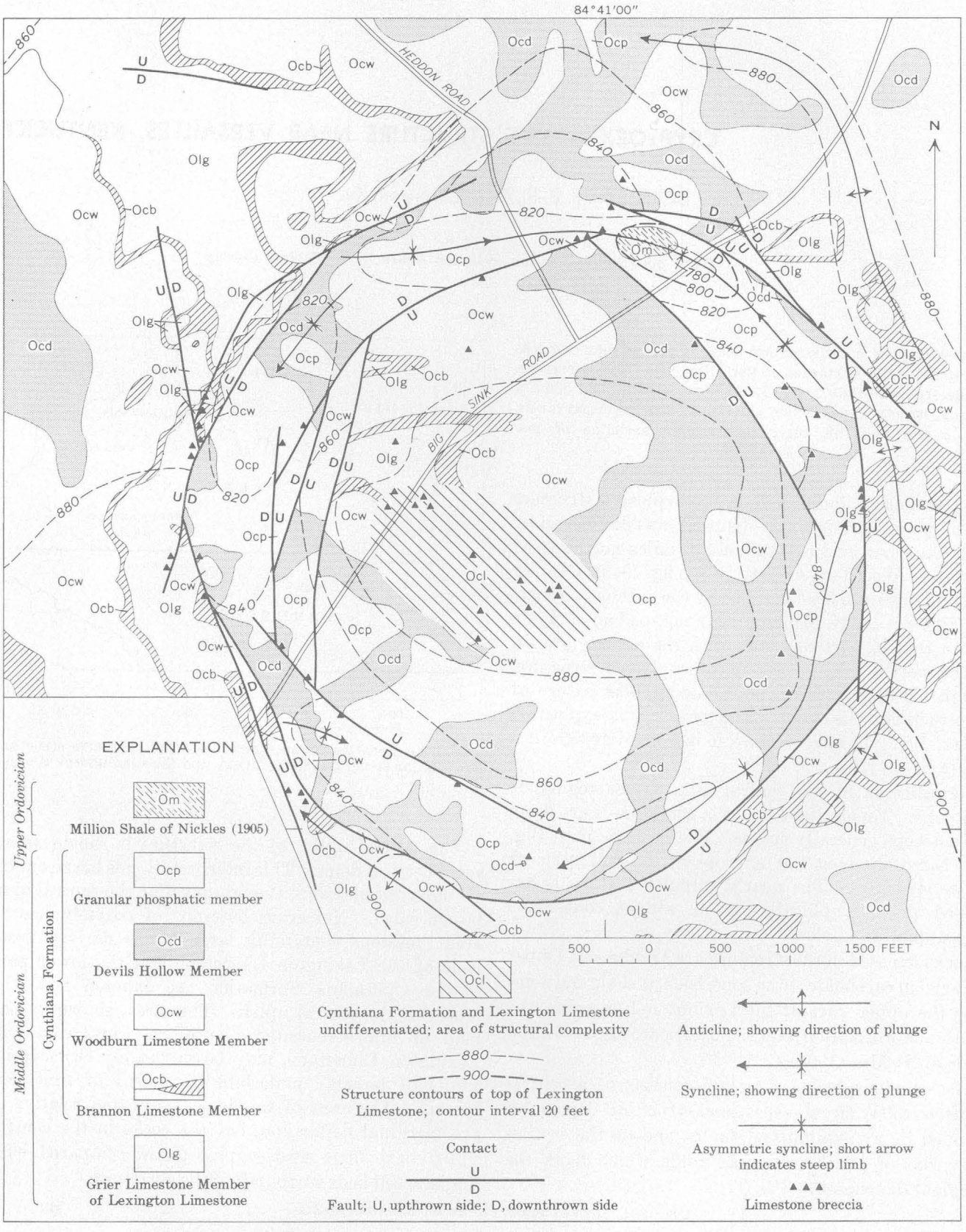

FIGURE 2.—Geologic map of the cryptoexplosive structure near Versailles, Ky.

The marginal structural depression is bounded, at least in part, by normal faults, many of which are readily defined by well-developed zones of breccia and in some cases by moderate to steeply dipping beds adjacent to the faults. The faults are presumed to be high-angle ones, but no accurate dip measurements were obtained because of poor exposure and very low topographic relief. The maximum downward displacement of strata in the depression is slightly more than 100 feet relative to undisturbed rocks surrounding the structure.

An asymmetrical synclinal fold in the marginal depression, having a steeper limb on the northeast, can be seen in upper Cynthiana and basal Million rocks exposed above the stock pond 1,000 feet northeast of the junction of the Heddon and Big Sink Roads. This folding may be the result of settling and readjustment of faulted blocks subsequent to initial faulting.

The curved anticlinal folds outside the marginal depression are apparently restricted to the eastern margins of the structure. These folds are generally of low amplitude and are located in the field only by small altitude differences on key beds. Folded strata with measurable dip occur locally along the southern edge of the structure.

The limestone breccias of this structure are believed to be finer grained than those described by Eggleton and Shoemaker (1961) from the Sierra Madera structure in Texas, but they seem otherwise very similar. The Versailles breccias consist of angular limestone blocks, some of which are several feet across, enclosed in a matrix of smaller fragments of more than one rock type.

The youngest rocks known to have been involved in this cryptoexplosive structure belong to the basal part of the Million Shale of Nickles (1905), thus, the structure is of Late Ordovician or younger age.

The similarity of the Versailles structure to structures of known and supposed meteorite-impact origin, and the high degree of brecciation, otherwise rare in this region, may indicate a similar origin for the Versailles structure. The possibility of volcanic origin as postulated by Bucher (1933, 1936) for some structures of this type cannot yet be abandoned here, although no evidence of volcanism has been found. Previously described structures which seem especially similar to this include the Crooked Creek structure, Missouri (Hendricks, 1954); Jeptha Knob, Kentucky (Bucher, 1925); Middlesboro Basin, Kentucky (Englund and Roen, 1963); the Flynn Creek disturbance, Tennessee (Wilson and Born, 1936; Conant and Swanson, 1961, p. 9–12); the Wells Creek Basin, Tennessee (Bucher, 1936, p. 1066–1070); the Howell structure, Tennessee (Born and Wilson, 1939); the Serpent Mound structure, Ohio (Bucher, 1936, p. 1061–1064; Heyl and Brock, 1962); and the Sierra Madera structure, Texas (King, 1930).

Because of the small diameter of the Versailles structure, further detailed study to determine its nature and origin might prove to be less costly than similar studies of larger cryptoexplosive structures. Such a study might include a closer search for shatter cones such as those described by Dietz (1959), a coring program designed to determine the subsurface structure, tests for shock-induced thermoluminescence, both at the surface and at depth (Angino, 1959; Roach and others, 1961, 1962), and tests for high-pressure minerals (Chao and others, 1960, 1962).

REFERENCES

Angino, E. E., 1959, Pressure effects on thermoluminescence of limestone relative to geologic age: Jour. Geophys. Research, v. 64, no. 5, p. 569–573.

Born, K. E., and Wilson, C. W., Jr., 1939, The Howell structure, Lincoln County, Tennessee: Jour. Geology, v. 47, p. 371–388.

Bucher, W. H., 1925, Geology of the Jeptha Knob: Kentucky Geol. Survey, ser. 6, v. 21, p. 193–237.

——— 1933, Volcanic explosions and overthrusts: Am. Geophys. Union Trans., 14th ann. mtg., p. 238–242.

——— 1936, Cryptovolcanic structures in the United States [with discussion]: Internat. Geol. Congress, 16th, v. 2, p. 1055–1084.

Chao, E. C. T., Shoemaker, E. M., and Madsen, B. M., 1960, First natural occurrence of coesite: Science, v. 132, no. 3421, p. 220–222.

Chao, E. C. T., Fahey, J. J., Littler, Janet, and Milton, D. J., 1962, Stishovite, SiO_2, a very high pressure new mineral from Meteor Crater, Arizona: Jour. Geophys. Research, v. 67, no. 1, p. 419–421.

Conant, L. C., and Swanson, V. E., 1961, Chattanooga shale and related rocks of central Tennessee and nearby areas: U.S. Geol. Survey Prof. Paper 357, 91 p.

Dietz, R. S., 1946, Geological structures possibly related to lunar craters: Pop. Astronomy, v. 54, p. 465–467.

——— 1959, Shatter cones in cryptoexplosion structures (meteorite impact?): Jour. Geology, v. 67, p. 496–505.

Eggleton, R. E., and Shoemaker, E. M., 1961, Breccia at Sierra Madera, Texas: Art. 342 *in* U.S. Geol. Survey Prof. Paper 424–D, p. D151–D153.

Englund, K. J., and Roen, J. B., 1963, Origin of the Middlesboro Basin, Kentucky: Art. 184 *in* U.S. Geol. Survey Prof. Paper 450–E, p. E20–E22.

Hendricks, H. E., 1954, The geology of the Steelville quadrangle, Missouri: Missouri Geol. and Water Resources Survey, v. 36, ser. 2, p. 52–70.

Heyl, A. V., and Brock, M. R., 1962, Zinc occurrence in the Serpent Mound structure of southern Ohio: Art. 148 *in* U.S. Geol. Survey Prof. Paper 450–D, p. D95–D97.

King, P. B., 1930, The geology of the Glass Mountains, Texas; pt. 1, Descriptive geology: Texas Univ. Bull. 3038, p. 123–125. [1931]

725–328 O—64——2

Miller, A. M., 1924, Geologic map of Woodford County, Kentucky: Kentucky Geol. Survey, ser. 6, 1950 reprint.

Nickles, J. M., 1905, The Upper Ordovician rocks of Kentucky and their Bryozoa: Kentucky Geol. Survey Bull. 5, 64 p.

Roach, C. H., Johnson, G. R., McGrath, J. G., and Spence, F. H., 1961, Effects of impact on thermoluminescence of Yule Marble: Art. 272 *in* U.S. Geol. Survey Prof. Paper 424–C, p. C342–C346.

Roach, C. H., Johnson, G. R., McGrath, J. G., and Sterrett, T. S., 1962, Thermoluminescence investigations at Meteor Crater, Arizona: Art. 149 *in* U.S. Geol. Survey Prof. Paper 450–D, p. D98–D103.

Wilson, C. W., Jr., and Born, K. E., 1936, The Flynn Creek disturbance, Jackson County, Tennessee: Jour. Geology, v. 44, p. 815–835.

A LATE TERTIARY LOW-ANGLE FAULT IN WESTERN JUAB COUNTY, UTAH

By DANIEL R. SHAWE, Denver, Colo.

Abstract.—A low-angle fault in western Juab County, Utah, has moved Cambrian carbonate rocks at least 1 mile over late Tertiary volcanic rocks. Tuff beneath the fault is probably correlative with tuff that contains large beryllium deposits at Spor Mountain; this or similar faults therefore may conceal additional deposits.

A low-angle fault about 10 miles southeast of the Spor Mountain beryllium deposits, in western Juab County, Utah (fig. 1), has moved Cambrian carbonate rocks at least 1 mile over volcanic rocks that are probably Miocene and Pliocene in age. It is thus the youngest low-angle fault of this magnitude now known in the region. A tuff unit underlying the fault may be correlative with tuff that contains large beryllium deposits at Spor Mountain, and therefore this fault or others like it may in places conceal additional beryllium deposits.

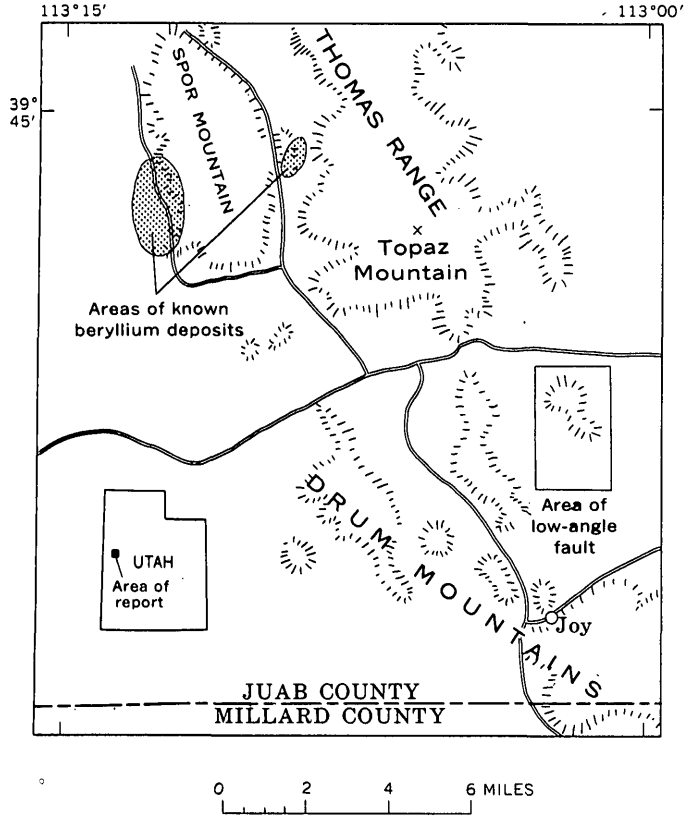

FIGURE 1.—Map showing location of low-angle fault and beryllium deposits.

The fault, which is exposed on three sides of a group of hills (fig. 2) about 2 miles east of the north end of the Drum Mountains, was mapped in August 1963 by the author and Stanley Bernold during a study of Tertiary volcanic rocks related to the beryllium deposits at Spor Mountain.

The upper plate of the low-angle fault consists of at least several hundred feet of carbonate rocks, mostly dolomite, that are folded and brecciated. The carbonate rocks are recrystallized and apparently unfossiliferous. They are dominantly thin- to thick-bedded gray dolomite, but locally they contain layers of light-pinkish-brown dolomite as much as several tens of feet thick. Probably the upper plate consists of more than one formation (M. H. Staatz, oral communication, 1963). On the State map of Utah the carbonate rocks in this area are termed the Notch Peak Limestone of Late Cambrian age (Stokes and Hintze, 1963).

The rocks beneath the low-angle fault consist of two units of gently tilted rhyolitic welded tuff and one of water-laid vitric-lithic tuff. The tuffs contain moderate to abundant amounts of quartz, sanidine, and biotite crystals, and lithic fragments.

The oldest unit is light-brown rhyolitic welded tuff a few hundred feet thick. It is lithologically similar to, and in the same stratigraphic position as, rhyolitic welded tuff of probable Miocene age in the Thomas Range about 10 miles to the northwest. The tuff in the Thomas Range is probably nearly the same age as quartz-sanidine crystal tuff which M. H. Staatz (1963, p. M12) reported as 20 million years old on the basis of a Larsen-method age determination on zircon (Jaffe and others, 1959, p. 71).

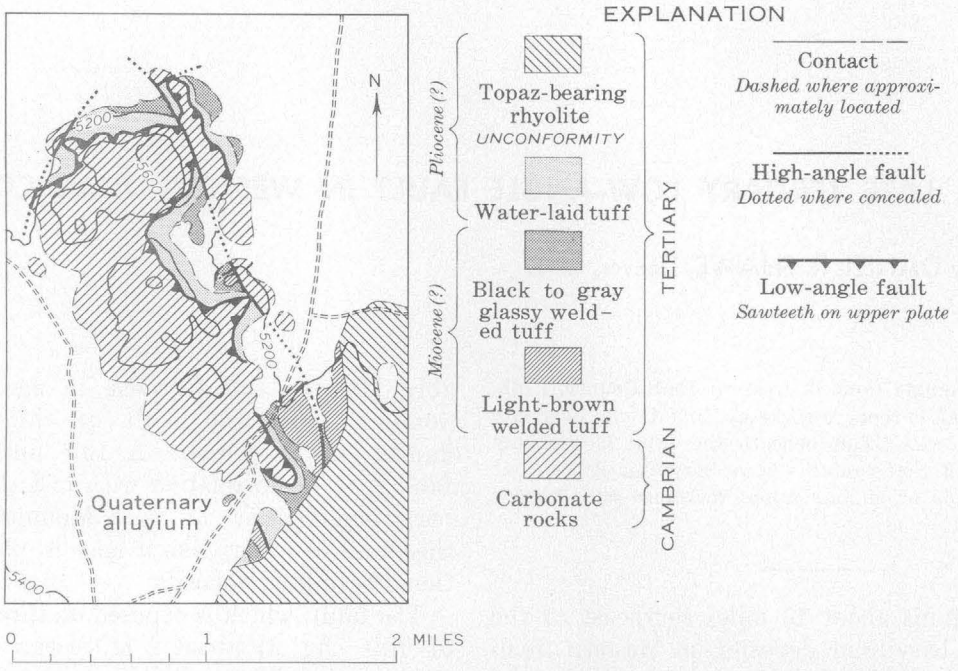

FIGURE 2.—Geologic map of area of low-angle fault. Location of area shown on figure 1.

Overlying the light-brown welded tuff is a sheet of black to gray glassy welded tuff 50 to 100 feet thick. The base of this unit is black vitrophyre that contains moderate amounts of crystals and fragments of carbonate rocks and volcanic rocks. The welded tuff above the basal vitrophyre contains abundant flattened perlitic lapilli of black pumiceous vitrophyre, as well as other fragments and crystals, all in a gray matrix. This unit is correlated here with a welded tuff that overlies the rhyolite of probable Miocene age 4 miles to the north in the Thomas Range.

Above the black to gray welded tuff is a unit of light-yellowish-brown and light-pinkish-brown water-laid bedded tuff, 50 to 200 feet thick, which contains numerous fragments of pumice, other volcanic rocks, carbonate rocks, and other sedimentary rocks, and crystals. This unit is correlated here with vitric tuff in the Thomas Range considered by Staatz (1963, pl. 1) to be Pliocene(?). Locally, near high-angle faults (fig. 2) the water-laid tuff unit has been hydrothermally altered to a soft rock that contains abundant montmorillonite showing ghostlike relics of original texture. Such rock looks lithologically very similar to the altered and mineralized tuff at Spor Mountain.

Southeast of the low-angle fault, topaz-bearing rhyolite flows aggregating as much as several hundred feet in thickness overlie these three tuff units unconformably; elsewhere the flows mostly lie conformably on the water-laid tuff. The topaz-bearing rhyolite is light gray, flow layered, and contains sparse phenocrysts of quartz and sanidine in an aphanitic groundmass. Locally abundant lithophysae and vugs contain small crystals of topaz and quartz. This rhyolite unit is also assigned to the Pliocene (?) by Staatz (1963, pl. 1).

The low-angle fault is nearly horizontal at the north end of the hills shown in figure 3 and dips about 15° southwest at the south end of the hills. Locally the dip of the fault surface may vary as much as 5°.

Beneath the fault, water-laid tuff is virtually undisturbed except in a zone of pulverized material within a few inches of the fault surface (fig. 4). Bedding in the tuff is virtually parallel to the fault. Decrease in thickness of the water-laid tuff from north to south (fig. 2) could be the result of slight truncation by the

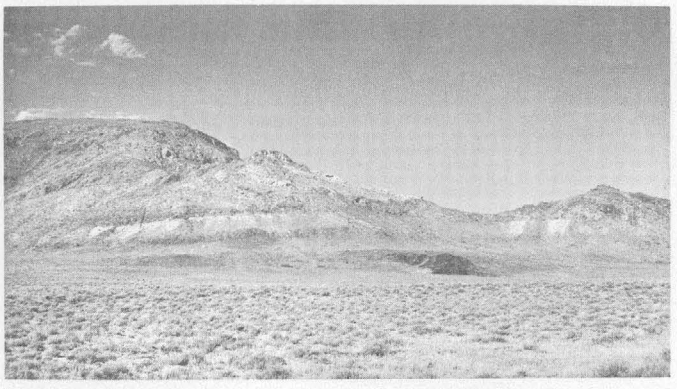

FIGURE 3.—View of low-angle fault at northeast side of mapped area. Black outcrop at foot of hills is part of basal vitrophyre of black to gray glassy welded tuff. White layer is water-laid tuff; upper contact of tuff is low-angle fault. Above the fault are Cambrian carbonate rocks.

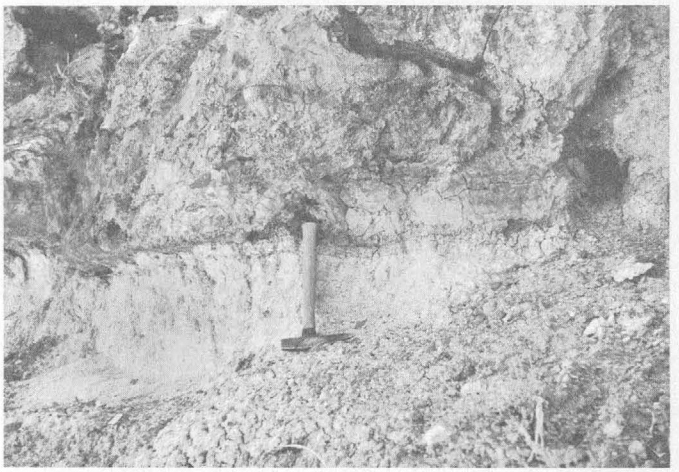

FIGURE 4.—Closeup view of low-angle fault at northwest side of mapped area. Brecciated carbonate rock overlies water-laid tuff along contact, near end of pick handle. Tuff is undisturbed except where pulverized within 2 inches of fault.

fault, although it also could be attributed to difference in original thickness.

Above the low-angle fault, carbonate rocks are considerably deformed. Strikes are variable, and beds dip as much as 30° into the underlying fault plane. Breccia cemented by carbonate and by dark-brown silica (jasperoid) is common in many places close to the fault and appears in some places 100 feet or more above the fault. Breccia consisting of pieces of carbonate rock separated by thin gouge layers is widespread within a few feet of the fault (fig. 4). Locally the gouge and breccia are irregularly sheeted subparallel to the low-angle fault. Folds with amplitudes of at least 100 feet are evident locally. The upper plate contains several high-angle and low-angle faults that do not extend into underlying rocks.

The low-angle fault cuts rocks as young as the water-laid tuff of Pliocene(?) age, and as it is offset by a normal fault older than the topaz-bearing rhyolite flows also of Pliocene(?) age (fig. 2), it is dated as Pliocene(?).

The high-angle faults that have displaced the low-angle fault (fig. 2) are probably of basin-range type. They bound a horst whose uplift accounts for a large part of the relief shown by the hills in which the low-angle fault is exposed.

The low-angle fault may mark the base of a regional plate or a local plate. This distinction would become important if beryllium deposits in water-laid tuff prove to be widespread in the vicinity of Spor Mountain. In other words, if the fault is local, the Cambrian rocks of the upper plate may conceal tuff only within the area of figure 2, but if regional, Cambrian rocks may conceal beryllium-bearing volcanic rocks in other places, making other carbonate-rock areas of potential interest for beryllium exploration.

REFERENCES

Jaffee, H. W., Gottfried, David, Waring, C. L., and Worthing, H. W., 1959, Lead-alpha age determinations of accessory minerals of igneous rocks (1953–1957): U.S. Geol. Survey Bull. 1097–B, p. 65–148.

Staatz, M. H., 1963, Geology of the beryllium deposits in the Thomas Range, Juab County, Utah: U.S. Geol. Survey Bull. 1142–M, p. M1–M36.

Stokes, W. L., and Hintze, L. F., 1963, Geologic map of northwestern Utah: Utah Geol. and Mineralog. Survey.

STRUCTURE OF PART OF THE TIMBER MOUNTAIN DOME AND CALDERA, NYE COUNTY, NEVADA

By W. J. CARR, Denver, Colo.

Work done in cooperation with the U.S. Atomic Energy Commission

Abstract.—The center of the Timber Mountain caldera northeast of Beatty is a structural dome in a thick sequence of ash-flow tuffs. Doming resulted in two episodes of faulting: an arcuate system of faults that were intruded by possible ring dikes, and graben faults that resulted in irregular collapsed segments in the middle of the dome.

Timber Mountain, on the western edge of the Nevada Test Site, is a domal uplift in the center of the Timber Mountain caldera (fig. 1). The uplift is dissected by a radial drainage system and culminates in 2 high points more than 7,000 feet in altitude. A central topographic trough trending roughly east-west between the high points contains Cat Canyon and its subordinate valleys (fig. 2). The dome is elliptical in plan, measuring about 10 by 8 miles; the long dimension trends northwest. An arcuate, relatively low lying area about 5 miles wide surrounds the dome on all but the west side. This moatlike depression is drained by Fortymile Canyon on the east and by Beatty Wash on the south. In general the rocks on Timber Mountain dip outward toward the moat.

The southeastern part of the dome, where erosion has cut into the flanks of the uplift and has exposed the underlying structure, is described in this preliminary article. Also, a brief history of the center of the caldera as interpreted from structural evidence in and around Timber Mountain is presented.

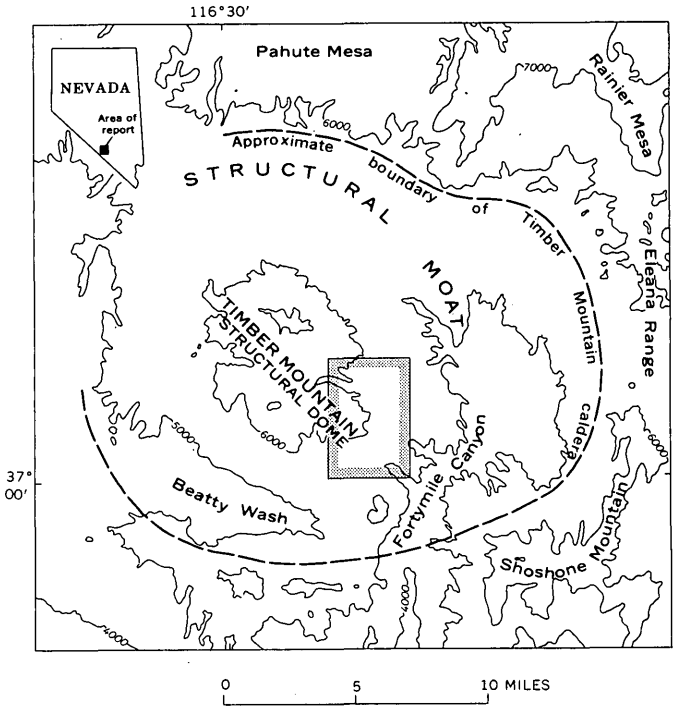

FIGURE 1.—Index map of the Timber Mountain caldera, showing topographic outlines and area of figure 2 (shaded outline).

STRATIGRAPHY

More than 3,000 feet of tuff is exposed within the Timber Mountain dome. The tuffs of Timber Mountain (fig. 2) are more than 2,500 feet thick and occupy most of the area discussed here. They are probably a composite ash-flow sheet as defined by Smith (1960, p. 158). No air-fall tuffs are present between ash flows in this sheet, and in some areas virtually the entire section of tuff is welded. In many places, individual ash flows can be distinguished only with difficulty, if at all. Devitrification of originally glassy pyroclastic material is complete nearly everywhere. In the following discussion the tuffs of Timber Mountain have been divided into units 1, 2, and 3, from oldest to

youngest (fig. 2). The base of the tuffs is not exposed, but the top is well exposed at the eastern end of Cat Canyon where the tuffs of Timber Mountain are unconformably overlain by bedded tuffs, tuffaceous sandstones, and ash-flow tuffs. These younger ash-flow tuffs lap out onto the dome in this area.

In the same area, at the mouth of Cat Canyon, but stratigraphically higher, are local silicic lava flows, basalt of Fortymile Canyon, poorly welded tuff of the Thirsty Canyon Tuff, basalt of Buckboard Mesa, and much interbedded, locally tuffaceous conglomerate, sandstone, and colluvium. These rocks fill the moat and lap out onto the dome.

No outcrops of the Piapi Canyon Formation, a thick sequence of ash-flow tuffs that is older than the tuffs of Timber Mountain, have been identified on the Timber Mountain dome. The Piapi Canyon is extensive elsewhere on the test site, but is exposed mainly outside the caldera.

STRUCTURE

Part of the structural history of the Timber Mountain uplift can be interpreted from the structural relations of the rocks exposed in the southeastern part of the dome (figs. 1 and 2). Large faults of the dome affect all rocks up to and including the tuffs and sandstones immediately overlying the tuffs of Timber Mountain, but displacements in the younger rocks locally are somewhat smaller than in the older rocks.

Minor faulting began in the Timber Mountain area before deposition of the tuffs of Timber Mountain was completed, but the oldest major structure of the southeastern part of the dome is an arcuate zone of faulting, here called the inner ring fracture, that cuts the tuffs of Timber Mountain near the edge of the moat fill (fig. 2). The zone, which is about a mile wide, is exposed for about 3 miles, and may extend farther in areas covered by younger rocks.

In general the inner ring-fracture zone parallels the strike of the tuffs and consists of branching normal faults which individually have small displacements, but which together have considerable displacement. The main fault of the zone can be traced for several miles. It probably dips toward the moat at about 45° to 65° in places, and is thus nearly parallel to the dip of the tuffs on the downthrown side (fig. 2, section). In most places it occurs at about the same stratigraphic position and results in the omission of several hundred feet of unit 2 of the tuffs of Timber Mountain. Many strike faults on the moat side of this main fault dip more steeply and cause numerous repetitions of unit 3. These faults are less persistent and some may dip inward and end against the main fault.

Along the main fault in the ring-fracture system is a chain of small rhyolitic intrusions. These dikes, together with stratigraphic position, aid in tracing this fault. Many of the intrusions are brecciated, but the wallrocks are relatively undisturbed, indicating either possible movement on the fault during emplacement of the dike, or autobrecciation of the dike.

Along the south side of the dome, tuffs inside the main fault of the inner ring-fracture zone generally dip away from the dome at angles of less than 35°. In the outer part of the zone, outside the main fault, the same tuffs commonly dip outward at more than 35°, and local dips as high as 65° are observed along the south edges of the dome.

A second large structural feature of the map area is a group of granite porphyry intrusions (fig. 2) containing alkali feldspar, zoned plagioclase, and biotite phenocrysts in a fine-grained matrix of quartz and alkali feldspar. The largest exposure of this rock is about 4,500 feet long and 1,500 feet wide. Although the intrusions are irregular in shape they tend to be elongated in a northeasterly direction, and they form a group that trends about N. 45° E., which closely parallels the ring-fracture zone. The mapped intrusions join at depth, as indicated by the downward widening of individual bodies, and by the presence of a roof pendant in one place. They are restricted to the stratigraphically lowest part of unit 1, and contacts with unit 2 are probably faults. In at least one place the line of intrusions is displaced by a system of northwestward-trending graben faults.

Horsts and grabens, which control the topography of the central trough area of the Timber Mountain dome, trend from nearly due west to about N. 50° W., and intersect the inner ring-fracture zone at fairly large angles in the southeastern part of the dome. Most of the northwest-trending faults clearly offset the inner ring-fracture system, and the faults bounding one graben displace the granite porphyry intrusions. The grabens appear to be the result of relative subsidence of elongate irregular blocks on fairly steep normal faults, perhaps as illustrated by Smith (1961, p. D148).

In the center of the graben zone of eastern Cat Canyon are several small, shallow rhyolitic intrusions (fig. 2) that tend to enlarge upward and probably reached the surface in places. They cut the youngest ash flows of unit 3, and in a few places overlie these tuffs, separated from them by a thin tuff breccia. The age of these intrusions with respect to faulting is uncertain, but their distribution suggests that they are related to the formation of the grabens.

Postgraben structural movement is not well recorded within the area shown on figure 2. Some small faults of northwesterly trend, parallel to the graben system,

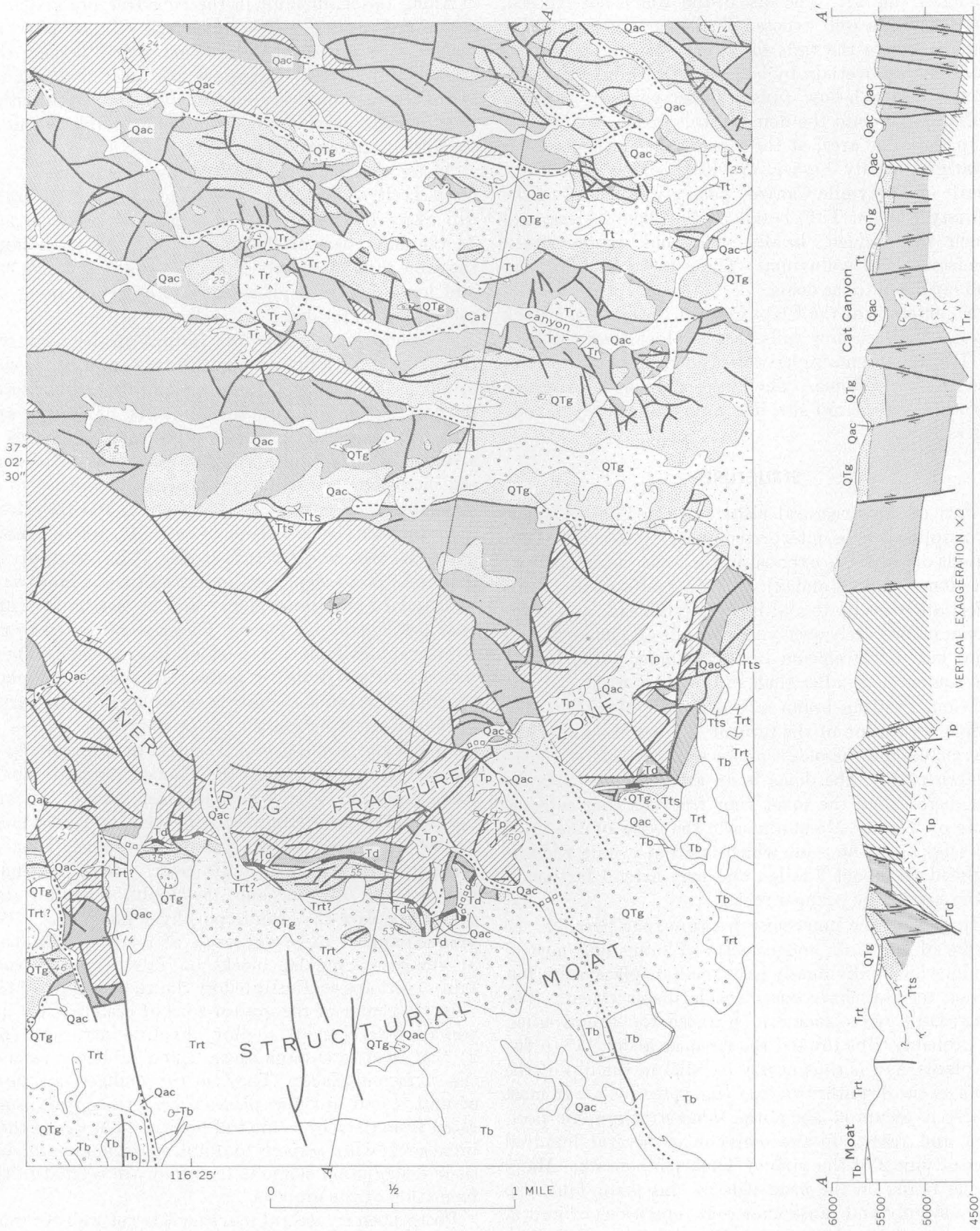
A
A'
Qac
QTg
Tr
Tt
Tts
Tp
Td
Trt
Tb
Cat Canyon
INNER RING FRACTURE ZONE
STRUCTURAL MOAT
Moat
37° 02′ 30″
116°25′
0
½
1 MILE
VERTICAL EXAGGERATION ×2
6000′
5500′
5000′
4500′

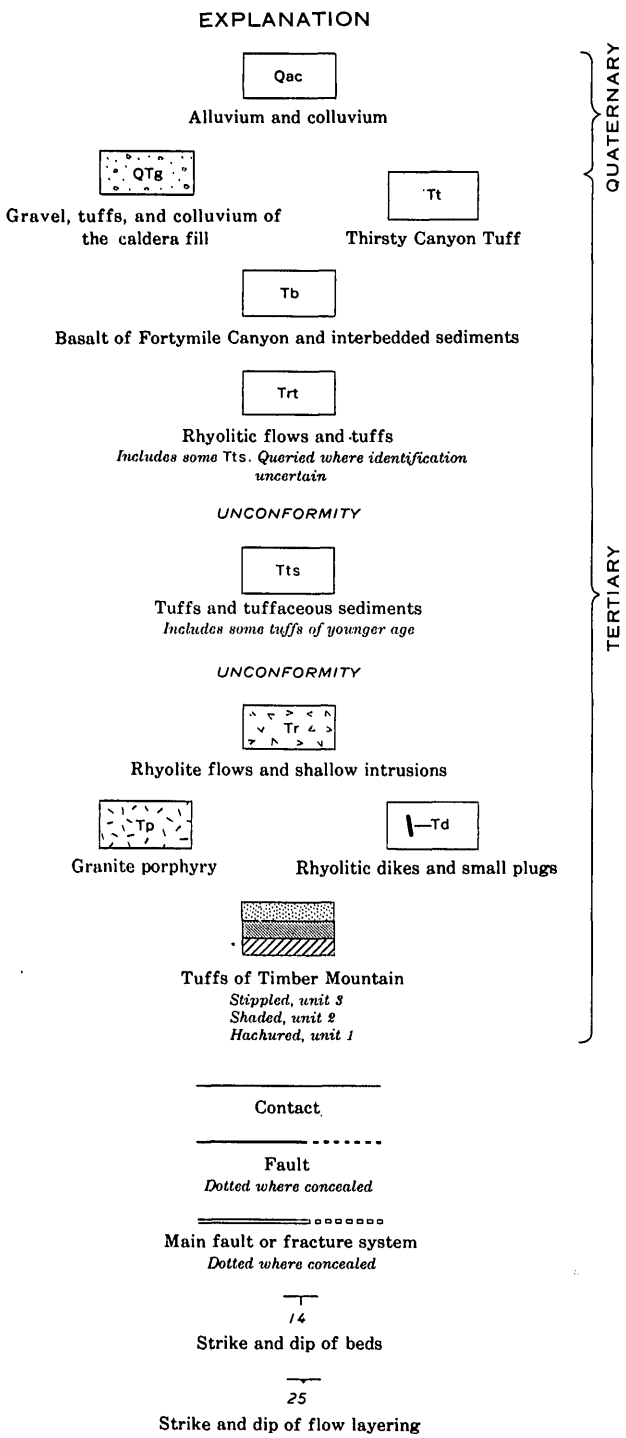

FIGURE 2.—Generalized geologic map and section of the southeastern corner of the Timber Mountain quadrangle, Nye County, Nev., by W. J. Carr and W. D. Quinlivan, 1962.

may be later than the grabens. A few minor faults, mostly of northerly trend, cut the younger rocks of the moat area, including the ash-flow tuffs of the Thirsty Canyon. Gravels (fig. 2, section) in the Cat Canyon area probably were not displaced significantly by movement on the graben faults, but the Thirsty Canyon Tuff exposures on the flanks of the dome in the Cat Canyon area (fig. 2) are about 500 feet structurally higher than in the moat to the east. Some post-Thirsty Canyon Tuff uplift seems necessary to account for this difference in altitude.

STRUCTURAL HISTORY

The foregoing evidence leads to a tentative interpretation of the history of the Timber Mountain dome and inner moat area.

Faulting began before deposition of the tuffs of Timber Mountain was completed, as some faults do not cut the youngest of these tuffs. Shortly after deposition of the tuffs, the Timber Mountain area was domed, probably by upward magma pressure. The central part of this "blister" failed along an inner ring-fracture zone that may have been controlled by fractures developed during caldera collapse. This zone consisted of a persistent outward-dipping fault with associated, possibly antithetic, faults. Blocks were rotated and dips steepened on the downthrown side of the main fault. The relatively consistent stratigraphic position of the main fault in the ring-fracture zone indicates that the zone predates most of the other faults in the area. Small silicic intrusions occurred along the main fault of the ring fracture, and granite porphyry was intruded into the lower part of the tuffs, coming nearest the surface in the general area of the inner ring-fracture zone to form a possible ring dike. Tuffs and sandstones were deposited on the rising dome with minor angular unconformity. In the later stages of doming, grabens were formed. This faulting was followed or accompanied by extrusion of rhyolite in the moat and intrusion of shallow rhyolite plugs in the Cat Canyon area. The moat rhyolites are cut by only a few very small faults. The moat was partially filled with sedimentary and volcanic rocks, including the ash-flow tuffs of the Thirsty Canyon. Structural relief of these tuffs on the dome indicates that minor uplift of Timber Mountain recurred subsequent to their deposition.

REFERENCES

Smith, R. L., 1960, Zones and zonal variations in welded ash flows: U.S. Geol. Survey Prof. Paper 354–F.

——— 1961, Structural evolution of the Valles caldera, New Mexico, and its bearing on the emplacement of ring dikes: Art. 340 *in* U.S. Geol. Survey Prof. Paper 424–D, p. D145–D149.

DIVERSE RECURRENT MOVEMENT ALONG SEGMENTS OF A MAJOR THRUST FAULT IN THE SCHELL CREEK RANGE NEAR ELY, NEVADA

By HARALD DREWES, Denver, Colo.

Abstract.—Normal faulting, then low-angle gravity sliding, and finally renewed normal faulting occurred along a segment of an earlier thrust fault. Along this segment the later faults appear to have followed virtually the same fault plane, but the relative direction of movement was reversed.

The Schell Creek Range extends north-south 100 miles in central-eastern Nevada. The part of the range shown in figure 1 is underlain by Paleozoic sedimentary rocks and Tertiary sedimentary and volcanic rocks. Some large structural features of this part of the range have been described briefly by Spurr (1903, p. 44–47), Misch and Easton (1954), and Drewes (1960). Part of the northern end of the range has been mapped by Young[1] (1960). Current work in the central part of the range indicates that there were at least four episodes of deformation: (1) Mesozoic or early Tertiary low-angle faulting, thought to be chiefly thrust faulting during which faults were formed and gently folded during or after faulting; (2) middle Tertiary normal faulting; (3) middle or late Tertiary low-angle faulting, thought to be glide faulting in which faults were formed solely by gravity and not pushed laterally; and (4) late Tertiary or Quaternary normal faulting.

Complicated relations between structures account for some of the difficulties in dating the faults and explaining their origin. Normal faults locally follow the plane of weakness of older structures and are deflected along parts of thrust faults, so that their strikes are changed slightly and their dips are decreased. Glide plates have moved on, or close to, stripped parts of earlier thrust faults. Parts of thrust plates that moved eastward or northeastward were later shifted westward along deflected normal faults, so that some blocks across the thrust faults apparently moved in different directions. The relations between these structures are generalized on figure 1. On the map the fault symbols overlap where recurrent movement is inferred; in the structure section the sequence of fault movements is indicated by numbers.

Low-angle, near-bedding-plane faults that cut the Paleozoic rocks have reduced the normal stratigraphic sequence from a thickness of about 5 miles to about 3½ miles. The Paleozoic rocks consist of marine limestone, dolomite, quartzite, and interbedded shale. The low-angle faults commonly lie along, or close to, the contacts between units of markedly different competence. In many places the faults parallel the bedding, although in other places, beds above or on both sides of such faults are inclined toward the faults at angles of more than 30°; thus the low-angle faults are not strictly bedding-plane faults.

The structures in the Paleozoic rocks differ from those in the Tertiary rocks, suggesting that the older structures were formed in a structural environment different from that of the younger ones. In the Paleozoic rocks, beds along the faults are generally missing rather than repeated, but locally some slices of rock are shingled. The plates between adjacent low-angle faults are broken into numerous large blocks that have been rotated along horizontal axes, with respect to adjacent blocks, mainly by normal faults but also by reverse faults and subsidiary low-angle faults. Some small low-angle faults die out along their strike, merge at low angles with adjacent faults, or separate disharmonic plates; some larger faults are truncated by others higher in the section or end against tear faults.

SCHELL CREEK RANGE THRUST FAULT

The Schell Creek Range thrust fault has been mapped for 18 miles along the range and may extend

[1] J. C. Young, 1960, Structure and stratigraphy in the north-central Schell Creek Range, eastern Nevada: Princeton Univ., Ph. D. thesis.

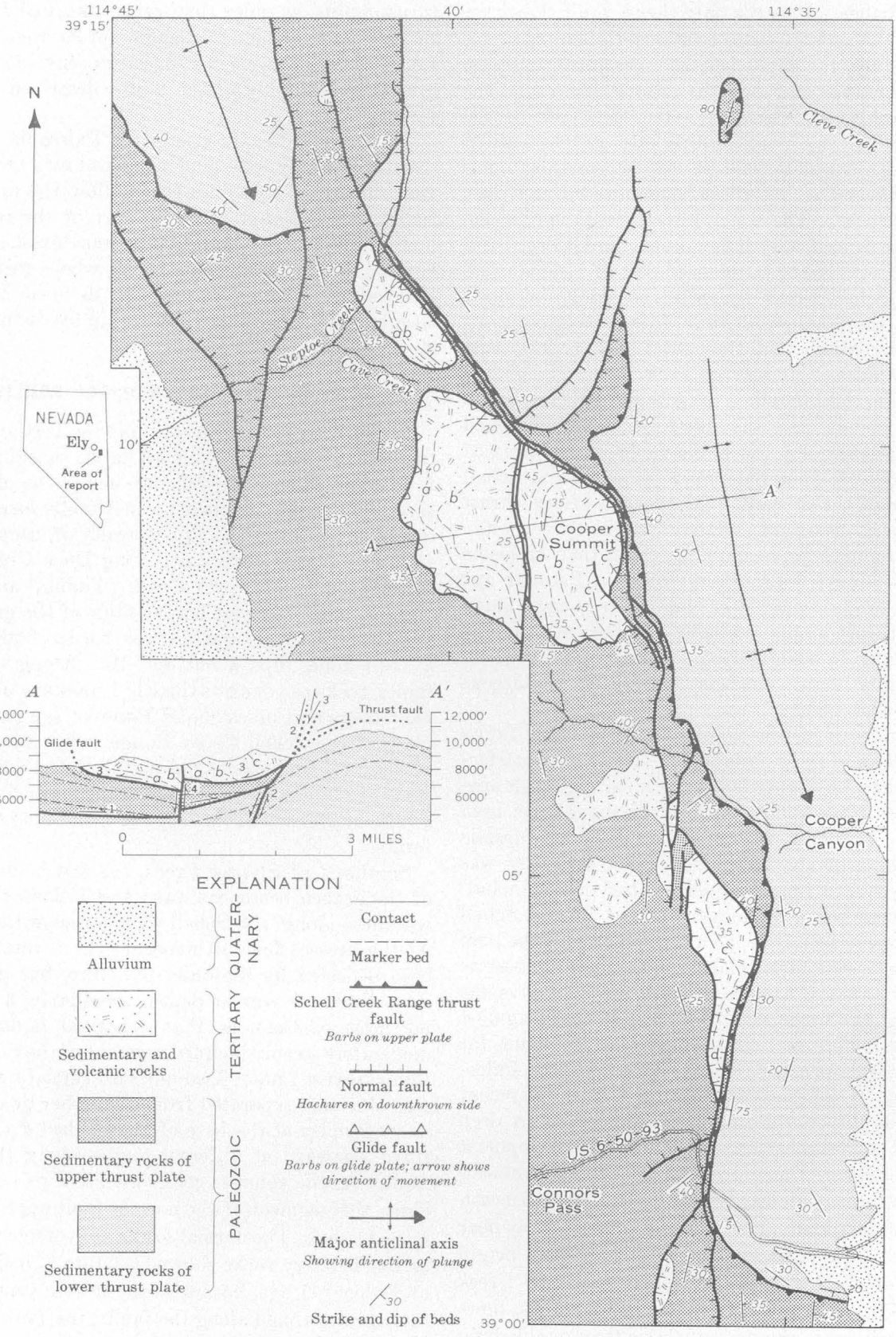

FIGURE 1.—Generalized geologic map of part of the Schell Creek Range, Nev., showing segments of a thrust fault, normal faults, and a glide fault. Where they merge they are shown by separate symbols only for clarity; actually they are superposed or very nearly parallel. Numbers in structure section indicate sequence of development.

30 miles farther. It is the only thrust fault shown on figure 1. Where structural relations are simple along the main trace, the fault dips 25° westward, but east of the main trace and over the crest of the range the fault is nearly horizontal. On the east flank of the range, near Cleve Creek, it dips eastward beneath a klippe. As much as 15,000 feet of beds is missing along the fault where Permian rocks have moved over Upper Cambrian rocks. The other low-angle faults in the area can be traced only a few miles, and along them only a few hundred to a thousand feet of beds is missing. The Schell Creek Range thrust fault described here is not the décollement fault (not shown on fig. 1) described by Misch and Hazzard (1962, p. 319) east of Connors Pass.

The inclination of minor drag folds with respect to the fault planes, and the offset of steeply inclined beds along subsidiary low-angle faults in the area of figure 1 indicate that the upper plates of the Schell Creek Range thrust fault and the subsidiary thrust faults moved eastward relative to the lower ones. Locally the faults can be dated no closer than Mesozoic or early Tertiary; the fault cuts rocks of Permian age but not those of Eocene(?) or Oligocene(?) age. However, the thrust faults probably are the same age as similar faults in neighboring ranges, some of which are probably Late Jurassic or Early Cretaceous (Misch, 1960, p. 33).

Local evidence for the origin of the low-angle faults in the Paleozoic rocks is indirect. Neither a satisfactory root area for thrust faults nor a suitable high area from which glide plates might have moved has been identified. However, at least as late as Early Jurassic time the base of the Paleozoic section evidently was covered by 6½ to 7 miles of sedimentary rocks, including Mesozoic rocks no longer present in the Schell Creek Range. Beneath such a column of rock the pore pressure may well have equaled the lithostatic pressure. If such a pressure balance existed, it would give the underlying Precambrian rocks great strength against further load deformation and may help account for their lack of deformation beneath much-faulted Paleozoic rocks. It seems easier to picture the development of thrust faults or squeezed-out plates in such a deep structural environment and to picture the development of glide faults in a shallower structural environment. In the absence of a clear décollement surface beneath widespread imbricate plates formed comparatively near the surface, I provisionally favor a thrust-fault origin for most of the low-angle faults in the Schell Creek Range. The genesis of the low-angle faults is, however, less critical to the present thesis than establishing the age of the low-angle faults, described above as thrust faults, as older than certain normal faults, and indicating that such low-angle faults were probably formed in a much deeper structural environment than other, younger low-angle faults described below as glide faults.

During or after thrusting, the Paleozoic rocks and the thrust faults were gently warped into broad southward-plunging anticlines that follow the crest of the Schell Creek Range and the crest of the topographically lower Duck Creek Range, northwest of Steptoe Creek. One of these folds, along whose western flank the beds and thrust fault were inclined moderately steeply, played an important part in localizing younger structures.

MIDDLE TERTIARY NORMAL FAULTS

Normal faults of probable middle Tertiary age cut the Schell Creek Range thrust fault, subsidiary thrust faults, and some rocks that lap across the older structures. The largest of these normal faults form a graben that extends from the upper reach of Steptoe Creek (fig. 1) 25 miles northward along Duck Creek Valley to the vicinity of North Creek (Young,[2] and Young, 1960, pl. 1). The west border fault of the graben dips steeply to the east, and the east border fault, actually a fault zone, dips about 45° W. Along the border faults, rocks as young as the Ely Limestone of Pennsylvanian age and limestone of Permian age in the upper plate of the Schell Creek Range thrust fault are displaced against rocks as old as the Pole Canyon Limestone of Middle Cambrian age in the lower plate, giving a false impression of the displacement along the normal faults.

Southeast of Steptoe Creek, the east bounding fault of the graben bends eastward and follows the zone of weakness along the Schell Creek Range thrust fault. At the present level of exposure the normal fault has been deflected by the older structure, but presumably these faults diverge at depth. Similarly, 3 to 4 miles northeast of Connors Pass a normal fault follows a moderately steeply inclined segment of the Schell Creek Range thrust fault. Two units of Tertiary conglomerate, which are separated from each other by an angular unconformity at the base of marker bed *d* (fig. 1), are tilted eastward at different angles along this normal fault. As the younger conglomerate dips less than the older, this segment of the normal fault appears to have moved twice. The normal faults are younger than some of the Tertiary rocks shown in figure 1, believed to be of Eocene(?) age, but as some volcanic vents of about this age are alined along the faults, the faults are prob-

[2] Op. cit.

ably not much younger. Provisionally they are assigned a middle Tertiary age. The later of the two episodes of normal faulting northeast of Connors Pass is considerably younger and probably is of late Tertiary or Quaternary age, for the younger faults cut rocks of Pliocene(?) age.

MIDDLE OR LATE TERTIARY GLIDE FAULTS

Low-angle faults believed to be glide faults underlie two plates of rocks of Eocene(?) or Oligocene(?) age. One plate is between Cooper Canyon and Cave Creek, and the other is north of Cave Creek (fig. 1). Rocks in these glide plates consist of a sequence, in ascending order, of conglomerate, a rhyolite vitrophyre lava flow, slightly welded rhyolite tuff, much unwelded tuff, and dacite vitrophyre lava flows and tuff. In the larger glide plate the sequence is about 1 mile thick, but in the other it is much thinner. The Tertiary rocks in these plates have been warped into open synclines that plunge gently eastward, and the larger plate is broken by several normal faults. The beds of the smaller plate and of the eastern half of the larger plate dip 20° to 45° into clay-rich, slightly gypsiferous Chainman Shale of Mississippian age and locally also into Ely Limestone (Pennsylvanian), both in the upper plate of the Schell Creek Range thrust fault. Where the eastern edge of the larger plate lies along or crosses the thrust fault, the beds of the glide plate dip into rocks of Cambrian or Ordovician age of the lower plate of the thrust fault. The surface beneath the larger plate ranges from saucer shaped to flat. Along the north and east sides, the basal contact dips about 40° southward and westward; along the south side of the block it is nearly horizontal; and along the west side it dips gently eastward. In the northern part of the Schell Creek Range, Young[3] reports that there, too, the Tertiary rocks are structurally discordant on Paleozoic rocks along low-angle faults.

The displaced Tertiary rocks in the glide plates are thought to have slid westward along glide faults from the flank of a highland, formed by uplift of the rocks east of the normal fault that farther north forms the east border of the graben near Steptoe Creek, and into a large valley underlain by Chainman Shale. A glide-fault interpretation is favored here because the fault surfaces are exposed all around the plates, because there is a slope down which the plates could have moved, and because the plates were formed under little cover.

The leading, western half of the larger glide plate moved westward a minimum of 3,500 feet to accommodate the rotation of about 40° of the trailing, eastern half of the plate. As the plate moved, drag along the flanks exceeding that beneath the center gently warped the beds within the plate. Locally, blocks of Ely Limestone that had been resting on the Chainman Shale were dragged along the base of the Tertiary rocks. A most significant point in this interpretation of the origin of the glide plate of tilted Tertiary rocks is that parts of the plate followed a part of the surface, stripped along or close to the older Schell Creek Range thrust fault and the normal fault of middle Tertiary age, thereby acquiring a structural position of rocks truly part of the upper plate of the thrust fault. Movement of the glide plates postdates the deposition of rocks of Eocene(?) or Oligocene(?) age in the plates, and presumably it postdates the normal fault along which the source area of the plates was raised. The glide faulting, therefore, is dated as middle or late Tertiary.

LATE TERTIARY OR QUATERNARY NORMAL FAULTS

Several normal faults cut the larger glide plate of Tertiary rocks and the underlying glide fault. Near Cave Creek the fault cutting across the center of the plate has a stratigraphic displacement of several thousand feet, for the marker beds *a* and *b* (fig. 1) east of the fault lie topographically and structurally far above the same beds to the west of the fault. Because it has large displacement near the north edge of the glide plate, the normal fault probably extends northward beyond the glide block. The only surface available for the extension of this fault is the surface already utilized by the Schell Creek Range thrust fault, by the normal fault of middle Tertiary age bounding the east side of the graben along Steptoe Creek, and possibly also by the glide fault beneath the smaller of the glide plates. Where the normal fault of middle Tertiary age diverges from the thrust fault, the later normal fault probably follows the plane of the older normal fault. Some movement along this younger fault may also have been contemporaneous with gliding, as beds *a* and *b* are offset more than the glide-fault plane. This late normal fault is dated as late Tertiary or Quaternary, because northeast of Connors Pass it cuts the unit above marker bed *d* which is as young as Pliocene(?) (fig. 1), and similar faults elsewhere in the area cut gravel of Pleistocene age. Apparently, glide faulting occurred at a time of active normal faulting and volcanism, during which the source area was uplifted. The tectonic activity of middle Tertiary age probably set the stage for glide faulting, and the activity continued after the gliding.

SUMMARY

In much of the central part of the Schell Creek Range, normal faults, thrust faults, and glide faults are

[3] Op. cit., p. 123–125.

abundant and form plainly decipherable map patterns. Complexity of map pattern arises along segments of the major thrust fault where younger faults have been deflected, and the complexity increases where the direction of movement along later normal faults was different from that along the thrust fault. As a result of post-thrust normal faulting, in several places Tertiary rocks younger than the thrust faults are faulted down into the rocks of the upper plate of the major thrust fault and against rocks of the lower plate. As a result, the map pattern formed by these bodies of Tertiary rocks mimics that formed by rocks that are actually part of the upper plate of the thrust fault, although the direction of movement of the hanging block of the normal faults that were deflected along segments of the thrust fault was opposite to that of the upper plate of the thrust fault. Under such circumstances of recurrent and diverse movement along some thrust faults, however local, detailed mapping of relatively large areas around the faults is essential to understanding the timing and dynamics of the thrust faults.

REFERENCES

Drewes, Harald, 1960, Bedding-plane thrust faults east of Connors Pass, Schell Creek Range, eastern Nevada: Art. 122 *in* U.S. Geol. Survey Prof. Paper 400–B, p. B270–B272.

Misch, Peter, 1960, Regional structural reconnaissance in central-northeast Nevada and some adjacent areas; observations and interpretations, *in* Intermountain Association of Petroleum Geologists, Guidebook, East central Nevada: p. 17–42.

Misch, Peter, and Easton, W. H., 1954, Large overthrust near Connors Pass in the southern Schell Creek Range, White Pine County, eastern Nevada [abs.]: Geol. Soc. America Bull., v. 65, no. 12, pt. 2, p. 1347.

Misch, Peter, and Hazzard, J. C., 1962, Stratigraphy and metamorphism of late Precambrian rocks in central northeastern Nevada and adjacent Utah: Am. Assoc. Petroleum Geologists Bull., v. 46, p. 289–343.

Spurr, J. E., 1903, Descriptive geology of Nevada south of the fortieth parallel and adjacent portions of California: U.S. Geol. Survey Bull. 208, 229 p.

Young, J. C., 1960, Structure and stratigraphy in north-central Schell Creek Range, *in* Intermountain Association of Petroleum Geologists, Guidebook, East central Nevada: p. 158–172.

FACIES RELATIONS OF EXPOSED ROME FORMATION AND CONASAUGA GROUP OF NORTHEASTERN TENNESSEE WITH EQUIVALENT ROCKS IN THE SUBSURFACE OF KENTUCKY AND VIRGINIA

By LEONARD D. HARRIS, Knoxville, Tenn.

Abstract.—The Rome Formation, Conasauga Shale, and Conasauga Group were deposited in a northwest transgressive phase of the Early, Middle, and Late Cambrian seas. Sandstone of the Rome in central Kentucky is by lateral gradation a facies equivalent of approximately the lower half of the Conasauga Group of northeastern Tennessee. The Rome probably ranges in age from Early Cambrian in eastern Tennessee to Middle Cambrian in central Kentucky.

In the Valley and Ridge province of extreme southwest Virginia and the adjacent part of Tennessee the oldest Cambrian formations exposed are the Rome Formation of Early Cambrian age and the Conasauga Shale or Group of Middle and Late Cambrian age. These formations plunge into the subsurface of Kentucky and are not exposed in that State. In recent years a series of deep test wells drilled to or near basement rocks in central and eastern Kentucky has provided the link necessary to show facies relations between the subsurface rocks of Kentucky and the surface exposure of the Rome and Conasauga in Virginia and Tennessee (fig. 1).

Early workers in Virginia and Tennessee (Campbell, 1894; and Keith, 1896) recognized that a facies relation exists between the Conasauga Shale and the unit now called the Conasauga Group (Rodgers, 1953, p. 47). They found that the thick limestone units of the group wedge out northward into a shale section. The name Conasauga Shale was used for the shale facies on the northwest, and to the east and south the equivalent sequence was divided in ascending order into four formations—the Rutledge Limestone, Rogersville Shale, Maryville Limestone, and Nolichucky Shale.

Later stratigraphic studies in eastern Tennessee have not altered the basic facies concept of the earlier workers; however, some of the terminology has been modified by restriction of the Rome Formation and recognition of additional formations considered to be equivalent to the Conasauga Shale (Rodgers and Kent, 1948). These later nomenclatural developments were summarized by Rodgers (1953, p. 43–53). In a diagram he (1953, p. 46) illustrated how the Conasauga Shale on the northwest side of the Valley and Ridge province is gradually supplanted to the southeast by six alternating units of shale and limestone, which he included in his Conasauga Group. These formations from oldest to youngest are the Pumpkin Valley Shale, Rutledge Limestone, Rogersville Shale, Maryville Limestone, Nolichucky Shale, and Maynardville Limestone. These later studies have done much to standardize and clarify the terminology and have established a firm base for regional stratigraphic work in northeast Tennessee. Consequently, I have used Rodgers' terminology as the basis for developing the subsurface nomenclature for eastern Kentucky and extreme southwest Virginia. This use of Tennessee surface nomenclature in the subsurface of southwest Virginia and central and eastern Kentucky is not without precedent. Tennessee terms have been used in most recent subsurface studies in southwest Virginia (Miller and Fuller, 1954) and eastern Kentucky (Thomas, 1960; Woodward, 1961; and Calvert, 1962), as shown on figure 2. One exception to this was Freeman (1953) who used midcontinent terms.

The rocks of the Valley and Ridge province in northeast Tennessee and southwest Virginia are cut by a series of northeast-trending thrust faults (fig. 1). Northwestward movement along many of these faults is probably measured in miles. This movement tends to obscure regional facies changes by bringing rocks deposited in different parts of the original basin of deposition in close proximity. Within particular fault belts the lithology of individual formations re-

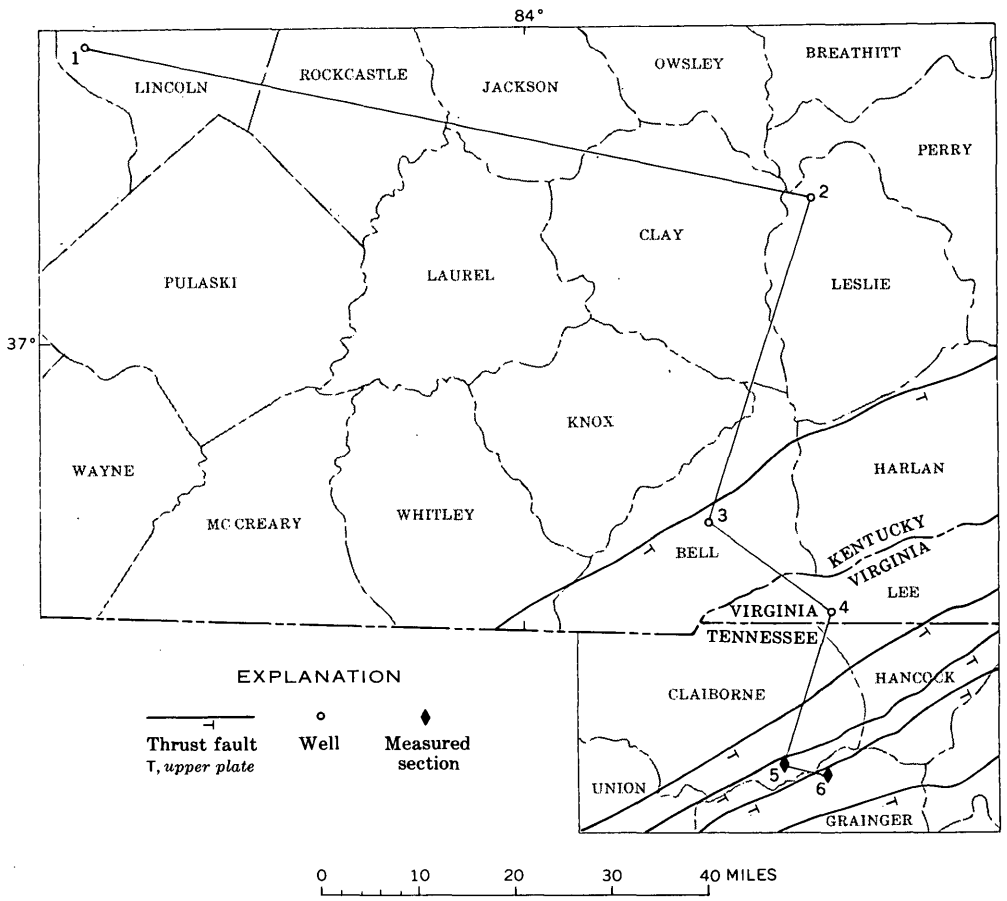

FIGURE 1.—Location of wells and measured sections referred to in text.

mains relatively constant, but across fault belts, facies are markedly different. In order to remove the effect of shortening of the depositional basin by thrusting, I have attempted to restore the sections and wells in figure 3 to their relative position before thrusting. At present, only the amount of movement on the northernmost fault—the Pine Mountain thrust—can be calculated accurately. Miller and Fuller (1954, p. 260) have shown that the displacement within the area discussed in this article along the Pine Mountain fault is about 6 miles. In the present study, 6 miles was used as a minimum displacement on the faults to the southeast and was added to the present geographic distance between sections in an attempt to restore them roughly to near their original position. Thus, the distance between sections 5 and 6 (fig. 3) was increased by 6 miles, and that between 4 and 5 by 12 miles. The distance between wells 3 and 4 was increased by 6 miles, as shown by the fact that well 4 was drilled through the Rome Formation and Conasauga Shale above the Pine Mountain thrust fault, whereas well 3 penetrated the same section below the fault.

ROME FORMATION

Stratigraphic studies of the exposed Rome Formation in northeast Tennessee are complicated because everywhere the "base" of the Rome is marked by a major thrust fault. Therefore, until key beds or zones were established in the formation, an estimate could not be made of how much or what part of the Rome was represented in any given section. Rodgers and Kent (1948) simplified the problem by pointing out a distinctive dolomite unit and a sandstone unit at the top of their restricted Rome Formation. Detailed mapping and measurement of sections have established that both these units can be used as key beds in regional stratigraphic studies.

On the outcrop in Tennessee the Rome Formation is a sequence of sandstone, siltstone, and shale containing a few beds and one thick zone of dolomite (fig. 3). Unweathered clastic rocks of the Rome are micaceous and abundantly glauconitic. The proportion of sandstone to shale and siltstone gradually increases toward the northwest. This relation holds true in the sub-

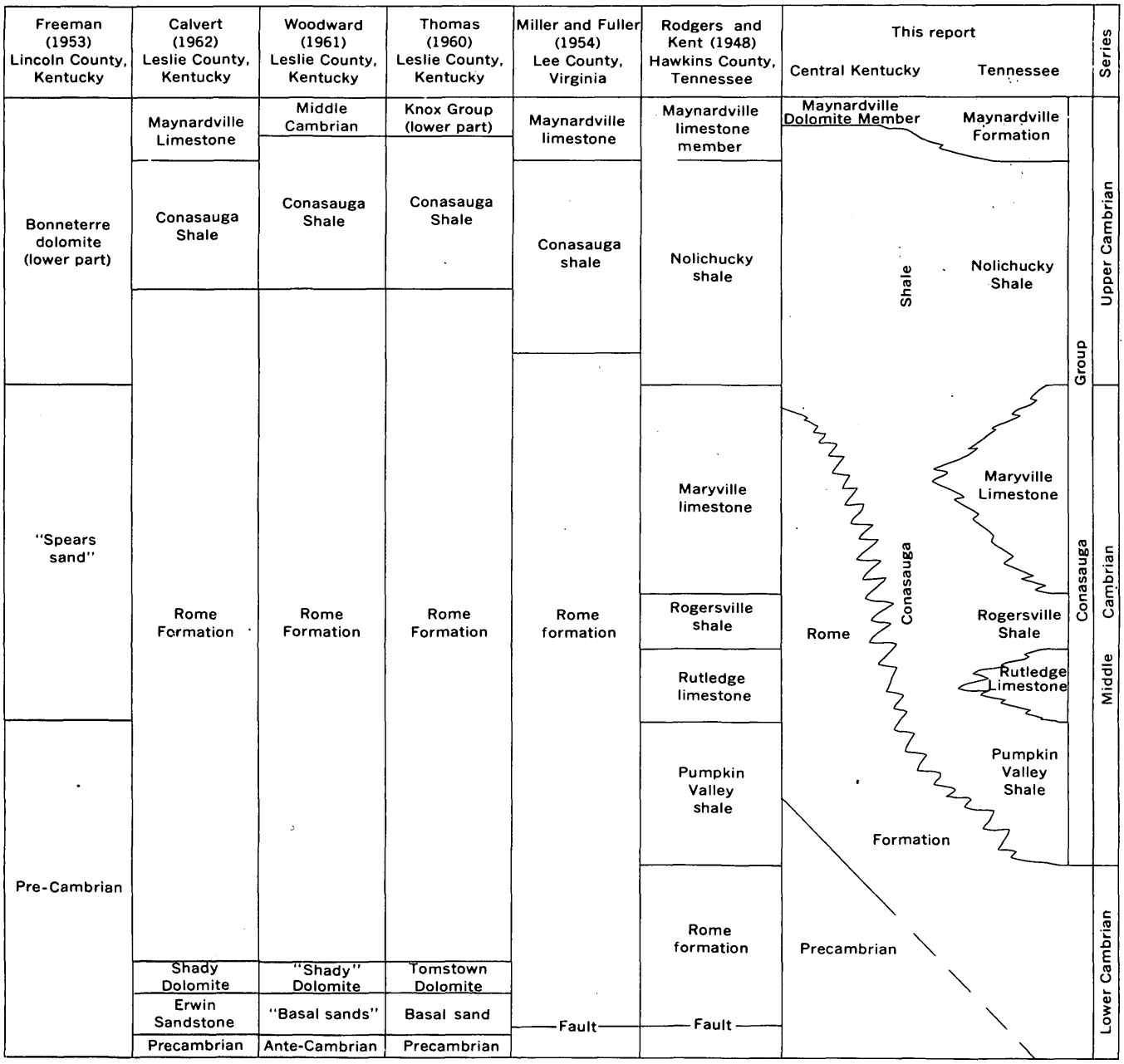

FIGURE 2.—Comparison of stratigraphic nomenclature used by various authors with that used in this article.

surface of Virginia and Kentucky, where the Rome is mainly a glauconitic micaceous sandstone with small amounts of siltstone, shale, and limestone. The lower dolomite unit of the Tennessee outcrop occurs in both the Fordson and Brooks wells (secs. 2 and 4, fig. 3). In each well the contact between the Conasauga Shale and Rome is placed, as it is in surface sections, at the first occurrence of abundant sandstone. Thus delineated, the contact rises in the wells toward the northwest.

CONASAUGA SHALE OR GROUP

The Conasauga Group of northeast Tennessee is composed of six alternating units of shale and limestone (fig. 3). The lowermost unit, the Pumpkin Valley Shale, is greenish gray to dark olive gray and usually contains numerous paper-thin beds of glauconitic siltstone. Siltstone becomes more abundant toward the northwest (sec. 5, fig. 3). The other shale units, the Rogersville and Nolichucky Shale, are less silty but

725-328 O—64——3

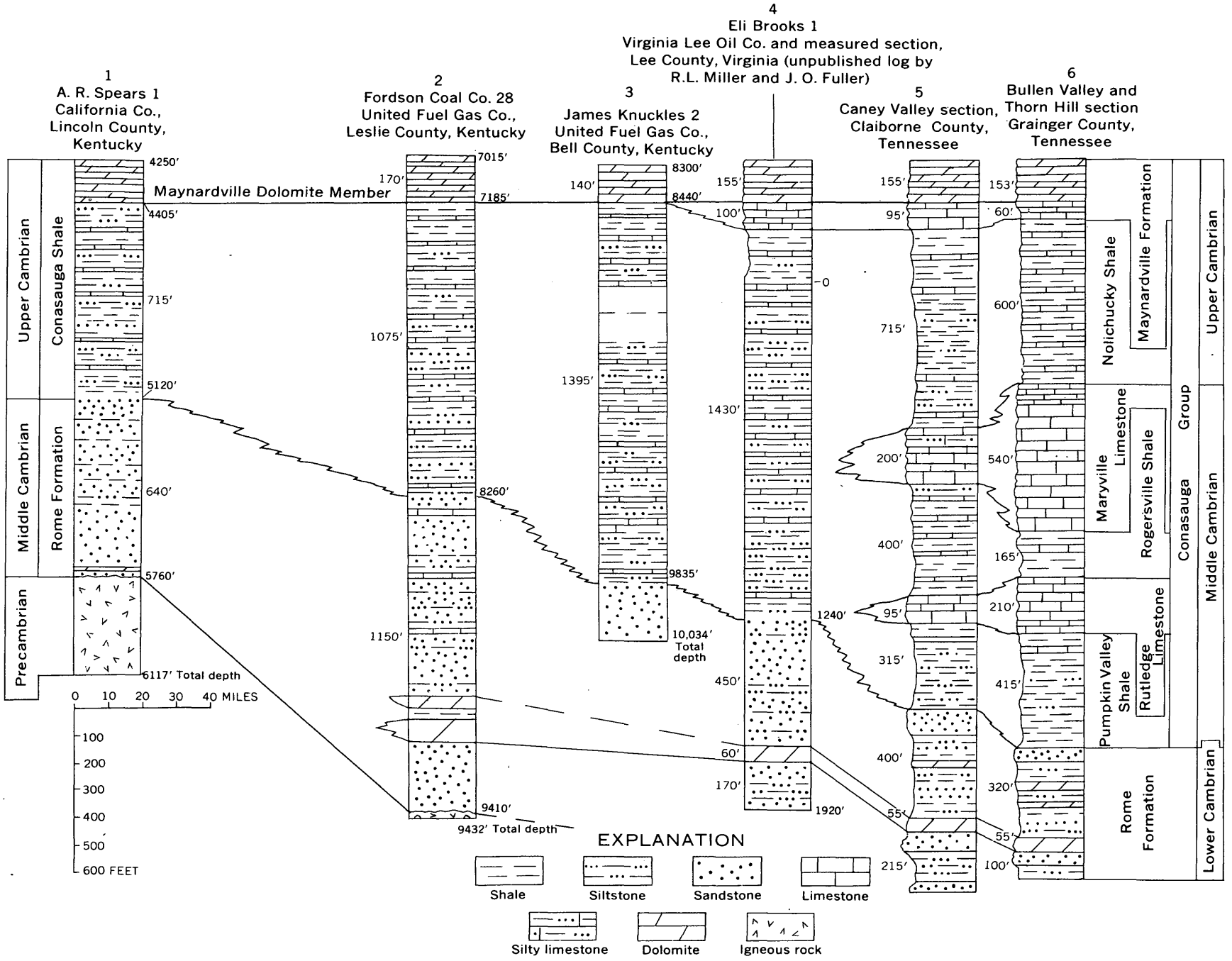

FIGURE 3.—Palinspastic diagram showing correlation of the outcropping Rome Formation and Conasauga Group in Tennessee with subsurface sections of the Rome and Conasauga Shale in Virginia and Kentucky. Distance between sections 3 and 4 and 4 and 5 is estimated, and that between 5 and 6 is exaggerated to show intertonguing relations. Location of sections is shown on figure 1. Datum is base of the Maynardville Dolomite Member.

contain thin beds of limestone which are either oolitic or contain intraformational conglomerate. The limestone units, Rutledge and Maryville Limestones, thin abruptly toward the northwest and are absent in the subsurface of Virginia and Kentucky. In outcrop the Maynardville Formation, the uppermost unit of the group, is composed of a lower limestone member and an upper dolomite member. Toward the northwest in the subsurface, the limestone member wedges out; however, the dolomite member persists and occurs in all the Kentucky wells. Where the limestone member is absent, the Maynardville is included in the Conasauga Shale as the Maynardville Dolomite Member.

In the subsurface where the limestone units of the Conasauga Group wedge out, there exists no good criterion to separate individual shale units; consequently, the entire sequence is termed the Conasauga Shale. The Conasauga Shale, which is remarkably uniform throughout, is characterized by grayish-red or medium-dark-gray shale with interbeds of glauconitic siltstone and numerous thin limestone beds, many of which are clearly oolitic. The Conasauga thins toward the northwest.

Age of at least the upper 300 feet of the Conasauga Shale in Kentucky has been established as Late Cambrian by the identification of trilobite fragments by Ulrich (Miller, 1921). The trilobite fragments were found in cuttings from the William Hoover 1 well in Jessamine County, about 30 miles north of the A. R. Spears 1 well (sec. 1, fig. 3).

FACIES RELATIONS

A comparison of measured sections of the Rome Formation and Conasauga Group with equivalent rocks in the subsurface shows two key units generally common to all sections. These units are a thick zone of dolomite near the base of the Rome, and the dolomitic part of the Maynardville Formation at the top of the section. Of the two, the Maynardville is the more persistent; hence, it was used as the reference datum for this study (fig. 3). With the sections and wells thus alined, it is readily apparent that Campbell's (1894) and Keith's (1896) concept of the intertonguing relation of the limestone of the Conasauga Group with shale and siltstone of the Conasauga Shale is but a part of a broader facies relationship involving the Rome and Conasauga. In addition, there is the suggestion that the regional sedimentary sequence overlaps the basement rocks from northeastern Tennessee to central Kentucky. Because of this overlap, it is assumed that the entire sedimentary body was deposited in a transgressive stage of the Cambrian seas. Within this transgressive framework, the regional facies pattern was developed by two fundamental processes—one a gradual change by lateral gradation from sandstone to shale, and the other a more abrupt change by intertonguing of clastic and carbonate rocks. Sandstone of the Rome in central Kentucky is by lateral gradation a facies equivalent of the siltstone and shale of approximately the lower half of the Conasauga in southeast Kentucky and southwest Virginia. In turn, the Conasauga Shale intertongues to the southeast with the limestone of the Conasauga Group. These relations show that the Rome probably ranges in age from Early Cambrian in northeast Tennessee to Middle Cambrian in central Kentucky.

REFERENCES

Calvert, W. L., 1962, Sub-Trenton rocks from Lee County, Virginia, to Fayette County, Ohio: Ohio Geol. Survey Rept. Inv. 45.

Campbell, M. R., 1894, Description of the Estillville quadrangle [Kentucky-Virginia-Tennessee]: U.S. Geol. Survey Geol. Atlas, Folio 12.

Freeman, L. B., 1953, Regional subsurface stratigraphy of the Cambrian and Ordovician in Kentucky and vicinity: Kentucky Geol. Survey Bull 12, Ser. IX.

Keith, Arthur, 1896, Description of the Briceville quadrangle [Tennessee]: U.S. Geol. Survey Geol. Atlas, Folio 33.

Miller, A. M., 1921, Nicholasville, Kentucky well [abs.]: Geol. Soc. America Bull., v. 32, p. 35–36.

Miller, R. L., and Fuller, J. O., 1954, Geology and oil resources of the Rose Hill district—the fenster area of the Cumberland overthrust block—Lee County, Virginia: Virginia Geol. Survey Bull. 71, 383 p.

Rodgers, John, 1953, Geologic map of East Tennessee with explanatory text: Tennessee Div. Geology Bull. 58, pt. II.

Rodgers, John, and Kent, D. F., 1948, Stratigraphic section at Lee Valley, Hawkins County, Tennessee: Tennessee Div. Geology Bull. 55.

Thomas, G. R. 1960, Geology of recent deep drilling in eastern Kentucky: Kentucky Geol. Survey, Ser. X, Spec. Pub. 3, p. 10–28.

Woodward, H. P., 1961, Preliminary subsurface study of southeastern Appalachian Interior Plateau: Am. Assoc. Petroleum Geologists Bull., v. 45, p. 1634–1655.

IN THE CUMBERLAND MOUNTAINS OF SOUTHEASTERN KENTUCKY STRATIGRAPHY OF THE LEE FORMATION

By KENNETH J. ENGLUND, Washington, D.C.

Work done in cooperation with the Kentucky Geological Survey

Abstract.—Division of the Lee Formation into seven mapped members in the type area is based on the lithologic contrast between cliff-forming conglomeratic sandstone and intervening beds of nonresistant sandstone, siltstone, shale, coal, and underclay. The Lee Formation has been regarded as basal Pennsylvanian in age and as resting unconformably upon the Pennington Formation of Mississippian age. This study has shown that the contact between the two represents a time transition, the lower beds of the Lee grading laterally into, and intertonguing with, the upper beds of the Pennington.

The name Lee was originally assigned by Campbell (1893, p. 36) to a section of massive conglomeratic sandstone of Carboniferous age exposed along Cumberland Mountain on the northwest margin of Lee County, Va. Lithologically similar sandstone in other outcrop belts of Kentucky, Tennessee, and Virginia has been correlated with the Lee, which is regarded as the basal formation of Pennsylvanian age. The Lee generally contains, or underlies, a sequence of economically important coal beds. In the Cumberland Mountain outcrop belt the formation is also of particular interest because of its transitional relation with underlying rocks of Mississippian age.

Recent geologic mapping along Cumberland Mountain has demonstrated that the Lee Formation contains seven mappable subdivisions that coincide with lithologic changes in a repetitious sequence of massive conglomeratic sandstone and nonresistant intervals of thin-bedded sandstone, siltstone, shale, coal, and underclay. The contrast in the topographic expression of cliff- or ledge-forming members as opposed to intervening members that underlie linear depressions provides a basis for the mapping of subdivisions both in the field and on aerial photographs. Recognition of these subdivisions has aided in the interpretation of structural and stratigraphic relations of the Lee Formation. In addition to a description of the contact relations of the Lee in the type area, five previously established informal members are herein named and defined.

In naming the Lee Formation, Campbell (1893) followed an early practice of designating a type area without specifying a type section, and as a result there are minor variations in references to type Lee. A "best exposed" section that was described by Campbell in Wise County, Va., is used as a type section in Virginia (Eby, 1923, p. 65). Publications dealing with the Lee Formation in Kentucky (Campbell, 1898, p. 2; Wanless, 1939, p. 89; and McFarlan, 1943, p. 99) tend to define the formation with reference to Lee County, Va., where the outcrop belt straddles the Kentucky-Virginia State line. Although a suitable type section was not available in Lee County, Va., at the time Campbell assigned the term Lee, recent highway and park road construction at Cumberland Gap (fig. 1) has uncovered a well-exposed readily accessible section across the outcrop belt of the type area. The members of the Lee Formation are herein described with reference to the section at Cumberland Gap, which is centrally located in the tristate area where the formation is recognized.

LOWER BOUNDARY OF THE LEE FORMATION

Regionally the criteria most commonly used to differentiate the Lee Formation from the underlying Pennington Formation is the predominance of massive quartzose conglomeratic sandstone with intervening coal beds in the Lee and the presence of greenish-gray and reddish-gray shale with thin limestone beds in the Pennington. The contact between the two formations was

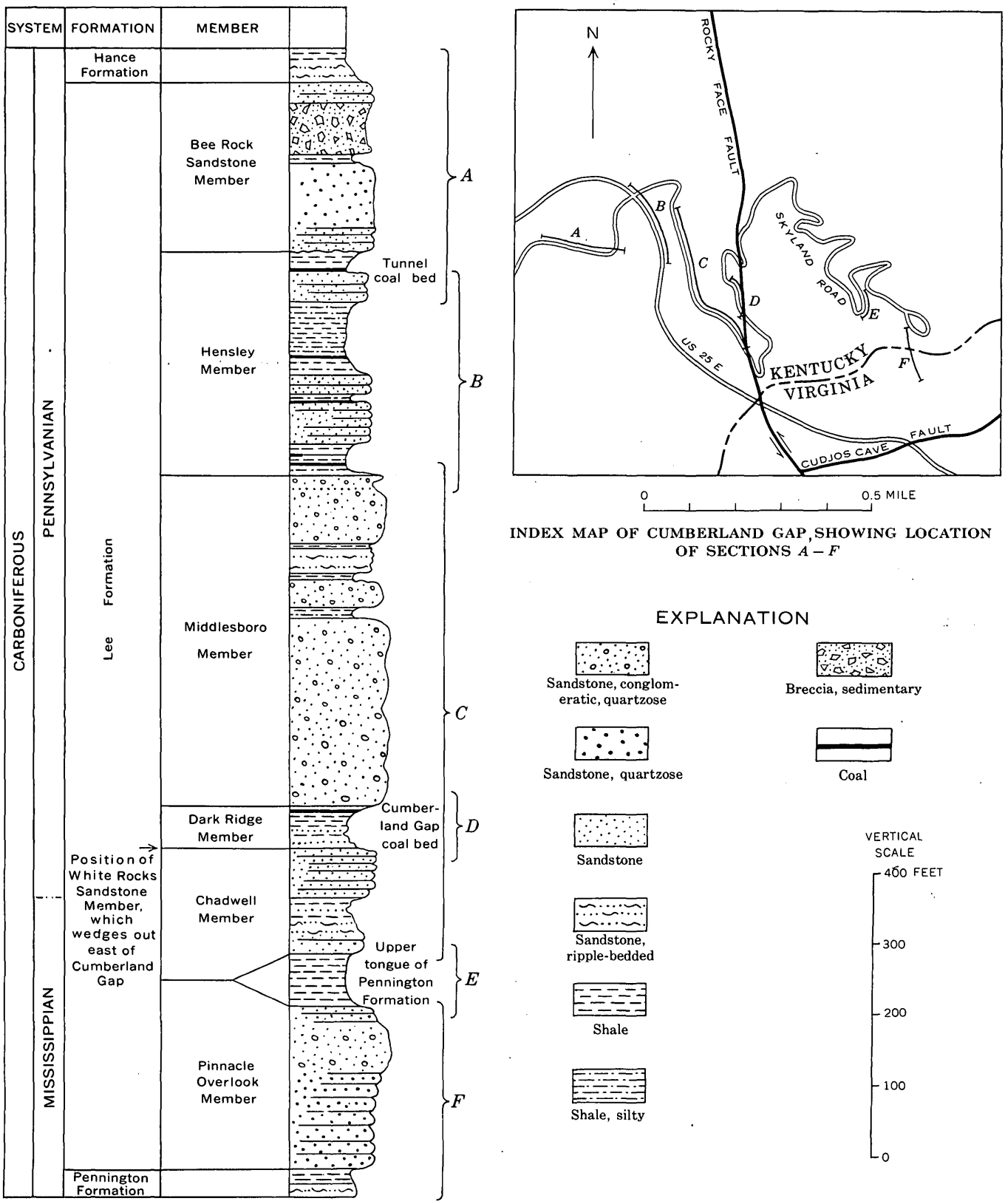

INDEX MAP OF CUMBERLAND GAP, SHOWING LOCATION OF SECTIONS *A* – *F*

FIGURE 1.—Composite section of the Lee Formation at Cumberland Gap in southeastern Kentucky and southwestern Virginia. Partial sections *A*–*F* are located on index map.

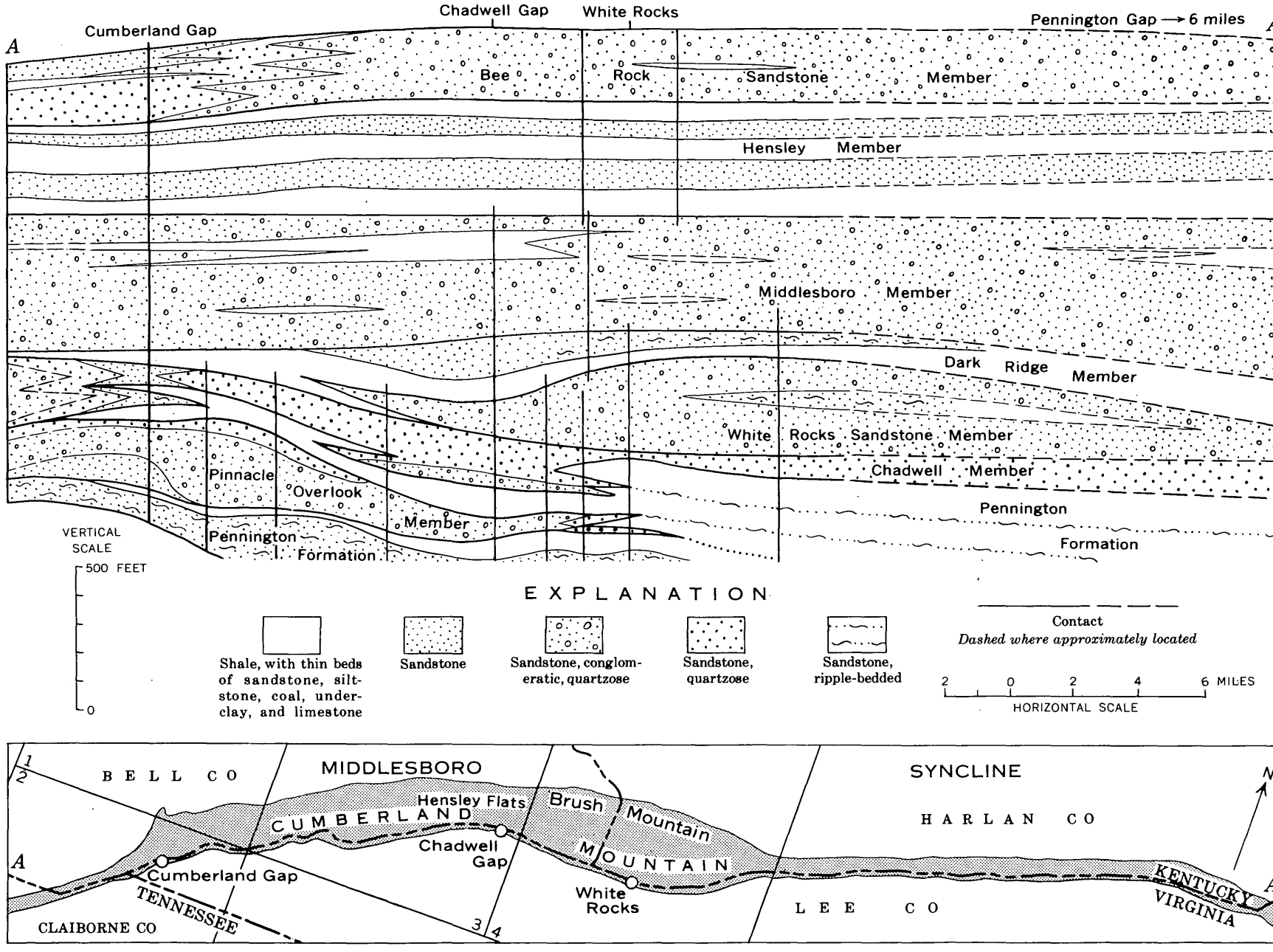

FIGURE 2. Geologic section *A–A′* illustrating the interrelation of members of the Lee Formation and intertonguing with the Pennington Formation. Measured intervals are shown by vertical lines. Shaded area on index map (below) shows the Cumberland Mountain outcrop belt of the Lee Formation. Numbers show quadrangles mapped in detail as follows: 1, Middlesboro North; 2, Middlesboro South; 3, Varilla; 4, Ewing.

generally considered to be an unconformity which supposedly corresponded to the Mississippian-Pennsylvanian systemic boundary. Evidence used in support of this interpretation includes: sharp scour-type contacts at the base of the Lee sandstones; variations in the total thickness of the Pennington; and the marked differences in the lithology and fossil content of the two formations.

Contrary to the interpretation of the contact as an unconformity, geologic mapping along Cumberland Mountain has demonstrated that the lower beds of the Lee grade laterally into, and intertongue with, the upper beds of the Pennington (Englund and Smith, 1960; Englund and Harris, 1961, fig. 5) to record a lateral change from paludal and marginal marine to marine deposition. In this transitional sequence the Lee intertongues with successively younger rocks of the Pennington, causing a gradual stratigraphic rise in the base of the Lee which is largely responsible for the increase in the thickness of the Pennington Formation from 120 feet at Cumberland Gap to about 850 feet at Pennington Gap, near the north end of the outcrop belt. A relatively similar contact relation was reported in the type area of Lower Pennsylvanian rocks in the Anthracite region of Pennsylvania (Wood and others, 1962, p. 40). Because of its time-transitional character, the Lee-Pennington contact in the Cumberland Mountain outcrop belt is not everywhere identical with the Mississippian-Pennsylvanian systemic boundary. As there is paleontological evidence to support a Mississippian age for the Pennington the part of the Lee which intertongues with the Pennington in the Cumberland Mountain outcrop belt is considered to be Mississippian in age.

LEE FORMATION

The Lee Formation crops out in a belt of northwestward-dipping hogbacks and ridges delineated on the southeast by a precipitous southeast-facing escarpment at the crest of Cumberland Mountain and on the northwest by the foot of Cumberland or Brush Mountains (fig. 2). The Lee averages about 1,600 feet in thickness in the Cumberland Mountain area, and it thins northwestward by the tonguing out of lower beds. The characteristic lithology is fine- to coarse-grained subangular to subrounded white to very light gray conglomeratic sandstone that is commonly composed of more than 90 percent quartz. In contrast, nearly all the sandstones of the underlying Pennington Formation and the overlying Hance Formation contain 50 to 75 percent quartz. The conglomerate consists largely of well-rounded white quartz pebbles that generally range from ½ to 1 inch in diameter, although a few are as much as 5 inches in diameter. In addition, the Lee contains lesser amounts of fine- to medium-grained massive sandstone, very fine to fine-grained thin-bedded sandstone, siltstone, shale, and several beds of coal and underclay. Lithologically, the Lee is divided into seven mapped members as follows: the Pinnacle Overlook, Chadwell, White Rocks Sandstone, Dark Ridge, Middlesboro, Hensley, and Bee Rock Sandstone Members.

Pinnacle Overlook Member

The name Pinnacle Overlook is herein applied to the lowermost member of the Lee Formation (fig. 3) that previously was referred to informally as the basal or lower tongue (Englund and Harris, 1961, fig. 4; Englund, Landis, and Smith, 1963). It is named for the Pinnacle, a scenic overlook formed by the member on the northeast side of Cumberland Gap, where the following section is exposed:

Type section of the Pinnacle Overlook Member exposed at the Pinnacle overlook

	Thickness Ft	Thickness In
Pennington Formation (in part):		
Shale, light-olive-gray; exposed on the northwest side of the hill crest	5+	0
Lee Formation:		
Pinnacle Overlook Member (230 ft):		
Sandstone, very light gray, fine-grained, thick-bedded, moderately quartzose, crossbedded	20	0
Sandstone, white to very light gray, medium-grained, massive, quartzose, crossbedded, conglomeratic; forms upper part of cliff	75	0
Sandstone, white to very light gray, fine-grained, crossbedded, well-sorted, thick-bedded; forms lower part of cliff	120	0
Sandstone, very light gray, very fine to fine-grained, partly ripple bedded, moderately quartzose	10	0
Sandstone, very light gray, fine-grained, massive, moderately quartzose	5	0
Pennington Formation (in part):		
Shale, greenish-gray	15	0

The lithology of the Pinnacle Overlook Member is typical of the Lee Formation and consists of thick-bedded well-sorted fine- to medium-grained quartzose sandstone in the lower and upper parts and massive conglomeratic quartzose sandstone in the middle part. Crossbedding is conspicuously developed throughout. The thickness increases from 230 feet at the Pinnacle overlook to 360 feet approximately 2 miles northeast of Cumberland Gap. From this point of maximum thickness, the member thins in a broad arc to form a northwestward-protruding lobe. Where the lobe is thickest the basal contact is sharp and locally undulates as much as 10 feet into the underlying varicolored shale. Toward the periphery of the lobe the contact is conform-

able and the typical Lee lithology grades gradually into partly argillaceous and ripple-bedded very fine to fine-grained sandstone, about 20 feet or less in thickness, in the upper part of the Pennington Formation. Along most of the outcrop belt the top of the member grades abruptly into greenish-gray or reddish-gray shale in an upper tongue of the Pennington Formation which immediately northwest of the outcrop area contains a thin bed of fossiliferous limestone. At the southwest end of the outcrop belt the Pinnacle Overlook Member is in contact with the overlying member of the Lee Formation.

Chadwell Member

The strata previously referred to as sandstone member A (fig. 3) are here designated the Chadwell Member for Chadwell Gap, a notch in Cumberland Mountain, located approximately 10 miles northeast of Cumberland Gap. The following section is exposed approximately 450 feet below the southeast side of the gap:

Type section of the Chadwell Member at Chadwell Gap

	Thickness Ft	Thickness In
Lee Formation:		
White Rocks Sandstone Member (in part):		
Sandstone, white to very light gray, fine- to medium-grained, massive, crossbedded, conglomeratic, quartzose; forms cliff; base sharp	5+	0
Chadwell Member (182 ft 6 in.):		
Sandstone, white to very light gray, fine- to medium-grained, massive, crossbedded, quartzose	24	0
Sandstone, light-gray, fine-grained; bedding is parallel and averages about 2 in. in thickness	4	0
Sandstone, light-gray, fine-grained; bedding is uneven and averages about 6 in. in thickness	15	0
Sandstone, light-gray, fine-grained; bedding is parallel and as much as 6 in. in thickness	24	0
Sandstone, light-gray, fine-grained; bedding ranges from parallel to wavy and from ½ to 3 in. in thickness	2	0
Sandstone, light-gray, fine-grained; beds are as thick as 7 in. and are parallel	8	0
Sandstone, very light gray, fine-grained; massive, quartzose, base sharp	9	6
Sandstone, light-gray, fine-grained; bedding is parallel and ¼ to 1 in. thick	2	0
Sandstone, white to very light gray, fine- to medium-grained, massive, conspicuously crossbedded	57	0
Sandstone, white to very gray, medium- to coarse-grained, massive, crossbedded, quartzose; sparsely conglomeratic with well-rounded quartz pebbles as much as ¾ in. in diameter; base sharp	37	0
Pennington Formation (in part):		
Shale, greenish-gray	5+	0

The member commonly crops out in two resistant ledges of well-sorted quartzose sandstone which are separated by an intervening tongue of greenish-gray Pennington shale northeast of Chadwell Gap. Near White Rocks the lower ledge wedges out and at its extremity grades into argillaceous ripple-bedded sandstone of the Pennington Formation. The two ledges are exposed in the Cumberland Gap section where they total 150 feet in thickness, including an intervening bed of carbonaceous shale with thin coal beds and associated underclay. Conglomerate is generally restricted to a thin basal bed, but it thickens abruptly southwest of Cumberland Gap and makes up most of the member. The basal contact is normally conformable but may be marked by several feet of scour into underlying beds, especially where the basal conglomerate is present.

White Rocks Sandstone Member

The White Rocks Sandstone Member (Englund, Smith, Harris, and Stephens, 1963, p. 13) was named for White Rocks, where its entire thickness of 300 feet is exposed in a precipitous cliff at the crest of Cumberland Mountain. The lithology is typical of the Lee; however, the main distinction of the member is an unusual abundance of large well-rounded vein-quartz pebbles that constitute 75 percent or more of some outcrops. The conglomerate is generally concentrated in the lower part of the member, which has a sharp undulatory contact with underlying beds. Southwestward from the type locality the member thins and wedges out about 2 miles southwest of Hensley Flats.

Dark Ridge Member

A section of thin-bedded sandstone and shale, previously referred to informally as sandstone and shale member B (fig. 3) is included in a unit herein named the Dark Ridge Member. The type locality is near the south end of Dark Ridge, a northward-trending ridge on the north side of Cumberland Gap, where the member occupies a poorly exposed interval between massive sandstones of the underlying and overlying members. There on Skyland Road the member consists of 60 feet of medium-dark-gray shale with a few thin beds of very fine to fine-grained sandstone (fig. 1) and includes at its top the Cumberland Gap coal bed (Ashley and Glenn, 1906, p. 115). The coal commonly ranges from 3 to 4 feet in thickness and is the most persistent coal bed of commercial thickness in this outcrop belt of the Lee. Elsewhere along Cumberland Mountain the Dark Ridge Member is rarely exposed, but its outcrop posi-

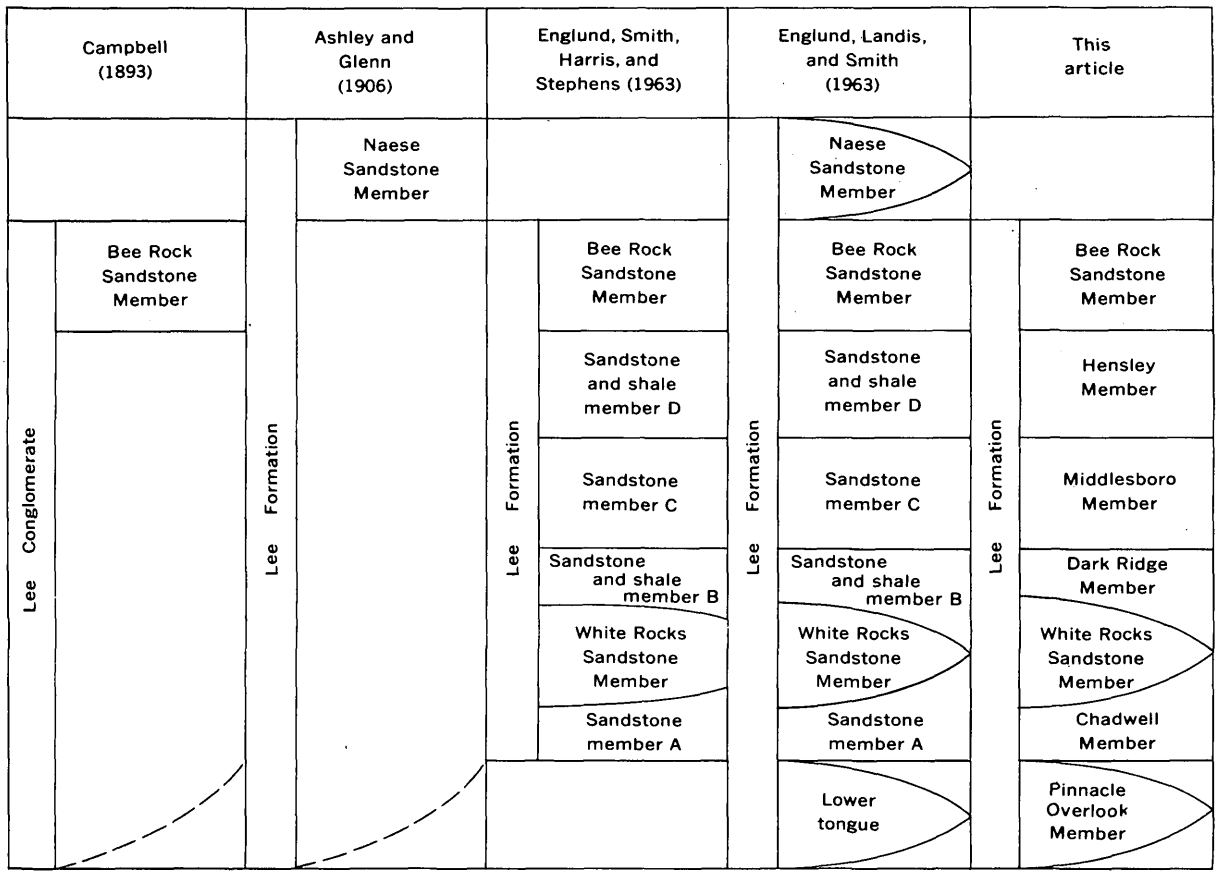

FIGURE 3.—Stratigraphic nomenclature of the Lee Formation in the Cumberland Mountain outcrop belt of southeastern Kentucky.

tion is marked by a linear depression or notch between massive Lee sandstones, or by mines and prospects in the Cumberland Gap coal bed. An argillaceous very fine to fine-grained partly ripple bedded sandstone in the upper part of the member thickens northeastward to about 100 feet in the vicinity of White Rocks, where it overlies 40 feet of medium-dark-gray shale in the lower part of the member. There the basal contact of the Dark Ridge Member is gradational with the underlying White Rocks Sandstone Member, and where the White Rocks wedges out the base is gradational with the Chadwell Member.

Middlesboro Member

A thick sequence of massive conglomeratic sandstone, previously included in sandstone member C (fig. 3), is herein designated the Middlesboro Member. It is named after the city of Middlesboro, which is situated at the northwest approach to Cumberland Gap. The type section is exposed on Skyland Road on the north side of the gap as follows:

Type section of the Middlesboro Member at Cumberland Gap

Lee Formation:	Thickness	
	Ft	In
Hensley Member (in part):		
Shale, medium-gray, silty, poorly bedded; base sharp	6	6
Middlesboro Member (469 ft 10 in.)		
Sandstone, white to very light gray, massive, quartzose, crossbedded, sparsely conglomeratic	12	6
Sandstone, very light gray, very fine grained, ripple-bedded, argillaceous		10
Sandstone, very light gray, fine-grained, quartzose; base sharp	1	6
Shale, medium-light-gray, clayey; base sharp		6
Sandstone, white to very light gray, fine-grained, massive, quartzose, crossbedded; base sharp	16	0
Shale, light-gray, clayey; base sharp		7
Sandstone, very light gray, fine-grained; base sharp		2
Shale, medium-gray, evenly bedded; base sharp		8
Sandstone, light-gray, weathers reddish brown, fine-grained; base sharp		3
Shale, medium-light-gray		6

Type section of the Middlesboro Member at Cumberland Gap—Continued

Lee Formation—Continued	Thickness	
Middlesboro Member—Continued	Ft	In
Sandstone, very light gray, fine- to coarse-grained, massive, quartzose; very conglomeratic in basal 20 ft, sparsely conglomeratic in upper part; base sharp	70	0
Shale, medium-dark-gray, evenly bedded; base sharp	3	0
Sandstone, medium-light-gray, very fine grained, lenticular; beds range from 1 to 3 in. in thickness	1	10
Shale, medium-gray, evenly bedded, clayey; base sharp	5	5
Sandstone, very light gray, very fine to fine-grained, moderately quartzose; in beds up to 1 ft 4 in. in thickness with a few ripple-bedded surfaces; base sharp	10	2
Siltstone, weathers reddish brown, evenly bedded; very fine grained sandstone occurs in some laminae; base sharp	1	1
Sandstone, very light gray, fine-grained, quartzose; in beds as much as 1 ft in thickness; base sharp	13	2
Shale, medium-dark-gray, evenly bedded; base sharp	2	2
Sandstone, very light gray, fine-grained, quartzose; bedding ranges from 6 in. to 1 ft in thickness with some ripple-bedded surfaces	6	6
Sandstone, light-gray, very fine grained, micaceous; ripple-bedded; some argillaceous laminae; base sharp	9	0
Sandstone, white to very light gray, medium-grained, subrounded, massive, quartzose, crossbedded, conglomeratic; quartz pebbles are well rounded and average ½ in. in diameter; base sharp	35	0
Shale, medium-dark-gray, evenly bedded; abundant fossil plant fragments	4	0
Sandstone, white to very light gray, medium-grained, quartzose, massive; base sharp	5	0
Shale, medium-gray, highly weathered	5	0
Sandstone, white to very light gray, medium-grained, quartzose, subrounded, massive, conglomeratic, crossbedded; base sharp	265	0
Dark Ridge Member (in part):		
Coal bloom (Cumberland Gap coal bed)	2+	0

The Middlesboro Member ranges from 400 to 500 feet in thickness and because of this great thickness of conglomeratic sandstone, it is the principal ridge- and cliff-forming unit along Cumberland Mountain and along Pine Mountain on the northwest limb of the Middlesboro syncline. The member also caps Rocky Face Mountain, which is formed by a large upwarp in the Middlesboro syncline about 5 miles north of Cumberland Gap. The member consists predominantly of fine- to coarse-grained white to very light gray quartzose sandstone with a abundance of well-rounded quartz pebbles that commonly range from ½ to 1 inch in diameter. Conglomeratic sandstone generally occurs in four beds that are locally separated by thin beds of shale, coal, underclay, and thin-bedded very fine to fine-grained sandstone. Where these intervening nonresistant beds are absent the member also tends to crop out in a series of four ledges or hogbacks. The basal contact is sharp and locally undulates several feet into the underlying beds.

Hensley Member

The nonresistant beds of the Lee Formation that lie between the top of the Middlesboro Member and the base of the Bee Rock Sandstone Member have been referred to informally as sandstone and shale member D (fig. 3). These beds are here designated the Hensley Member from Hensley Flats, an upland area between the crests of Brush and Cumberland Mountains, which is underlain by the member. The type section is exposed along Skyland Road and U.S. Highway 25E on the northwest side of Cumberland Gap as follows:

Type section of the Hensley Member at Cumberland Gap

Lee Formation:	Thickness	
	Ft	In
Bee Rock Sandstone Member (in part):		
Sandstone, very light gray, fine- to medium-grained, thick-bedded to massive; base sharp	12	0
Hensley Member (319 ft 6 in.):		
Shale, very dark gray to black, evenly bedded; few ironstone nodules	21	0
Coal (Tunnel coal bed)	2	0
Underclay, medium-light-gray; abundant fossil rootlets; base gradational	4	6
Sandstone, light-gray, very fine grained, poorly bedded, silty	2	0
Coal		2
Underclay, medium-light-gray; rootlets; base gradational	1	6
Sandstone, light-gray, very fine grained, poorly bedded, silty	6	6
Sandstone, very light gray, fine- to medium-grained, moderately quartzose, thick-bedded to massive; base sharp	33	0
Shale, medium-gray, silty, evenly bedded	30	0
Shale, dark-gray, evenly bedded; ironstone nodules and beds as much as 1 in. thick	25	0
Ironstone, sideritic, nodular		4
Shale, medium-gray, evenly bedded	4	0
Shale, medium-gray, very silty	15	0
Shale, medium-gray, evenly bedded	4	6
Coal; few shale laminae		10
Underclay, medium-light-gray; rootlets; base gradational	2	0
Shale, medium-gray, silty, poorly bedded	8	0
Shale, medium-gray, evenly bedded; few very fine grained sandstone lenses as much as 3 in. thick; base sharp	5	0
Sandstone, light-gray, very fine to fine-grained, unevenly bedded	1	8
Shale, medium-gray, poorly exposed; base sharp	4	0

Type section of the Hensley Member at Cumberland Gap—Con.

	Thickness Ft	In
Lee Formation—Continued		
Hensley Member—Continued		
Sandstone, very light gray, very fine to fine-grained, partly crossbedded; bedding ranges from 2 in. to 3 ft in thickness; base sharp	28	0
Sandstone, very light gray, very fine grained; bedding ranges from 1 to 6 in. in thickness; interbedded with medium-gray silty shale; base sharp	12	10
Sandstone, very light gray, very fine grained, moderately quartzose; bedding is parallel and ranges mostly from 6 in. to 1 ft in thickness; partly crossbedded; base sharp	60	0
Shale, medium-gray, silty; fine mica flakes on bedding planes; evenly bedded	8	6
Shale, dark-gray, evenly bedded	7	0
Coal	1	3
Shale, black, abundant coal laminae		8
Underclay, medium-gray, rootlets	1	10
Shale, medium-dark-gray, poorly bedded; abundant fossil plant fragments	6	0
Coal, few shale laminae		5
Underclay, medium-gray, silty, rootlets; base gradational	1	6
Shale, medium-gray, silty, poorly bedded	7	0
Sandstone, light-gray, very fine grained, silty; in beds as much as 18 in. thick; base sharp	7	0
Shale, medium-gray, silty, poorly bedded; base sharp	6	6
Middlesboro Member (in part):		
Sandstone, white to very light gray, massive, quartzose, crossbedded, sparsely conglomeratic	12	6

The Hensley Member ranges from about 320 to 400 feet in thickness and consists mostly of shale in the lower, middle, and upper parts with two very fine to medium-grained thin- to thick-bedded sandstones in between. In contrast to the excellent exposures of adjacent beds of conglomeratic sandstone, the outcrop belt of the Hensley Member is commonly a concealed interval with scattered outcrops of sandstone. The sandstones are persistent and resistant enough to form low ridges in the outcrop belt. In addition to several thin coal beds, the member contains near its top the Tunnel coal (Ashley and Glenn, 1906, p. 115), which ranges from 24 to about 50 inches in thickness and has been mined at several localities. The basal contact is conformable and is placed where the conglomeratic quartzose sandstone of the underlying Middlesboro Member is succeeded by shale and thin-bedded nonconglomeratic sandstone.

Bee Rock Sandstone Member

The Bee Rock Sandstone Member (Campbell, 1893, p. 17) is the uppermost conglomeratic sandstone in the Lee Formation along Cumberland Mountain. The name is well established in the Pennington Gap area of the outcrop belt (Giles, 1925, p. 21; Wanless, 1946, p. 136), and it has been extended southwestward to the Cumberland Gap area by tracing the member on aerial photographs and by field mapping. The best development and exposure of the Bee Rock Sandstone Member, as mapped in the Cumberland Gap area, is at the northeast end of Brush Mountain where the following reference section crops out in a cliff overlooking Martins Fork:

Reference section of the Bee Rock Sandstone Member at the northeast end of Brush Mountain

	Thickness Ft	In
Hance Formation (in part):		
Sandstone, light-gray, very fine to fine-grained, argillaceous, partly ripple bedded; base gradational	5+	0
Lee Formation:		
Bee Rock Sandstone Member (258 ft 6 in.):		
Sandstone, white to very light gray, fine- to medium-grained, quartzose, sparsely conglomeratic; base sharp	125	0
Shale, medium-gray, evenly bedded; base gradational	3	6
Sandstone, white to very light gray, fine- to medium-grained, quartzose, conglomeratic, crossbedded; base sharp	130	0
Hensley Member (in part):		
Shale, dark-gray, evenly bedded	6+	0

The Bee Rock Sandstone Member ranges generally from 200 to 250 feet in thickness and consists of two massive sparsely conglomeratic quartzose sandstone beds of about equal thickness, separated by a thin shale bed. Quartz pebbles decrease in size and number southwestward along the outcrop belt and are absent southwest of Cumberland Gap. In the section at Cumberland Gap (fig. 1) most of the sandstone in the upper part of the member is very fine to fine-grained and occurs as sedimentary breccia in several beds. The base of the member is sharp and undulatory, and the top is gradational with overlying beds.

UPPER BOUNDARY OF THE LEE FORMATION

In the Cumberland Mountain outcrop belt the upper boundary of the Lee Formation was placed by Campbell (1893, p. 36) at the top of the Bee Rock Sandstone Member. The overlying rocks consist of relatively nonresistant beds of shale, siltstone, sandstone, coal, and underclay that make up the Hance Formation of the Breathitt Group. In contrast to the sandstones of the Lee Formation, those of the Hance Formation are nonconglomeratic and are typically more micaceous and less quartzose. In the nearby Pine Mountain outcrop belt the top of the Lee Formation was placed by Ashley and Glenn (1906, p. 35) at the top of the Naese

Sandstone Member, which is lithologically similar to the Lee sandstones but stratigraphically above the Bee Rock Sandstone Member.

Recent geologic mapping and stratigraphic studies have shown that the Naese Sandstone Member is a southeastward protruding lobe of partly conglomeratic and quartzose sandstone, as much as 250 feet in thickness, that overlies a regional disconformity and tongues out southeastward in the lower part of the Hance Formation. The southeastern edge of the Naese Sandstone Member grades gradually into sandstone that is lithologically typical of sandstones in the Hance Formation. Below the disconformity the sandstones in the Lee Formation tongue out to the northwest, whereas the Naese and other sandstones above the disconformity tongue out to the east or southeast. This reversal in the depositional trend is interpreted as a change from an eastern or southeastern source to a local northwestern source which may have originated from the uplift and reworking along the erosional surface of previously deposited Lee sediments. Such a reworking hypothesis would account for the deposition of lithologically similar sediments above the disconformity. In view of its diverse depositional trend and higher stratigraphic position, the Naese Sandstone Member could be excluded from the Lee Formation. Its lithologic similarity to the Lee Formation rather than to the Hance Formation, however, favors the previously established practice of recognizing the Naese Sandstone Member as a tongue of the Lee Formation in the Pine Mountain outcrop belt. Only the extremity of the Naese Sandstone Member is present locally in the Cumberland Mountain outcrop belt, where it is a thick-bedded to massive moderately quartzose nonconglomeratic sandstone. Except for this local occurrence of the Naese, which is mapped as a tongue of the Lee that wedges out in the Hance Formation, the top of the Lee is placed as originally designated by Campbell at the top of the Bee Rock Sandstone Member in the Cumberland Mountain outcrop belt.

REFERENCES

Ashley, G. H., and Glenn, L. C., 1906, Geology and mineral resources of part of the Cumberland Gap coal field, Kentucky: U.S. Geol. Survey Prof. Paper 49, 239 p.

Campbell, M. R., 1893, Geology of the Big Stone Gap coal field of Virginia and Kentucky: U.S. Geol. Survey Bull. 111, 106 p.

——— 1898, Description of the London quadrangle: U.S. Geol. Survey Geol. Atlas, Folio 47, 3 p.

Eby, J. B., 1923, The geology and mineral resources of Wise County and the coal-bearing portion of Scott County, Virginia: Virginia Geol. Survey Bull. 24, 617 p.

Englund, K. J., and Smith, H. L., 1960, Intertonguing and lateral gradation between the Pennington and Lee Formations in the tri-state area of Kentucky, Tennessee, and Virginia [abs.]: Geol. Soc. America Bull., v. 71, no. 12, pt. 2, p. 2015.

Englund, K. J., and Harris, L. D., 1961, Itinerary—geologic features of the Cumberland Gap area, Kentucky, Tennessee, and Virginia: Geol. Soc. Kentucky Field Trip, April 1961, Guidebook, 30 p.

Englund, K. J., Landis, E. R., and Smith, H. L., 1963, Geology of the Varilla quadrangle, Kentucky and Virginia: U.S. Geol. Survey Geol. Quad. Map GQ–190.

Englund, K. J., Smith, H. L., Harris, L. D., and Stephens J. G., 1963, Geology of the Ewing quadrangle, Kentucky and Virginia: U.S. Geol. Survey Bull. 1142–B, 23 p.

Giles, A. W., 1925, The geology and coal resources of the coal-bearing portion of Lee County, Va.: Virginia Geol. Survey Bull. 26, 177 p.

McFarlan, A. C., 1943, Geology of Kentucky: Kentucky Univ., 531 p.

Wanless, H. R., 1939, Pennsylvanian correlations in the Eastern Interior and Appalachian coal fields: Geol. Soc. America Spec. Paper 17, 130 p.

——— 1946, Pennsylvania geology of a part of the southern Appalachian coal field: Geol. Soc. America Mem. 13, 162 p.

Wood, G. H., Jr., Trexler, J. P., and Arndt, H. H., 1962, Pennsylvanian rocks of the southern part of the Anthracite region of eastern Pennsylvania: Art. 74 *in* U.S. Geol. Survey Prof. Paper 450–C, p. C39–C42.

THE LITTLE STONE GAP MEMBER OF THE HINTON FORMATION (MISSISSIPPIAN) IN SOUTHWEST VIRGINIA

By RALPH L. MILLER, Washington, D.C.

Abstract.—A limestone member of the Hinton Formation has been mapped at the surface and recognized in the subsurface in southwest Virginia. Reger applied the name Avis to this unit, but the name was preoccupied. The member is here rename the Little Stone Gap Member.

Various writers have described a limestone or calcareous shale 35 to 55 feet thick in the Hinton Formation of the Pennington Group of southwest Virginia and in the Hinton Group, as used by the West Virginia Geological Survey, in southern West Virginia. These beds of late Chester (Mississippian) age, are persistent at the surface and in the subsurface. They form a highly fossiliferous unit in a relatively unfossiliferous sequence. Until recently no attempt has been made to map this unit as a separate entity, but with the publication of topographic maps on the scale of 1:24,000 for parts of this region, it is now feasible to map these calcareous strata separately on detailed geologic maps. The writer, in mapping this calcareous shale unit in Scott, Wise, and Lee Counties, Va. (fig. 1), has been faced with the necessity of designating it only as an informally named unit or else applying a new name. Because these calcareous strata comprise such a distinctive and areally extensive unit, a formal name seems more appropriate. Hence, the name Little Stone Gap Member is here proposed. It is the uppermost of three mapped members of the Hinton Formation in this part of Virginia, of which the basal member is named the Stony Gap Sandstone Member and the middle member is called the middle red member (Wilpolt and Marden, 1959).

Campbell and Mendenhall (1896, p. 487–489) first applied the name Hinton Formation to a series of predominantly clastic sedimentary rocks about 1,100 feet thick along the New River Gorge near Hinton, W. Va. (fig. 1). They noted the presence of several fossiliferous limestone zones within the Hinton. Although

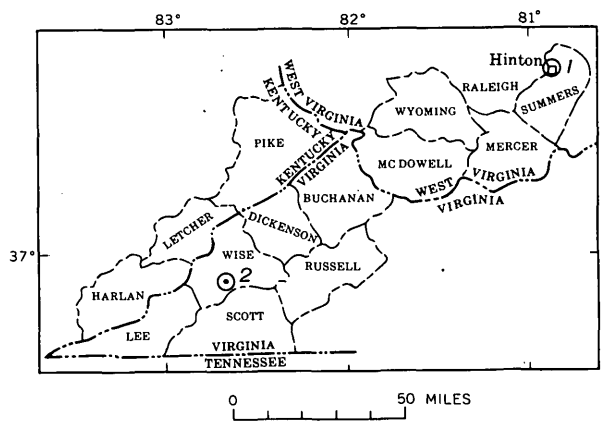

FIGURE 1.—Map showing the type localities of the Hinton Formation (*1*) and the Little Stone Gap Member of the Hinton Formation (*2*).

they did not map or measure detailed sections of the sequence, apparently the most conspicuous of the limestones that they mention is the one with which this article is concerned.

Two names previously have been applied to this limestone, both in southern West Virginia. Neither name is, however, in good standing. Krebs (1916) in a report on Raleigh County and parts of Mercer and Summers Counties, W. Va., seems to have been the first to single out and name this limestone. Without describing it, he called it the Hinton Limestone in measured sections in Raleigh County (1916, p. 76) and Summers County (1916, p. 88). Reger (1926) recognized the same unit in his report on Mercer, Monroe, and Summers Counties. Because the name Hinton Formation was originally proposed by Campbell and Mendenhall (1896) for a much thicker heterogeneous sequence of sedimentary rocks, Krebs' restriction of the name to one relatively thin limestone within the sequence was not followed by Reger. Instead, Reger

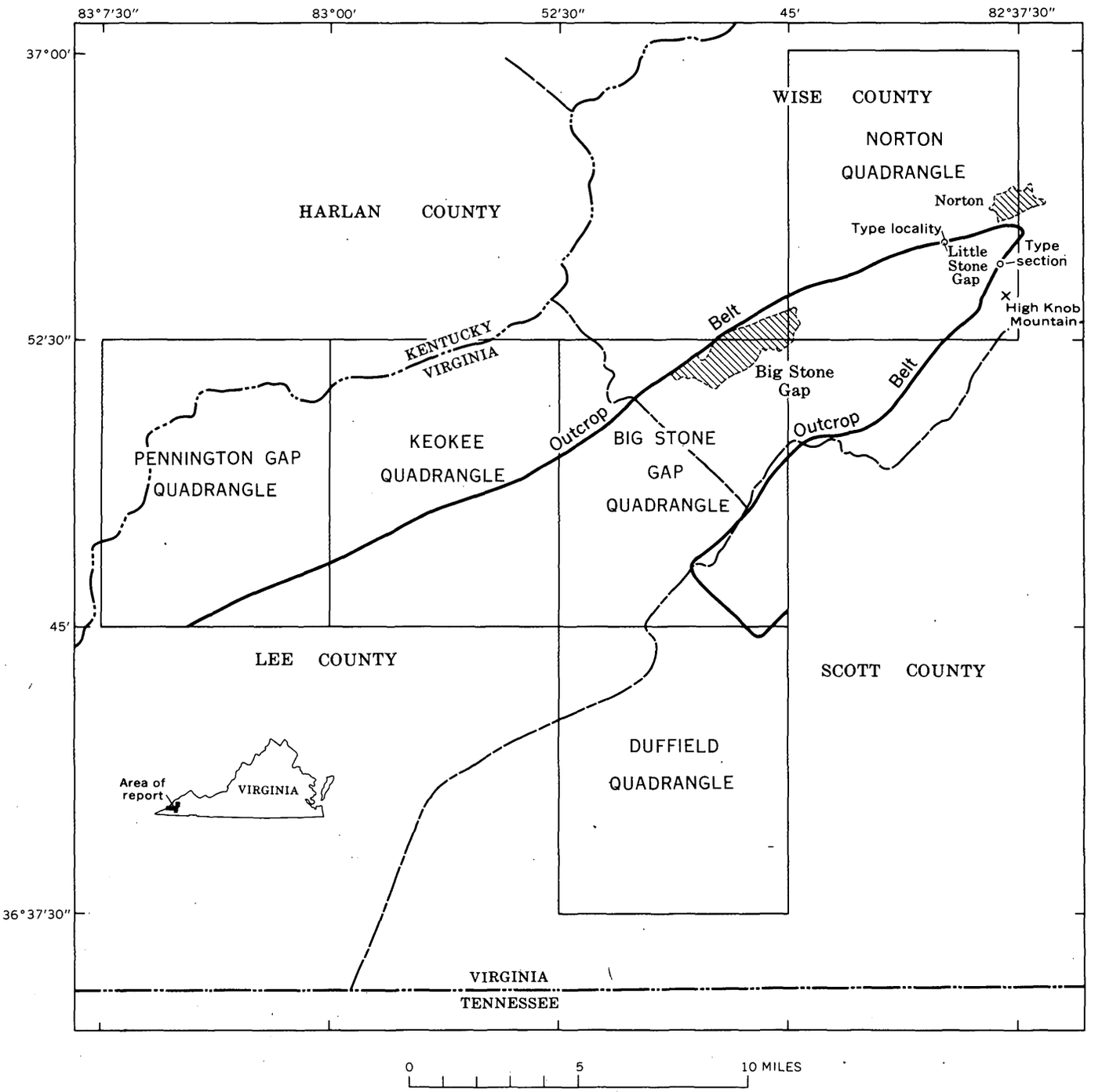

FIGURE 2.—Map showing the outcrop belt of the Little Stone Gap Member of the Hinton Formation and the type locality.

raised the Hinton Formation to group status, and proposed 44 named units within the group, of which 5 were named coals. Presumably the other 39 units were formations. On the county geologic maps of his report, scale 1:62,500, however, Reger lumped all these 44 named units as one mapped unit, the Hinton Group. The limestone, with which this article is concerned, was called by Reger the Avis Limestone (1926, p. 347–351). However, the name Avis was preoccupied. Furthermore, Reger used the name Lower Avis Shale for a shale underlying his Avis Limestone, Upper Avis Shale for a shale overlying his Avis Limestone, and Avis Sandstone for a unit overlying his Upper Avis Shale. Because the name Avis is preoccupied, and because of the proliferation of uses of the name to cover four different lithologic units in southern West Virginia, the strati-

graphic name Avis is best dropped from West Virginia and Virginia nomenclature.

Recent workers in Virginia, who have recognized and mapped or measured sections of the unit that Reger called the Avis Limestone in West Virginia have called it the limestone member (Avis of Reger) of the Hinton Formation (Wilpolt and Marden, 1949, 1959) or the claystone member of the Hinton Formation (Harris and Miller, 1958).

No complete surface section of this calcareous member of the Hinton Formation is known to the writer in southwest Virginia. The upper part of the member is, however, well exposed at Little Stone Gap, near Norton in Wise County (fig. 2). The member is here named Little Stone Gap Member of the Hinton Formation from this locality. The exposures are along the county road at Little Stone Gap through Stone Mountain. In Little Stone Gap the steeply dipping resistant ledges at the highest point of the road consist of the basal or Stony Gap Sandstone Member of the Hinton, the next 279 feet of beds of sandstone and shale cropping out intermittently northeastward down the road is the informally named middle red member of the Hinton (Wilpolt and Marden, 1959, p. 639). At the top of the middle red member is a covered interval of 47.5 feet within which is concealed the contact with the overlying Little Stone Gap Member. Only the upper 22 feet, or approximately the upper half, of the Little Stone Gap Member crops out. The exposed beds consist of deeply weathered highly fossiliferous mudstone from which the carbonate content has been leached. At the sharp curve in the highway 800 feet northeast of the Gap, the Princeton Sandstone forms resistant ledges that conformably overlie the Little Stone Gap Member.

The writer in association with others has recently mapped this unit in the Duffield, Big Stone Gap, and Keokee quadrangles of Scott, Wise, and Lee Counties, Va. (fig. 2). It consists of about 45 feet of calcareous mudstone and shale with thin interbeds of impure limestone, some of which are nodular. Numerous beds are highly fossiliferous, with bryozoa and brachiopods most abundant. The member seems to be everywhere present in the Big Stone Gap district, but it is deeply weathered, and good outcrops are scarce. It is easily recognized in well cuttings because of its high carbonate and fossil content. Wilpolt and Marden (1959) have traced this member by correlating between detailed measured surface sections and deep wells from the vicinity of Big Stone Gap northeastward into southern West Virginia, where they believe it to be the same unit as Reger's Avis Limestone.

Although the Little Stone Gap Member is named for this locality, a more complete section nearby is designated as the type section. This is along the paved county road from Norton southward to High Knob at the hairpin turns shown near the 3,000-foot contour on the topographic map. The section at this locality, designated the type section of the Little Stone Gap Member, is given below:

Type section of the Little Stone Gap Member of the Hinton Formation, along the county road from Norton to High Knob, Wise County, Va. Section begins at 2,950 feet elevation at first sharp curve of hairpin-turn complex, proceeds up small quarry face and through woods to top of hairpin-turn complex, and ends with exposures in small ditch and low roadcut along southeast stretch of road at top of turn complex.

	Thickness (feet)
Princeton Sandstone (+5 feet):	
9. Sandstone, medium-grained, yellow-weathering; almost in place	+5
Hinton Formation:	
Little Stone Gap Member (±44.5 feet):	
8. Shale, calcareous; in ditch at southwest side of road	1.2
7. Covered	5.6
6. Mudstone, calcareous, poorly bedded, medium-light-gray; interbeds of nodular fossiliferous impure limestone 1 to 2 inches thick	22.5
5. Mudstone, calcareous, poorly bedded, medium-light-gray; weathers light gray and also grayish orange	7.6
4. Mudstone, calcareous, weathered (found by digging)	2.8
3. Limestone and shale; limestone, argillaceous, light-olive-gray; weathers yellowish gray, in beds up to 4 inches thick; shale, calcareous, irregularly bedded. Unit very fossiliferous	4.4
2. Covered. Contact estimated to be about 4 feet below top of this covered interval	12.8
Middle red member (+20 feet):	
1. Mudstone, grayish-red; weathers to earthy chips in roadcut. A sandstone bed in the roadbank at the curve of the road near top of this unit is either out of place or lenses out in 10 feet	+20

In Wise and Scott Counties, Va., the Little Stone Gap Member of the Hinton conformably overlies the middle red member, which consists of red and gray shale and siltstone and fine- to coarse-grained sandstone. According to Wilpolt and Marden (1959) both the Stony Gap and middle red members continue northeastward into southern West Virginia, the type region of the Hinton Formation. The Little Stone Gap Member in Wise and Scott Counties, Va., is disconformably overlain by the Princeton Sandstone, a resistant cliff-forming unit about 50 feet thick. Northeastward, however, rocks similar to those in the underlying middle red member in places overlie the Little Stone Gap Member and underlie the Princeton. Wilpolt and Marden (1959, p. 601) have designated these beds as the upper

red member of the Hinton Formation. Thus the Little Stone Gap Member does not form the topmost unit of the Hinton Formation at every place where this formation is present in southwest Virginia.

REFERENCES

Campbell, M. R., and Mendenhall, W. C., 1896, Geologic section along the New and Kanawha Rivers in West Virginia: U.S. Geol. Survey 17th Ann. Rept., pt. 2, p. 487–489.

Harris, L. D., and Miller, R. L., 1958, Geology of the Duffield quadrangle, Virginia: U.S. Geol. Survey Geol. Quad. Map GQ–111.

Krebs, C. E., 1916, Raleigh County and the western portions of Mercer and Summers Counties, West Virginia: West Virginia Geol. Survey County Rept., p. 76, 88.

Reger, D. B., 1926, Mercer, Monroe, and Summers Counties, West Virginia: West Virginia Geol. Survey County Rept., p. 330–378.

Wilpolt, R. H., and Marden, D. W., 1949, Upper Mississippian rocks of southwestern Virginia, southern West Virginia, and eastern Kentucky: U.S. Geol. Survey Oil and Gas Inv. Prelim. Chart 38, 3 sheets.

——— 1959, Geology and oil and gas possibilities of upper Mississippian rocks of southwest Virginia, southern West Virginia and eastern Kentucky; U.S. Geol. Survey Bull. 1072–K, p. 587–655.

THE CHATTANOOGA SHALE (DEVONIAN AND MISSISSIPPIAN) IN THE VICINITY OF BIG STONE GAP, VIRGINIA

By JOHN B. ROEN, RALPH L. MILLER, and JOHN W. HUDDLE, Washington, D.C.

Abstract.—Three lithologic subdivisions of the Mississippian-Devonian black-shale sequence have been mapped in parts of southwest Virginia by previous workers. These subdivisions can be recognized in only part of the Big Stone Gap area. The name Chattanooga Shale is reestablished for the sequence, and the three lithologic subdivisions are designated as members. The uppermost subdivision is the Big Stone Gap Member.

Recent mapping of an area in the vicinity of Big Stone Gap in southwest Virginia has involved the writers in "the black-shale problem." This problem concerns the nomenclature, correlation, and age of the organic-rich fine-grained clastic sediments that were deposited over much of the eastern and central United States in Late Devonian time, and which in places continued to be deposited into early Mississippian time. From New York to Alabama, the problems presented by the "black shales" have been among the most difficult and the most popular in Appalachian stratigraphy. Hass (1956), and Conant and Swanson (1961) have recently reviewed the abundant literature on the black shales as it pertains to central Tennessee and adjacent areas. For a broad preview of the problems, the reader is referred to their publications.

In the Big Stone Gap area of southwest Virginia (fig. 1), the black shales are nearly 1,000 feet thick, or nearly 30 times as thick as in central Tennessee. A threefold subdivision of this sequence has been recognized by some previous workers in southwest Virginia, and Roen and Miller have been able to map these three units separately in part but not all of the Big Stone Gap area. The nomenclature and age of the black shale as a whole in the Big Stone Gap area, and of its mapped units where is has been subdivided, form the subject matter of this article.

Campbell (1893, p. 38) first applied the name Chattanooga black shale, as used in Tennessee and Georgia to the black-shale sequence at Big Stone Gap in southwest Virginia. He (Campbell, 1894) recognized three lithologic units within the sequence, which were not, however, mapped separately by him. These units were: (1) a lower black carbonaceous shale, (2) a middle ash-colored sandy or micaceous shale, and (3) an upper black carbonaceous shale (see accompanying table). In the Big Stone Gap area Stose (1923, p. 43, 45, 46) recognized and mapped separately the three lithologic divisions of Campbell. He abandoned Campbell's usage of the name Chattanooga, and treated each of the three mapped units as a separate formation. Because of faunal affinities, Stose assigned the New York names Genesee and Portage to Campbell's lower and middle lithologic divisions, respectively. For Campbell's upper unit Stose proposed the name Big Stone Gap Shale (see table). Ulrich (Stose, 1923, p. 47–53), who measured a section and collected fossils in the Big Stone Gap area, correlated the Big Stone Gap Shale with the Huron-Cleveland-Sunbury sequence of Ohio, which he believed to be of Mississippian age. Stose (1924, p. 315) regarded the Big Stone Gap Shale as equivalent to the Chattanooga Shale in Tennessee, but was uncertain about the age, as some paleontologists (Stose, 1923, p. 47, 48) considered it to be of Devonian age. Stose was unable to resolve these opposing viewpoints, and hence assigned a Devonian and Mississippian age to his Big Stone Gap Shale. It is interesting to note that recent intensive conodont studies by Hass (1956, and written communications, 1953, 1954) and additional conodont studies by Huddle indicate that the Devonian-Mississippian boundary lies within the Big Stone Gap Shale of Stose.

U.S. GEOL. SURVEY PROF. PAPER 501-B, PAGES B43-B48

725-328 O—64——4

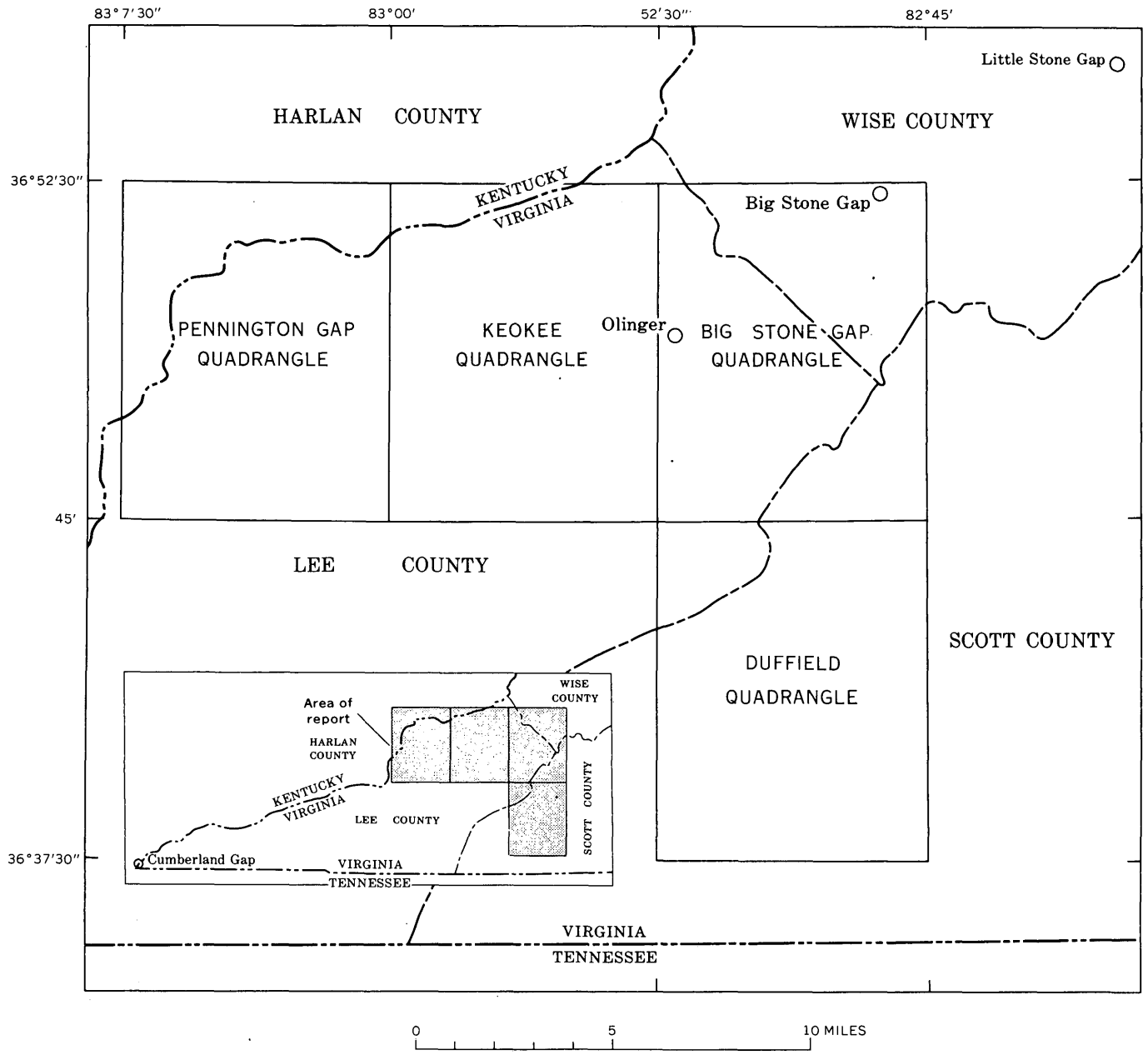

FIGURE 1.—Map of part of southwest Virginia, showing the location of localities and topographic quadrangles mentioned in text.

Swartz (1926a, b; 1927; 1929a, b) made stratigraphic studies consisting principally of measurement of detailed sections at favorable places from the type locality of the Chattanooga in southeast Tennessee northeastward to southwest Virginia. In the Big Stone Gap area, he restricted the name Chattanooga Shale, which Campbell had used for the whole black-shale sequence, to the uppermost part, which Stose had named the Big Stone Gap Shale. He divided his restricted Chattanooga into three members. Rather than abandon completely the name Big Stone Gap, he applied it to his new upper member of his redefined Chattanooga. He named the middle member the Olinger Member from a town southwest of Big Stone Gap, and the lower member the Cumberland Gap Member from exposures near this gap at the tristate junction of Virginia, Kentucky, and Tennessee (fig. 1 and table). We have found Swartz' subdivisions of the Big Stone Gap Shale, based as they were on detailed section measuring and paleontologic studies at the most favorable exposures, impractical for field mapping in the Big Stone Gap area. This may be partly

Comparison of names used for geologic units in the Big Stone Gap area, Virginia

Campbell (1894)			Stose (1923)		Swartz (1929a)			Butts (1940)		Harris and Miller (1958)		This article		
Devonian	Chattanooga black shale	Black carbonaceous shale unit	Devonian and Mississippian	Big Stone Gap shale	Mississippian	Chattanooga shale	Big Stone Gap member	Devonian	Brallier shale	Devonian and Mississippian	Big Stone Gap Siltstone	Mississippian	Chattanooga Shale	Big Stone Gap Member
							Olinger member					Devonian or Mississippian		
		Ash-colored sandy or micaceous unit	Devonian	Portage	Devonian	Chemung and Portage formations	Cumberland Gap member			Devonian	Siltstone	Devonian		Middle gray siltstone member
		Black carbonaceous shale unit		Genesee					Genesee(?)-Millboro		Shale			Lower black-shale member

because of few and poor outcrops in the black shale belts in the structurally complex region, but it is also due in part to difficulty in recognizing Swartz' divisions by lithologic criteria alone, a difficulty which Swartz himself also met in his studies.

In a report on an area southwest of Big Stone Gap, Bates (1939) followed Swartz' usage of the name Chattanooga. To the lower and middle parts of the black-shale sequence, he applied Stose's names Genesee and Portage. A year later, Butts (1940) extended the name Brallier Shale from its type region in south-central Pennsylvania to southwest Virginia, applying it to the beds that Stose referred to as Portage and Big Stone Gap Shales. At Big Stone Gap, Butts (1940, p. 312, pl. 45) designated the beds underlying his Brallier Shale as Genesee(?). He also suggested that these beds may be equivalent to his Millboro Shale (Butts, 1940, p. 308–312) in Bath County, Va., the fossils of which he believed to range from as old as Marcellus age to as young as Naples age. Butts' introduction of the name Brallier into the Big Stone Gap region and his reference to Millboro seem to us only to confuse an already complex picture, and his usage does not conform to subdivisions of the black shale that we have been able to map.

Harris (Harris and Miller, 1958) mapped a threefold division of the black-shale sequence in the Duffield quadrangle, Virginia (fig. 1). These were the same three major lithologic units originally recognized by Campbell and subsequently termed Genesee, Portage, and Big Stone Gap Shales by Stose (see table). Hass (Harris and Miller, 1958), who studied the conodont faunas from this area, has indicated that Stose's lower unit (Genesee) is of Genesee (of early New York usage) and younger age (lower and middle Late Devonian), and that Stose's middle unit (Portage) is of Late Devonian age, but younger than Portage of early New York usage.[1] Hass assigned a Late Devonian and Early Mississippian age to the Big Stone Gap Shale (of Stose) in the Duffield quadrangle. Harris therefore did not use the names Genesee and Portage, but called the lower unit shale (unnamed), the middle unit siltstone (unnamed), and the upper unit Big Stone Gap Siltstone.

In mapping and measuring sections, the writers have recognized and found it practicable to use the lithologic divisions that correspond to those of Campbell (1893),

[1] Current nomenclature for the Upper Devonian of central New York, compared with early nomenclature, is given in a recent paper by de Witt and Colton (1959).

Stose (1923), and Harris and Miller (1958) in all of the Big Stone Gap quadrangle and most of the Keokee quadrangle. These lithologic divisions are: a lower black-shale unit, a middle unit of gray siltstone with interbedded black shale, and an upper unit of black shale and silty shale. Accurate measurements of thickness of these units are exceedingly rare because of few exposures, intertonguing of the black and gray facies, and the possibility of folds and faults in covered intervals. The lower black-shale unit appears to be from 300 to 400 feet thick, the middle gray-siltstone unit from 140 to 400 feet thick, and the upper black-shale unit from 200 to 325 feet thick. In the Keokee quadrangle (fig. 1), mapping of these three units became uncertain because the scarcity of good outcrops did not permit accurate mapping of the apparently thinning middle gray siltstone which divides the otherwise continuous black-shale sequence. In the Pennington Gap quadrangle, which adjoins the Keokee quadrangle on the west, the middle gray siltstone unit could not be recognized, and the whole black-shale sequence was mapped as an undivided unit. In logging deep wells a few miles north of the Big Stone Gap area, Roen and Miller also were unable to recognize the middle gray siltstone unit. It thus appears that the threefold lithologic division is confined to a relatively small area in southwest Virginia. Where the subdivision into thinner mapped units fails, the most appropriate name for the undivided sequence is Chattanooga Shale.

It seems better to treat the Chattanooga Shale in southwest Virginia as a formation locally divisible into three members that can be mapped separately, rather than as three formations. We therefore propose that the Big Stone Gap Shale be reduced in rank to the Big Stone Gap Member of the Chattanooga Shale. The two underlying mapped units, because of their limited areal extent, do not merit new formal member names. Rather, we propose that they be called the lower black-shale member and the middle gray-siltstone member of the Chattanooga Shale.

In the Big Stone Gap area the Chattanooga Shale is overlain by the Price Siltstone of Early Mississippian age. The contact is conformable. Locally the gray siltstone of the Price and the black shale of the Chattanooga are interbedded in a zone that may be as much as 12 feet thick. In the vicinity of Big Stone Gap, the Chattanooga disconformably overlies the Wildcat Valley Sandstone of Early and Middle Devonian age [Miller and others, 1964, p. B51 (this chap.)]. To the northwest, west, and south of the Big Stone Gap area, the Wildcat Valley Sandstone thins to extinction in a few miles, and the Chattanooga lies on the next older Hancock Dolomite (Limestone) of Late Silurian age.

Stose (1923, p. 46, 47) gives two reconnaissance sections of his Big Stone Gap Shale in the Big Stone Gap area, one on the Powell River just north of the town of Big Stone Gap, and the other at Little Stone Gap, 7 miles northeast of the town. He does not indicate, however, which of these he intended for the type section of the Big Stone Gap Shale. We have remeasured both of these sections. The Powell River section, given below, is the better of the two for the upper part of the shale sequence, and is here designated the type section of our Big Stone Gap Member of the Chattanooga Shale.

Type section of the Big Stone Gap Member of the Chattanooga Shale. Section is located along the southwest bank of the Powell River at Big Stone Gap, Va., 0.6 mile north-northwest of the center of the town of Big Stone Gap. Measured by R. L. Miller and J. B. Roen, November 28, 1962.

	Thickness (feet)
Price Siltstone (+25 feet):	
20. Siltstone, medium-gray; even beds average 1 foot in thickness; concretionary structures present; sandstone very fine grained at top, slightly wavy bedded	25.4
Chattanooga Shale:	
Big Stone Gap Member (242.6 feet):	
19. Shale, grayish-black, silty; with conspicuous beds of medium-dark-gray siltstone as much as 2 inches thick; contact with Price appears conformable; siltstone of this unit indistinguishable from Price, indicating apparent transitional sedimentation	1.3
18. Siltstone, grayish-black, thin- to shaly-bedded; few grayish-black silty shale beds	4.8
17. Shale, grayish-black, silty; ¼-inch bed of medium-dark-gray siltstone in middle of unit	4.5
16. Covered	15.4
15. Shale, dark-gray, silty; slightly more resistant siltstone laminae	10.1
14. Shale, dark-gray; no siltstone; top drawn at first siltstone laminae	10.1
13. Shale, grayish-black, silty; similar to unit 12; 1-inch ironstone bed at top and 2-inch ironstone bed 1 foot below top; pronounced gully in middle of unit	10.7
12. Shale, grayish-black; thin bedded but bedding not as conspicuous as in units 7 and 8; top of unit is conspicuous 3-inch medium-gray ironstone bed	12.9
11. Shale, grayish-black, silty; a few siltstone beds; appears similar to units 10 and 12	41.2
10. Shale, grayish-black; thin, even bedded	40.4
9. Clay shale, medium-dark-gray; bedding contorted and indistinct; unit contains lenses and concretions of light-olive-gray siltstone and grayish-black well-bedded shale; small brachiopods and pelecypods collected 3 feet above base	24.5
8. Shale, grayish-black; fault repeats 9.7 feet of beds including contact between unit 9 and this unit	4.9
7. Shale, grayish-black; three grayish-black silty shale beds 3 to 6 inches thick; irregular pits on weathered surface	3.2

Type section of the Big Stone Gap Member of the Chattanooga Shale—Continued

Chattanooga Shale—Continued	Thickness (feet)
Big Stone Gap Member—Continued	
6. Shale and siltstone; shale, grayish-black, silty; siltstone, grayish-black; irregular pits as much as ½ inch in diameter scattered on weathered surface, which has a slaglike luster	3.5
5. Shale, grayish-black, very thin bedded	32.8
4. Covered	14.3
3. Shale, grayish-black, even-bedded; weathers to plates less than 1/16 inch thick; conformable contact with unit 2 placed at highest prominent siltstone	8.0
Middle gray siltstone member (+23 feet):	
2. Shale, grayish-black, silty, with occasional laminae of medium-dark-gray siltstone	13.6
1. Clay shale, olive-gray, with resistant medium-dark-gray siltstone and shale interbedded in a zone 6 inches to 2 feet thick	9.3

The Chattanooga Shale in the Big Stone Gap area ranges in age from earliest Late Devonian, or possibly late Middle Devonian to Early Mississippian. These age determinations were made by W. H. Hass (written communications, 1953, 1954) and Huddle, and are based on conodont collections made by Hass in 1944, Harris and Hass in 1952–53, and the writers in 1962–63. Conodonts found in the basal beds of the lower black-shale member of the Chattanooga Shale in the Duffield quadrangle, Virginia, include *Polygnathus linguiformis* Hinde and *Icriodus latericrescens* Branson and Mehl. These species are common in the Middle Devonian rocks of New York but are also found in the Upper Devonian part of the Genesee Formation of New York. The age of the basal beds is therefore not definitely determined. Most of the lower black shale member has a Late Devonian conodont fauna including several species of *Palmatolepis*. *Palmatolepis glabra* Ulrich and Bassler, *Palmatolepis perlobata* Ulrich and Bassler, and *Ancyrognathus bifurcata* (Ulrich and Bassler) occur in the upper part of the lower member and represent the conodont assemblage found in the Upper Devonian Perrysburg Formation in New York (middle Late Devonian).

The middle gray-siltstone member of the Chattanooga Shale has yielded few conodonts. Two collections from this unit in the Duffield quadrange contain *Spathognathodus inornatus* (Branson and Mehl) and *Palmatolepis perlobata* Ulrich and Bassler. These species suggest a correlation of the middle gray member in the Big Stone Gap area with part of the Gassaway Member of the Chattanooga in central Tennessee and the upper part of the Ohio Shale in Ohio.

The Big Stone Gap Member of the Chattanooga Shale contains both Early Mississippian and Late Devonian conodont faunas. The lower part of this member, up to and including unit 5 in the Powell River section at Big Stone Gap (see stratigraphic section), contains *Spathognathodus inornatus* (Branson and Mehl), *S. strigosus* (Branson and Mehl), and *S. aculeatus* (Branson and Mehl), and several species of bar-type conodonts. This part of the member is considered Late Devonian in age. Units 7 and 8 in the Powell River section contain *Spathognathodus inornatus* (Branson and Mehl), *S. anteposicornis* Scott, *S. strigilis* (Huddle), and several species of *Hindeodella*. *S. anteposicornis* occurs with *S. inornatus* in the Louisiana Limestone in the Mississippi Valley, the Bedford Shale of Ohio, and in the Knapp Formation of northwestern Pennsylvania. These formations have been classified as Early Mississippian by some authors and as Late Devonian by others. No identifiable conodonts have been found in the medium-dark-gray clay shale, unit 9, of the Powell River section of the Big Stone Gap Member. Units 7, 8, and 9 of the Powell River section are here regarded as being Mississippian or Devonian in age.

The lowest definitely Mississippian conodont fauna occurs in the basal 0.3 feet of unit 10 in the Powell River section. This is the base of the Big Stone Gap Member of Swartz (1929a). The fauna is characterized by *Siphonodella* and occurs throughout the upper part of our Big Stone Gap Member at Big Stone Gap and Little Stone Gap, Va. The following species have been found:

Elictognathus lacerata (Branson and Mehl)
Polygnathus communis (Branson and Mehl)
Polygnathus inornatus (E. R. Branson)
Pseudopolygnathus sp.
Siphonodella duplicata (Branson and Mehl)
Siphonodella quadruplicata (Branson and Mehl)
Spathognathodus aciedentatus (E. R. Branson)

This fauna is clearly Early Mississippian Kinderhookian in age, and hence units 10–19 in the Powell River section are considered Kinderhookian in age. This fauna also occurs in the Maury Formation of Tennessee and the Sunbury Shale of Ohio, but has not been found in New York.

REFERENCES

Bates, R. L., 1939, Geology of Powell Valley in northeastern Lee County, Virginia: Virginia Geol. Survey Bull. 51, pt. 2, p. 31–94.

Butts, Charles, 1940, Geology of the Appalachian Valley in Virginia: Virginia Geol. Survey Bull. 52, pt. 1, 568 p.

Campbell, M. R., 1893, Geology of the Big Stone Gap coal field of Virginia and Kentucky: U.S. Geol. Survey Bull. 111, 106 p.

——— 1894, Description of the Estillville quadrangle (Ky-Tenn-Va): U.S. Geol. Survey Geol. Atlas, Folio 12.

Conant, L. C., and Swanson, V. E., 1961, Chattanooga shale and related rocks of central Tennessee and nearby areas: U.S. Geol. Survey Prof. Paper 357, 91 p.

de Witt, Wallace and Colton, G. W., 1959, Revised correlations of lower Upper Devonian rocks in western and central New York: Am. Assoc. Petroleum Geologists Bull., v. 43, no. 12, p. 2810–2828.

Harris, L. D., and Miller R. L., 1958, Geology of the Duffield quadrangle, Virginia: U.S. Geol. Survey Geol. Quad. Map GQ–111.

Hass, W. H., 1956, Age and correlation of the Chattanooga Shale and the Maury Formation: U.S. Geol. Survey Prof. Paper 286, 47 p.

Miller, R. L., Harris, L. D., and Roen, J. B., 1964, The Wildcat Valley Sandstone (Devonian) of southwest Virginia, *in* Geological Survey Research 1964: U.S. Geol. Survey Prof. Paper 501–B, p. B49–B52.

Stose, G. W., 1923, Pre-Pennsylvanian rocks, *in* Eby, J. B., The geology and mineral resources of Wise County and the coal-bearing portion of Scott County, Virginia: Virginia Geol. Survey Bull. 24, 617 p.

——— 1924, The black shale of southwestern Virginia: Jour. Geology v. 32, no. 4, p. 311–315.

Swartz, J. H., 1926a, The Big Stone Gap shale of southwestern Virginia: Science, new ser., v. 64, p. 226.

——— 1926b, The age of the Big Stone Gap shale of southwestern Virginia: Am. Jour. Sci., 5th ser., v. 12, p. 522–531.

——— 1927, The Chattanooga age of the Big Stone Gap shale: Am. Jour. Sci., 5th ser., v. 14, p. 485–499.

——— 1929a, The age and stratigraphy of the Chattanooga shale in northeastern Tennessee and Virginia: Am. Jour. Sci., 5th ser., v. 17, p. 431–448.

——— 1929b, The Devono-Mississippian boundary in the southeastern United States: Science, new ser., v. 70, p. 609.

THE WILDCAT VALLEY SANDSTONE (DEVONIAN) OF SOUTHWEST VIRGINIA

By RALPH L. MILLER,[1] LEONARD D. HARRIS,[2] and JOHN B. ROEN,[1]
[1]Washington, D.C., [2]Knoxville, Tenn.

Abstract.—A conspicuous formation in Wise, Scott, and Lee Counties, Va., has previously been called Helderberg Limestone or Helderberg Limestone of Stose. Helderberg is not a formation in its type region but a stage of Devonian time. The formation in southwest Virginia is renamed the Wildcat Valley Sandstone.

In Scott, Wise, and Lee Counties of southwest Virginia, the Devonian System is represented by a calcareous sandstone about 45 feet thick, overlain by a black shale sequence hundreds of feet thick. The black shale is the Chattanooga Shale, largely of Late Devonian age. The underlying calcareous sandstone has in the past been called Helderberg Limestone (Stose, 1923). Because Helderberg has been used as a time stratigraphic term in this area, that is, for a stage of Devonian time (Cooper, G. A., and others, 1942), and also because in places the topmost beds of the sandstone contain post-Helderberg fossils, the new name Wildcat Valley Sandstone is here introduced for this rock stratigraphic unit.

In the Estillville folio covering this region (Campbell, 1894), the Wildcat Valley Sandstone was included with underlying limestones of Late Silurian age in the Hancock Limestone (or Dolomite). Stose (1923) later mapped the calcareous sandstone as a separate formation in his section of the Virginia Geological Survey report on Wise County, calling it the Helderberg Limestone because of faunal similarities to the Helderberg of New York. Butts (1940) calls the unit "Helderberg undivided" in his classic report on the Appalachian Valley of Virginia.

The new formation name is derived from Wildcat Valley in southwestern Wise County, Va. (Big Stone Gap topographic quadrangle map, scale 1 : 24,000, 1957). Wildcat Valley lies about 2 miles south of the town of Big Stone Gap between Wallen Ridge on the northwest and Powell Mountain on the southeast (fig. 1). It is drained northeastward by Wildcat Creek, which flows into the South Fork of the Powell River. Along the lower course of the creek, southeast-dipping beds of Hancock Limestone form a line of low knobby hills on the southeast side of the valley. The crests of the knobs are in most places capped by the Wildcat Valley Sandstone. On most of the hills the basal beds of the Chattanooga Shale lie on the back slopes of the knobs, and the remainder of the formation underlies the lowest slopes of Powell Mountain. The type section of the Wildcat Valley Sandstone was measured at the southwest end of the peninsula-shaped knob 0.15 mile south of Irondale Church, which is in the small community of Irondale on U.S. Highway 23. The section of the upper part of the Hancock Limestone and of the Wildcat Valley Sandstone exposed at this locality follows.

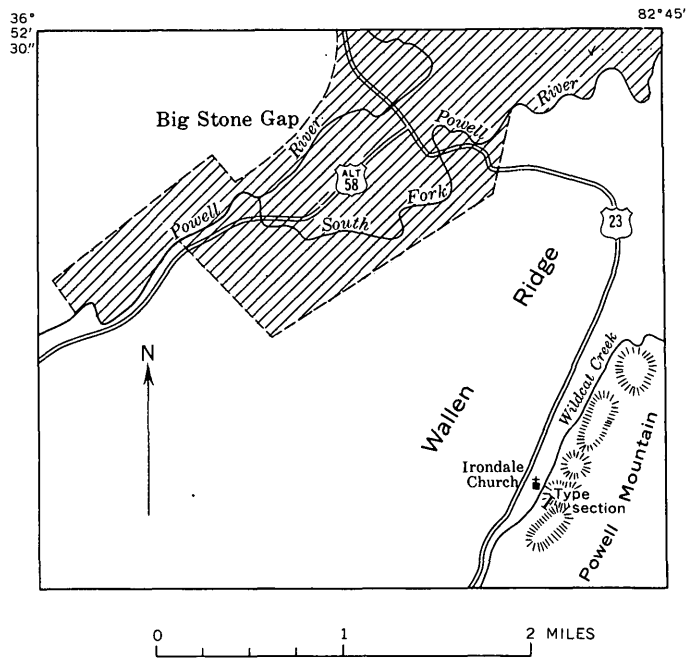

FIGURE 1.—Sketch map showing type locality of the Wildcat Valley Sandstone in the northeast part of the Big Stone Gap quadrangle, Virginia.

Type section of the Wildcat Valley Sandstone, and upper part of the Hancock Limestone. Section is located 2 miles south-southeast of Big Stone Gap, Wise County, Va., on a spur overlooking Wildcat Creek, 0.15 mile south of Irondale Church on U.S. Highway 23. Section begins with lowest beds exposed on southwest slope of spur and ends with black-shale exposures on highest point of spur. Measured by Ralph L. Miller, August 26, 1963.

	Thickness (feet)
Chattanooga Shale:	
16. Black shale, almost in place on crest of spur.	
Wildcat Valley Sandstone (41 feet):	
15. Covered; float from upper part is fine-grained, porous, fossiliferous, sandstone that weathers pale yellowish brown and is partly replaced by granular white chert; abundant fossils, principally brachiopods; float from lower part is similar sandstone, but more dense, and without fossils	13+
14. Sandstone, fine-grained, porous, friable; in irregular beds	13.5
13. Sandstone, fine-grained, pale-yellowish-brown, little-weathered, laminated; interstitial calcium carbonate. Contains *Leptaena* sp. and other brachiopods. Before weathering, unit 14 probably had similar lithology	3.7
12. Sandstone, fine-grained, calcareous; abundant brachiopods; tiny patches of white chert. Might be called sandy limestone, but after dissolving of carbonate, coherent sandstone remains	2.1
11. Covered	4.3
10. Sandstone, very fine grained, calcareous, pale-yellowish-brown; numerous fragmented fossils	1.3
9. Sandstone, fine-grained, light-brownish-gray, calcareous; in uneven thin beds with indistinct fossils	3.4
Hancock Limestone (66+ feet):	
8. Limestone, very fine crystalline, olive-gray, faintly laminated; petroliferous odor after fracturing; beds somewhat slumped	8±
7. Limestone, fine and very fine crystalline, brownish-gray; in beds 2 to 6 inches thick; petroliferous odor after fracturing	12.6
6. Limestone, dolomitic, dense, olive-gray, faintly laminated. Not as dolomitic as units 2 and 4	11.7
5. Limestone like unit 3; weathers thin bedded in upper part; petroliferous odor after fracturing	10.2
4. Dolomite, very fine crystalline, dense, olive-gray with steely luster; even beds as much as 3 feet thick	10.5±
3. Limestone, very fine crystalline, olive-black; in even beds 1 inch to 2 feet thick; silty laminae show faintly on weathered surfaces; petroliferous odor after fracturing	9.7
2. Dolomite, very fine crystalline, olive-gray, irregularly bedded and faintly laminated	1.6
1. Limestone, fine crystalline, light-olive-gray; in irregular beds; conspicuous vertical joints; weathers very dark gray with white blotches	1.8

Miller and Roen have mapped the Wildcat Valley Sandstone throughout its outcrop belt in the Big Stone Gap and Keokee quadrangles (maps in preparation). Harris and Miller have also mapped this unit under the name "Sandstone (Helderberg as used by Stose)" in the Duffield quadrangle (Harris and Miller, 1958), which lies just south of the Big Stone Gap quadrangle (fig. 2). In all three quadrangles, sandstone is the predominant rock type at the outcrop. Before weathering, probably all the sandstone beds were calcareous. Northeast of the Big Stone Gap quadrangle, at the extreme east end of the Powell Valley, sandy and argillaceous limestone is dominant according to Stose (1923), which is why he referred to this unit as the Helderberg Limestone. Even here, however, sandstone seems to predominate over limestone in roadside exposures we have seen. A facies change to still more calcareous beds appears to take place northeast of the Big Stone Gap area (Butts, 1940, p. 264–291).

The Wildcat Valley Sandstone in most surface (that is, weathered) exposures consists of fine-, medium-, and coarse-grained porous and friable sandstone normally stained light shades of yellow or very light brown. In places, particularly near faults, the sandstone is stained or recemented with limonite or hematite and appears red, brown, or nearly black. In some places, the weathered sandstone is no longer coherent, and the outcrop consists of a sand pile which may still preserve traces of original bedding. Elsewhere, however, the sandstone is moderately resistant in spite of its porous character. It caps small hills, causes changes of slope, and may form a sparse blocky float. Fossils, predominantly large brachiopods, are abundant and where not replaced by chert consist principally of external and internal molds. The fossiliferous nature of the rock may be deduced from the fact that we used the field term "Devonian fossil sand" for the unit in mapping it in the Duffield quadrangle. White chert is a variable constituent of the formation and occurs principally as replacements of fossils or fillings of cracks, but in some beds it fills interstices between sand grains or replaces sand grains. Calcium carbonate generally forms the cement between sand grains, where the rock is little weathered, but in most outcrops the carbonate is completely dissolved. Nodular chert is scarce, and fragments of chert in the soil derived from weathering of the rock are mostly small and thin. In the type section, chert is abundant in the uppermost beds. Locally, a few feet of very cherty sandstone is present at the top. These beds contain corals in abundance in some places.

Where we have mapped the formation in the Duffield and Big Stone Gap quadrangles it is consistently about 40 to 45 feet thick. It thins southwestward, in the Keokee and Stickleyville quadrangles, and is absent in the Pennington Gap quadrangle and the western part of the Stickleyville quadrangle (fig. 2). Northward

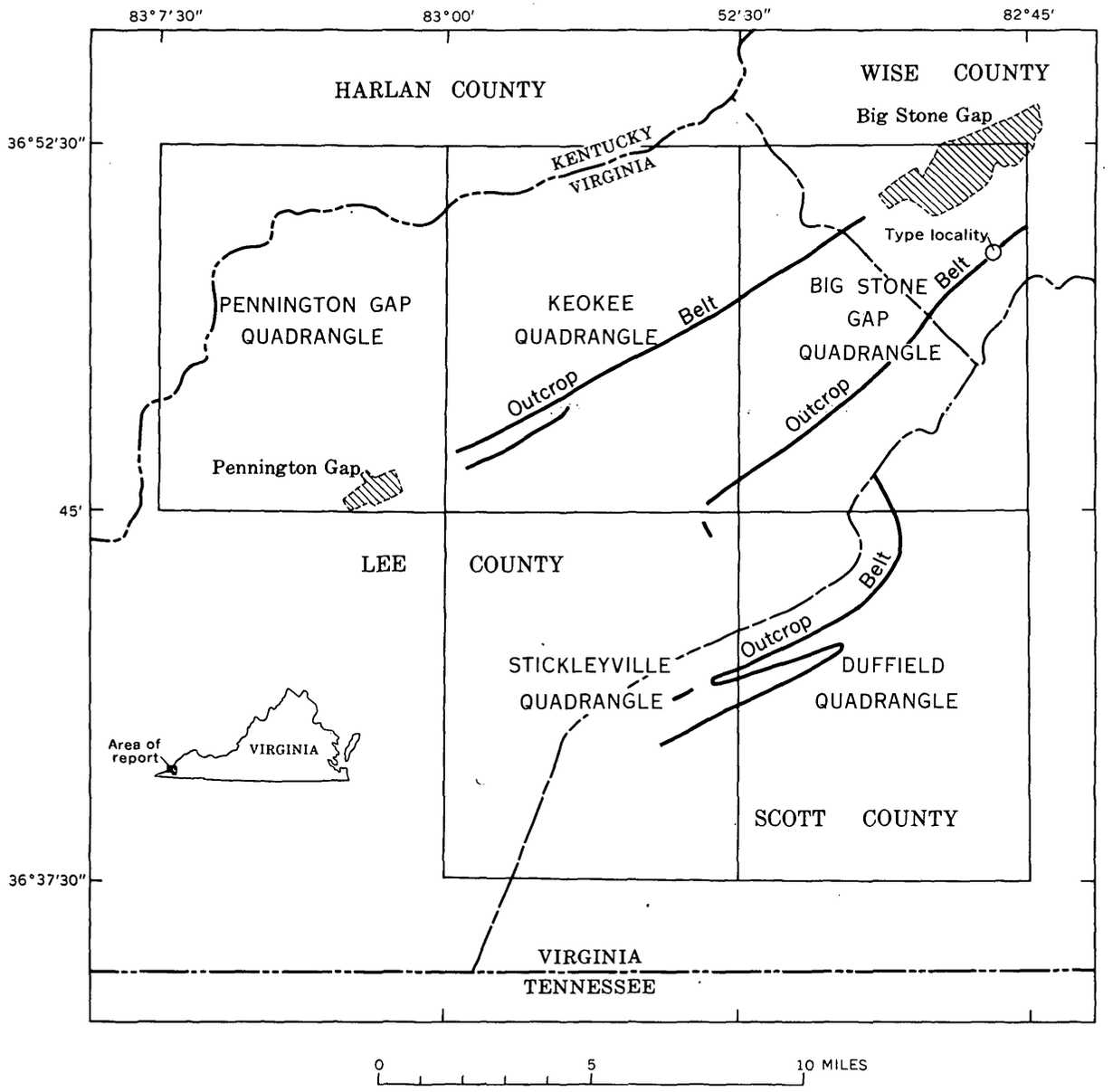

FIGURE 2.—Map of part of southwest Virginia, showing belts of outcrop and the type locality of the Wildcat Valley Sandstone.

and northwestward, within a few miles of Big Stone Gap, it also feathers out beneath the younger strata of the Cumberland Plateau, as shown by deep wells in western Wise County.

The Wildcat Valley Sandstone, disconformably overlies the Hancock Limestone (or Dolomite) of Late Silurian age. The contact is sharp but with little apparent erosion of the Hancock. Disconformably overlying the Wildcat Valley Sandstone is the black Chattanooga Shale, without apparent significant erosion of the beds beneath the contact.

Although the Wildcat Valley Sandstone is relatively thin and is virtually a lithologic unit, it is not a paleontologic entity. Various geologists have collected from the formation in sections near Big Stone Gap. Campbell (1894) mapped the Big Stone Gap region but included all the Wildcat Valley Sandstone with the underlying Hancock Limestone (Silurian). H. S. Williams, whose fieldwork postdated that of Campbell, mentions the sandstone underlying the black shale at Big Stone Gap from the top beds of which he collected "corals of Corniferous (Onondaga) age" (Williams, 1897, p. 398–399). His reference to the Helderberg Limestone beneath the sandstone appears to mean the Hancock Limestone, now considered Late Silurian. Kindle (1905, p. 27–29) lists faunas collected from four

localities near Big Stone Gap, two of which he dates as "Oriskany" (quotes are Kindle's). The other two faunules are not dated. Later, Kindle (1912, p. 50–53) collected again, this time from the topmost beds beneath the black shales at two localities near Big Stone Gap. He dated these coral-rich faunules as Onondaga, but noted correctly that the coral-rich beds were not everywhere present overlying the more sandy and less cherty beds that he had previously called "Oriskany".

Stose (1923) called the unit that he mapped in Wise County the Helderberg Limestone, apparently basing this designation on sections measured and paleontologic studies made in the area by E. O. Ulrich. The main body of the formation was correlated by Ulrich and Stose with the New Scotland and Becraft Limestones of the Helderberg Group of New York. The coral-rich faunules noted by Kindle were also recognized by Ulrich as having Onondaga affinities, but he "found that the coral fauna occurs in several bands in the upper 50 feet or more of the formation and that the intervening beds contain an unquestionable Becraft fauna. He therefore regards these corals as representing an earlier invasion of species that are elsewhere known only in limestones of Onondaga age" (Stose, 1923, p. 42). Stose therefore assigned these coral-bearing beds as well as the underlying rocks to the Helderberg. We believe that the recurrence in several bands of the coral faunas noted by Ulrich was probably due to repetition of beds by faulting, although this cannot be verified because Ulrich's localities are not specified. Bates (1939) followed Stose in assigning a New Scotland and Becraft age to the Helderberg Formation in northeastern Lee County, Va.

Harris (Harris and Miller, 1958) in collaboration with A. J. Boucot collected fossils from the formation, here named the Wildcat Valley Sandstone, in the Duffield quadrangle and also in the Big Stone Gap area. Boucot (written communications, 1954), who studied the brachiopods from these new collections as well as the earlier collections made by other paleontologists in the Big Stone Gap area, has indicated that the lowest part of the Wildcat Valley Sandstone contains fossils of probable Helderberg age, whereas the middle and most of the upper parts of the formation are of New Scotland or Becraft age. As with others before them, Harris and Boucot at some localities found post-Helderberg fossils in the top few feet of the formation. These seemed to Boucot to be of Schoharie or Onondaga age, and at one locality Boucot identified brachiopods of Oriskany age between the beds of Helderberg age and those of Schoharie or Onondaga age. W. A. Oliver, Jr. (oral communication, 1963) has recently examined the corals from these faunules designated by Boucot as Schoharie or Onondaga and believes that they are of Schoharie age.

In spite of the fact that beds of diverse ages are apparently present in the Wildcat Valley Sandstone, it is virtually one geologic unit for mapping purposes. At some localities in the Big Stone Gap area, it seems to be entirely of Helderberg age, but at other places in the same region, as much as 8 feet of beds of probable Schoharie age is included at the top, and a few localities have yielded fossils of apparent Oriskany age between the two. These thin zones of post-Helderberg age are probably remnants of a more extensive but thin layer of late Lower Devonian and possibly early Middle Devonian sedimentary rocks that has only locally been preserved from pre-Chattanooga erosion. The erosion of only a few feet of beds in Onondaga and Hamilton time would account for the spotty occurrences of the post-Helderberg beds. Thus, the Wildcat Valley Sandstone is largely of Early Devonian age, but in places lower Middle(?) Devonian beds are present at the top of the formation.

REFERENCES

Bates, R. L., 1939, Geology of Powell Valley in northeastern Lee County, Va.: Virginia Geol. Survey Bull. 51–B, p. 31–94.

Butts, Charles, 1940, Geology of the Appalachian Valley of Virginia: Virginia Geol. Survey Bull. 52, p. 264–291.

Campbell, M. R., 1894, Description of the Estillville quadrangle (Ky.-Tenn.-Va.): U.S. Geol. Survey Geol. Atlas, Folio 12.

Cooper, G. A., and others, 1942, Correlation of the Devonian sedimentary formations of North America: Geol. Soc. America Bull. v. 53, p. 1729–1794.

Harris, L. D., and Miller, R. L., 1958, Geology of the Duffield quadrangle, Virginia: U.S. Geol. Survey Geol. Quad. Map GQ–111.

Kindle, E. M., 1905, Sections in Virginia and West Virginia, *in* Williams, H. S., and Kindle, E. M., Fossil faunas of the Devonian and Mississippian ("Lower Carboniferous") of Virginia, West Virginia, and Kentucky: U.S. Geol. Survey Bull. 244, p. 144.

——— 1912, The Onondaga fauna of the Allegheny region: U.S. Geol. Survey Bull. 508, p. 144.

Stose, G. W., 1923, Pre-Pennsylvanian rocks, *in* Eby, J. B., The geology and mineral resources of Wise County and the coal-bearing portion of Scott County, Virginia: Virginia Geol. Survey Bull. 24, p. 40–43.

Williams, H. S., 1893, On the southern Devonian Formations: Am. Jour. Sci., 4th ser., v. 3, p. 393–403.

THE GOOSE EGG FORMATION IN THE LARAMIE RANGE AND ADJACENT PARTS OF SOUTHEASTERN WYOMING

By EDWIN K. MAUGHAN, Denver, Colo.

Abstract.—The name Goose Egg Formation is applied in southeastern Wyoming to that part of the Permian and Triassic red-bed sequence that contains interstratified carbonate and sulfate rocks. These strata compare with those of the type section near Casper, Wyo., composed of Opeche Shale, Minnekahta Limestone, Glendo Shale, Forelle Limestone, Difficulty Shale, Ervay, Freezeout Shale, and Little Medicine Members.

Discussion of red beds of Permian and Triassic age in southeastern Wyoming has been difficult heretofore owing to inadequate nomenclature for these rocks. The Goose Egg Formation was named by Burk and Thomas (1956) for exposures near the Goose Egg Post Office, NW¼ sec. 12, T. 32 N., R. 81 W. (fig. 1), in central Wyoming, for that part of this red-bed sequence that is interstratified with carbonate and sulfate rocks. Units that compose the Goose Egg Formation at the type section near Casper (table 1) can be identified in surface and subsurface sections throughout most of southeastern Wyoming. For this reason, and to establish a consistent nomenclatural system for the red beds and other rocks, the name Goose Egg Formation is extended into the southeastern part of the State. The stratigraphic relations of the members that make up the formation in southeastern Wyoming are discussed in this article.

All the red beds in southeastern Wyoming now known to be of Permian and Triassic age were included originally in the Chugwater Formation by Darton (1904, p. 397–398). Strata equivalent to the Minnekahta Limestone and Opeche Shale, which Darton (1901, p. 513–514) had previously named in the Black Hills, were not differentiated in his definition of the Chugwater. Subsequently, strata in the lower part of the original Chugwater were excluded in the Laramie Basin and named there the Satanka Shale and overlying Forelle Limestone (Darton, 1908).

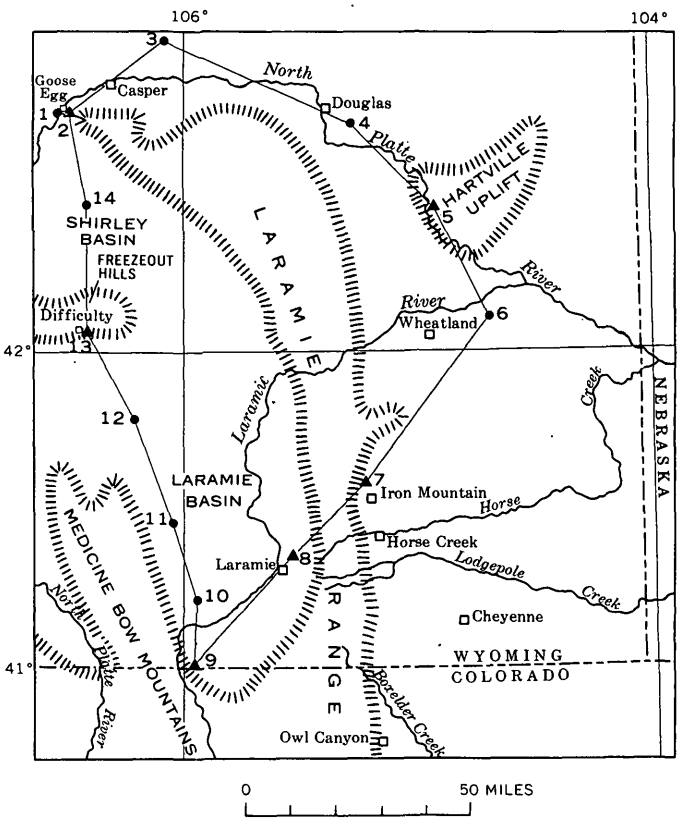

FIGURE 1.—Index map showing location of places referred to in text. Numbers indicate geologic sections illustrated on figure 2. Triangle, outcrop section; dot, subsurface section.

Thomas (1934) established the age for the part of the red-bed sequence that is interstratified with carbonate and sulfate rocks by tracing these strata westward into rocks of known Permian and Triassic age. The Ervay tongue in central Wyoming he correlated with the uppermost part of the Park City Formation (then known as the Phosphoria Formation) in the Wind River Range of western Wyoming and established it

TABLE 1.—*Nomenclature of Permian and Lower Triassic rocks in southeastern Wyoming.*

LARAMIE BASIN (Darton, 1908)	EAST FLANK OF LARAMIE RANGE AND HARTVILLE UPLIFT (Condra and others, 1940)	CASPER AREA (Burk and Thomas, 1956)		SOUTHEASTERN WYOMING (this article)		
				System	Series	Stratigraphic unit
Chugwater formation	Spearfish shale (redefined)	Chugwater formation		TRIASSIC	Lower Triassic	Red Peak equivalent of Chugwater Formation
	Dinwoody sandstone	Goose Egg formation	Little Medicine member			Little Medicine Member
	Freezeout shale		Ervay member / Freezeout member	PERMIAN	Upper Permian	Freezeout Shale Member / Ervay Member? / Difficulty Shale Member
Forelle limestone	Forelle limestone		Forelle limestone member			Forelle Limestone Member
Satanka shale	Glendo shale		Glendo shale member			Glendo Shale Member
	Minnekahta limestone		Minnekahta limestone member		?	Minnekahta Limestone Member
	Opeche shale		Opeche shale member		Lower Permian	Opeche Shale Member
	Lyons sandstone	Casper formation				Owl Canyon Formation[1]
	Owl Canyon formation					Casper or Hartville Formation

[1]Condra and others (1940).

as the uppermost unit of Permian age. Red beds enclosing the Ervay he named the Freezeout Tongue of the Chugwater Formation. The part of the Freezeout that overlies the Ervay was correlated westward by Thomas with the lower part of the Dinwoody Formation of Early Triassic age and is overlain by a bed of limestone that Thomas named the Little Medicine Tongue of the Dinwoody Formation. The Little Medicine is found in most of eastern Wyoming.

Condra and others (1940) introduced additional names for red beds of Permian age in southeastern Wyoming. The Owl Canyon Formation and a thin sandstone locally found at its top, which they provisionally correlated with the Lyons Sandstone, were recognized beneath the Opeche Shale. These strata are the equivalent of the lower part of the Satanka Shale (Darton, 1908). The Opeche Shale and Minnekahta Limestone, names extended from the Black Hills, and the Glendo Shale, a name which Condra and others introduced for the red-bed unit between the Minnekahta and the Forelle, were applied along the east flank of the Laramie Range for strata equivalent to the upper part of the Satanka Shale. The Freezeout Shale was applied to the red beds above the Forelle and below their Dinwoody sandstone (Little Medicine Tongue). The Freezeout as used by Condra and others includes thin limestone and gypsum beds of the Ervay.

The Goose Egg Formation of Burk and Thomas (1956) included in ascending order: Opeche Shale, Minnekahta Limestone, Glendo Shale, Forelle Limestone, lower part of the Freezeout, Ervay, upper part of the Freezeout, and Little Medicine Members. This nomenclature has been extended throughout the Powder River Basin in northeastern Wyoming by Privrasky and others (1958) with the exception that the two parts of the Freezeout were left unnamed.

Units that comprise the Goose Egg Formation at its type section can be traced into southeastern Wyoming and differentiated in most places from other Permian and Triassic red beds (fig. 2 and table 2). They are distinct in exposures in the Laramie Range, except in the southern part, and in the Hartville uplift. Electric logs of the formation throughout southeast Wyoming differ only slightly from the electric log of the formation in the Mississippi River Fuel Co. 1 Government-Goose Egg well, which Burk and Thomas (1956, fig. 1, p. 6) compare with the surface type section.

The base of the Goose Egg Formation is the base of the lowest gypsum beds in the Opeche Shale Member; the underlying red beds lack bedded gypsum. The top of the formation is the top of the highest dolomite or gypsum in the Little Medicine Member; these kinds of rocks are absent in the overlying red beds. It is a distinctive sequence in most of southeastern Wyoming where exposures are moderately good; however, in the southern Laramie Basin and along the eastern front of the southern part of the Laramie Range, identification of the Goose Egg is difficult. Near Laramie, the equivalents of the members of the Goose Egg are present and can be identified at the few places where these rocks are well exposed, although some of the units are much thinner than correlative strata farther north. However, because all units except the Forelle are poorly exposed at most places in the Laramie area, the Goose Egg cannot be readily subdivided nor differentiated, and the nomenclature of Darton (1908) should be retained.

ROCKS BELOW THE GOOSE EGG FORMATION

Underlying the Goose Egg Formation throughout southwestern Wyoming is the Owl Canyon Formation of Condra and others (1940) or equivalent strata. The formation is composed dominantly of reddish siltstone and very fine grained sandstone. Southward in Colorado the Owl Canyon Formation grades into the Lyons Sandstone, and southwestward in the Laramie Basin it similarly grades into sandstone (Maughan and Wilson, 1960) that probably is a remnant of the Lyons in that area. The Owl Canyon thins northward in the Laramie Range and also grades into sandstone in the northern part of the range where it forms part of the Casper Formation. Consequently, strata equivalent to the Owl Canyon probably underlie the Goose Egg in the Casper area.

Strata similar and perhaps equivalent to the Owl Canyon Formation are included as a lower part of the Opeche Shale at some places in the southern Black Hills. Where these strata grade into sandstone they are included as a part of the Minnelusa Formation. Throughout southeastern Wyoming the Opeche has been restricted to the overlying dominantly claystone unit described below.

ROCK UNITS IN THE GOOSE EGG FORMATION

Opeche Shale Member

The Opeche Shale Member is a thin but very widespread unit which extends throughout most of eastern Wyoming at the base of the Goose Egg Formation (Burk and Thomas, 1956, p. 9). At the type section of the Goose Egg the Opeche Member is 70 feet thick. In the Hartville uplift area and as far south as Horse Creek in the Laramie Range the Opeche ranges between 20 and 70 feet in thickness. At Horse Creek the Opeche is about 70 feet thick, but it thins markedly southward and probably is very thin or absent at Lodgepole Creek and farther south, in Colorado. A similar abrupt thinning of the Opeche occurs in the subsurface in the northern part of the Laramie Basin and in exposures in the Freezeout Hills northwest of the basin. At a few places on the margins of the southern part of the Laramie Basin and south of Boxelder Creek in Colorado, red and purplish-red claystone directly above strata equivalent to the Owl Canyon probably are a wedge edge of the Opeche equivalent.

The Opeche is composed mostly of moderate-reddish-orange claystone. The upper part is purplish in most places where it grades upward into the overlying Minnekahta. The claystone generally is composed of strata ranging from parallel thin laminae to thin beds and is moderately fissile. At many places the lowermost strata are silty or sandy, but more commonly they include beds of dolomite or gypsum, which in the Laramie Basin are moderately thick.

The Opeche is believed to be of late Leonard age. Southeastward it seems to correlate and probably is contemporaneous with the Flowerpot Shale of that age in Kansas. Westward it intertongues in central Wyoming with the Park City Formation at about the stratigraphic position of the Meade Peak Phosphatic Shale Member of the Phosphoria Formation, also of Leonard age.

Minnekahta Limestone Member

The Minnekahta Limestone is about 50 feet thick in the Black Hills and gradually thins southwestward to about 30 feet in the Hartville uplift, and to between 10 to 30 feet at most places in the northern parts of the Laramie Range and the Laramie Basin where it is a member of the Goose Egg. The Minnekahta and Opeche are thin in the same areas. In the south half of the Laramie Basin the Minnekahta is less than 10 feet thick, and at some places it is missing (fig. 2). On

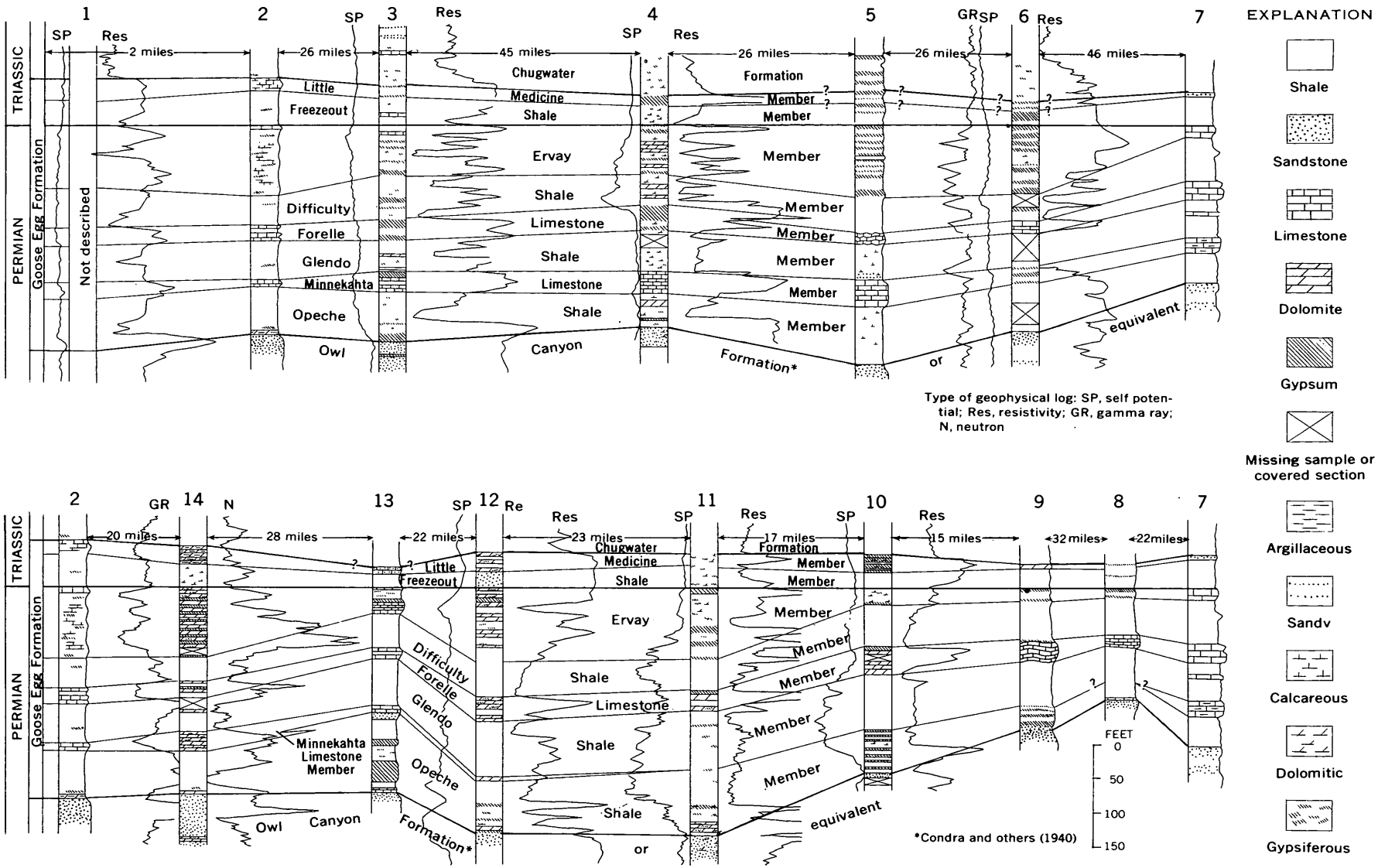

FIGURE 2.—Cross sections of the Goose Egg Formation in southeastern Wyoming. The top line of sections is from the Goose Egg type area near Casper, Wyo., to the east side of the Laramie Range near Iron Mountain, by way of Sand Canyon in the Hartville uplift. The bottom line is from the Goose Egg type section to the east side of the Laramie Range, by way of the Freezeout Hills and Laramie Basin. Lines of sections are shown on figure 1 and description of location and source of sections are given in table 2.

TABLE 2.—*Location and source of sections shown on figure 2*

No. on figure 2	Well or geologic section	Location			Source
		Section	Township (north)	Range (west)	
1	Mississippi River Fuel 1 Government–Goose Egg	9	32	81	Burk and Thomas (1956).
2	Goose Egg Formation type section	12	32	81	Do.
3	Socony Vacuum 32X–21G	21	35	77	[1].
4	Mobil Producing F–14–19–G	19	32	70	[1].
5	Section in Sand Canyon	29	29	67	Denson and Botinelly (1949).
6	Seaboard Oil 1 Wilson	29	25	65	[1].
7	Section at Iron Mountain	29	19	70	This article.
8	Section in vicinity of Laramie	[2] 23	16	73	Do.
9	Section at Red Mountain	18	12	76	Do.
10	Pacific Western 1 Strom	32	15	76	[1].
11	California Co. 3 Seven Mile Unit	9	17	77	[1].
12	British-American 2 State–Horn Bros	17	21	78	[1].
13	Section at Difficulty	10	24	80	Modified from Thomas (1934, p. 1680).
14	Tidewater-Associated 81–22 Lawn Creek	22	29	80	[1].

[1] Sample information from log by American Stratigraphic Co.
[2] Approximate.

the east side of the Laramie Range the Minnekahta is about 25 feet thick at Horse Creek, but it is generally less than 5 feet thick at Lodgepole Creek and farther south. At places in the Boxelder Creek area, where strata equivalent to the Minnekahta are 4 feet thick, this unit rests directly upon Lyons Sandstone and is itself moderately sandy.

The Minnekahta generally is composed of thin even parallel beds and laminae of finely crystalline pinkish- and purplish-gray dolomitic limestone. Commonly, the Minnekahta contains interstratified thin beds of purplish-red claystone, especially in the lower part; geodes incrusted with gypsum, and lenses of gypsum, are common in the upper part. Southeastward from the Laramie Range and Hartville area, the Minnekahta is increasingly gypsiferous. At Owl Canyon, gypsum quarried from a few feet above the Lyons may be a facies of the Minnekahta. However, it is more likely that a dolomite bed half a foot thick and 8 feet above the top of the gypsum is the Minnekahta, and that the gypsum is the bed included in the Opeche Shale Member at Red Mountain (fig. 2, section 9) and elsewhere in the Laramie Basin.

In central Wyoming the Minnekahta Member intertongues with the Franson Member of the Park City Formation. In Nebraska and Kansas it correlates with the Blaine Formation (M. R. Mudge, oral communication, 1959), which is stratigraphically above the Blaine Gypsum of the type section in Oklahoma. At Boxelder Creek in northern Colorado the Minnekahta and Opeche may intertongue with the upper part of the Lyons Sandstone; but these units seem to thin and lap onto the previously deposited sandstone which locally is reworked into overlying and younger Minnekahta.

Glendo Shale Member

The Glendo Shale Member is between 50 and 60 feet thick at most places, but is as much as 80 feet thick at some places. The type locality of the Glendo designated by Condra and others (1940, p. 5) is "in Spring Creek Valley 1 mile south and 2 miles west of Glendo, Wyoming; [and] comprises the interval between the Forelle and Minnekahta limestones . . ." This member, also, is widespread throughout most of eastern Wyoming and because of the characteristic lithologic features described below can be identified in the Laramie Basin where Minnekahta and Opeche are absent and the Glendo rests upon somewhat similar strata of the Owl Canyon Formation.

The Glendo is composed dominantly of moderate reddish-orange mudstone and siltstone. The rock is mottled by abundant yellowish-gray to light-greenish-gray spots as much as ¾ inch in diameter, which are a characteristic feature and aid identification of this member throughout southeastern Wyoming. This member probably was originally formed in parallel thin beds and laminae and tabular sets of low-angle small-scale cross laminae; however, at most places the bedding is now complexly contorted, perhaps because of slumping or flowage penecontemporaneous with deposition or during very early stages of compaction of the sediments. Locally, in the Laramie Basin, the Cheyenne area, and farther south along the Laramie Range in north-central Colorado, the Glendo or equivalent strata include anhydrite and gypsum lenses about 20 to 30 feet below the top of the member. These lenses grade into dolomite or limestone still farther south along the Front Range.

In central Wyoming the Glendo intertongues with the Franson Member of the Park City Formation. It cor-

relates southeastward in Kansas, northeastern Colorado, and Nebraska with rocks equivalent to the Permian Whitehorse Sandstone of Oklahoma. Equivalent rocks in the Golden, Colo., area are the Harriman Shale, Falcon Limestone, and Bergen Shale Members of the Lykins Formation of LeRoy (1946). The Falcon previously has been correlated with the Minnekahta;[1] however, in parts of the Laramie Basin and on the east side of the Laramie Range both Falcon and Minnekahta are present and are separated by about 45 feet of typical Glendo Shale Member.

Forelle Limestone Member

The Forelle Limestone Member, although only about 30 feet thick, is very widespread and extends throughout most of eastern Wyoming.

The Forelle is generally a threefold unit consisting of finely crystalline dolomitic limestone in the upper and lower parts and an argillaceous limestone in the middle. Crenulated laminae and thin beds, probably algal, are characteristic of the Forelle, and at some places the upper part is formed of closely spaced domes 2 to 4 feet in diameter that are probably algal heads. The Forelle changes into anhydrite and gypsum east of the Laramie Range in eastern Wyoming. In the southern Black Hills, equivalent strata, included in the lower part of the Spearfish Formation, locally are partly composed of dolomite that retains the characteristic "crinkly" lamination of the Forelle (D. E. Wolcott, oral communication, 1959).

The Forelle connects westward through the Big Horn Basin in north-central Wyoming with the middle or upper part of the Franson Member of the Park City Formation. A westward connection was illustrated by Thomas (1934, fig. 3, p. 1664), who showed the Forelle in central Wyoming as an eastward-extending tongue of the Park City Formation.

The Forelle crops out discontinuously along the east side of the Laramie and Front Ranges in southern Wyoming and northern Colorado and is equivalent to the "Crinkly Sandstone" of Fenneman (1905, p. 25) or Glennon Limestone Member of the Lykins Formation of LeRoy (1946, p. 44) near Golden, Colo. The correlation of the Forelle with the "Crinkly" or Glennon is based on similarities of lithologic detail, especially the supposed algal structures, stratigraphic position above mudstone characteristic of the Glendo Shale Member, as well as correlations (M. R. Mudge, oral communication, 1957) of both the Forelle and "Crinkly" into the Day Creek Dolomite of Kansas and Nebraska.

[1] T. L. Broin, 1957, Stratigraphy of the Lykins Formation of eastern Colorado: Colorado Univ., Ph. D. dissert.

Difficulty Shale Member

The Freezeout Tongue of the Chugwater Formation of Thomas (1934) is divided into an upper and a lower part by the eastward extension of the Ervay Member of the Park City Formation. Because of this division of the Freezout by the Ervay the concept of the Freezeout as a tongue is untenable, and consequently Thomas (oral communication, 1960) has recommended revision of the Freezeout. The lower part of the Freezeout, like other units of Upper Permian rocks in eastern Wyoming, is widespread and nearly uniform in thickness, generally about 50 feet thick. This unit, bounded by the Forelle and the Ervay Members is herein named the Difficulty Shale Member of the Goose Egg Formation. The type section for this unit is in the Freezeout Hills, in the SW¼ sec. 10, T. 24 N., R. 80 W., about ¼ mile northeast of the location of the old Difficulty Post Office, and seems to be in the same location as the section described near Difficulty by Thomas (1934, p. 1680).

Strata composing the Difficulty Shale Member are mostly moderate-reddish-orange parallel-laminated and thinly bedded mudstone and siltstone. The unit grades upward within a few feet into dolomite or gypsum of the overlying member.

Westward the Difficulty Member grades laterally into carbonate rock of the upper part of the Franson Member of the Park City Formation in central Wyoming. In Colorado, equivalent strata are included in the Lykins Formation, probably in the lower part of the Strain Shale Member of LeRoy (1946). In Kansas the Difficulty seems to correlate with the Taloga Formation (Cragin, 1897).

Ervay Member

The Ervay Member at the Goose Egg type section is 6 feet thick according to Burk and Thomas (1956). However, the underlying 98 feet of interbedded gypsum, carbonate rcok, and shale seems to be a facies of a thicker limestone section included in the Ervay farther west. In this article this gypsum is included in the Ervay. Strata equivalent to the Ervay extend throughout eastern Wyoming and are moderately well exposed in the Black Hills, Hartville area, and the northern part of the Laramie Range. The Ervay in southern Wyoming and its equivalent in northern Colorado is mostly gypsum ranging from 5 to 10 feet in thickness and is generally poorly exposed.

The Ervay is mostly limestone and dolomitic limestone in western Wyoming but grades eastward to dolomite in central Wyoming and to gypsum in most of the eastern half of the State. The gypsum facies is com-

posed of beds of gypsum or anhydrite interstratified with thin beds of reddish claystone or mudstone.

The Ervay and equivalent strata are the youngest Permian rocks in Wyoming and are overlain with seeming conformity at most places by correlatives of the Dinwoody Formation of Early Triassic age. Southward thinning of the Ervay in the Laramie Basin as illustrated on figure 2 seems most likely due to truncation of the member prior to deposition of the overlying strata, although a slower rate of deposition in this area may account for the thinning. The truncation or depositional thinning suggests a minor tectonic movement of the nearby ancestral Front Range highland during or closely following the time of deposition of the Ervay.

Freezeout Shale Member (restricted)

The upper part of the Freezeout Tongue of the Chugwater Formation of Thomas (1934) lies above the Ervay Member and is overlain by the Little Medicine Member. The name Freezeout is restricted to this unit designated herein as the Freezeout Shale Member of the Goose Egg Formation. The type section of the restricted Freezeout is in the NE¼ sec. 2, T. 24 N., R. 80 W., and 1½ miles northeast of Difficulty in the Freezeout Hills and is near the section described by Thomas (1934, p. 1680). It is 35 feet thick at the type section and ranges between 10 and 50 feet in thickness in southeastern Wyoming.

The Freezeout, like the Difficulty Member, is mostly moderate-reddish-orange, parallel-laminated and thinly bedded mudstone and siltstone. It is gradational with the overlying member and commonly contains gypsiferous siltstone and thin beds of gypsum in its upper part.

The Freezeout Shale Member grades westward into yellowish calcareous siltstone in the lower part of the Dinwoody Formation of Early Triassic age. On the basis of the blanketlike distribution of this member and of the strata which enclose it, the Freezeout is of the same age as the equivalent strata in the Dinwoody.

Little Medicine Member

The Little Medicine Member, although thin, is widespread and forms the top of the Goose Egg Formation. At the Goose Egg type section this member is 20 feet thick but ranges between 5 and 25 feet in thickness in southeastern Wyoming. It correlates westward into a part of the Dinwoody Formation of Early Triassic age in western Wyoming.

The Little Medicine Member is gypsiferous and argillaceous dolomite or limestone in the northern Laramie Range, the Shirley Basin, and the Freezeout Hills. Southeastward of these areas this member is mostly gypsum or anhydrite. At most places it includes thin beds of reddish siltstone and claystone interbedded with the sulfate and carbonate rocks. Similarities such as gradation of reddish mudstone of the Freezeout Member upward into the sulphate and carbonate of the Little Medicine, much like the gradation of the Difficulty into the Ervay Member, indicate that the pattern of sedimentation in Early Triassic time repeated that of Late Permian time.

725-328 O—64——5

ROCKS ABOVE THE GOOSE EGG FORMATION

The Goose Egg Formation is conformably overlain by a thick sequence of moderate-reddish-orange siltstone and very fine grained sandstone very similar to the older Owl Canyon Formation. These rocks are equivalent to the Red Peak Member of the Chugwater Formation of Love (1939).

SEDIMENTATION AND ENVIRONMENT

Sediments that formed the red beds within the Goose Egg Formation probably were the initial deposits in a sea that overspread a nearly level plain in most of eastern Wyoming and parts of adjacent States. This area probably was a vast shallow lagoon or tidal flat that extended from the edge of the deeper Phosphoria sea in central Wyoming eastward to the north end of, and far to the south along the east side of, the nearly buried ancestral Front Range highland. The hematitic claystone and associated evaporitic rocks, dolomite, and limestone, indicate a probable marginal marine environment with relatively high salinity and suggest a warm arid climate.

The chemically deposited rocks suggest submergence of the detrital source areas or an increased rate of evaporation. Differences of salinity are indicated by deposition of dominantly carbonate rock of the Minnekahta and Forelle Members and of gypsum of the lower part of the Opeche, the Ervay, and the Little Medicine Members. These differences probably reflect variations in the strength and direction of currents within the lagoon and in variations in the inflow of water from the open ocean, but climatic variations may have affected the rate of evaporation also and accounted for the differences of salinity.

REFERENCES

Burk, C. A., and Thomas, H. D., 1956, The Goose Egg Formation (Permo-Triassic) of eastern Wyoming: Wyoming Geol. Survey Rept. Inv. 6, 11 p.

Condra, G. E., Reed, E. C., and Scherer, O. J., 1940, Correlation of the formations of the Laramie Range, Hartville uplift, Black Hills, and western Nebraska: Nebraska Geol. Survey Bull. 13A [revised ed., 1950].

Cragin, F. W., 1897, Observations on the Cimarron series: Am. Geologist, v. 10, p. 703–737.

Darton, N. H., 1901, Geology and water resources of the southern half of the Black Hills and adjoining regions in South Dakota and Wyoming, *in* U.S. Geol. Survey Ann. Rept. 21, pt. 4; p. 489–599.

———1904, Comparison of the stratigraphy of the Black Hills, Bighorn Mountains, and Rocky Mountain Front Range: Geol. Soc. America Bull., v. 15, p. 379–448.

———1908, Paleozoic and Mesozoic of central Wyoming: Geol. Soc. America Bull., v. 19, p. 403–470.

Denson, N. M., and Botinelly, Theodore, 1949, Geology of the Hartville uplift, eastern Wyoming: U.S. Geol. Survey Oil and Gas Inv. Prelim. Map 102, Sheet 2.

Fenneman, N. M., 1905, Geology of the Boulder district, Colorado: U.S. Geol. Survey Bull. 265.

LeRoy, L. W., 1946, Stratigraphy of the Golden-Morrison area, Jefferson County, Colorado: Colorado School Mines Quart., v. 41, no. 2.

Love, J. D., 1939, Geology along the southern margin of the Absaroka Range, Wyoming: Geol. Soc. America Spec. Paper 20.

Maughan, E. K., and Wilson, R. F., 1960, Pennsylvanian and Permian strata in southern Wyoming and northern Colorado, *in* Guide to the Geology of Colorado: Denver, Colo., Geol. Soc. America, Rocky Mountain Assoc. Geologists, and Colorado Sci. Soc., p. 34–42.

Privrasky, N. C., and others, 1958, Preliminary report on the Goose Egg and Chugwater Formations in the Powder River Basin, Wyoming, *in* Wyoming Geol. Assoc. Guidebook 13th Ann. Field Conf.: p. 48–55.

Thomas, H. D., 1934, Phosphoria and Dinwoody tongues in the lower Chugwater of central and southeastern Wyoming: Am. Assoc. Petroleum Geologists Bull., v. 18, p. 1655–1697.

FORAMINIFERA FROM THE *EXOGYRA PONDEROSA* ZONE OF THE MARSHALLTOWN FORMATION AT AUBURN, NEW JERSEY

By J. F. MELLO, J. P. MINARD, and J. P. OWENS, Washington, D.C.

Abstract.—The Upper Cretaceous Marshalltown Formation, near the top of the Matawan Group, is exposed at Auburn, N.J., where it contains abundant specimens of *Exogyra ponderosa* (Roemer) and *Ostrea* species. A rock sample from this locality yielded an abundant foraminiferal fauna consisting of 30 identified species, 8 of which are planktonic. Comparison of these Foraminifera, listed but not described here, with the age ranges of the same species on the Gulf Coastal Plain suggests that the sample is of late Taylor age.

A sample collected from an outcrop of the Upper Cretaceous Marshalltown Formation near Auburn in southwest New Jersey (fig. 1) has yielded an abundant microfauna. The microfossils occur in association with numerous megafossils, the most conspicuous of which are the thick shelled *Exogyra ponderosa* (Roemer) and thin-shelled *Ostrea* species. The outcrop is at the head of the small gully in the south bank of Oldmans Creek at Camp Kimble.

As defined by Stuart Weller (1907, p. 17), the Marshalltown is near the top of the Matawan Group of New Jersey (table 1), and below the *Exogyra costata* zone of the overlying Monmouth Group. A report on the microfauna from the base and middle of the Monmouth Group was published earlier (Minard and others, 1961).

TABLE 1.—*Marine Upper Cretaceous formations of New Jersey*

[Adapted from Richards and others, 1957]

Group	Subdivision	*Exogyra* zone
Monmouth	Red Bank Sand Navesink Formation Mount Laurel Sand	*Exogyra costata*
Matawan	Wenonah Formation Marshalltown Formation Englishtown Formation Woodbury Clay Merchantville Formation	*Exogyra ponderosa*

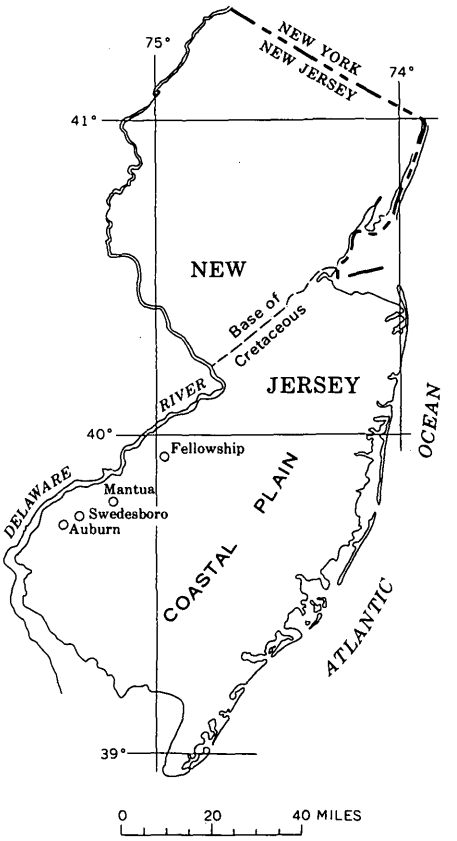

FIGURE 1.—Index map showing localities discussed in text.

Throughout much of its outcrop to the northeast, the Marshalltown is unfossiliferous. Foraminifera have been reported by Joyce Mumby (1961, p. 38) from Fellowship, N.J., and by Harold Gill [1] from Mantua and Swedesboro, N.J., but no faunal lists accompanied either article. The Swedesboro locality may be the

[1] Harold Gill, 1956, A stratigraphic analysis of the Matawan Group: Rutgers Univ., unpub. Ph. D. thesis.

same as either locality 177 or 180 of Weller (1907, p. 82–84), both of which are only a short distance from the locality cited in this article.

The Marshalltown outcrop at Auburn appears relatively unweathered. The rock is an unconsolidated olive-gray (5 Y 4/1) to olive-black (5 Y 2/1) clayey medium-grained feldspathic quartz-glauconite sand. Small clusters of pyrite are abundant. A high percentage of the glauconite grains are accordion forms (Galliher, 1935), a characteristic of glauconite from the Marshalltown Formation (Owens and Minard, 1960, p. B430). Heavy minerals include abundant apatite and some staurolite, sillimanite, kyanite, andalusite, biotite, chlorite, chloritoid, and horndblende.

At Auburn, the Marshalltown is approximately 18 feet thick and is underlain by the very micaceous and clayey deposits of the Englishtown Formation (fig. 2). A similar relation has been observed along the strike from north of Fellowship to as far south as Auburn.

This article lists the Foraminifera recovered from the Marshalltown sample and also indicates the time-stratigraphic position of this part of the Marshalltown with respect to the Upper Cretaceous sequence of the Gulf Coastal Plain.

The Marshalltown sample contains a large foraminiferal fauna both in terms of number of specimens and number of species. Because the aim of this study was to determine the age of this part of the Marshalltown, no attempt was made to identify all the species present. More intensive analysis probably would add to the number of species.

The identified species indicate that this assemblage is of Taylor age. Two additional samples from the Marshalltown Formation near Auburn, previously examined by Ruth Todd (written communication, 1963), also contained Foraminifera of Taylor age, although fewer species were listed. The accompanying list of species (table 2) does not include data on the samples examined by Miss Todd.

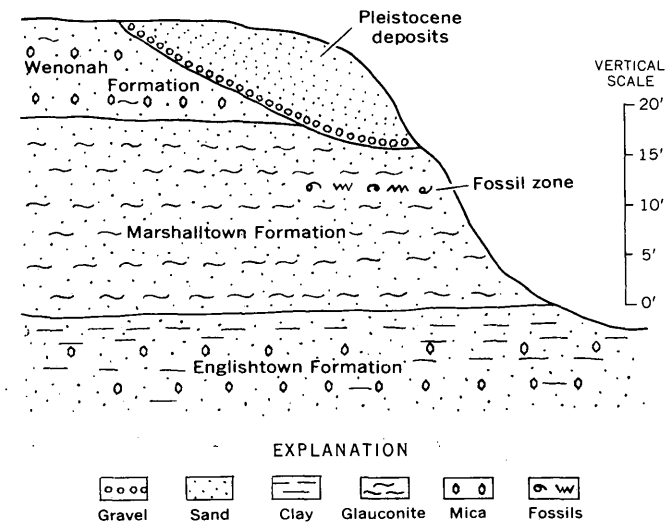

FIGURE 2.—Outcrop section at fossil locality, Camp Kimble, Auburn, N.J.

The ranges given for the identified species illustrate their known age ranges in the Cretaceous deposits of the Gulf coast. If a species has not been reported from the Gulf coast, or if its range is increased by an occurrence elsewhere, a notation is added. The correlation of L. W. Stephenson and others (1942, chart 9) between the standard European stages and the Gulf coast stratigraphic sequence is followed. The terms Austin age, Taylor age, and Navarro age are adopted from J. A. Cushman (1946), with time-stratigraphic boundaries between these units as defined by Stephenson and others (1942, p. 448, explanation of chart 9).

Of the 30 identified species, 27 occur in the Gulf coast Cretaceous deposits and all but 3 of this number have ranges that include a Taylor age. All three Gulf coast species that have not been reported from the Taylor have been reported from the Navarro. One of these species, *Fissurina marginata*, is probably nondiagnostic. Another, *Globigerina* (*Rugoglobigerina*) *rugosa*, has been reported from older beds elsewhere than on the Gulf coast. The third species, *Biglobigerinella biforaminata*, has been seen by the senior author in samples from the upper part of the Taylor Marl (Cushman Colln. 64875, 64877) and Pecan Gap Chalk Member of the Taylor Marl (Cushman Colln. 64876).

Six of the eight planktonic species are reported from beds of Austin, Taylor, and Navarro ages on the Gulf coast, or from their age equivalents elsewhere. The two species with more restricted ranges are *Globotruncana wilsoni* (Santonian) and *Hedbergella planispira* (Albian, Cenomanian, and Turonian). The age restriction presently ascribed to *G. Wilsoni* can be discounted because this species has been reported only once before. Careful comparison of the Marshalltown specimens included under *Hedbergella planispira* with the type specimens of *Globorotalia? youngi* Fox, a junior synonym of *H. planispira*, leaves no doubt that they belong in the same species. It can only be concluded that *H. planispira* is longer ranging than was previously supposed.

Pseudogaudryinella capitosa, *Nonionella austinana*, and *Bolivinitella eleyi* do not occur in beds younger than Taylor age in the Gulf coast deposits and have not been reported from younger beds elsewhere. Typical Taylor species, found in the Marshalltown sample, but which are not restricted to beds of this age, are: *Bulimina reussi*, *Dentalina basitorta*, *Eouvigerina americana*, and *Planulina taylorensis*. We conclude that the foramini-

TABLE 2.—*Foraminifera from the Marshalltown Formation near Auburn, N.J.*

Species	Recorded ranges			
	Gulf coast			Elsewhere
	Austin	Taylor	Navarro	
Anomalina rubiginosa Cushman	------	x	------	Lower Cretaceous of Australia; Tertiary of Trinidad.
Biglobigerinella biforaminata (Hofker)	------	------	x	
Bolivina incrassata Reuss	------	x	x	
Bolivinitella eleyi (Cushman)	x	x	------	
Bulimina prolixa Cushman and Parker	------	x	x	
Bulimina reussi Morrow	x	x	x	
Bulimina kickapooensis Cole	x	x	x	
Caucasina vitrea (Cushman and Parker)	x	x	x	
Dentalina basitorta Cushman	------	x	x(?)	One possible occurrence in beds of Navarro age.
Eouvigerina americana Cushman	x	x	x	Especially common in beds of Taylor age.
Fissurina marginata (Walker and Jacob)	------	------	x	Early Campanian of California; Tertiary of Trinidad.
Globigerina (Rugoglobigerina) rugosa Plummer?	------	------	x	Turonian to Maestrichtian of Trinidad.
Globotruncana cretacea Cushman	x	x	x	
Globotruncana lapparenti bulloides Vogler	------	------	------	Turonian to Maestrichtian in several areas.
Globotruncana wilsoni Bolli	------	------	------	Santonian of Trinidad.
Gyroidina depressa (Alth)	x	x	x	Eagle Ford Shale of Texas; Tertiary of Trinidad.
Hedbergella planispira (Tappan)	------	------	------	Albian, Cenomanian.
Heterohelix globulosa (Ehrenberg)	------	x	x	Santonian and Coniacian of western interior United States.
Heterohelix pulchra (Brotzen)	x	x	------	Maestrichtian of New Jersey.
Hoeglundina supracretacea (ten Dam)?	------	x	x	Hauterivian of the Netherlands; Turonian of California.
Lagena cf. *acuticosta* Reuss	x	x	x	Hauterivian of the Netherlands.
Marginulina cf. *taylorana* Cushman	------	x	x	
Neobulimina canadensis Cushman and Wickenden	x	x	x	Eagle Ford Shale of Texas.
Neobulimina spinosa Cushman and Parker	------	x	x	
Nonionella austinana Cushman	x	x	------	Cenomanian of Egypt.
Planulina taylorensis (Carsey)	x	x	x	
Pseudogaudryinella capitosa (Cushman)	x	x	------	
Pseudoglandulina cf. *lagenoides* (Olszewski)	------	x	x	
Pyrulina cylindroides (Roemer)	------	x	x	Albian of the Netherlands; Tertiary of Trinidad.
Textularia ripleyensis Berry	------	x	x	

feral evidence indicates a Taylor age for the Marshalltown sample, and that the large number of species which range into the Navarro suggest that the sample is probably of late rather than early Taylor age.

REFERENCES

Cushman, J. A., 1946, Upper Cretaceous Foraminifera of the Gulf coastal region of the United States and adjacent areas: U.S. Geol. Survey Prof. Paper 206, 241 p.

Galliher, E. W., 1935, Geology of glauconite: Am. Assoc. Petroleum Geologists Bull., v. 19, no. 11, p. 1569–1601.

Minard, J. P., Owens, J. P., and Todd, Ruth, 1961 Redefinition of the Mount Laurel Sand (Upper Cretaceous) in New Jersey: Art. 173 *in* U.S. Geol. Survey Prof. Paper 424–C, p. C64–C67.

Mumby, Joyce, 1961, Second annual field conference: Atlantic Coastal Plain Geol. Assoc. Guidebook, p. 38.

Owens, J. P., and Minard, J. P., 1960, Some characteristics of glauconite from the coastal plain formations of New Jersey: Art. 196 *in* U.S. Geol. Survey Prof. Paper 400–B, p. B430–B432.

Richards, H. G., Groot, J. J., and Germeroth, R. M., 1957, Cretaceous and Tertiary geology of New Jersey, Delaware, and Maryland: Geol. Soc. America, Guidebook for field trips, Atlantic City mtgs. 1957, p. 183–230.

Stephenson, L. W., King, P. B., Monroe, W. H., and Imlay, R. W., 1942, Correlation of the outcropping Cretaceous formations of the Atlantic and Gulf Coastal Plain and Trans-Pecos Texas: Geol. Soc. America Bull., v. 53, p. 435–448.

Weller, Stuart, 1907, A report on the Cretaceous paleontology of New Jersey: New Jersey Geol. Survey Paleontology Ser., v. 4, 871 p.

RARE-EARTH SILICATIAN APATITE FROM THE ADIRONDACK MOUNTAINS, NEW YORK

By MARIE LOUISE LINDBERG and BLANCHE INGRAM, Washington, D.C.

Abstract.—An apatite unusually rich in rare-earth oxides and silica, $R^{+3}_{3.1}(Ca,Mn)_7(SiO_4)_{2.8}(PO_4)_{3.2}F_{1.9}(OH)_{0.6}$, from the Adirondack Mountains, N.Y., contains 36.7 percent rare-earth oxides and 12.9 percent SiO_2. Unit-cell dimensions are: $a=9.43\pm0.02$, $c=6.93\pm0.015$ A; hexagonal; spaces group $P6_3/m$; uniaxial negative; $\omega=1.703\pm0.002$, $\epsilon=1.699\pm0.002$.

An apatite unusually rich in rare earths and silica, $R^{+3}_{3.1}(Ca,Mn)_7(SiO_4)_{2.8}(PO_4)_{3.2}F_{1.9}(OH)_{0.6}$, was submitted as a public sample from the Adirondack Mountains of New York. The exact locality is unknown, but the ratio of the rare-earth elements present is similar to that reported in apatite from the Mineville district, Essex County, N.Y. (McKeown and Klemic, 1956).

The rare-earth apatite here described occurs as coarse (average size 1.0 mm) anhedral grains embedded in a black glassy matrix. It is yellow to pale reddish brown. Its unusual chemical composition was first indicated by the indices of refraction, very high for an apatite mineral, of $\omega=1.703\pm0.002$, $\epsilon=1.699\pm0.002$ (uniaxial negative). The specific gravity is 3.83 ± 0.05, measured with a specific gravity bottle and toluene. The unit-cell size is: $a=9.43\pm0.02$, $c=6.93\pm0.015$ A. The apatite is partially metamict; the sharpness of the reflections and resolution of the 211–112 doublet is increased by heating. The X-ray diffraction data, given in table 1, are not unlike data of other apatite.

The chemical analysis and molecular ratios are given in table 2. The analyzed sample of apatite contained no separate grains of impurity, no visible inclusions, and was significantly free of titanium, one of the principal constituents of the matrix. The ratio of titanium in the mineral to that in the matrix is 1:500, calculated from 0.015 percent Ti in the purified apatite sample and 7 percent Ti in the matrix (Helen Worthing, written communication). Approximately three atoms of rare-earth elements, valence +3, substitute for calcium

TABLE 1.—*X-ray diffraction data on rare-earth apatite*

[Symmetry: hexagonal; space group: $P6_3/m$ (No. 176)]

Calculated [1]		Measured [2] Cu/Ni, λ=1.5418 A			
		Unheated		Heated	
hkl	d_{hkl}(A)	*I*	d_{hkl} (A)	*I*	d_{hkl} (A)
100	8. 17				
001	6. 93				
101	5. 285				
110	4. 717				
200	4. 085	6	4. 095	15	4. 073
111	3. 900	3	3. 909	12	3. 880
201	3. 519				
002	3. 465	50	3. 466	50	3. 435
102	3. 190	28	3. 193	35	3. 173
210	3. 088	14	3. 085	30	3. 087
211	2. 820	} 100	2. 811	{ 100	2. 817
112	2. 793	}		{ 50	2. 775
300	2. 723	23	2. 724	50	2. 721
202	2. 642	16	2. 647	18	2. 629
301	2. 535				
220	2. 358				
003	2. 310				
212	2. 306				
310	2. 266	8	2. 265	20	2. 263
221	2. 233				
103	2. 223				
311	2. 154	4	2. 152		
302	2. 141				
113	2. 075	10	2. 080	18	2. 069
400	2. 043				
203	2. 011				
		15	1. 949	40	1. 946
		4	1. 900	15	1. 895
		25	1. 850	60	1. 845
		4	1. 812	15	1. 828
		4	1. 780	12	1. 784
		4	1. 758	20	1. 759
		22	1. 735	35	1. 724
		4	1. 514	15	1. 507
		4	1. 464	12	1. 479
				20	1. 458
		4	1. 439	12	1. 436

[1] d_{hkl} calculated from $a=9.43\pm0.02$ A, $c=6.93\pm0.015$ A, the cell dimensions derived by precession camera techniques from unheated apatite crystals.

[2] 114.59-mm camera. Film measurements corrected for shrinkage. Lower limit of 2θ measureable approximately 7°. Intensities of reflections given for the unheated apatite are a percentage of the combined (unresolved) 211 and 112 reflections; intensities for the heated sample are in percentage of the resolved 211 reflection. Heating the apatite, which is partially metamict, increases the crystallinity; the cell size is decreased, the reflections are sharpened, and the absorption of radiation with increasing θ is decreased.

atoms, with a concomitant substitution of three SiO_4^{-4} for three PO_4^{-3} anionic groups.

The black glassy matrix in which the apatite is embedded is radioactive and metamict; the unheated sample gives no X-ray pattern. The heated samples give five broad and diffuse reflections poorly resolved from the radioactive-radiation background; the *d*-spacings (in angstrom units) are 3.08, 2.83, 2.714, 2.151, and 1.953. The patterns from heated matrix are similar but not identical with patterns of allanite and heated chevkinite. The semiquantitative spectrographic analysis of the matrix material shows Si, major; Fe, Ti, Ce, 7 percent each; Ca and La, 3 percent each; F, Nd, Pr, 0.7 percent each; Al, Gd, Nb, Sm, Y, 0.3 percent each; Mg, P, Mn, Dy, 0.15 percent each; Ag, B, Ba, Cr, Cu, Er, Eu, Ho, Lu, Mo, Ni, Pb, Sc, Sn, Sr, Tb, Tm, V, Yb, and Zr, present in quantities of <0.1 percent each (Helen Worthing, written communication).

TABLE 2.—*Chemical and spectrographic analyses of rare-earth apatite* [1]

[Analysts: Blanche Ingram, chemical analyses; Nola B. Sheffey, spectrographic analyses]

Constituent	Weight percent	Molecular ratios	Metal equivalent	Oxygen equivalent	Atoms per unit cell [2]	
Chemical analyses						
SiO_2	12.9	0.2147	0.2147	0.4294	Si	2.81
P_2O_5	17.3	.1219	.2437	.6094	P	3.19
CaO	29.7	.5296	.5296	.5296	R^{+2}	6.96
MnO	0.15	.0021	.0021	.0021		
Fe_2O_3	0.39	.0024	.0049	.0073		
Ce_2O_3	12.9	.0393	.0786	.1179	R^{+3}	3.09
RE_2O_3 [3]	23.8	.07615	.1523	.2285		
CeO_2	<0.5	<.0029	<.0029	<.0058	Ce^{+4}	<0.09
ThO_2	0.93	.0035	.0035	.0070	Th^{+4}	0.05
F	2.8	.1474		−.0737	F	1.93
H_2O [4]	0.4	.0222	.0444	.0222	H	0.58
Total	101.27			1.8855		
Less O=F	−1.2					
Total	100.07					
Quantitative spectrographic analyses [5]						
Y_2O_3	4.4	0.01948	0.03896	0.05844		
La_2O_3	5.2	.01595	.03190	.04785		
Pr_2O_3	1.2	.00363	.00726	.01089		
Nd_2O_3	6.0	.01782	.03564	.05346		
Sm_2O_3	2.7	.00774	.01548	.02322		
Eu_2O_3	0.03	.00008	.00016	.00024		
Gd_2O_3	1.4	.00386	.00772	.01158		
Tb_2O_3	0.28	.00076	.00152	.00228		
Dy_2O_3	1.1	.00294	.00588	.00882		
Ho_2O_3	0.24	.00063	.00126	.00189		
Tm_2O_3	0.09	.00023	.00046	.00069		
Er_2O_3	0.64	.00167	.00334	.00501		
Lu_2O_3	0.06	.00015	.00030	.00045		
Yb_2O_3	0.48	.00121	.00242	.00363		
Total	23.8	.07615	.1523	.2285		

[1] Formula derived from analyses: $R^{+3}_{3.1}(Ca,Mn)_7(SiO_4)_{2.8}(PO_4)_{3.2}F_{1.8}(OH)_{0.6}$.
[2] Calculated from metal and oxygen equivalents on basis of Si+P=6.
[3] Rare-earth content, excluding Ce_2O_3, which was determined both chemically (12.9 percent) and spectrographically (12.2 percent). The chemical value for Ce_2O_3 is used in the calculations, since the spectrographic method is not sensitive to the determination of small increments if the total cerium content is large.
[4] Total water by Robert Meyrowitz.
[5] Oxide values, in weight percent, calculated from a spectrographic analysis of the sample.

The unusually high content of rare-earth oxides, 36.7 percent, is well above the average rare-earth-oxide content, 11.14 percent, of 14 apatite samples from the Mineville district, Essex County, N.Y. The latter apatite contains 1–10 percent of Ce, La, Nd, Y, and 0.1–1.0 percent of Pr, Dy, Er, Gd, Yb, and Th, the same rare earths found in the new apatite; the omega index of refraction varies in the range 1.65–1.68. The apatite from the Mineville district is intergrown with fine-grained monazite and bastnaesite, minerals not identified in the apatite sample here described (data on Mineville apatites from McKeown and Klemic, 1956).

Rare-earth silicate minerals with the apatite structure include britholite (Winther and Böggild, 1901) and spencite (Frondel, 1961; Jaffe and Malinski, 1962). Britholite from Naujakasik, Greenland, contains 60.54 percent rare earths and 16.77 percent silica (Winther and Böggild, 1901); spencite from Sussex County, N.J., contains 24 percent silica and 28 percent rare-earth oxides.

REFERENCES

Frondel, Clifford, 1961, Two yttrium minerals; spencite and rowlandite: Canadian Mineralogist, v. 6, p. 576–581.

Jaffe, H. W., and Malinski, V. J., 1962, Spencite, the yttrium analogue of tritomite from Sussex County, New Jersey: Am. Mineralogist, v. 47, p. 9–25.

McKoewn, F. A., and Klemic, Harry, 1956, Rare-earth-bearing apatite at Mineville, Essex County, New York: U.S. Geol. Survey Bull. 1046–B, p. 9–23.

Winther, C., and Böggild, 1901, On some minerals from the nepheline syenite at Julianehaab, Greenland: Med. Grönland, v. 24, p. 181–213.

FERROAN NORTHUPITE IN THE GREEN RIVER FORMATION OF WYOMING

By CHARLES MILTON and ROBERT MEYROWITZ, Washington, D.C.

Abstract.—A green ferroan variety of the sodium magnesian chloro-carbonate, northupite, containing as much as 8.7 percent FeO occurs in the trona-bearing beds of the Green River Formation of southwestern Wyoming. The habit is massive or stubby striated prismatic; octahedra, in which colorless (iron-free) northupite often is found, have not been observed. The specific gravity varies, with the iron content, up to 2.52. The X-ray powder pattern is virtually identical with that of ordinary northupite. Optically, the mineral is isotropic, with indices of refraction up to 1.550.

In drill cores from holes several miles apart in the Green River Formation of Sweetwater County, southwestern Wyoming, a bright-green mineral, usually massive, sometimes prismatic, has been noted. First observed in minute quantity along with abundant ordinary colorless northupite in the John Hay, Jr., well 1 (Fahey, 1962), it appeared in relatively large quantity in the Diamond Alkali Co. Finley 2 well at a core depth of 2,196 feet, thus permitting its isolation and analysis.

It is isotropic, bright clear green, occasionally brownish green, and crystals have the prismatic habit shown in figure 1. No octahedral crystals (the common habit of northupite) have been found. It also is massive, intergrown with authigenic acmitic pyroxene, and is associated with trona, shortite, pyrite, halite, and other minerals. The index of refraction of clear-green grains is 1.550±0.002; of brownish or yellow green, slightly less; and of almost colorless grains, 1.530±0.002 (fig. 2). The specific gravity is 2.52. The deep-green prismatic northupite, with the highest measured index of refraction, grades into the massive yellow or brownish-green variety, and this in turn into the almost colorless northupite, which still, however, contains substantial iron. All the northupite contains extremely minute black opaque inclusions, possibly sulfide, that are always in relatively very small proportion, less than 1 percent.

FIGURE 1.—Deep-green striated prismatic crystals of ferroan northupite. × 20.

X-RAY POWDER DATA—ISOMORPHOUS SUBSTITUTIONS

The powder pattern of ferroan northupite matches very closely that of northupite from the John Hay, Jr., well 1 (Fahey, 1962). It also matches closely two other patterns, those of clear colorless massive northupite and dirty-greenish-yellow massive northupite, both associated with the clear-green ferroan northupite.

This virtual identity of powder patterns may be explained by the closeness of ionic radii of magnesium and

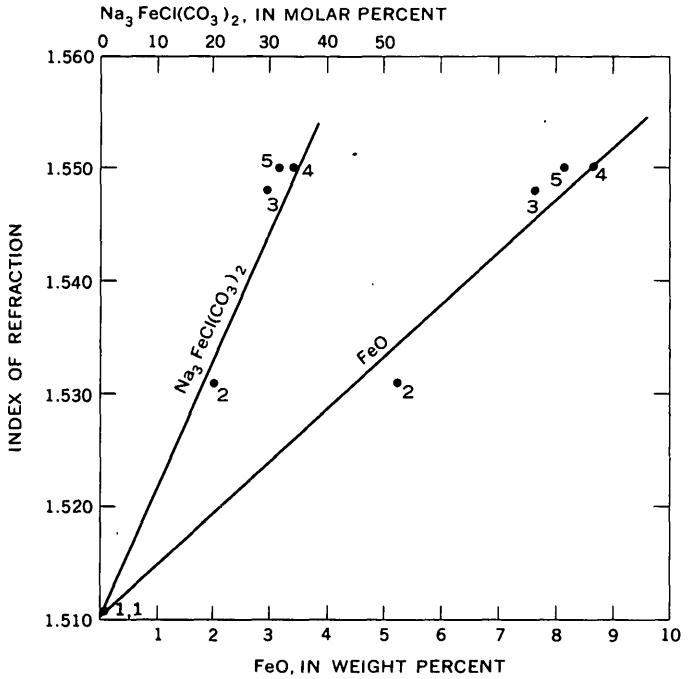

FeO	FeO (percent)		$Na_3FeCl(CO_3)_2$ (molar percent)	n	d
1. (Fahey, 1962).	0. 23	(quantitative spectroscopic).	0. 9	1. 513	2. 407
2. Almost colorless.	5. 2	(X-ray fluorescence).	20. 3	1. 531	-----
3. Yellow green.	7. 7	(X-ray fluorescence).	30. 0	1. 548	-----
4. Clear green.	8. 7	(X-ray fluorescence).	33. 9	1. 550	-----
5. Do---	8. 1	(chemical)------	31. 7	1. 550	2. 52

FIGURE 2.—Variation of index of refraction and density with FeO content in northupite.

ferrous iron (Mg, 0.78; and Fe, 0.83). Because of the virtual identity of the *d*-spacings of the John Hay, Jr., northupite, as measured by M. E. Mrose (Fahey, 1962) with those of the ferroan northupite, the cell constant, *a*, is presumably the same for both within the limits of measurement.

ANALYTICAL PROCEDURES

The selection of methods for the chemical analysis of ferroan northupite was guided by the microspectrochemical analysis of the mineral (table 1). Table 2 compares the results of the chemical analysis with the calculated compositions of the theoretical ferroan and magnesian end members. Micro- and semimicrochemical procedures were used for the various determinations upon separate splits of a sample totaling 80 mg. One portion of the sample was used for the carbon dioxide determination; a second portion for the chlorine determination; a third portion for the FeO and total iron determinations; and a fourth portion for determinations of (1+1) HCl insoluble residue, MgO, Na_2O, CaO, and K_2O.

TABLE 1.—*Microspectrochemical analysis of ferroan northupite*

[Analyst: Helen Worthing; method of analysis described by Waring and Worthing (1961) and Waring (1962)]

Elements	*Weight percent*
Na	>10
Mg, Fe	10
Ca, K	0. 3
Si, Mn	0. 1
Al, Ti, Ba	0. 03

TABLE 2.—*Microchemical analysis of ferroan northupite,* $Na_3(Mg, Fe)Cl(CO_3)_2$, *with* Mg:Fe *69:31, from Sweetwater County, Wyo.*

[Analyst: Robert Meyrowitz; analyses in weight percent]

	Ferroan northupite	$Na_3FeCl(CO_3)_2$ *(theoretical)*	$Na_3MgCl(CO_3)_2$ *(theoretical)*
Na_2O	35. 6	33. 2	37. 37
K_2O	<0. 2	--------	---------
MgO	10. 5	--------	16. 21
FeO	7. 6	25. 6	---------
Fe_2O_3	0. 6	--------	---------
CaO	<0. 2	--------	---------
CO_2	33. 6	31. 4	35. 38
Cl	13. 9	12. 7	14. 25
Insoluble residue in (1+1) HCl	2. 2	--------	---------
Subtotal	104. 0	102. 9	103. 21
O=Cl	−3. 1	−2. 9	−3. 21
Total	100. 9	100. 0	100. 00
Specific gravity	2. 52	--------	[1] 2. 407
Index of refraction	1. 550±0. 002	--------	[1] 1. 514

[1] Fahey (1962).

The first portion of the sample was decomposed by ignition at 900°C in a stream of oxygen. V_2O_5 was added to the sample to insure complete decomposition of all carbonates present. Total carbon dioxide was determined by use of a modified microcombustion train of the type used for the determination of carbon and hydrogen in organic compounds.

The second portion of the sample was dissolved in nitric acid and filtered. An aliquot of the filtrate was used for the gravimetric determination of the chlorine as AgCl. An Emich microbeaker and sintered glass filterstick were used.

The third portion of the sample was dissolved in 2.4*N* HCl. Aliquots of this solution were used for the spectrophotometric determination of FeO and total iron using o-phenanthroline. The determinations of FeO and total iron were identical except that the addition of hydroxylamine hydrochloride was omitted for the determination of FeO. The concentration of Fe_2O_3 in the sample was calculated using the values for total iron and FeO.

The fourth portion of the sample was boiled with (1+1) HCl to determine the insoluble residue. An

Emich microbeaker and sintered glass filterstick were used for the separation of the insoluble residue, which was dried to constant weight at 110°±5°C. The residue was washed with water before drying to constant weight.

Aliquots of the filtrate from the acid-insoluble determination were used for the MgO, Na_2O, CaO, and K_2O determinations.

MgO was determined by photometric microtitration with approximately 0.001 *M* standard disodium ethylenediamine tetra-acetate (Versene) using Eriochrome Black T as the indicator. Na_2O was determined by flame photometry (wavelength=589 mμ). The solution was compared to standard sodium solutions containing approximately the same concentrations of HCl, iron, and magnesium present in the solution analyzed. CaO was determined by flame photometry (wavelength=554 mμ). The solution was compared to standard calcium solutions containing approximately the same concentrations of HCl, iron, magnesium, and sodium present in the solution analyzed. K_2O was determined by flame photometry (wavelength=768 mμ). The solution was compared to standard potassium solutions containing approximately the same concentrations of HCl, iron, magnesium, and sodium present in the solution analyzed.

Total iron (as Fe_2O_3) was determined by X-ray fluorescence (table 3) in almost colorless massive and yellow-green massive northupite, and also in the associated clear-green prismatic northupite. This last has a somewhat higher iron content than the sample analyzed in table 2 (total iron as FeO, 8.7 percent compared with 8.1 percent).

TABLE 3.—*X-ray fluorescence determination of total iron in ferroan northupite*

[Analyst: Robena Brown]

Type of ferroan northupite	*Total iron as* Fe_2O_3 *(weight percent)*	*Total iron as* FeO *(weight percent)*
Almost colorless, massive	5.8	5.2
Yellow green, massive	8.4	7.6
Clear green, prismatic	9.7	8.7

The iron content of the deepest colored specimens, 8.7 percent FeO, is equivalent to about ⅓ molar ferroan northupite, and therefore is not enough to class the mineral as a species, its marked dissimilarity to ordinary northupite notwithstanding. The varietal name, ferroan northupite, however, does seem well justified.

Why this variety should form where it does, in limited zones as compared with the far more abundant and widespread virtually iron-free northupite, is not known. The necessary iron is present almost throughout the formation as pyrite and (or) pyrrhotite. Siderite, though, is extremely rare, if not absent, in much of the Wyoming trona series of the Green River Formation. W. H. Bradley (personal communication) has observed siderite associated with pyrrhotite in relative abundance in upper beds of the Tipton Shale Member of the Green River Formation below the Wilkins Peak Member in which the trona series with ferroan northupite occurs.

Various ionic modifications of the ordinary northupite structure are known, but ferroan northupite appears to be the first recognized with significant substitution of other ions for magnesium. The chlorine ion is replaced by SO_4 in the mineral tychite, and artificially, by Br^{-1} and CrO_4^{-2} (Watanabe, 1933a, b). Also, Penfield and Jamieson (1905) prepared octahedral crystals of composition $2MgCO_3 \cdot 2Na_2CO_3 \cdot MgCO_3$, presumably carbonate tychite.

The recognition of ferroan northupite in the trona series may have some economic or technologic interest in soda-ash refining, as it presents a possible source of soluble iron, which discolors the soda-ash product unless removed (W. E. Bauer, personal communication).

REFERENCES

Fahey, J. J., 1962, Saline minerals of the Green River Formation, with a section on X-ray powder data for saline minerals of the Green River Formation, by M. E. Mrose: U.S. Geol. Survey Prof. Paper 405, 50 p.

Penfield, S. L., and Jamieson, G. S., 1905, On tychite, a new mineral from Borax Lake, California, and on its artificial production and its relations to northupite: Am. Jour. Sci., 4th. ser., v. 22, p. 217–224.

Waring, C. L., 1962, The microspectrochemical analysis of minerals, II: Am. Mineralogist, v. 47, p. 741–743.

Waring, C. L., and Worthing, H. W., 1961, Microspectrochemical analysis of minerals, with an accompanying mineralogical note by Alice D. Weeks: Am. Mineralogist, v. 46, p. 1177–1186.

Watanabe, Tokonosuké, 1933a, Synthese de la northupite, de la tychite et de nouveaux mineraux de meme groupe: Tokyo, Inst. Phys. and Chem. Research, Scientific Papers, v. 21 p. 1–29.

——— 1933b, Les structures crystalline de la northupite $2MgCO_3 \cdot 2Na_2CO_3 \cdot Na_2SO_4$: Tokyo, Inst. Phys. Chem. Research, Scientific Papers, v. 21, p. 40–62.

WALSEN COMPOSITE DIKE NEAR WALSENBURG, COLORADO

By ROSS B. JOHNSON, Denver, Colo.

Abstract.—The Walsen composite lamprophyre dike of Eocene or early Oligocene age was intruded in three distinct stages into a tension joint trending normal to the northerly strike of the sedimentary wallrocks. The earliest dike was a soda-minette containing scattered xenoliths. The second dike, a minette, was emplaced along the north contact of the soda-minette. Finally, another minette was injected into shrinkage cracks in the earlier dikes.

The Walsen dike (Knopf, 1936, p. 1764), an easterly-trending composite dike of late Eocene or early Oligocene age (Johnson, 1961, p. 580) made up of three separate lamprophyric intrusives, extends for 6½ miles near Walsenburg, in south-central Colorado (fig. 1). The Walsen dike does not form a high vertical wall as do many of the nearby more silicic porphyry dikes of the Spanish Peaks radial dike system; however, the dike and the indurated sedimentary rocks adjacent to the dike form a conspicuous serrate ridge that stands 50 to 100 feet above the surrounding country.

At the surface the sedimentary rocks cut by the Walsen dike (fig. 1) include Pierre Shale, Trinidad Sandstone, Vermejo Formation, Raton Formation, and Poison Canyon Formation (Johnson, 1958, p. 563–565). The Trinidad Sandstone and Poison Canyon Formation are mainly sandstone and conglomerate; the other formations are predominantly shale. Coal occurs in the Vermejo and Raton Formations.

The Walsen dike is one of a large system of subparallel dikes that transect the radial dikes associated with the Spanish Peaks (Johnson, 1961, p. 581–586) southwest of Walsenburg. The dikes of this system extend for 36 miles from the Purgatoire River on the south to the Huerfano River on the north (Johnson and others, 1958), and they trend normal to the general strike of the folded sedimentary rocks. The strike of these dikes ranges from N. 60° E. in the southern part to N. 86° E. in the northern part of their outcrop area. It is believed that the dikes were intruded along tension fractures formed during folding of the structural Raton basin in southern Colorado and northern New Mexico (Johnson, 1961, p. 588).

Most of the dikes are lamprophyres, and many are composite or multiple. They are easily eroded and generally not well exposed. However, the Walsen dike is transected by several roadcuts, a railroad cut, and an arroyo, and thus it can be more completely studied petrographically and structurally than other composite dikes in the Spanish Peaks region.

The width of the dike is fairly uniform throughout most of its extent, varying between 20 and 30 feet. The dike is vertical, although its contacts with the enclosing rocks are locally irregular. Small high-angle reverse faults with several inches of displacement cut wallrock along the northern margin of the dike (fig. 2). The faults strike parallel to the dike, dip 60° to 70° toward the dike, and are separated vertically by as little as 10 feet. As a result of several inches of reverse dip-slip displacement along each fault, the preexisting tension fracture tends to widen upward. Otherwise, there is no apparent differential vertical displacement of the wallrock. Visible baking of the invaded sedimentary rocks extends as far as 10 feet on both sides of the dike and extends farther from the dike in shale than in sandstone and conglomerate.

PETROGRAPHY

The Walsen dike comprises three intrusives; a composite dike of soda-minette and minette, and a later minette intruded into shrinkage cracks and locally along both margins of the earlier dike (fig. 2). The composite nature of the dike was recognized by Knopf (1936, p. 1764–1765), who distinguished two intrusives, a biotite-augite vogesite, and a biotite lamprophyre. Hills (1900,

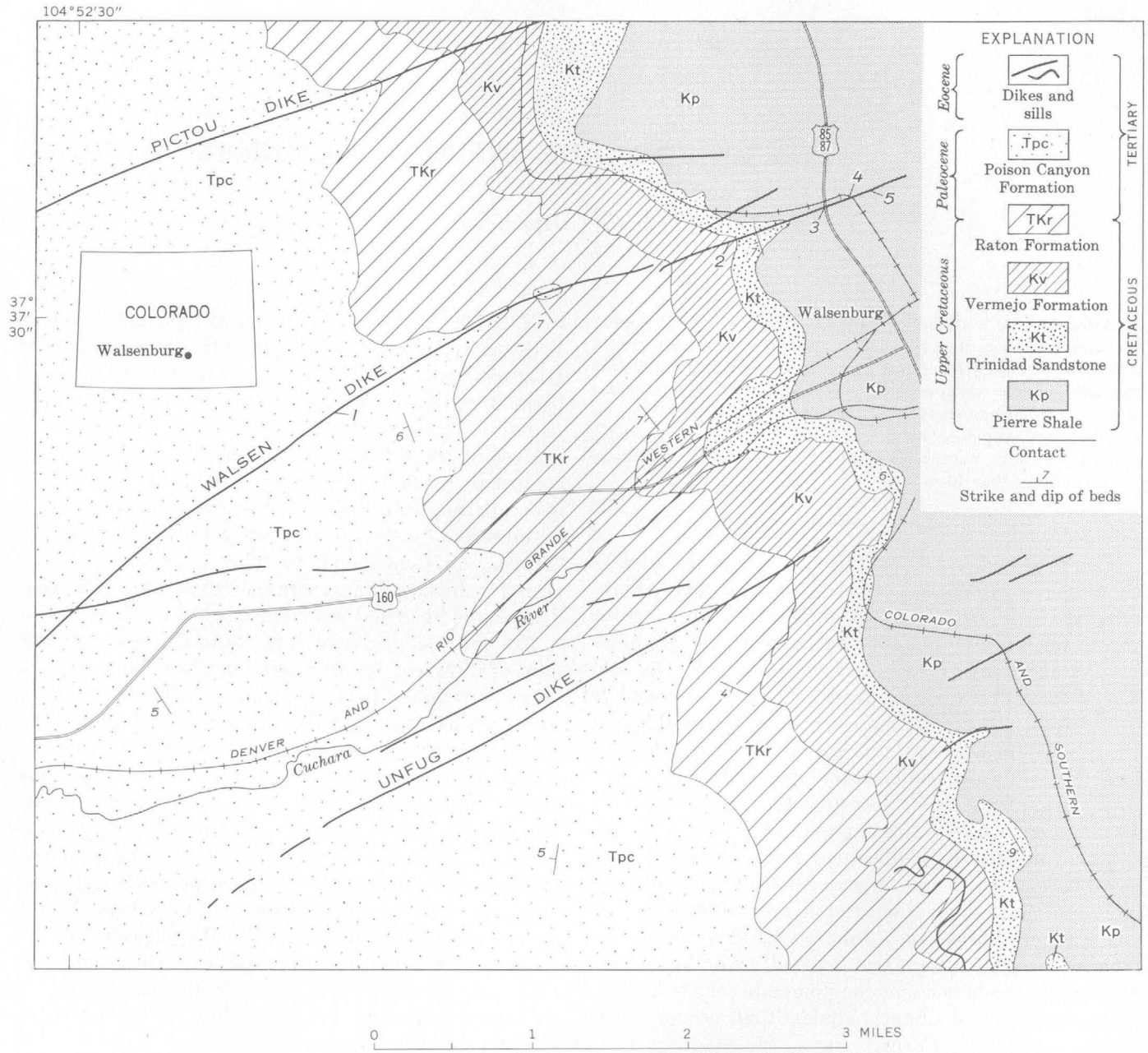

FIGURE 1.—Geologic map of the area adjacent to the Walsen dike near Walsenburg, south-central Colorado.

igneous geology sheet) apparently recognized only one intrusive and classed it as basalt.

The earliest intrusive, a greenish-gray weathered soda-minette, makes up the southeastern part of the composite dike, and ranges from 10 to 13 feet in width. It was sampled at three places (locs. *1*, *2*, and *5*, fig. 1). Phenocrysts are mainly biotite with augite as much as 2 mm across, and olivine as much as 4 mm across. The groundmass is microcrystalline and in thin section consists of analcitized sanidine, analcitized andesine (An_{35}), red and brown biotite, diopsidic augite, apatite, ilmenite, and magnetite, and locally hematite, chlorophaeite, bowlingite, iddingsite, clay, and an unidentified zeolite. The mineralogic composition (table 1) of the soda-minette varies slightly throughout the dike, but local variation is probably due to deuteric alteration. The only xenoliths found in the composite dike occur in this intrusive. At locality *1* a spherical 6-inch cobble of Precambrian gneiss is enclosed in the soda-minette. At locality *5* a highly baked angular block of Pierre Shale in almost its original orientation is separated from the south wall of the dike by 10 inches of soda-minette.

FIGURE 2.—Exposure of the Walsen dike at a highway cut on U.S. Highway 85, 87 (loc. 3) at the north limits of Walsenburg, Colo. *Kp*, Pierre Shale; *Kpm*, baked Pierre Shale; *S–M*, soda-minette intrusive; M_1, first minette intrusive; *M–Z*, mixed zone; and M_2, second minette intrusive. View is toward the southwest.

The second intrusive, a fairly hard durable light-gray minette, makes up the northwestern part of the composite dike. It ranges from 12 to 16 feet in width, but locally it is more than 20 feet wide. The minette was sampled at three places (locs. *1*, *2*, and *4*, fig. 1). Phenocrysts are mainly red biotite as much as 2 mm across with some olivine crystals as much as 4 mm across, a few augite crystals as much as 1 mm across, and local crystals of sanidine as much as 3 mm across. Under the microscope the groundmass consists of analcitized sanidine, analcitized andesine (An_{35}), red biotite, augite, apatite, ilmenite and magnetite, hematite, and locally serpentine, clay, and an unidentified zeolite.

The soda-minette (first intrusive) and the minette (second intrusive) are separated by 2 to 3 feet of fine-grained very hard and durable medium-gray micro-minette. This rock was sampled at three places (locs. *1*, *2*, and *4*, fig. 1). The microscopic phenocrysts are mainly biotite, augite, and olivine. Serpentine and zeolite replace olivine, and a few crystals of olivine are rimmed with minute augite crystals and replaced by zeolite. Some of the biotite phenocrysts show resorbed ends. The modal composition is intermediate between that of the soda-minette and the minette (table 1), but is closer to that of the minette.

The third intrusive, a minette that fills shrinkage fractures in the earlier rocks, was sampled at three localities (locs. *2*, *4*, and *5*, fig. 1). This intrusive ranges

TABLE 1.—*Average modal composition, in volume percent, of rocks of the Walsen dike*

[Compositions based on three samples from each zone]

	First intrusive (soda-minette)	Mixed zone (micro-minette)	Second intrusive (minette)	Third intrusive (minette)
Sanidine	17	26	28	24
Oligoclase(An_{25})	----	----	----	18
Andesine (An_{35})	24	22	19	----
Biotite	24	20	21	27
Augite	8	10	9	·4
Olivine	2	4	5	----
Apatite	4	3	4	4
Magnetite and ilmenite	17	15	13	11
Serpentine	----	Tr.	Tr.	2
Chlorophaeite	Tr.	----	----	----
Bowlingite	Tr.	----	----	----
Iddingsite	Tr.	----	----	----
Hematite and limonite	3	Tr.	1	7
Clay	Tr.	----	Tr.	----
Calcite	----	Tr.	----	1
Zeolite	Tr.	Tr.	Tr.	2

from 3 inches to 3 feet in width. It is a friable rock, but on fresh exposures displays conspicuous flow banding (fig. 3). Although its structure gives the rock an appearance resembling some types of spheroidal weathering, the effect is quite distinct from the small amount of spheroidal weathering noted along some of the joint surfaces in the earlier dike rocks. It is medium light gray where fresh and medium reddish brown where highly weathered. In the weathered rock, sanidine and oligoclase (An_{25}) are highly analcitized, and the rock breaks up into small pea-sized pebbles.

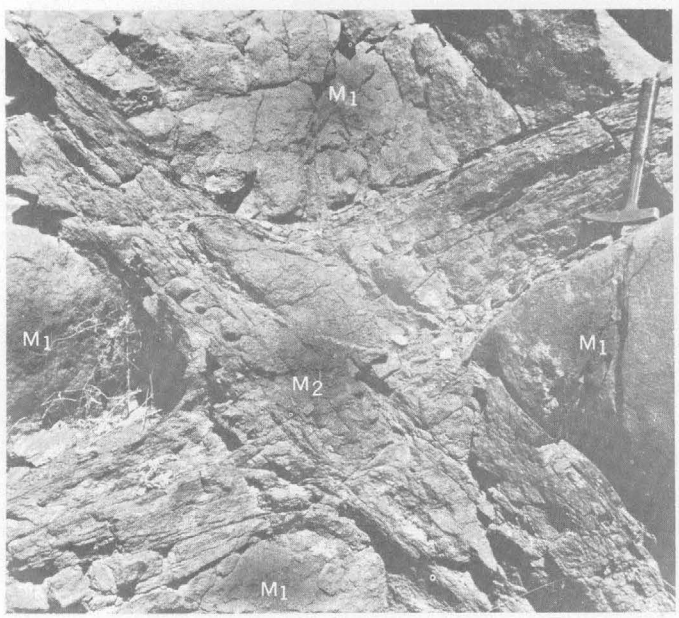

FIGURE 3.—Closeup view of the Walsen dike, showing flow-banding in a minette, M_2, here intruding an earlier minette, M_1. View is toward the north.

Red biotite occurs in serial sizes up to phenocrysts as large as 3 mm across, olivine is absent, and augite occurs as clustered small crystals in the groundmass. In all samples, small vesicles make up 1 to 6 percent of the volume of the rock and are filled by calcite and an unidentified zeolite.

TABLE 2.—*Chemical analyses, in weight percent, of rocks of the Walsen dike*

[Rocks from loc. 2 (fig. 1); rapid rock analyses by P. Elmore, S. Botts, G. Chloe, L. Artis, and H. Smith, analysts]

	First intrusive (soda-minette)	Mixed zone (microminette)	Second intrusive (minette)	Third intrusive (minette)
SiO_2	45. 3	47. 1	47. 1	46. 7
Al_2O_3	11. 2	11. 5	11. 6	10. 9
Fe_2O_3	8. 2	6. 0	6. 4	9. 5
FeO	3. 6	3. 9	3. 4	1. 8
MgO	7. 0	8. 0	8. 3	6. 8
CaO	9. 6	9. 5	9. 4	8. 6
Na_2O	2. 6	2. 6	2. 3	2. 1
K_2O	4. 0	4. 3	4. 5	4. 6
H_2O-	. 90	. 71	1. 3	2. 0
H_2O+	2. 5	2. 2	2. 2	2. 8
TiO_2	2. 3	2. 2	2. 1	2. 0
P_2O_5	2. 3	1. 3	1. 4	1. 8
MnO	. 15	. 14	. 16	. 16
CO_2	<. 05	<. 05	<. 05	<. 05
Total	100	100	100	100

TABLE 3.—*Spectrographic analyses (semiquantitative) of rocks of the Walsen dike*

[J .C. Hamilton, analyst. Results reported in percent to nearest number in the series 1, 0.7, 0.5, 0.3, 0.2, 0.15, and 0.1, etc., which represents approximate midpoints of group data on a geometric scale. The assigned group for semiquantitative results includes the quantitative value about 30 percent of the time. Symbols: M, major constituent (greater than 10 percent); 0, looked for but not detected; --, not looked for]

	First intrusive (soda-minette)	Mixed zone (micro-minette)	Second intrusive (minette)	Third intrusive (minette)
Si	M	M	M	M
Al	7. 0	M	7. 0	7. 0
Fe	7. 0	7. 0	7. 0	7. 0
Mg	3. 0	5. 0	5. 0	5. 0
Ca	M	M	M	5. 0
Na	3. 0	3. 0	3. 0	3. 0
K	5. 0	5. 0	5. 0	7. 0
Ti	1. 5	2. 0	1. 5	1. 5
P	. 7	. 5	. 5	. 5
Mn	. 07	. 07	. 07	. 05
Ba	. 5	. 7	. 7	. 5
Be	. 0002	. 0002	0	. 00015
Ce	<. 05	<. 05	<. 05	0
Co	. 005	. 005	. 005	. 003
Cr	. 03	. 05	. 05	. 03
Cu	. 01	. 01	. 01	. 015
Ga	. 003	. 003	. 003	. 007
La	. 015	. 015	. 015	. 007
Nb	. 005	. 005	. 005	. 007
Ni	. 02	. 02	. 02	. 03
Pb	. 0015	. 0015	. 0015	. 0015
Sc	. 002	. 003	. 003	. 003
Sr	. 5	. 7	. 7	. 3
V	. 05	. 05	. 05	. 03
Y	. 003	. 003	. 003	. 003
Yb	----	----	----	----
Zr	. 03	. 03	. 03	. 02
Nd	. 03	. 03	. 03	. 015

Petrographically, the minettes are typical biotite-syenite lamprophyres, and the soda-minette is a typical biotite-syenodiorite lamprophyre; the two types differ mainly in the ratio of the plagioclase feldspars to sanidine (table 1).

CHEMISTRY

The soda-minette and minette of the Walsen dike are chemically (table 2) classified as basic and unsaturated, metaluminous, and alkalic. In comparison with other syenites and syenodiorites in the Spanish Peaks region, they are high in Fe_2O_3, MgO, CaO, K_2O, H_2O, TiO_2, and P_2O_5 content (table 2); the lamprophyres of the Walsen dike also have a relatively high content of Ba, Ce, Cr, Cu, Ni, Sc, Sr, V, Zr, and Nd (table 3). The chemical analyses (table 2) indicate that the lamprophyric intrusives of the Walsen dike were derived from a low-viscosity high-volatile olivine-nepheline-basalt parent magma (table 4).

TABLE 4.—*Normative composition, in weight percent, of rocks of the Walsen dike*

	First intrusive (soda-minette)	Mixed zone (microminette)	Second intrusive (minette)	Third intrusive (minette)
or	23. 63	25. 41	26. 59	27. 18
ab	18. 38	13. 93	13. 61	17. 76
an	7. 08	7. 02	8. 04	6. 73
ne	1. 95	4. 36	3. 16	----------
mt	5. 43	6. 65	5. 39	. 53
hm	4. 46	1. 41	2. 68	9. 14
il	4. 37	4. 18	3. 99	3. 80
ap	5. 45	3. 08	3. 32	4. 26
di	19. 86	24. 61	22. 91	18. 81
hy	----------	----------	----------	3. 66
ol	5. 76	5. 96	7. 04	3. 19
Total	96. 37	96. 61	96. 73	95. 06

SEQUENCE AND MECHANICS OF EMPLACEMENT

The soda-minette magma (*S–M*, fig. 2) appears to have been the first to be intruded. During its emplacement, blocks were torn from the wallrock to form xenoliths; some were brought up from great depths, whereas others were merely separated from the wall and remained close to their original position and orientation. There does not appear to have been much melting or assimilation of the wallrock.

The second magma, a minette (M_1, fig. 2), was intruded along the north wall of the soda-minette, apparently before the soda-minette had cooled and completely solidified. The magma of the minette may have worked its way between the soda-minette and the wallrock, and then forced its way upward by separating the north wall from the soda-minette by creating a series of small reverse faults (fig. 2) which widened the fracture upward. The amount of assimilation of the invaded rock seems to have been of the same order as that for the soda-minette (table 2).

The microminette (*M–Z*, fig. 2) between the soda-minette and minette intrusives appears to be a mixture of the two rocks. Reaction rims of minute augite crystals on some of the olivine phenocrysts, partial resorption of some of the biotite phenocrysts, and a chemical composition (table 2) intermediate between the compositions of the soda-minette and minette intrusives confirm the mixed origin of this rock. It resembles a chilled margin of minette against soda-minette; however, there is no corresponding chilled margin against the sedimentary wallrock, which certainly must have been as cool or cooler than the soda-minette at the time of the invasion of the minette magma.

The third magma, a minette (M_2, fig. 2), was injected after the first two intrusives had cooled and shrunk away from the wallrock. Cracks had formed across both of the early intrusives as well as the intervening mixed zone. A magma was forced upward through these shrinkage cracks along narrow tortuous channels. At the levels now exposed the magma appears to have been more viscous than the previous two magmas. This may be demonstrated by the flow banding observed in this intrusive. However, from the chemical analyses (table 2) and from the presence of vesicles, the magma appears to have remained fairly volatile until solidified.

REFERENCES

Hills, R. C., 1900, Description of the Walsenburg quadrangle, Colorado: U.S. Geol. Survey Geol. Atlas, Folio 68.

Johnson, R. B., 1958, Geology and coal resources of the Walsenburg area, Huerfano County, Colorado: U.S. Geol. Survey Bull. 1042–0, p. 557–583.

——— 1961, Patterns and origin of radial dike swarms associated with West Spanish Peak and Dike Mountain, south-central Colorado: Geol. Soc. America Bull., v. 72, p. 579–590.

Johnson, R. B., Wood, G. H., Jr., and Harbour, R. L., 1958, Preliminary geologic map of the northern part of the Raton Mesa region and Huerfano Park in parts of Las Animas, Huerfano, and Custer Counties, Colorado: U.S. Geol. Survey Oil and Gas Inv. Map OM–183.

Knopf, Adolph, 1936, Igneous geology of the Spanish Peaks region, Colorado: Geol. Soc. America Bull., v. 47, p. 1727–1784.

ZONAL FEATURES OF AN ASH-FLOW SHEET IN THE PIAPI CANYON FORMATION, SOUTHERN NEVADA

By P. W. LIPMAN and R. L. CHRISTIANSEN, Denver, Colo.

Work done in cooperation with the U.S. Atomic Energy Commission

Abstract.—Chemical analyses from devitrified, lithophysal, and vapor-phase zones of an ash-flow sheet in southern Nevada, newly named the Yucca Mountain Member, indicate limited compositional variation. Nonwelded vitric tuff at the edges of the ash-flow sheet differs appreciably in composition from crystallized tuff because of incipient secondary alteration of metastable glass shards.

In the vicinity of the southwestern part of the Nevada Test Site (fig. 1) a previously undescribed sheet of nonwelded to densely welded ash-flow tuff wedges into the Piapi Canyon Formation. The Piapi Canyon Formation has been dated by the potassium-argon method as about 13 million years old, near the Miocene-Pliocene boundary (R. Kistler, written communication, 1963). As originally described the Piapi Canyon Formation comprises 5 members, of which 4 are ash-flow sheets—in ascending order, the Stockade Wash, Topopah Spring, Tiva Canyon, and Rainier Mesa Members (Poole and McKeown, 1962). The fifth member, the Survey Butte, consists of lithologically distinctive ash-fall tuffs into which the three lower ash-flow sheets wedge out. The newly recognized sheet occurs immediately below the Tiva Canyon Member and conformably overlies a thick sequence of bedded tuffs correlative with the Survey Butte Member. In accordance with previous designation of major ash-flow sheets of the Piapi Canyon Formation as members, the newly described sheet is here named the Yucca Mountain Member. The northwest end of the mesalike part of Yucca Mountain in the Topopah Spring 15-minute quadrangle is designated the type locality because the member is best exposed there and because all its zones are represented.

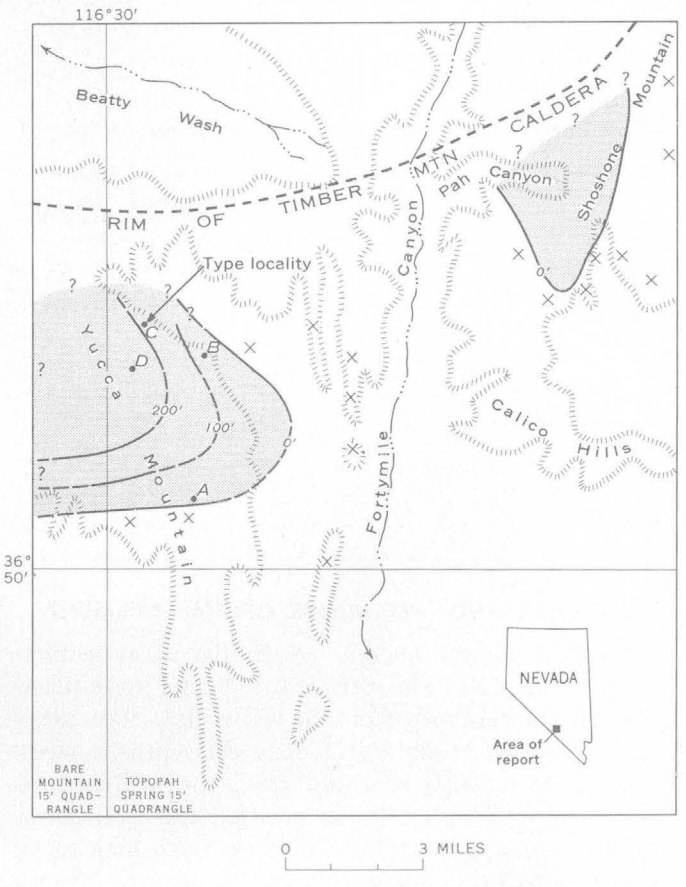

FIGURE 1.—Map of the southwestern part of the Nevada Test Site and vicinity, showing areal extent (stippled), thickness, and type locality of the Yucca Mountain Member of the Piapi Canyon Formation. Isopachs show approximate thickness; contour interval is 100 feet. ×, outcrop at which Yucca Mountain Member is absent. *A*, *B*, *C*, *D*, locations of measured sections that are shown on figure 2.

Outcrops of the Yucca Mountain Member are confined to about 20 square miles near the type locality and 5 square miles near Pah Canyon; the unit appears to have a more limited areal extent than other members of the Piapi Canyon Formation. From a maximum thickness of 250 feet near the type locality the sheet thins to the east and south. It underlies the entire west-central part of the Topopah Spring 15-minute quadrangle, and its depositional edge can be located almost continuously around the east and south sides of Yucca Mountain (fig. 1). The original distribution of the sheet has not been satisfactorily reconstructed to the north or west because of erosion, faulting, and cover by younger rocks. About 100 feet of the unit is present east of Fortymile Canyon, at Pah Canyon, and the depositional edge of the sheet has been mapped 2½ miles south of that locality. Adequate exposures demonstrate that the sheet was not deposited between Yucca Mountain and Pah Canyon, and that the two outcrop areas apparently represent the southeastern ends of separate lobes of an ash-flow sheet which originated to the north and northwest.

PETROLOGIC DESCRIPTION

The Yucca Mountain Member before welding and crystallization was a distinctively uniform shard tuff containing only very small amounts of pumice, phenocrysts, and lithic inclusions. The original character of the tuff can be determined by examination of the nonwelded glassy margins of the ash-flow sheet. Refractive indices of unaltered glass shards average about 1.50. The phenocryst content of the tuff, mainly alkali feldspar and some oligoclase, is constant at about 1 percent. Quartz and mafic minerals are scarce. Pumice typically makes up 3 to 4 percent of the tuff but increases in abundance toward the edges of the ash-flow sheet, where it locally makes up as much as 10 percent. A few small grayish-red aphanitic lithic inclusions are present. The abundance of these constituents does not vary significantly in vertical sections of the sheet. This uniformity contrasts with other major ash-flow sheets of the Piapi Canyon Formation, especially the Topopah Spring and Tiva Canyon Members, in which pumice and phenocrysts increase in abundance upward in vertical sections. Tuffs of the Yucca Mountain Member closely resemble crystal-poor pumice-poor lower parts of the Topopah Spring and Tiva Canyon Members.

Although relict shard textures and the proportions of pumice, phenocrysts, and lithic inclusions demonstrate initial vertical and lateral uniformity of the Yucca Mountain Member, differential welding and crystallization during cooling produced a variety of rocks that differ in color, density, crystallinity, and other physical properties. These variations are zonal in character and show a consistent pattern throughout the exposed part of the ash-flow sheet. Such zonal variations in welded ash flows have been discussed recently by Smith (1960). Smith's concepts of welding and crystallization zones, although based on extensive field observations, were presented as hypothetical models. The Yucca Mountain Member provides a particularly fine example to illustrate Smith's concepts because of its uniform simple composition, its uncomplicated cooling history, and because the distal end of the sheet, rarely preserved in prehistoric ash flows (Smith, 1960, p. 150), is well exposed in several places.

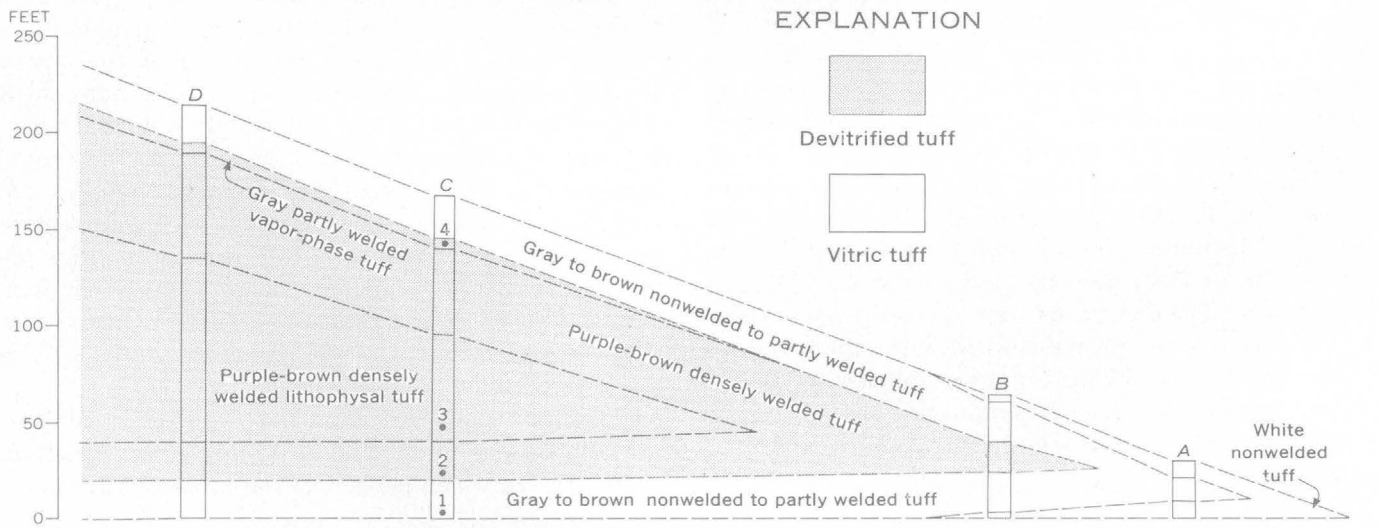

FIGURE 2.—Diagrammatic longitudinal cross section showing measured sections of the Yucca Mountain Member and schematic zonal variations of the ash-flow sheet. Numbers in section *C* indicate positions of analyzed samples (tables 1 and 2). Locations of sections shown on figure 1. The sections are plotted in order of decreasing distance from the distal edge of the sheet in such a manner as to emphasize the wedgelike character of the separate zones.

725-328 O—64——6

In Smith's terminology, the Yucca Mountain Member is a simple cooling unit. The sheet is wedge shaped in cross section (fig. 2) and on a large scale can be divided into a nonwelded to welded glassy envelope enclosing a welded devitrified core. Where the devitrified core is thickest and most densely welded, it contains an inner zone characterized by lithophysal cavities (see Smith, 1960, pl. 21L).

Most of the glassy part of the Yucca Mountain Member is nonwelded. Where the sheet is less than about 50 feet thick, the outermost part of the nonwelded zone is white to pink tuff that grades inward into gray tuff with the inception of welding. The gray tuff owes its color to magnetite crystallites, and the pink color of the peripheral tuff probably resulted from oxidation of magnetite to hematite where the outer part of the ash-flow sheet was in contact with air during cooling. Where the sheet is thicker, either nonwelded or incipiently welded gray tuff extends to the base of the sheet, and underlying ash-fall and reworked tuffs are reddened to a depth of 6 to 10 inches indicating baking by the overlying ash-flow sheet. The nonwelded vitric shard tuffs of the Yucca Mountain Member appear unaltered in hand specimen, and the shards are transparent in thin section. Fine-grained dusty material is present around the edges of the shards, however, and X-ray analysis indicates that this material is a calcic montmorillonitic clay constituting 5 to 10 percent of the glassy tuffs.

The transition from nonwelded to partly welded tuff, marked by the first recognizable deformation of shards or compaction of pumice (Smith, 1960, p. 151), is approximately coincident with a change in color from gray to orange brown or red brown. The partly welded rock commonly forms bluffs and has imperfect columnar jointing. In the area studied, devitrification extended into the zone of partial welding, and no vitrophyre zone was formed. In most places the boundary between glassy and devitrified tuff is abrupt and can be located within a few inches. The boundary between zones of partial and dense welding, being within the zone of devitrification, cannot be precisely located because the primary porosity has been obscured by crystallization. The devitrified zone typically is composed of dense purple-brown welded tuff with closely spaced platy or semiconchoidal fractures subparallel to the eutaxitic foliation. X-ray examination shows that the devitrified rock consists mainly of alkali feldspar and cristobalite.

Where the Yucca Mountain Member is thickest, the devitrified zone contains in its center a distinctive subzone characterized by lithophysal crystallization in roughly spherical to lenticular gas cavities. These cavities are as much as 5 cm in diameter and may produce as much as 25 percent bulk porosity. The lithophysal minerals are mainly alkali feldspar and tridymite.

The zone of partial welding near the top of the sheet is thin and shows evidence of vapor-phase crystallization. This vapor-phase zone is inconspicuous, mainly because drusy crystallization of alkali feldspar and tridymite in the cavities of pumice fragments, the most distinctive feature of the zone (Smith, 1960, p. 156), was limited by the scarcity of pumice in the Yucca Mountain Member. Tuff of the vapor-phase zone is pale gray, in contrast to the brownish colors of welded tuff from the main part of the devitrified zone.

CHEMICAL AND SPECTROGRAPHIC ANALYSES

Some writers (for example, Smith, 1960, p. 156) have suggested that different crystallization zones which have developed in an initially homogeneous tuff might have chemical variations as a result of volatile transfer during crystallization. The possibility of such chemical variation in the Yucca Mountain Member resulting from devitrification, formation of lithophysae, or vapor-phase crystallization was tested by a series of chemical and semiquantitative spectrographic analyses. The Yucca Mountain ash-flow sheet is in certain respects a nearly ideal unit for such a study; it is quite homogeneous in composition and has a very low content of crystals and lithic inclusions throughout. A bulk analysis approximates the composition of the glass shards. Analyses were made of samples of four lithologic zones collected from a single vertical section of the Yucca Mountain Member, as follows: (1) the basal nonwelded glassy gray shard zone, (2) the densely welded devitrified zone, (3) the lithophysal zone, and (4) the vapor-phase zone. Positions of the analyzed samples are shown in figure 2. Chemical and semiquantitative spectrographic analyses are given in table 1. For direct comparison of the cationic constituents of the four zones, the chemical analyses have been recalculated free of water and calcite and are presented in table 2 as cation percentages.

The cation percentages of the four zones sampled indicate, for the most part, strikingly little variation. Silicon averages 71.4 percent of the cations with a max-

TABLE 1.—*Chemical and spectrographic analyses of ash-flow tuffs of the Yucca Mountain Member*

[Analyses given in weight percent; numbers in boxheads refer to locations shown on fig. 2; sample numbers in parentheses]

Component	1 Nonwelded vitric zone (62L–50o)[1]	2 Densely welded devitrified zone (62L–50q)	3 Lithophysal zone (62L–50qq)	4 Vapor-phase zone (62L–50y)
Chemical analyses:[2]				
SiO_2	71.5	76.0	75.4	76.4
TiO_2	.14	.13	.14	.15
Al_2O_3	12.6	13.0	12.3	12.7
Fe_2O_3	.80	.81	.82	.94
FeO	.14	.17	.16	.03
MnO	.10	.12	.12	.10
MgO	.86	.20	.30	.07
CaO	.41	.12	.32	.18
Na_2O	2.8	4.3	4.0	4.2
K_2O	4.8	4.7	4.6	4.6
H_2O total	5.6	.68	.93	.40
CO_2	.10	<.05	.19	<.05
P_2O_5	.02	.02	.02	.03
Total	99.9	100.3	99.3	99.9
Spectrographic analyses:[3,4]				
Ba	0.01	0.01	0.01	0.01
Be	.0005	.0007	.0007	.0005
Cu	.0003	.0003	.0003	.0005
Ga	.003	.003	.003	.003
La	.003	.003	.003	.003
Mo	.001	.001	.001	.001
Nb	.002	.003	.003	.002
Pb	.005	.005	.003	.005
Sr	.005	.003	.003	.002
V	.001	.001	.002	0
Y	.003	.003	.003	.003
Yb	.0003	.0003	.0003	.0003
Zr	.02	.02	.02	.02
Powder density	2.39	2.45	2.54	2.51

[1] Refractive index of glass from the nonwelded vitric zone=1.498±0.001.
[2] By rapid methods (Shapiro and Brannock, 1962) by P. Elmore, S. Botts, G. Chloe, L. Artis, and H. Smith.
[3] By J. C. Hamilton. Results reported to the nearest number in the series 0.02, 0.015, 0.01, 0.007, 0.005, 0.003, 0.002, 0.0015, 0.001, 0.0007, 0.0005, 0.0003, which represent approximate midpoints of group data on a geometric scale. Assigned group for semiquantitative results will include the quantitative value about 30 percent of the time.
[4] Other elements looked for but not found in any specimen: Ag, As, Au, B, Bi, Cd, Ce, Co, Cr, Eu, Ge, Hf, Hg, In, Li, Ni, Pd, Pr, Pt, Re, Sb, Sc, Sm, Sn, Ta, Te, Th, Tl, U, W, Zn.

imum deviation of only 0.6 percent of that value. Total iron is virtually constant within a range of 2.5 percent of the mean value of 0.70 cation percent. The minor constituents titanium, manganese, and phosphorus are practically constant for all four zones, and the trace constituents have no major variations. The Fe^{+2}/Fe_{total} ratio is almost constant in all except the sample from the vapor-phase zone, a relation which indicates considerable oxidation in that zone.

Of the remaining cations, all except possibly magnesium are constant within the limits of determinative error for the three crystallized zones, but they vary significantly between the glassy and crystalline rocks. It is notable that crystallization from a vapor phase, either in primary pore spaces of partly welded tuff or

TABLE 2.—*Cation weight-percentage compositions of ash-flow tuffs of the Yucca Mountain Member*

[Numbers in boxheads refer to locations shown on fig. 2; sample numbers in parentheses]

Cation	1 Nonwelded vitric zone (62L–50o)	2 Densely welded devitrified zone (62L–50q)	3 Lithophysal zone (62L–50qq)	4 Vapor-phase zone (62L–50y)
Si	71.2	71.0	71.8	71.7
Ti	.10	.09	.10	.10
Al	14.8	14.3	13.8	14.0
Fe^{+3}	.60	.57	.58	.66
Fe^{+2}	.11	.13	.12	.02
Mn	.08	.09	.09	.08
Mg	1.27	.25	.42	.10
Ca	.33	.12	.13	.18
Na	5.4	7.8	7.4	7.6
K	6.0	5.6	5.6	5.5
P	.01	.01	.01	.02
Total	100.0	100.0	100.0	100.0
Fe_{total}	.71	.70	.70	.68
Fe^{+2}/Fe_{total}	.16	.18	.17	.03

in the formation of lithophysae, has no measureable effect on the bulk composition of the rocks; only the local redistribution of major elements and the oxidation of iron in the vapor-phase zone appear to have been involved.

The glassy tuff is higher in aluminum, magnesium, calcium, and potassium content and is much lower in sodium content than the crystallized rocks. Similar variations in several other paired analyses of glassy and devitrified ash-flow tuffs from the Piapi Canyon Formation indicate that these differences are not fortuitous (analyses 5 and 6 of Cornwall, 1962, table 2, are from the Tiva Canyon Member; other such analyses made by the U.S. Geological Survey and still unpublished have a similar pattern). The higher aluminum, magnesium, and calcium content of glassy tuff of the Yucca Mountain Member is explained by the presence of 5 to 10 percent calcic montmorillonitic clay coating glass shards as indicated by X-ray determination and optical estimates. The significance of the excess potassium in the glass is not entirely clear; possibly potassium has been added by base exchange within the glass. Although low sodium and high calcium content might indicate some base exchange between the clay mineral or the glass and ground water, only a small part of the sodium deficiency can be explained in this way. Considerable additional sodium would appear to have been leached from the metastable glass by percolating fluids. The noted presence of similar chemical patterns for other paired analyses indicates that leaching of sodium and formation of montmorillonitic clays may be common alteration features of rhyolitic glasses. Analyses

of even apparently fresh glasses should be regarded with some caution as representatives of an original magma.

REFERENCES

Cornwall, H. R., 1962, Calderas and associated volcanic rocks near Beatty, Nye County, Nevada, *in* Engel, A. E. J., and others, eds., Petrologic studies (Buddington volume) : New York, Geol. Soc. America, p. 357–371.

Poole, F. G., and McKeown, F. A., 1962, Oak Spring Group of the Nevada Test Site and vicinity, Nevada: Art. 10 *in* U.S. Geol. Survey Prof. Paper 450–C, p. C60–C62.

Smith, R. L., 1960, Zones and zonal variations in welded ash flows: U.S. Geol. Survey Prof. Paper 354–F, p. 149–159. [1961]

Shapiro, Leonard, and Brannock, W. W., 1962, Rapid analysis of silicate, carbonate, and phosphate rocks: U.S. Geol. Survey Bull. 1144–A, p. A1–A56.

A WELDED-TUFF DIKE IN SOUTHERN NEVADA

By P. W. LIPMAN, Denver, Colo.

Work done in cooperation with the U.S. Atomic Energy Commission

Abstract.—A small welded-tuff dike in an ash-flow sheet is thought to represent an underlying nonwelded tuff that was remobilized and intruded into a dilatant tensional fracture in the still-hot sheet.

During mapping of the 7½-minute Thirsty Canyon SE quadrangle in southern Nevada, a small tuff dike with welded pyroclastic textures was observed in intrusive contact with ash-flow tuff wallrock. Although a relatively minor feature, this dike is significant because pyroclastic intrusives, despite relatively widespread occurrence, rarely show compaction or welding features and are not known to occur within ash-flow sheets as feeders (Smith, 1960a, p. 817–818). A welded-tuff dike might readily be interpreted as a fissure vent, but in the present occurrence, substantial evidence favors an alternative interpretation—that the dike is part of a stratigraphically lower ash-flow tuff that was emplaced upward into hot dilatantly fractured volcanic country rock. Such an origin would be analogous to formation of clastic sandstone dikes.

The dike occurs at lat 37°02′15″ N., long 116°35′12″ W. (about 15 miles northeast of Beatty, Nev., at the Nevada Test Site), in a talus block near the contact between two petrologically distinct cooling units[1] of ash-flow tuff of the Rainier Mesa Member of the Piapi Canyon Formation (Pliocene or younger) (Poole and McKeown, 1962). The lower cooling unit of the Rainer Mesa Member is nonwelded to partly welded near the dike locality and contains 20 to 30 percent phenocrysts (varying mainly with degree of welding). The dominant phenocrysts are alkali feldspar and quartz, with minor plagioclase. Biotite forms 1 percent or less of the phenocrysts, and clinopyroxene is very scarce (absent in most thin sections). The upper cooling unit, eroded at its top, is densely welded to its base at the dike locality and averages about 35 percent phenocrysts. Its phenocryst proportions contrast strikingly with those of the lower cooling unit—plagioclase is almost twice as abundant as quartz, biotite averages 4 to 5 percent of the phenocrysts, and augite is fairly abundant.

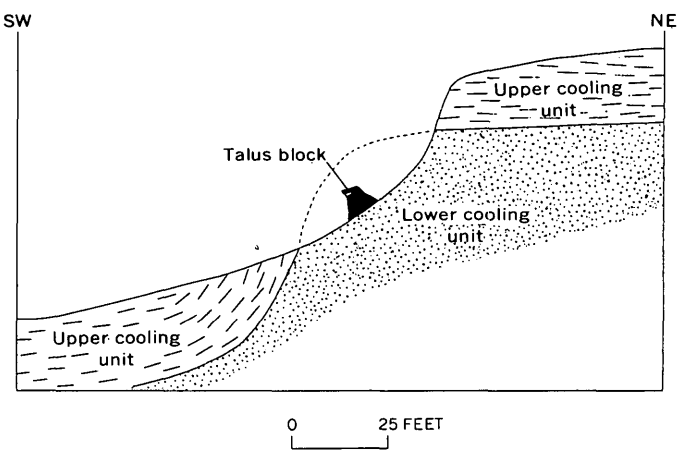

FIGURE 1.—Sketched cross section, showing relations between lower cooling unit and upper cooling unit of the Rainier Mesa Member, and location of talus block containing the dike. Patterning of upper cooling unit indicates approximate orientation of eutaxitic foliation.

The upper cooling unit overlies the lower cooling unit unconformably, but the surface of uncomfority is barely discordant in most places. In a few places, including the dike locality, the upper cooling unit was deposited on an irregular surface of several hundred feet of relief eroded on the lower cooling unit. Zones of welding in the lower cooling unit are truncated, and the compaction foliation of the upper unit dips at high angles, locally approaching vertical. The structural relations between the two cooling units at the dike locality are shown in figure 1.

[1] Terminology of ash-flow tuffs as used by Smith (1960a, 1960b).

The dike is nowhere exposed in place. The talus block in which it occurs is about 5 feet across and lies about 20 feet below the base of the upper cooling unit (fig. 1). Despite the detrital nature of this block, the original position of the dike can be closely determined because of certain zonal welding and crystallization changes in the upper cooling unit. Both the wallrock of the dike and the lithologically similar basal part of the upper cooling unit are dark gray because of the presence of abundant microlites of magnetite. Since the upper cooling unit changes color and becomes red brown about 10 feet above its base because of oxidation of the magnetite microlites to hematite, the block containing the dike must have come from within a few feet of the contact between the upper and lower cooling units.

The dike is red brown, in contrast to the dark-gray wallrock; it has generally planar parallel contacts and averages about 16 inches in width (fig. 2). Its exposed length is about 4 feet. It truncates the well-developed eutaxitic foliation of its country rock at about 65° and contains a lenticular inclusion of the country rock oriented parallel to the walls of the dike. The eutaxitic foliation of the inclusion is at an angle of about 25° to foliation in the wallrock, indicating rotation of the inclusion during emplacement of the dike. This inclusion shows that the dike was emplaced after welding of the upper cooling unit. The pyroclastic texture of the dike is obscure in outcrop, but is evident in thin section (fig. 3). Pumice lapilli are thoroughly compacted and are parallel to sides of the dike at a large angle to foliation in the wallrock.

Petrographically the dike closely resembles tuff of the lower cooling unit of the Rainier Mesa Member, except that it shows a greater degree of welding. The proportions of major and minor phenocrysts are strikingly similar. As in the lower cooling unit, the phenocrysts in the dike are mainly alkali feldspar and quartz, with little plagioclase; only about 1 percent of biotite is present, and clinopyroxene is absent. Figure 4,

FIGURE 2.—Welded-tuff dike cutting upper cooling unit of the Rainier Mesa Member. Dark inclusions in center of dike are recognizable wallrock. Pencil on wallrock shows scale.

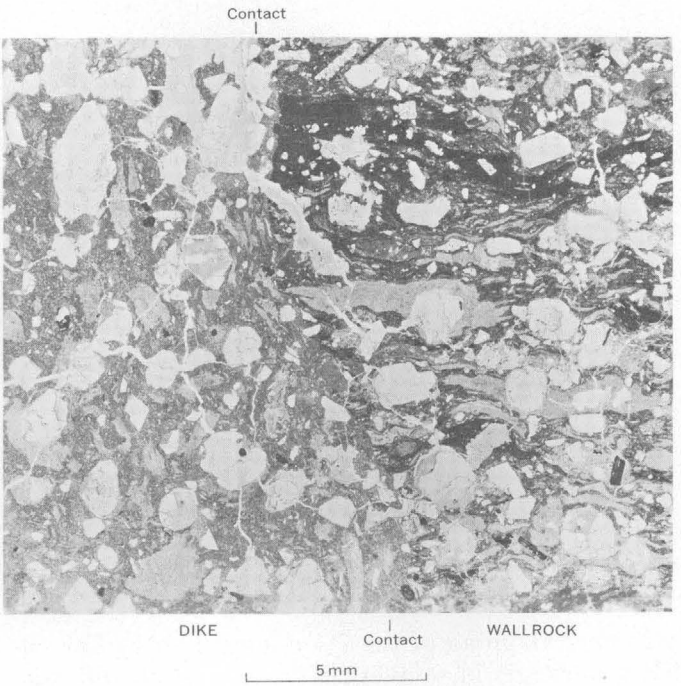

FIGURE 3.—Photomicrograph showing truncation of wallrock foliation by eutaxitic foliation of dike.

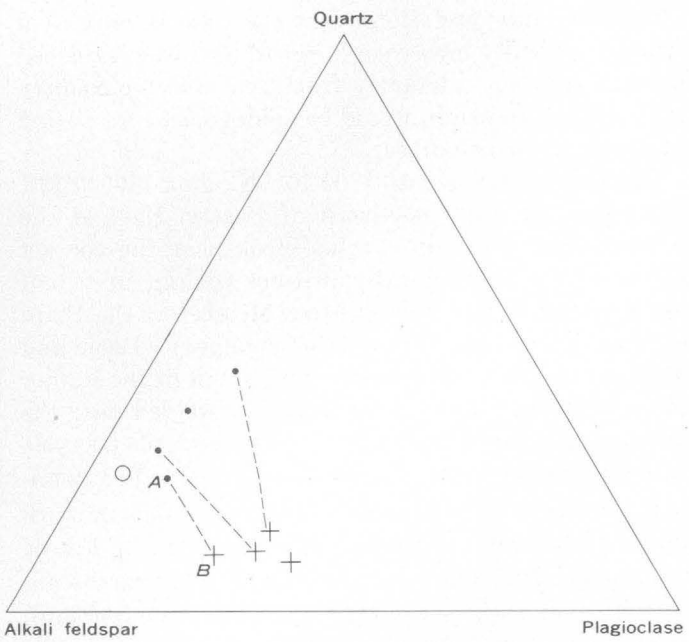

FIGURE 4.—Triangular diagram showing variations in proportions of quartz and feldspar phenocrysts in the dike (open circle), the lower cooling unit (dots), and the upper cooling unit (crosses) of the Rainier Mesa Member. Dashed lines are tie lines connecting samples from the same vertical section.

based on modal counts of 1,400 to 2,000 points in single thin sections, shows proportions of feldspar and quartz, which together account for most of the phenocrysts in both ash-flow and dike rocks. All samples of the Rainier Mesa Member were collected within 1 mile of the dike locality and either within a few feet above the base of the upper cooling unit or within a few feet below the uppermost exposures of the lower cooling unit. Samples *A* and *B* are from an outcrop immediately above the dike locality. The compositional range of the lower cooling unit is greater than that of the upper, probably because irregular erosion of its top has led to sampling of different despositional levels within the cooling unit. In contrast, all samples of the upper cooling unit should be from the same depositional level, and the spread of points for these samples in figure 4 probably represents the expectable degree of scatter from sampling and counting inaccuracies.

The petrologic similarity of the dike to the lower cooling unit and the structural position of the dike only a few feet above the contact between cooling units strongly suggest that the dike was formed by secondary mobilization of tuff from the lower cooling unit and that it is not a primary igneous feature. By this hypothesis the heat for welding ("fusion") of the dike would have come from the wallrock, and intrusion of the dike would have immediately followed emplacement and welding of the upper cooling unit. Perhaps a tensional fracture developed in the upper cooling unit as a result of small-scale flowage during welding and compaction on a slope and provided structural control for intrusion of the dike. The nonwelded tuff of the lower cooling unit then would have been mobilized by the pressure potential arising from dilatant fracturing, perhaps assisted by expansion and volatilization of interstitial water heated by the overlying ash-flow sheet. A similar mechanism of emplacement has been deduced by Walton and O'Sullivan (1950) for a clastic sandstone dike that was injected into a hot dolerite sill.

REFERENCES

Poole, F. G., and McKeown, F. A., 1962, Oak Spring Group of the Nevada Test Site and vicinity, Nevada: Art. 80 *in* U.S. Geol. Survey Prof. Paper 450–C, p. C60–C62.

Smith, R. L., 1960a, Ash flows. A review: Geol. Soc. America Bull., v. 71, p. 795–842.

Smith, R. L., 1960b, Zones and zonal variations in welded ash flows: U.S. Geol. Survey Prof. Paper 354–F, p. 149–159. [1961]

Walton, M. S., Jr., and O'Sullivan, R. B., 1950, The intrusive mechanics of a clastic dike: Am. Jour. Sci., v. 248, p. 1–22.

A NEW URANYL TRICARBONATE, $K_2Ca_3(UO_2)_2(CO_3)_6 \cdot 9–10H_2O$

By ROBERT MEYROWITZ, DAPHNE R. ROSS, and MALCOLM ROSS, Washington, D.C.

Abstract.—A new uranyl tricarbonate, $K_2Ca_3(UO_2)_2(CO_3)_6 \cdot 9–10H_2O$ has been synthesized using $UO_2(NO_3)_2 \cdot 6H_2O$, K_2CO_3, and $Ca(NO_3)_2 \cdot 4H_2O$. The green-yellow crystals show parallel extinction. They are biaxial positive, $2V=20°–30°$; $\alpha=1.544\pm0.003$, $\beta=1.549\pm0.003$, and $\gamma=1.563\pm0.003$ (white light). The measured and calculated specific gravities are 2.93 and 3.01 g/cm^3 respectively. The compound is orthohombic, space group *Pnmn* (No. 58) or *Pn2n* (No. 34), with $a=17.98$ A, $b=18.29$ A, $c=16.95$ A, V=5,574 A^3, and Z=8. Two quantitative chemical analyses and X-ray powder data are given.

A new uranyl tricarbonate, $K_2Ca_3(UO_2)_2(CO_3)_6 \cdot 9–10H_2O$, has been synthesized. This green-yellow crystalline compound was obtained either alone or with liebigite, $Ca_2UO_2(CO_3)_3 \cdot 10H_2O$, using K_2CO_3 as a source of the carbonate (Meyrowitz and others 1963). Its powder X-ray diffraction pattern is identical to that of a crystalline substance obtained by M. E. Thompson (oral communication, 1953) while attempting to synthesize liebigite by a procedure similar to that used by Axelrod and others (1951) in the synthesis of bayleyite.

The initial crop of crystals obtained by M. E. Thompson by allowing the solution containing the proper salts to evaporate at room temperature contained potassium. At that time (1953) the compound was considered to be an unknown substance because its powder X-ray diffraction pattern could not be identified. Because this compound formed in so many experiments performed by Meyrowitz in 1958, we decided it was a stable compound worth further investigation. The following reproducible procedure for the synthesis of this compound was developed.

Twenty milliliters of an aqueous solution containing 5.02 grams $UO_2(NO_3)_2 \cdot 6H_2O$ equivalent to 0.01 mole UO_3 is added dropwise with constant stirring to 200 ml of an aqueous solution containing 4.15 g anhydrous K_2CO_3 equivalent to 0.03 mole CO_2. The mixed solution is allowed to stand until the small amount of yellow amorphous precipitate that forms coagulates and settles to the bottom of the beaker. The mixture is filtered through a fine filter paper. Twenty ml of an aqueous solution containing 3.54 g $Ca(NO_3)_2 \cdot 4H_2O$ equivalent to 0.015 mole CaO is added slowly with constant stirring to the filtered solution. The pH of the solution is then adjusted to 8.5 by the dropwise addition of a dilute solution of K_2CO_3. The beaker is sealed with a plastic film to retard evaporation and is allowed to stand for approximately 4 weeks. The crystals are then detached from the sides and bottom of the beaker and washed a few times by decantation with water. Most of the excess water is removed by rolling the crystals on absorbent paper. The crystals (some as large as 1×4 mm) are finally air dried.

Two preparations of the compound were analyzed (table 1) by semimicrochemical procedures. Carbon dioxide was determined on one portion of each sample by decomposing with HCl and absorbing the CO_2 in a microabsorption train. Water was determined on a second portion with a modified microcombustion train of the type used for carbon and hydrogen determinations in organic compounds. The samples were decomposed by ignition at 900°C in a stream of oxygen. The third portion of each sample was dissolved in dilute nitric acid, and aliquots of this solution were used for determining UO_3, CaO, and K_2O. UO_3 was determined spectrophotometrically with ammonium thiocy-

TABLE 1.—*Chemical composition of a new uranyl tricarbonate* [1]

[Analyst: Robert Meyrowitz; analyses in weight percent]

Constituent	*Sample SRM-8*	*Sample SRM-10*	$K_2Ca_3(UO_2)_2(CO_3)_6 \cdot 9H_2O$ *(theoretical)*	$K_2Ca_3(UO_2)_2(CO_3)_6 \cdot 10H_2O$ *(theoretical)*
K_2O	7.6	7.4	7.4	7.4
CaO	14.0	14.4	13.3	13.2
UO_3	44.3	44.8	45.4	44.7
CO_2	20.7	20.7	21.0	20.6
H_2O	13.7	12.9	12.9	14.1
Total	100.3	100.2	100.0	100.0

[1] Specific gravity, 2.93

TABLE 2.—*X-ray powder data for* $K_2Ca_3(UO_2)_2(CO_3)_6 \cdot 9\text{–}10\ H_2O$ [1]

[Sample SRM-10]

I(A)[2]	d(A) (meas.)	d (A) (calc.)[3]	hkl	I(A)[2]	d (A) (meas.)
		12.82	110	6	3.40
		12.43	011	2	3.34
		12.33	101	5	3.28
		10.23	111	6	3.22
		9.15	020	6b	3.17
		8.99	200	6	3.15
100	8.7	8.48	002	9b	3.13
		7.94	201	14	3.10
		7.67	102	9b	3.07
		7.35	121	6	3.05
		7.28	211	4	3.02
		7.07	112	4	2.96
36	6.40	6.41	220	4	2.93
4	6.25	6.22	022	7	2.91
		6.17	202	11	2.86
7	6.03	6.00	221	4	2.83
13	5.95	5.87	122	18	2.75
		5.84	212	7	2.72
		5.77	130	2	2.70
4	5.73	5.74	031	4	2.63
		5.70	310	4	2.60
		5.65	301	4	2.59
11	5.50	5.47	131	6	2.57
		5.40	311	4	2.52
4	5.43	5.40	013	9	2.50
		5.39	103	4	2.478
46	5.17	5.17	113	4	2.445
		5.11	222	6	2.428
6	4.94	4.89	302	6	2.421
		4.84	231	7	2.412
		4.81	321	4	2.406
		4.78	203	7	2.371
		4.77	132	7	2.366
		4.73	312	7	2.358
		4.64	123	6	2.352
31	4.60	4.63	213	6	2.313
		4.57	040	4	2.225
11	4.51	4.50	400	6	2.203
11	4.37	4.34	401	7	2.148
		4.34	232	4	2.143
20	4.32	4.31	322	6	2.111
		4.29	141	16	2.105
		4.27	330	11	2.100
		4.24	223	7	2.092
		4.24	004	7	2.087
14	4.21	4.23	411	4	2.069
4	4.17	4.14	331	4	2.064
		4.14	033	6	2.052
		4.12	104	7	2.040
		4.11	303	6	2.036
24	4.06	4.08	240	7	2.018
		4.04	133	6	2.014
		4.03	420	4	1.995
		4.02	042	4	1.924
11	4.00	4.02	114	11	1.913
		4.01	313	11	1.908
9	3.96			4	1.826
7	3.92			11	1.766
11	3.82			7	1.761
24	3.59			4	1.708
9	3.55			9	1.701
14	3.51			7	1.696

[1] CuKα radiation, Ni filter (λ=1.5418 A) Camera diameter: 114.59 mm. Lower limit d measurable: approximately 11.0 A.

[2] Intensities were measured with a calibrated intensity strip.

[3] d-spacings were calculated from the following unit-cell data: orthorhombic, *Pnmn*, a=17.98 A, b=18.29 A, c=16.95 A. All calculated spacings ≥ 4.00 permitted by the space group are listed.

anate in an acetone-water medium. CaO was determined by flame photometry (wave length=554 mμ). The solution was compared with standard calcium solutions containing approximately the same concentration of uranium and potassium present in the solution analyzed. K_2O was determined by flame photometry (wave length=768 mμ). The solution was compared with standard potassium solutions containing approximately the same concentration of uranium and calcium present in the solution analyzed. The specific gravity (sample SRM–10) was determined by the hydrostatic weighing method. A 5-ml Erlenmeyer flask and toluene were used. The sample size for the specific-gravity determination was approximately 600 milligrams.

Single-crystal studies of $K_2Ca_3(UO_2)_2(CO_3)_6 \cdot 9\text{–}10H_2O$ (sample SRM–10) were made with the Buerger precession camera using molybdenum (λ=0.7107 A) and copper (λ=1.5418 A) radiation. Patterns were taken of the *hk*0, 0*kl*, *hkl*, 1*kl*, and 2*kl* reciprocal lattice nets. The compound is orthorhombic, space group *Pnmn* (No. 58) or *Pn2n* (No. 34), with a=17.98 A, b=18.29 A, c=16.95 A, V=5,574 A^3, and Z=8. The calculated (for $K_2Ca_3(UO_2)_2(CO_3)_6 \cdot 9H_2O$) and observed specific gravities are 3.01 and 2.93 g/cm^3, respectively. The indexed X-ray powder data for this compound are given in table 2.

The optical properties of sample SRM–10 as determined by Thomas L. Wright, U.S. Geological Survey, using white light are: biaxial positive, α=1.544±0.003, β=1.549±0.003, γ=1.563±0.003, and 2V=20°–30°. The crystals show parallel extinction.

The synthetic compound described in this article belongs to a group of compounds in which the uranyl tricarbonate complex is the only anion. However, the new substance is the only member of this group in which the ratio of monovalent to divalent cations is 2:3. The other members of the group have either all monovalent cations, all divalent cations, or a ratio of monovalent to divalent cations of 2:1.

REFERENCES

Axelrod, J. M. Grimaldi, F. S., Milton, Charles, and Murata, K. J., 1951, The uranium minerals from the Hillside mine, Yavapai County, Arizona: Am. Mineralogist, v. 36, p. 1–22.

Meyrowitz, Robert, Ross, D. R., and Weeks, A. D., 1963, Synthesis of liebigite: Art. 43 *in* U.S. Geol. Survey Prof. Paper 475–B, p. B162–B163.

FRACTIONATION OF URANIUM ISOTOPES AND DAUGHTER PRODUCTS IN WEATHERED GRANITE AND URANIUM-BEARING SANDSTONE, WIND RIVER BASIN REGION, WYOMING

By J. N. ROSHOLT, E. L. GARNER,[1] and W. R. SHIELDS,[1]
Denver, Colo., Washington, D.C.

Abstract.—Isotopic ratios of U^{235}/U^{234} for three samples representing different stages of weathering of granite show 7 to 23 percent deficient U^{234}. The slightly weathered rock is most deficient, suggesting major U^{234} leaching at an early stage in the decomposition. Isotopic ratios in samples from a uranium deposit in sandstone showed slight excess U^{234} in unoxidized sandstone and up to 72 percent excess U^{234} in parts of the adjoining oxidized sandstone characterized by relatively high uranium content. Th^{230}/U^{234} ratios indicate relatively recent deposition of redistributed uranium in parts of the oxidized sandstone where the U^{234}/U^{235} ratio is high. The low U^{234}/U^{235} ratios prevailing in uranium-poor parts of the oxidized sandstone are believed to have resulted from preferential leaching of U^{234} in these places and over a considerable time.

The use of abundance of uranium isotopes in geochronology of the Pleistocene, as suggested by Thurber (1962, 1963), in Pa^{231}/Th^{230} chronology (Rosholt and others, 1961), and in Th^{230}/Th^{232} chronology (Goldberg and Koide, 1962), depends on an extensive knowledge of the fundamental physico-chemical behavior of U^{234} daughter product in relation to parent U^{238} in hydrologic environments. It has been shown that significant fractionation exists between U^{234}, with a 250,000-year half life, and the longer lived isotopes, U^{238} and U^{235}, in sandstone-type uranium deposits (Rosholt and others, 1963). Most phases of the hydrologic environment should be investigated, including the environmental effect on uranium in its ultimate source, igneous rocks. Preferential leaching of U^{234} from a variety of rock types has been demonstrated by measurements of U^{234}/U^{238} ratios in waters draining uranium-bearing host rocks (Ancarani and Bettinali, 1960; Koshelev and Syromyatnikov, 1961). Ratios of U^{234}/U^{238} and Th^{230}/Th^{234} in natural waters, fossil bones, soils, and shells of fresh-water mollusks have been investigated by Cherdyntsev and others (1963).

More detailed study of the mechanism of fractionation, starting from the ultimate source of uranium and progressing through the hydrologic cycle of uranium, is needed to throw light on the specific controls involved.

This article compares the U^{235}/U^{234} fractionation pattern observed in 3 samples of granite from the Owl Creek Mountains, Wyo., with that noted in 11 samples of ore and barren rock taken across the contact of a typical roll-type sandstone deposit of uranium in the adjoining Gas Hills area of the Wind River basin, Wyo. In addition, the study of the variation of the radioactive-equilibrium ratios of Th^{230} to U^{234} and of Pa^{231} to U^{235} or U^{238} within the part of the deposit sampled provides a further useful tool in working out the mechanism of uranium-isotope fractionation. Investigation of uranium-bearing sandstones that have been saturated with ground water provide a desirable area for preliminary study because of the abundant supply of uranium and extensive geological and geochemical knowledge of this type of deposit.

PROCEDURE

Isotopic ratios of uranium were measured on a 12-inch, 60°-sector mass spectrometer (Rosholt and others, 1963). Uranyl nitrate was prepared from the rock samples by extraction with ethyl acetate after dissolution of uranium from rock or ore with concentrated nitric acid. Sufficient sample was used to yield from 1 to 5 milligrams of uranium. Approximately 50-microgram uranium aliquots of the uranyl nitrate solution

[1] National Bureau of Standards.

were used for each mass-spectrometric measurement. Variations of the ratios were determined by comparison of the ratios of $U^{235}/^{234}$ and $U^{235}/^{238}$ in the National Bureau of Standards reference sample with ratios in the sample. The reference sample is Republic of Congo pitchblende ore. No significant variations in the U^{235}/U^{238} ratio were found at the ½-percent confidence level in the samples.

Direct comparison of isotopic ratios in reference standards and in samples is shown in tables 1 and 2. Illustration of the roll feature shows the relation of each sample to its percentage isotopic variation, δ, where

$$\delta \text{ (percent)} = 100\left[\frac{U^{235}/U^{234} \text{ (reference)}}{U^{235}/U^{234} \text{ (sample)}} - 1\right],$$

as shown in figure 2. The isotope-ratio term in the above equation is shown in tables 1 and 2. The numerical result is the same as the U^{234}/U^{235} (sample) ratio, expressed in radioactive equivalent units; and the ratio is stated in this form in much of the subsequent discussion. Since no significant variation in the U^{235}/U^{238} ratio occurs, U^{234} daughter is frequently compared to U^{238} parent rather than to U^{235}. Radiochemical methods (Rosholt, 1957; Rosholt and Dooley, 1960) were used for the determination of the radioactive daughter products in the decay series below uranium. The results for these daughter products and for U^{234} in table 3 are expressed as equivalents to the parent nuclides in terms of percent equivalent.

GRANITE

Samples of weathered granite, weighing approximately 5 pounds each, were collected from Copper Mountain in the Owl Creek Mountains which flank the north side of the Wind River basin, as shown by Woodmansee (1958, fig. 1). It is not known whether this particular granite contributed to the detritus making up a large part of the upper coarse-grained facies of the Wind River Formation in the Gas Hills area (Zeller, 1957, p. 157); however, in general, it may be similar to granite which contributed uranium and sediments to a typical intermontane basin. Fresh rock could not be obtained from the outcrops at Copper Mountain. The fresh granite sample (256179) was taken from a drill core at a 50-foot depth in granite on the south side of Heath's Peak, sec. 14, T. 27 N., R. 84 W., in the Pedro Mountains, Carbon County, Wyo. (Bell and Harshman, report in preparation). Uraninite is known to occur in granite in this area, and the rock sampled is apparently mineralized, as indicated by its uranium content.

The results in table 1 show a correlation between the U^{234}/U^{235} ratio and the degree of weathering. The slightly decomposed granite has the lowest U^{234}/U^{235} ratio, indicating that U^{234} is preferentially leached with respect to U^{238} and U^{235} at an early stage in the decomposition of the rock. Enrichment by uranium with a higher U^{234}/U^{235} ratio may have occurred in the very weathered rock, as indicated by the anomalously high uranium content.

URANIUM-BEARING SANDSTONE

Uranium-ore samples from sandstone were collected by D. H. Norton, U.S. Atomic Energy Commission, in 1958 from the south pit wall of Lucky Mc Project 4A mine, sec. 26, T. 33 N., R. 90 W., Gas Hills area, Fremont County, Wyo. The deposit is in the Wind River Formation of the Wind River basin and has been described by Zeller (1957, fig. 1), together with the stratigraphy and structure of the Gas Hills area.

The lithologic features shown in figure 1 indicate a contact between oxidized and unoxidized sandstone in the wall of the mine, several feet below the water table. Normally, in this area, sandstone is oxidized above the water table and unoxidized below; thus, oxidized sandstone on the concave side of the contact may be the result of a geochemical process different from the surface oxidation above the water table. Somewhat similar contacts between altered and unaltered sandstone have been reported in deposits below the water table in the Shirley basin (Harshman, 1962, fig. 122.1). Results of analyses of 18-inch vertical channel samples taken at approximately 6-inch intervals across the contact are shown in tables 2 and 3.

TABLE 1.—*Isotopic ratios of uranium in granite samples from Fremont and Carbon Counties, Wyo.*

USGS sample number	*Degree of weathering*	*Uranium* [1] *(percent)*	U^{235}/U^{234} (reference) / U^{235}/U^{234} (sample)	U^{235}/U^{238} (reference) / U^{235}/U^{238} (sample)
256179 [2]	Very fresh	0.040	0.9907	1.0027
256175	Slightly weathered	.002	.7677	1.0041
256176	Weathered	.002	.8852	1.0014
256177 [2]	Very weathered	.013	.9251	1.0045

[1] Uranium analyses by fluorimetric method by E. J. Fennelly, U.S. Geological Survey.
[2] Relatively high uranium content; may be mineralized.

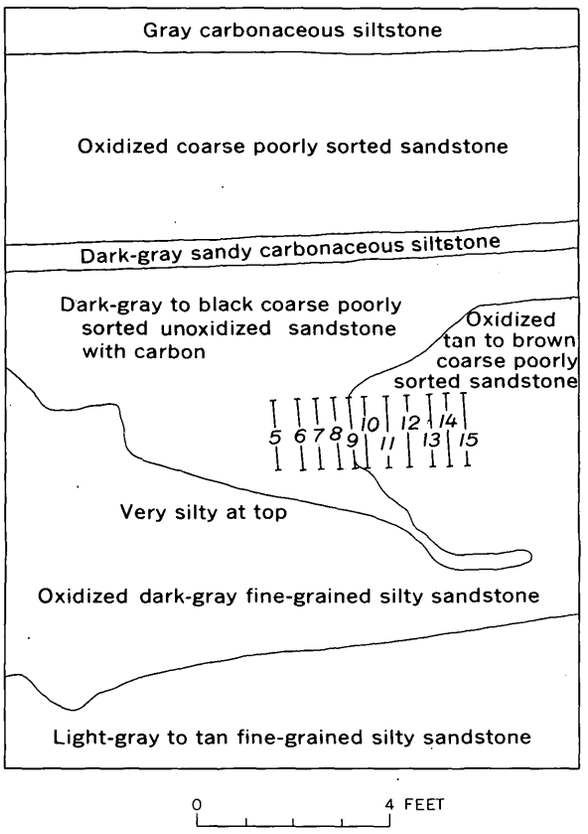

FIGURE 1.—Geologic section showing lithology and location of channel samples taken across oxidized-unoxidized sandstone contact in the wall of the Lucky Mc Project 4A mine, Gas Hills area, Fremont County, Wyo. Redrawn from photograph taken by D. H. Norton, U.S. Atomic Energy Commission.

TABLE 2.—*Isotopic ratios of uranium in sandstone samples from Gas Hills roll, Fremont County, Wyo.*

USGS sample No.	Field No. (figs. 1 and 2)	U^{238}/U^{234} (reference) / U^{238}/U^{234} (sample)	U^{235}/U^{238} (reference) / U^{235}/U^{238} (sample)
273084	15	0.8464	1.0016
273085	14	1.718	1.0019
273086	13	1.630	1.0027
273087	12	.9283	1.0009
273088	11	1.604	1.0033
273089	10	1.369	.9985
273090	9	1.292	1.0012
273091	8	1.014	1.0014
273092	7	1.096	1.0027
273093	6	.9930	1.0019
273094	5	.9688	1.0015

TABLE 3.—*Radioactive disequilibrium analyses of sandstone samples from Gas Hills roll, Fremont County, Wyo.*

[Isotopes given as percent equivalent of parent nuclide, except as noted]

USGS sample No.	Field No. (figs. 1 and 2)	U^{238} (percent)	Pa^{231}	U^{234}	Th^{230}	Ra^{226}	Rn^{222}	Pb^{210}
273084	15	0.004	0.01	0.003	0.004	0.010	0.01	0.010
273085	14	.018	.02	.031	.004	.010	.01	.009
273086	13	.030	.03	.049	.006	.012	.01	.010
273087	12	.004	.01	.004	.004	.013	.01	.011
273088	11	.018	.02	.029	.005	.019	.02	.017
273089	10	.062	.07	.085	.011	.10	.10	.092
273090	9	.11	(1)	.14	.04	.05	.04	.052
273091	8	.50	.54	.51	.52	.14	.10	.12
273092	7	.52	.52	.57	.58	.14	.12	.12
273093	6	.091	.08	.090	.11	.032	.03	.023
273094	5	.010	.02	.010	.014	.016	.02	.014

[1] Pa^{231} could not be determined because of exceptionally high content of Ac^{227}. Analyses for additional isotopes in this sample: Th^{232}, 0.01 percent; Ac^{227}, 0.86 percent equivalent.

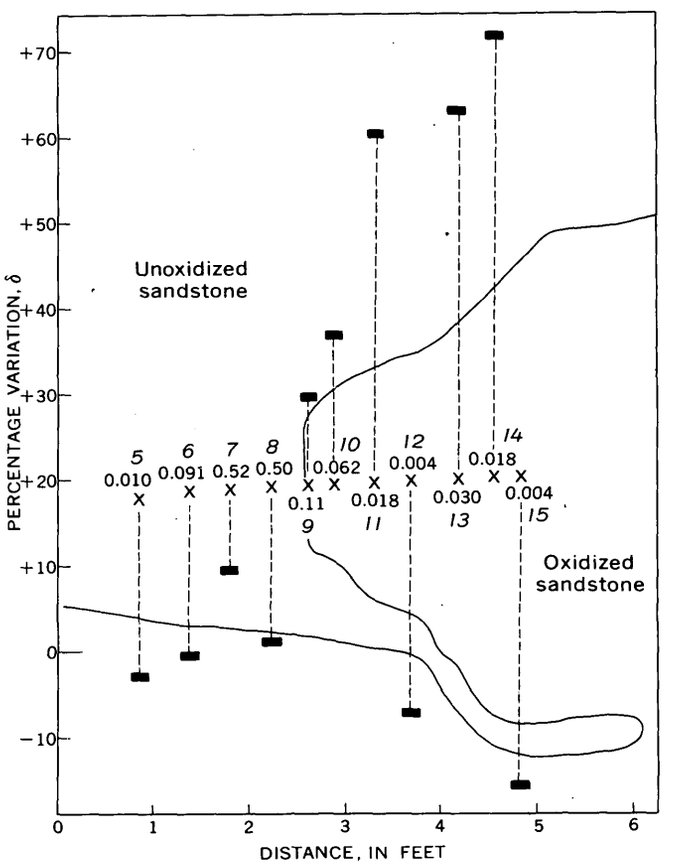

FIGURE 2.—Variations of percentage total uranium (numbers) and percentage $U^{235/234}$ ratio, δ, (solid blocks) across the oxidized-unoxidized sandstone contact in the Lucky Mc Project 4A mine. Locations of midpoints of individual channel samples are denoted by ×. Italic numbers are field numbers referred to in tables 2 and 3.

Comparison of the percentage isotopic variation, δ, of U^{234}/U^{235} ratios for each sample, together with the uranium content indicated at the location of each channel sample, is shown in figure 2. The peak concentration of uranium occurs in a 1½-foot interval in the unoxidized sandstone near the oxidized contact, and slight enrichment in uranium occurs at a few places in the oxidized sandstone. U^{234}/U^{235} ratios show a large excess of U^{234} in the more uraniferous samples of oxidized sandstone and a slight excess to a slight deficiency of U^{234} in the unoxidized sandstone. Two samples (12 and 15) with low uranium content are deficient in U^{234}.

At the peak concentration of uranium, as shown by the data in table 3, Pa^{231} and Th^{230} are present in radioactive-equilibrium amounts with uranium-isotope parents, U^{235} and U^{234}, respectively. This indicates that the process of uranium accumulation began at least

100,000 years ago. Th^{230} is deficient at the places of slight uranium enrichment in the oxidized sandstone, suggesting that the excess U^{234} accumulation was a relatively recent event. The relation of low Th^{230} content to high U^{234} content in the oxidized sandstone suggests deposition of uranium from ground water containing a high concentration of uranium enriched in U^{234}. This probably represents redistribution of uranium with a high U^{234}/U^{335} ratio derived by preferential leaching of U^{234} from nearby deposits undergoing slight oxidation. The two samples with low uranium content may be from part of the sampled mine wall with a small amount of uranium which has been in place for a considerable length of time; some of the U^{234} has been preferentially leached from these two samples. A similar low uranium content with deficient U^{234} may have existed throughout the oxidized sandstone; this effect may be masked by redistributed uranium that was deposited erratically at a later time.

CONCLUSIONS

To describe the mechanism of uranium-isotope fractionation, it has been suggested (Rosholt and others, 1964) that total U^{234} is contributed in two ways to the environment in which it is found: (1) those atoms that have been mixed and transported with U^{238} and U^{235} remain with these two isotopes and are not subject to removal by preferential leaching, and (2) atoms generated in place from the radioactive disintegration of U^{238} are subject to differential migration with respect to the U^{238}. One result of the latter process is a deficiency of U^{234} caused by its being preferentially leached from a uranium source in the solid phase; on the other hand, small amounts of excess U^{234} can result from accumulation, on particulate matter, of its parent isotopes, Th^{234} and Pa^{234}, generated from soluble U^{238} in pore water.

The weathered granites are primarily examples of the second type that show a deficiency of U^{234} from preferential leaching. Samples of uranium-enriched areas in oxidized sandstone in the Gas Hills suite are examples of the first type. These oxidized sandstones give the following clue that may be useful in many occurrences of excess U^{234}. The presence of excess U^{234}, together with considerably less than equilibrium amounts of Th^{230}, indicates relatively recent accumulation of transported uranium.

REFERENCES

Ancarani, L., and Bettinali, C., 1960, Analisi isotopica dell'Uranio e dello Zolfo nello studio delle mineralizzazioni di Canale Monterano: Studi e Ricerche della Divisione Geomineraria, v. III. Comitato Nazionale per le Ricerche Nucleari, Roma, p. 1–22.

Cherdyntsev, V. V., Kazachevski, I. V., and Kuzmina, E. A., 1963, Istotopic composition of uranium and thorium in the zone of hypergenesis. Investigation of fossil bones, soil and shells of mollusks: Geokhimiya, no. 3, p. 254–266.

Goldberg, E. D., and Koide, M., 1962, Geochronological studies of deep sea sediments by the ionium/thorium method: Geochim. et Cosmochim. Acta, v. 26, p. 417–435.

Harshman, E. N., 1962, Alteration as a guide to uranium ore, Shirley Basin, Wyoming: Art. 122 in U.S. Geol. Survey Prof. Paper 450–D, p. D8–D10.

Koshelev, I. P., and Syromyatnikov, N. G., 1961, Some regularities in the migration of uranium-234 and uranium-238 isotopes: Fzvest. Akad. Nauk Kazakh. SSR, Ser. Geol., no. 3, p. 73–82.

Rosholt, J. N., Jr., 1957, Quantitative radiochemical methods for the determination of the sources of natural radioactivity: Anal. Chem., v. 29, p. 1398–1408.

Rosholt, J. N., Jr., and Dooley, J. R., Jr., 1960, Automatic measurements and computations for radiochemical analyses: Anal. Chem., v. 32, p. 1093–1098.

Rosholt, J. N., Jr., Emiliani, C., Geiss, J., Koczy, F. F., and Wangersky, P. J., 1961, Absolute dating of deep-sea cores by the Pa^{231}/Th^{230} method: Jour: Geology, v. 69, p. 162–195.

Rosholt, J. N., Jr., Harshman, E. N., Shields, W. R., and Garner, E. L., 1964, Isotopic fractionation of uranium related to roll features in sandstone, Shirley Basin, Wyoming: Econ. Geology. [In press]

Rosholt, J. N., Jr., Shields, W. R., and Garner, E. L., 1963, Isotopic fractionation of uranium in sandstone: Science, v. 139, p. 224–226.

Thurber, D. L., 1962, Anomalous U^{234}/U^{238} in nature: Jour. Geophys. Res., v. 67, p. 4518–4520.

——— 1963, Natural variation in the ratio U^{234}/U^{238} and an investigation of the potential of U^{234} for Pleistocene chronology: Columbia Univ. Ph. D. thesis, 153 p.

Woodmansee, W. C., 1958, Ground water in sandstone-type uranium deposits: United Nations Internat. Conf. on Peaceful Uses of Atomic Energy, 2d, Geneva, 1958, v. 2, p. 351–357.

Zeller, H. D., 1957, The Gas Hills uranium district and some probable controls for ore deposition: Wyo. Geol. Assoc. Guidebook, 12th Ann. Field Conf., p. 156–160.

HAFNIUM CONTENT AND Hf/Zr RATIO IN ZIRCON FROM THE SOUTHERN CALIFORNIA BATHOLITH

By DAVID GOTTFRIED and CLAUDE L. WARING, Washington, D.C.

Abstract.—The hafnium content and the Hf/Zr ratio in zircon indicate a progressive enrichment of hafnium in relation to zirconium from the mafic to the more siliceous rocks. Zircon from the gabbro studied contains 1.0 percent hafnium and has a Hf/Zr ratio of 0.020. Zircon from the granite has a hafnium content ranging from 1.3 to 2 percent and Hf/Zr ratios ranging from 0.027 to 0.040. Within the rocks of a single stock of Woodson Mountain granodiorite, hafnium and the Hf/Zr ratio are highest in the zircon of finest mesh sizes.

Zircon is one of the most common accessory minerals in the igneous rocks of the southern California batholith and occurs in variable amounts in rocks ranging in composition from gabbro to granite. Because hafnium and zirconium are one of the best known pairs of geochemically coherent elements, a study of the hafnium content and Hf/Zr ratio in zircon was undertaken to determine the behavior of hafnium during magmatic differentiation and perhaps to shed some light on the paragenesis of zircon. Earlier data for zircon from rocks of this batholith were summarized and briefly discussed (Gottfried and others, 1959) with regard to the much debated problem of the crystallization history of zircon. This article presents the results obtained on additional samples of zircon from a wide range of chemically analyzed rocks to show (1) the relation of hafnium and the Hf/Zr ratio in zircon to the bulk composition of the host rock, (2) the variation of Hf and the Hf/Zr ratio in zircon from rocks from a single stock, and (3) the variation of Hf and the Hf/Zr ratio in zircon fractions of different mesh size from the same rock.

The hafnium content and the Hf/Zr ratio were determined with a direct-reading spectrometer using a 1-milligram sample of zircon mixed with 5 mg of graphite and arced for 3 minutes in a controlled atmosphere [Waring, 1964, p. B146 (this chap.)]. The method yields results reproducible to better than ±5 percent as determined by replicate analyses.

Cross checks with data obtained by X-ray fluorescence show satisfactory agreement.

SOUTHERN CALIFORNIA BATHOLITH

Forty analyses for hafnium and the Hf/Zr ratio of zircon concentrates separated from 32 rocks ranging in composition from gabbro to granite are listed in table 1. Nearly all these rocks are similar to those studied by Larsen (1948) and Everhart (1951). Chemical analyses are available for 27 of the rocks; figure 1 shows how the hafnium content and Hf/Zr ratio in zircon vary with the chemical composition of the rocks. The position of each rock in figure 1 is calculated, from its chemical analysis, by the method described by Larsen (1938).

The lowest hafnium content (1.00 percent) and Hf/Zr ratio (0.020) are found in zircon from the gabbroic rocks. In the 8 tonalites studied the zircon averages 1.10 percent hafnium and has a Hf/Zr ratio of 0.022. The data in table 1 show a wide variation in the hafnium content and Hf/Zr ratio in zircon from the different types of granodiorite. Those variations that exceed the experimental error appear to be related to significant differences in the chemical composition and relative age of the rocks. Another factor that helps account for the observed variation in hafnium content and Hf/Zr ratio is related to variations in grain size of the zircon.

Figure 2 summarizes data on zircon from 10 rocks from a single stock of Woodson Mountain Granodiorite located a few miles below Temecula, Calif. Particularly striking are the variations between 100–200- and 200–325-mesh zircon separated from the same rock. In each instance the finer mesh zircons have a higher

TABLE 1.—*Hafnium content and* Hf/Zr *ratio in zircon from igneous rocks of the southern California batholith*

Sample No.	Mesh size	Rock type	Position ⅓ SiO_2+ K_2O-CaO-FeO-MgO	Hafnium content (percent)	Hf/Zr ratio
SM	100–200	San Marcos Gabbro		1.00	0.020
BL 60–5	100–200	San Marcos Gabbro (quartz-biotite-norite)	+1.9	1.00	.020
BL 60–6	100–200	Green Valley Tonalite	+1.5	1.05	.021
G–3	100–200	Tonalite		1.01	.021
BL 60–1BB	100–200	Bonsall Tonalite		1.10	.022
BL 60–1B	100–200	Inclusion in BL 60–1BB	−6.2	1.10	.022
Z–19	100–200	Bonsall Tonalite		1.15	.023
LTS–3 [1]	100–200	do	+9.4	1.05	.021
BL 60–1	100–200	do	+9.5	1.10	.022
S–1	100–200	Lakeview Mountain Tonalite	+8.7	1.20	.024
BL 60–2	100–200	do	+8.6	1.10	.022
G–13	100–200	Granodiorite	+15.6	1.12	.024
BL 60–7	100–200	Indian Mountain Leucogranodiorite (granodiorite)	+22.0	1.24	.025
BL 60–8	100–200	Stonewall Formation (granodiorite)	+16.9	1.25	.025
S–17	100–200	Woodson Mountain Granodiorite		1.28	.027
S–9	100–200	do	+20.6	1.28	.026
	100–200			1.30	.026
S–8	100–200	do	21.2	1.32	.027
	200–235			1.48	.030
S–13	100–200	do	+22.2	1.32	.027
	200–325			1.35	.028
S–2	100–200	do	+23.2	1.37	.028
LTS–4 [1]	100–200	do	+23.9	1.40	.029
S–11	100–200	do	+22.9	1.35	.027
S–12	100–200	do	+26.4	1.50	.030
	200–325			1.60	.032
S–15	100–200	do	+24.3	1.35	.027
	200–325			1.60	.032
S–14	100–200	do	+25.7	1.28	.026
	200–325			1.37	.028
S–10	100–200	do	+28.8	1.37	.028
	200–325			1.65	.033
S–6	100–200	do	+20.9	1.60	.033
G–12	100–200	do	+26.5	1.48	.030
Z–17	100–200	Mount Hole Granodiorite	+22.4	1.75	.035
	200–325			1.80	.036
El 38–167	100–200	Quartz monzonite of Rubidoux Mountain, coarse phase.	+25.5	1.32	.026
LTS–2	100–325	do	+26.1	1.60	.032
El 38–265	100–200	Quartz monzonite of Rubidoux Mountain fine phase	+27.7	1.73	.036
BL 60–4	100–200	Roblar Leucogranite (granite)	+27.4	1.32	.026

[1] Provided by Dr. L. T. Silver, Dept. of Geology, California Institute of Technology.

hafnium content and Hf/Zr ratio. Moreover, it was found that there is a strong tendency for the zircon in the more siliceous rocks of this stock to be concentrated in the finer mesh sizes. Hence it is clear that an analysis on a particular fraction of zircon is not necessarily representative of all the zircon in the rock. Taking into consideration the relative amounts of zircon in the different size fractions, the data show a progressive increase in the hafnium content and Hf/Zr ratio in zircon from the relatively mafic to the more siliceous granodiorite. Zircon from rocks most typical of this stock average about 1.35 percent hafnium and have a Hf/Zr ratio of about 0.028.

Zircon of the porphyritic Mount Hole Granodiorite, which is younger than the Woodson Mountain Granodiorite (Larsen, 1948), has a minimum hafnium content (1.75 percent) and a minimum Hf/Zr ratio (0.035) greater than zircon from any other granodiorite in this study. Zircon from the quartz monzonite of Rubidoux Mountain and granite contains from about 1.32 to 1.73 percent hafnium and has a Hf/Zr ratio ranging from 0.026 to 0.036, thus overlapping the range shown by zircon of the granodiorite.

MOJAVE DESERT AREA

The hafnium content and Hf/Zr ratio of zircon from a granodiorite, quartz monzonite, and five samples of granite from satellitic instrusions exposed in the desert ranges east of the batholith are listed in table 2. Zircon from one of these granites (G–24) has a greater hafnium content (2.02 percent) and Hf/Zr ratio (0.042) than any of the zircon from the batholithic rocks listed in table 1. These few data also show the enrichment of hafnium in zircon in the more siliceous rocks.

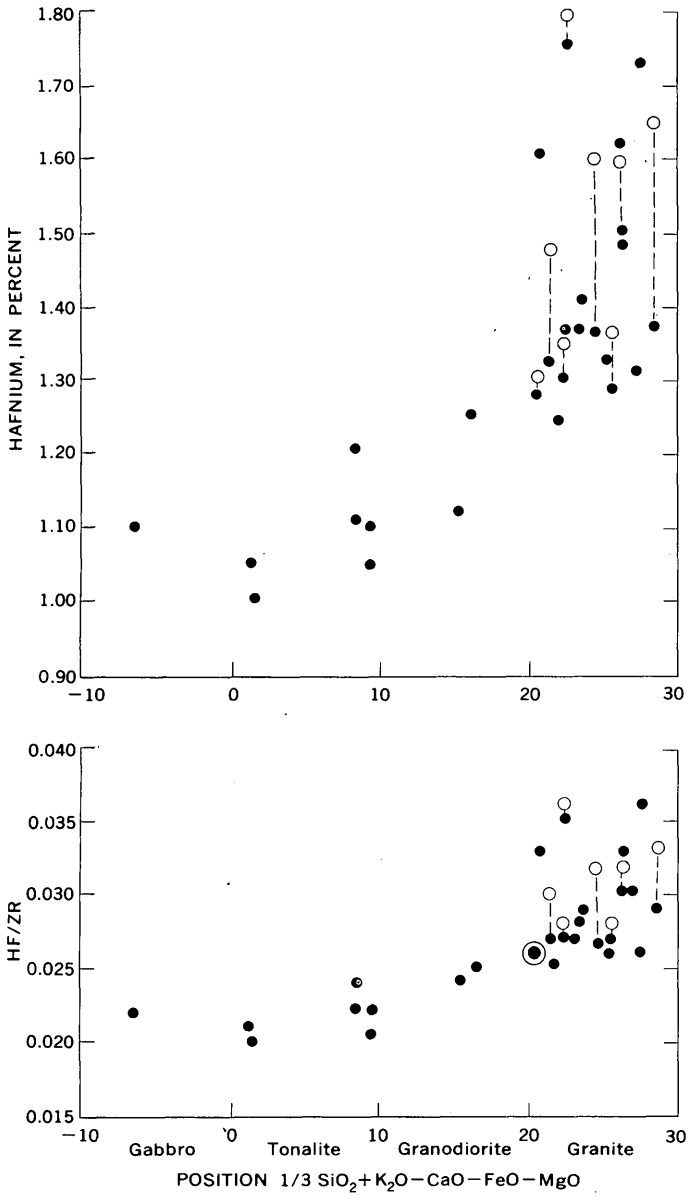

FIGURE 1.—Hafnium content and Hf/Zr ratio in zircon plotted against composition of the rocks. Dots, 100–200-mesh-size zircon; circles, 200–325-mesh-size zircon.

TABLE 2.—*Hafnium content and Hf/Zr ratio in zircon from igneous rocks of the Mojave Desert*

Sample No.	Mesh size	Rock type	Hafnium content (percent)	Hf/Zr ratio
RCE–28 A	100–200	Granodiorite	1. 15	0. 023
RCE–14 C	do	Quartz monzonite	1. 40	. 028
RCE–18 A	do	Granite	1. 35	. 027
RCE–27 C	do	do	1. 45	. 029
RCE–14 B	do	do	1. 60	. 032
RCE–28 B	do	do	1. 60	. 032
G–24	do	do	2. 02	. 042

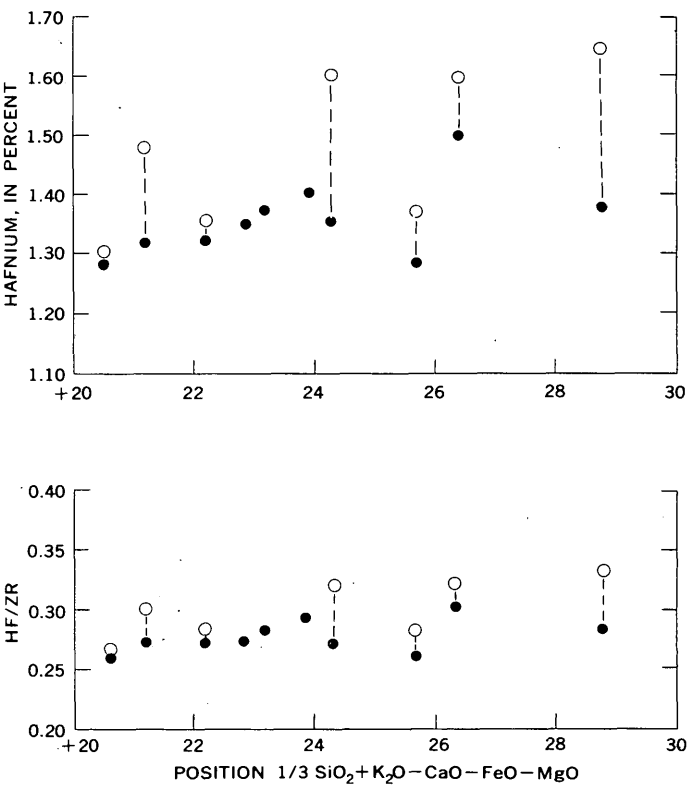

FIGURE 2.—Hafnium content and Hf/Zr ratio in zircon of analyzed rocks from a stock of Woodson Mountain Granodiorite. Dots, 100–200-mesh-size zircon; circles, 200–325-mesh-size zircon.

DISCUSSION

If it is assumed that the zirconium present in the rocks is contained in zircon and that the zircon analyzed is representative of the zircon in the rocks, the data presented above provide a basis for following the behavior of hafnium relative to zirconium during crystallization of the batholithic rocks. Both hafnium and the Hf/Zr ratio on the average show a progressive increase from the early formed gabbroic rocks to the late siliceous differentiates. The general trend shown by the data on samples from separate plutons of different composition is also shown on a more detailed scale by samples from a single differentiated stock. Much of the scatter of the data on the variation diagram (fig. 1) is probably caused by separate subparallel trends that may be present in individual plutonic units. Considerable scatter of the data may also be observed on a finer scale (fig. 2) where wide differences are found between zircon crystals differing in grain size from the same rock. If these uncertainties are taken into account, the hafnium and Hf/Zr data appear to vary in a systematic manner and to clearly show an enrichment of hafnium

relative to zirconium as differentiation of the magma progresses. From this hafnium enrichment it appears that within a given rock the finer sized crystals of zircon are formed later than the coarser ones in the normal course of crystallization.

With regard to the time of crystallization of zircon, the data lend further support to the belief (Gottfried and others, 1959) that in plutonic rocks, zircon crystallizes continuously throughout most of the interval of magmatic differentiation. The wide variations in its composition clearly show that zircon crystallizes in a continuously changing physico-chemical environment, its composition being approximately fixed for any stage in the differentiation of the magma. Lyakhovich and Shevaleyevskii (1962) have reached similar conclusions from a study of the Hf/Zr ratios in some plutonic rocks from the Soviet Union.

Based on the estimates of the abundance of the various rock types of the batholith published by Larsen (1948), the weighted average hafnium content and Hf/Zr ratio for zircon of the batholith are about 1.12 percent and 0.023, respectively. This ratio agrees with the estimate given by Fleischer (1955) for the Hf/Zr ratio in the earth's crust based on previously published data.

REFERENCES

Everhart, D. L., 1951, Geology of the Cuyumaca Peak quadrangle, San Diego County, California: Calif. Dept. Nat. Res., Div. Mines Bull. 159, p. 51–115.

Fleischer, Michael, 1955, Hafnium content and hafnium-zirconium ratio in minerals and rocks: U.S. Geol. Survey Bull. 1021–A, 13 p.

Gottfried, David, Jaffe, H. W., and Senftle, F. E., 1959, Evaluation of the lead-alpha (Larsen) method for determining ages of igneous rocks: U.S. Geol. Survey Bull. 1097–A, 63 p.

Larsen, E. S., Jr., 1938, Some new variation diagrams for groups of igneous rocks: Jour. Geology, v. 46, p. 505–520.

——— 1948, Batholith and associated rocks of Corona, Elsinore, and San Luis Rey quadrangles, southern California: Geol. Soc. America Mem. 29, 182 p.

Lyakhovich, V. V., and Shevaleyevskii, I. D., 1962, Zr: Hf ratio in the accessory zircon of granitoids: Geochemistry, no. 5, p. 508–524.

Waring, C. L., 1964, Determination of hafnium content and Hf/Zr ratios in zircon with the direct-reading emission spectrometer, *in* Geological Survey Research 1964: U.S. Geol. Survey Prof. Paper 501–B, p. B146–B147.

725–328 O—64——7

GEOCHEMICAL ANOMALIES IN THE LOWER PLATE OF THE ROBERTS THRUST NEAR CORTEZ, NEVADA

By R.L. ERICKSON, HAROLD MASURSKY, A. P. MARRANZINO, UTEANA ODA, and W. W. JANES, Denver, Colo.

Abstract.—Arsenic-antimony-tungsten anomalies have been discovered in jasperoid and fracture fillings in limestone in the lower-plate rocks of the Roberts thrust about 4 miles north of Cortez, Nev. Skarn pods and abundant quartz-bearing dike rocks in the limestone suggest the presence of a shallow buried intrusive mass.

Anomalous amounts of arsenic, antimony, and tungsten have been discovered in fracture fillings and jasperoid in limestone of Silurian and Devonian age in the lower-plate rocks of the Roberts thrust (Cortez window) near the Crescent fault about 4 miles north of Cortez, Nev. (fig. 1). Geochemical anomalies (copper, lead-zinc-silver, arsenic, and bismuth) in the siliceous clastic rocks of the upper plate of the Roberts thrust were reported by Erickson and others (1961); the reader is referred to their article for geographical orientation and a more complete geological and geochemical discussion of the general area of the investigation reported here.

Discontinuous alined masses of skarn and abundant fine-grained quartz-bearing dike rocks in the limestone of the lower plate (fig. 1) suggest that a shallow-buried intrusive mass underlies at least a part of the area of investigation. The skarn consists of calcite marble with porphyroblasts of idocrase, grossularite, and scapolite (meionite) in crystals as much as 2 inches across. This is the most intense contact metamorphic aureole in the Cortez area and it is suggested that the metal anomalies may be leakage halos emanating from concealed ore deposits in shear zones and fractures near the contact with the postulated buried intrusive.

The samples collected and analyzed in this study are not representative of rock units but are grab samples of the most favorable looking host material for introduced metals (fracture fillings, jasperoid masses, and intensely altered rocks). Thus, the density of sample sites shown on figure 1 is a crude index to the abundance of "favorable-looking material." Most of the traverses were made along drainages where bedrock exposure is best. Arsenic was determined chemically; all other metals were determined by semiquantitative spectrographic methods.

The largest arsenic-antimony-tungsten anomaly extends about 1 mile in a northeasterly direction roughly parallel to the Crescent fault (fig. 1). Maximum metal values detected in a few samples from the most intensely mineralized area are: arsenic, 6,000 parts per million; antimony, 3,000 ppm; tungsten, 1,500 ppm; zinc, 2,000 ppm; lead, 200 ppm; molybdenum, 200 ppm; beryllium, 100 ppm; and silver, 30 ppm. The smaller anomalies to the south are chiefly arsenic-antimony anomalies of lesser intensity. All the metals occur in highest concentration in the most iron-rich fracture fillings or jasperoid (>10 percent iron).

In the light of the previously described zoned metal anomalies in the upper plate of the Roberts thrust (Erickson and others, 1961), the discoveries reported here in the lower-plate rocks enhance the overall favorability of the Cortez district as a promising area for discovery of concealed ore deposits.

Location, description, and semiquantitative spectrographic and chemical analyses of the rocks collected in this investigation are described more fully by Erickson and others (1964).[1]

[1] Report obtainable at cost from the U.S. Geological Survey, Federal Center, Denver, Colo.

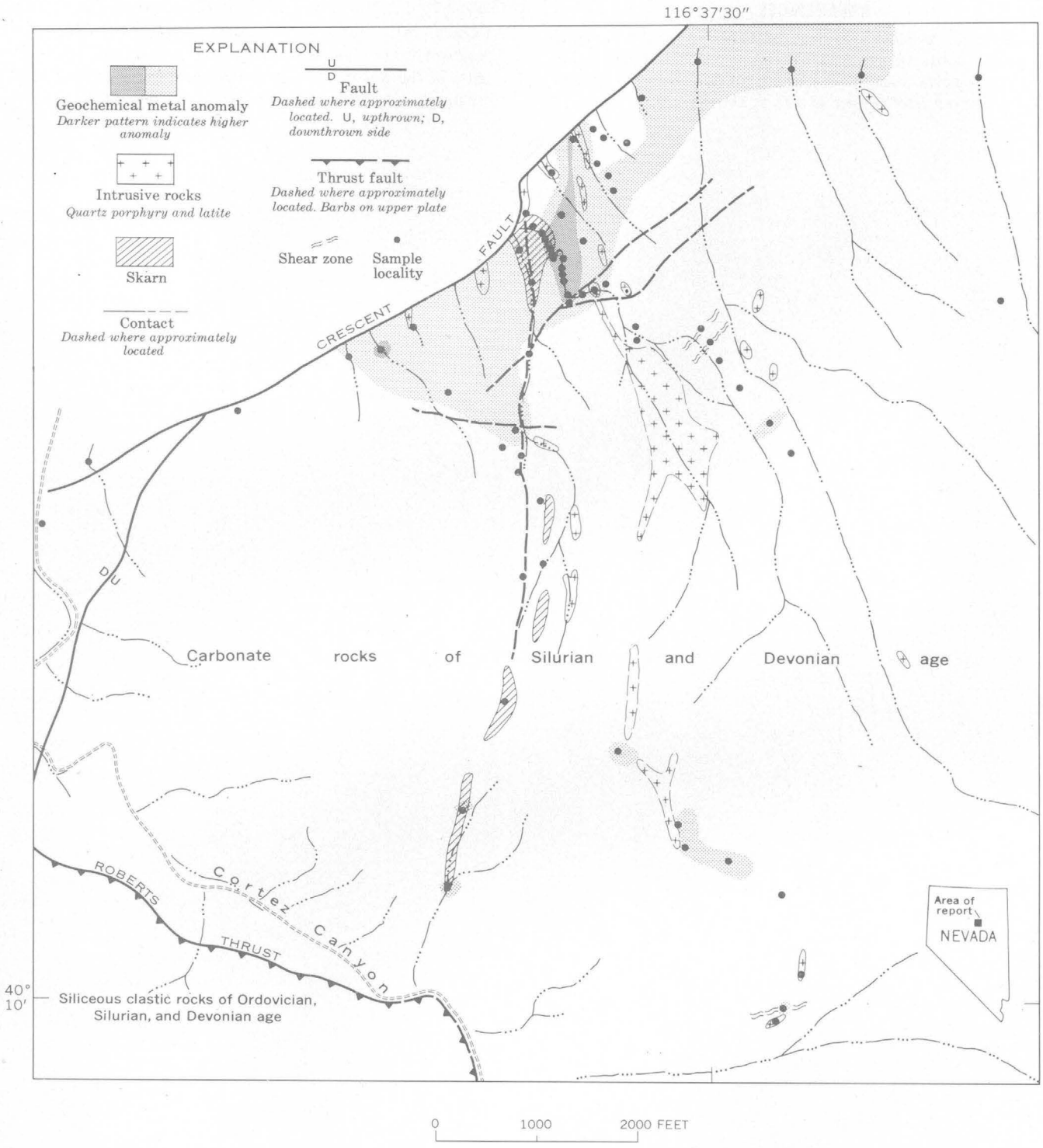

FIGURE 1.—Preliminary geochemical and geologic map of an area in the north-central part of the Cortez quadrangle, Nevada. Geology modified from work of James Gilluly and Harold Masursky, 1957–59. Density of pattern shows intensity of geochemical metal anomaly.

REFERENCES

Erickson, R. L., Masursky, Harold, Marranzino, A. P., and Oda, Uteana, 1961, Geochemical anomalies in the upper plate of the Roberts thrust near Cortez, Nevada: Art. 401 *in* U.S. Geol. Survey Prof. Paper 424–D, p. D316–D320.

Erickson, R. L., Masursky, Harold, Marranzino, A. P., Oda, Uteana, and Janes, W. W., 1964, Semiquantitative spectrographic and chemical analyses of rocks from the lower plate of the Roberts thrust, north-central part of the Cortez quadrangle, Nevada: U.S. Geol. Survey open-file report.

CESIUM AND STRONTIUM SORPTION STUDIES ON GLAUCONITE

By MARIAN M. SCHNEPFE, IRVING MAY, and CHARLES R. NAESER,
Washington, D.C.

Work done in cooperation with the U.S. Atomic Energy Commission

Abstract.—Studies of the ion-exchange behavior of cesium and strontium with glauconite in column experiments at pH 3, 6, and 10 indicate that increasing the pH increases the uptake of these ions. The strontium uptake averages 95 percent of capacity values at pH 10, while the cesium uptake is approximately 50 percent. Initial acid-treatment of glauconite increases the exchange with cesium to near capacity levels at pH 10, but reduces the strontium uptake by about 30 percent.

The interaction of three New Jersey glauconite mineral samples with cesium- and strontium-bearing solutions was studied to evaluate glauconite as a possible scavenging agent for cesium-137 and strontium-90 in nuclear-waste solutions.

Glauconite is a term used with dual connotation (Burst 1958a, 1958b). It is the name of a micaceous hydrous silicate mineral of iron, aluminum, and potassium, and it is also a general morphological term for rocks consisting of small spherical green pellets. The mineral, glauconite, has a dioctahedral illite structure with a charge deficiency in both tetrahedral and octahedral layers. These charge deficiencies are balanced by interlayer cations which are generally K^{+1}, but may be Ca^{+2}, or Na^{+1}. There is a considerable replacement of Al^{+3} by Fe^{+3}, Fe^{+2}, and Mg^{+2}.

Glauconite occurs typically in sand-size lobate aggregates of generally spherical shape. It is well known as "greensand" or "greensand marl". It is of marine origin and is abundant in the Cretaceous and early Tertiary marls and sands of the east coast of the United States. It has been mined for use as a fertilizer and as a natural "zeolite". Glauconite is now mined in New Jersey but is available in many other areas as well.

The ion-exchange properties of glauconite are well established. A completely reversible exchange reaction between potassium, sodium, and calcium is the basis for its use as a water softener. Glauconite is stable in neutral or slightly alkaline solutions but is appreciably soluble in 24 percent HCl (Hutton and Seelye, 1941) and somewhat soluble in weaker acid. Because of the reversible nature of its exchange reactions, glauconite might be expected to serve as a concentrating agent in the removal of radionuclides from nuclear-waste solutions.

Although glauconite has a lower exchange capacity than other clays such as montmorillonite, its granular nature makes it particularly desirable as an ion exchanger. It is not ordinarily subject to the undesirable swelling and consequent impedance to solution flow so often present in other clays in ion-exchange reactions.

Hendricks and Ross (1941) give the following formula as characteristic of many glauconites:

$$[K, Ca_{0.5}, Na]_{0.84}\,[Al_{0.47}Fe^{+2}_{0.19}Fe^{+3}_{0.97}Mg_{0.4}]\,[Si_{3.65}Al_{0.35}O_{10}](OH)_2$$
$$\textstyle\sum = 0.84 \qquad \sum = 2.03 \qquad \sum = 4.00$$

Owens and Minard (1960) computed structural formulas from chemical analyses of glauconite concentrates from various formations of the New Jersey coastal plain. Their formulas for glauconites with the same origin as those used in this study are:

Red Bank Sand (Upper Cretaceous),

$$[K_{0.636}Na_{0.009}Ca_{0.01}]\ [Mg_{0.35}Fe^{+2}_{0.18}Fe^{+3}_{1.0}Al_{0.48}Ti_{0.004}]\ [Si_{3.68}Al_{0.32}O_{10}](OH)_2$$
$$\Sigma=0.655 \qquad \Sigma=2.014 \qquad \Sigma=4.00$$

Hornerstown Sand (Paleocene),

$$[K_{0.764}Na_{0.009}Ca_{0.007}]\ [Mg_{0.384}Fe^{+2}_{0.204}Fe^{+3}_{1.08}Al_{0.36}Ti_{0.003}]\ [Si_{3.68}Al_{0.32}O_{10}](OH)_2$$
$$\Sigma=0.780 \qquad \Sigma=2.031 \qquad \Sigma=4.00$$

Manasquan Formation (Eocene),

$$[K_{0.722}Na_{0.018}Ca_{0.10}]\ [Mg_{0.46}Fe^{+2}_{0.16}Fe^{+3}_{0.925}Al_{0.42}Ti_{0.003}]\ [Si_{3.69}Al_{0.31}O_{10}](OH)_2$$
$$\Sigma=0.84 \qquad \Sigma=1.968 \qquad \Sigma=4.00$$

The glauconite concentrates used in these exchange studies were washed and sieved; the −35- to +60-mesh (sieve openings 0.50 and 0.25 mm) portions were then magnetically fractionated on the Franz Isodynamic Separator, the more magnetic fraction being taken for the exchange studies. Cesium was determined spectrographically to be<0.003 percent and strontium ≦0.007 percent by H. W. Worthing, U.S. Geological Survey. The chemical analyses of these fractionated samples are shown in table 1. These analyses correspond reasonably well with those of Owens and Minard (1960). X-ray studies of the glauconites described in the present article (Owens, personal communication, 1963) show them to be the disordered type of glauconite as classified by Burst (1958b).

TABLE 1.—*Chemical analyses of glauconites*

[Analyses by Rapid Rock Analysis Laboratory, U.S. Geological Survey. Analyses in percent]

	No. 1 (New Egypt, N.J.)	*No. 2 (New Egypt, N.J.)*	*No. 6 (Pemberton, N.J.)*
SiO_2	49.0	48.5	48.4
Al_2O_3	8.4	6.6	7.6
Fe_2O_3	17.7	19.9	17.1
FeO	3.3	3.9	2.6
MgO	3.2	3.3	3.7
CaO	.53	.62	2.1
Na_2O	.04	.03	.05
K_2O	6.9	7.4	7.0
H_2O	10.7	9.2	9.6
TiO_2	.10	.10	.08
P_2O_5	.28	.28	1.2
MnO	.02	.02	.01
CO_2	<.05	.61	<.05
Total	100.2	100.5	99.4

No. 1, glauconite from Red Bank Sand, Upper Cretaceous in age.
No. 2, glauconite from Hornerstown Sand, Paleocene in age.
No. 6, glauconite from Manasquan Formation, Eocene in age.

The glauconite samples were provided by James P. Owens and Dorothy Carroll, U.S. Geological Survey. We also wish to acknowledge their assistance and advice regarding the purification and characterization of these samples.

TECHNIQUE

Because of the obvious partial acid-decomposition of glauconite sample 2 during a column experiment, portions of the various glauconites were pretreated with acid. Samples were treated at room temperature with 2.5*M* HCl for a total of 6 hours and then washed with distilled water until the washings had a pH of 4. The samples were air dried. The acid leachings from each sample were evaporated and then ignited over a burner yielding residues weighing approximately 4 percent of the original sample. Spectrographic analyses showed that the residues were largely iron, aluminum, and silicon.

The total exchange capacities of both the acid-treated and the natural glauconites were determined by a batch method in which the samples were treated first with 2.5*N* ammonium acetate, and then the exchanged ammonium ions were removed by a Kjeldahl procedure employing barium hydroxide. Table 2 lists these exchange capacities.

TABLE 2.—*Total exchange capacity of glauconites (meq/100 g)*

	No. 1 (New Egypt, N.J.)	*No. 2 (New Egypt, N.J.)*	*No. 6 (Pemberton, N.J.)*
Untreated	26.0	19.6	22.3
Acid treated	27.2	21.2	2.3

All column studies were made with 12-mm-diameter glass columns immersed in a constant-temperature water bath. Column charges of 1 gram of glauconite were used, and the eluates were collected in 10-milliliter fractions.

Feed solutions prepared from the chlorides were 50 parts per million in either cesium or strontium with the

pH adjusted to 3, 6, or 10 by the addition of hydrochloric acid or sodium hydroxide. In the experiments at pH 10 the sodium hydroxide contributed a sodium-ion concentration of 2.3 ppm. Because the cesium and strontium concentrations were more than 20 times greater than that of sodium and because both cesium and strontium generally have greater replacing power than sodium it was felt that the competing effect of the sodium ions could be ignored.

The strontium feed solutions were spiked with strontium-89 to give counts approximately 500 times the background level of 20 counts per minute. The concentration of strontium in the glauconite-treated solutions was determined with a beta counter. The beta activity was determined on 1-ml aliquots of eluate fractions evaporated in aluminum planchets.

The cesium feed solutions were spiked with cesium-137 to give gamma activity approximately 700 times the background level. The activity of the glauconite-treated solutions was measured with a sodium iodide crystal scintillation counter.

Flow rates of approximately 10 ml per 15 minutes (0.6 ml cm^{-2} min^{-1}) were maintained when possible. Despite the granular nature of the glauconite, very slow flow rates were found for one of the glauconites (sample 2) at pH ranges from 3 through 10 for both the cesium and strontium solutions. An analysis of the eluate from this sample showed the presence of both aluminum and silicon, indicating partial decomposition of the sample.

Typical break-through curves[1] were obtained for both the acid-treated and natural glauconites. Figures 1 through 4 are the break-through curves for cesium and for strontium from the acid-treated and the natural glauconite (sample 1). The other glauconites give similar break-through curves. The C/C_o values represent the ratios of the concentration of cesium or strontium in the eluate to their concentration in the feed solution.

The experimental data are summarized in table 3. The uptake values in this table apply only to the extent to which the experiments were carried to completion, this being controlled largely by convenience. In table 4 the exchange capacities have been calculated from uptake values when C/C_o equals 0.5. If V is the volume of the eluate collected up to the point when C/C_o equals 0.5, then the exchange capacity equals the product, $V \times C_o$ (Samuelson, 1953, p. 48). Many of the elution curves are not completely symmetrical and therefore the calculated capacities may differ somewhat from the true values.

[1] The point at which the exchanging ion is first detected in the eluate is called the break-through point. In figure 1, at pH 3 the break-through of cesium occurs at 50 ml and at pH 10 at 400 ml.

TABLE 3.—*Experimental uptake of cesium and strontium*

Glauconite (sample No.)		Feed solution (50 ppm)	pH of feed solution	Eluate volume (ml)	Flow rate (ml cm^{-2} min^{-1})	Uptake (meq/100 g)	
Untreated form	Acid-treated form					Cs	Sr
1		Cesium	3	670	0.3	6.7	
1		do	6	800	.5	12.0	
1		do	10	800	.5	16.7	
	1	do	3	500	.3	7.5	
	1	do	6	850	.4	16.7	
	1	do	10	700	.3	23.6	
1		Strontium	3	700	.8		13.5
1		do	6	800	.5		20.1
1		do	10	850	.5		28.4
	1	do	3	600	.3		16.1
	1	do	6	900	.5		21.2
	1	do	10	600	.3		23.0
2		Cesium	3	455	.3	3.9	
2		do	6	<10	<.005		
2		do	10	180	.02	6.3	
	2	do	3	500	.4	6.2	
	2	do	6	800	.5	13.0	
	2	do	10	400	.06	14.9	
2		Strontium	3	455	.05		8.6
2		do	6	490	.1		16.0
2		do	10	340	.03		21.6
	2	do	3	600	.4		14.2
	2	do	6	800	.5		16.3
	2	do	10	650	≈.1		22.7
6		Cesium	3	400	.5	4.3	
6		do	6	565	.1	9.5	
6		do	10	800	.5	13.4	
	6	do	3	500	.4	6.6	
	6	do	6	800	.5	12.5	
	6	do	10	400	.05	15.0	
6		Strontium	3	650	.4		12.1
6		do	6	695	.2		19.5
6		do	10	700	.5		24.2
	6	do	3	600	.4		13.1
	6	do	6	800	.5		17.7
	6	do	10	650	.5		20.8

TABLE 4.—*Calculated exchange capacities of glauconites*

[Exchange capacity (meq/100 g) calculated from uptake when $C/C_o=0.5$]

Glauconite (sample No.)	pH of feed solution	Untreated form		Acid-treated form	
		Cs	Sr	Cs	Sr
1	3	4.7	10.6	6.0	14.9
	6	8.8	18.8	12.6	17.3
	10	13.9	23.9	25.2	19.0
2	3	3.5	8.1	5.8	6.2
	6	[1]	13.6	9.8	9.8
	10	[2] >6	20.0	[2] >13	15.2
6	3	3.0	6.0	5.8	8.4
	6	10.8	17.3	9.2	11.4
	10	11.5	20.2	22.4	14.0

[1] Run discontinued early because of excessively slow flow rate.
[2] Discontinued before $C/C_o=0.5$.

DISCUSSION

The total ion-exchange capacities of the New Jersey glauconites as determined by their saturation with ammonium ions range from 20 to 27 meq/100 g. The exchange capacities given in table 4 show that, as would be expected, the uptake of both cesium and strontium increase with pH. At the pH levels of 3, 6, and 10 the cesium uptake of the natural glauconites is approximately 16, 41, and 52 percent, respectively of the total capacity. The strontium uptake under similar conditions is appreciably higher than the uptake of cesium, amounting to 36, 73, and 94 percent.

Initial acid treatment of the glauconites causes an increase in the cesium uptake at all pH values studied,

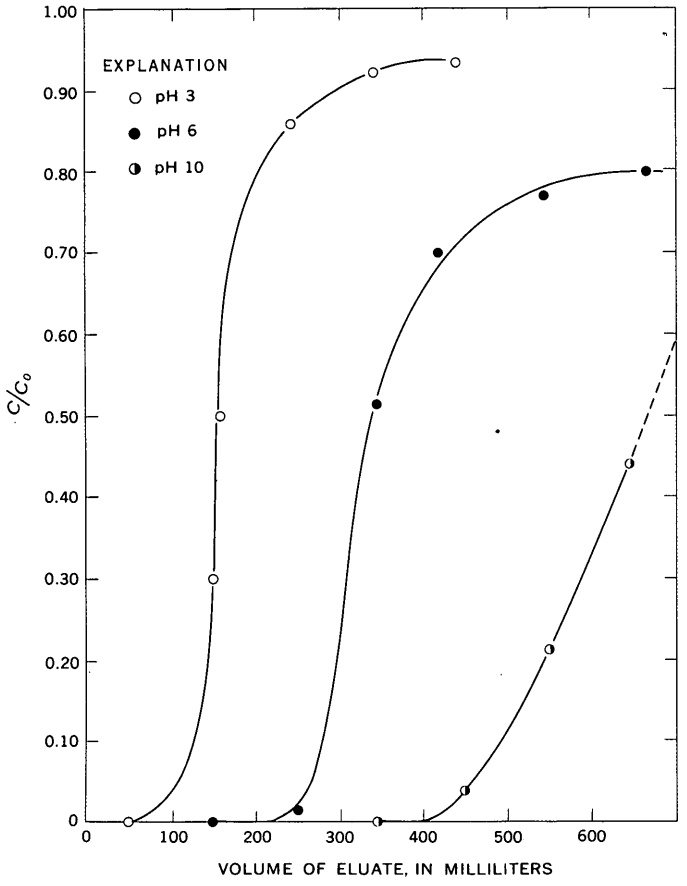

FIGURE 1.—Break-through curves for cesium from acid-treated glauconite of sample 1. C, concentration of cesium in the eluate; C_0, concentration of cesium in the feed solution.

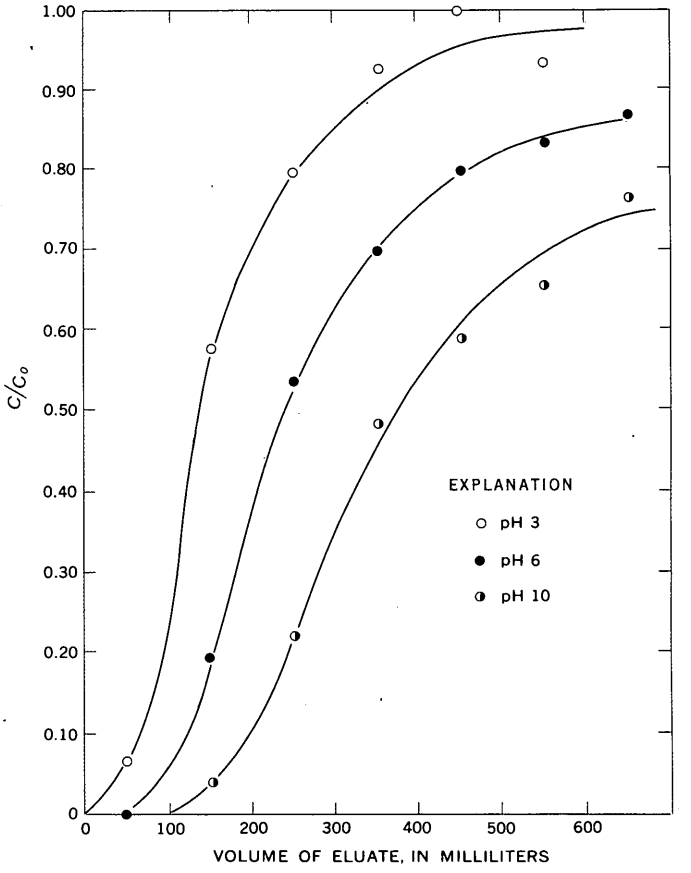

FIGURE 2.—Break-through curves for cesium from the untreated form of glauconite of sample 1. C, concentration of cesium in the eluate; C_0, concentration of cesium in the feed solution.

and at pH 10 the uptake approaches the capacity value. In contrast to the uptake of cesium, the change in strontium uptake after acid treatment is less predictable. Table 4 shows that strontium uptake is reduced as much as 30 percent at pH 6 and pH 10 after acid treatment. At pH 3, strontium uptake increased in 2 out of 3 samples and decreased in the third after acid treatment.

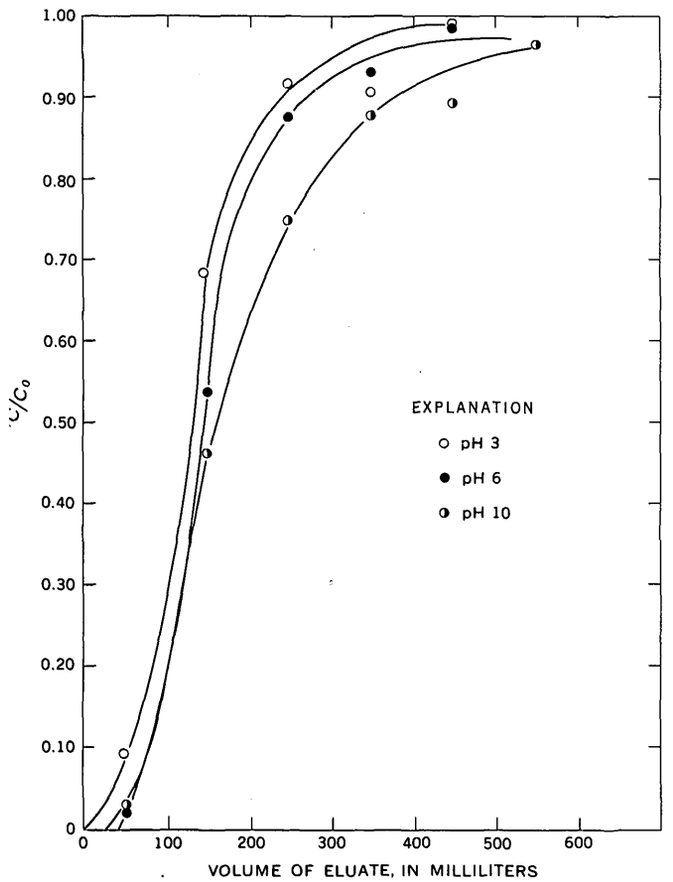

FIGURE 3.—Break-through curves for strontium from acid-treated glauconite of sample 1. C, concentration of strontium in the eluate; C_o, concentration of strontium in the feed solution.

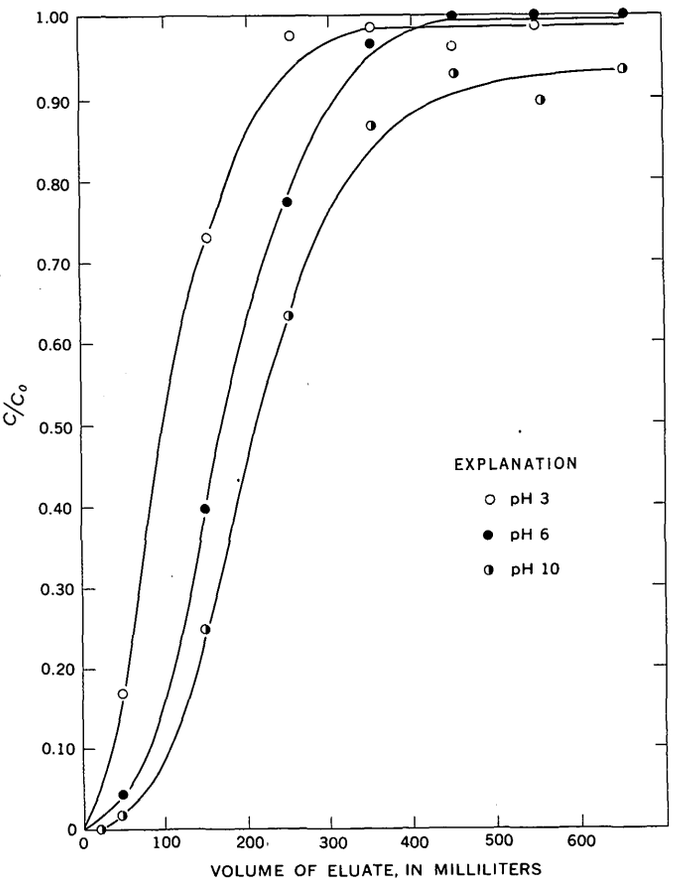

FIGURE 4.—Break-through curves for strontium from untreated form of glauconite of sample 1. C, concentration of strontium in the eluate; C_o, concentration of strontium in the feed solution.

REFERENCES

Burst, John F., 1958a, "Glauconite" pellets; their mineral nature and applications to stratigraphic interpretations: Am. Assoc. Petroleum Geologists Bull., v. 42, p. 310–327.

——— 1958b, Mineral heterogeneity in "glauconite" pellets: Am. Mineralogist, v. 43, p. 481–497.

Hendricks, S. B., and Ross, C. W., 1941, Chemical composition and genesis of glauconite and celadonite: Am. Mineralogist, v. 26, p. 683–708.

Hutton, C. O., and Seelye, F. T., 1941, Composition and properties of some New Zealand glauconites: Am. Mineralogist, v. 26, p. 595.

Owens, James P., and Minard, James P., 1960, Some characteristics of glauconite from the coastal plain formations of New Jersey: Art. 196 *in* U.S. Geol. Survey Prof. Paper 400–B, p. B430–B432.

Samuelson, Olof, 1953, Ion exchange in analytical chemistry: New York, John Wiley and Sons, 291 p.

DISTRIBUTION OF BERYLLIUM IN IGNEOUS ROCKS

By DANIEL R. SHAWE and STANLEY BERNOLD, Denver, Colo.

Abstract.—Beryllium concentration in igneous rocks tends to increase with increase in silica content, but reaches a maximum in rocks containing less-than-maximum amounts of silica. Among rocks having alkalic and silicic compositions, plutonic types normally contain the greatest average amount of beryllium, hypabyssal types an intermediate amount, and volcanic types the smallest amount.

The abundance and general distribution of beryllium in igneous rocks have been summarized by a number of authors (Goldschmidt and Peters, 1932; Sandell, 1952; Beus, 1956; Norton and others, 1958; Warner and others, 1959; and Turekian and Wedepohl, 1961). A study of the detailed relation between the beryllium content and other chemical components of these rocks, however, was not a major part of these studies. Some of these workers recognized that beryllium is most abundant in alkalic rocks, less abundant in silicic rocks, and still less abundant in mafic rocks. This distribution led several authors to the conclusion that beryllium is concentrated by processes of magmatic differentiation and that it is more abundant, along with silica and alkali oxides, in late-stage differentiates (Norton and others, 1958, p. 25; Warner and others, 1959, p. 18, 24; Griffitts and others, 1962, p. 1). In addition, a provincial variation in beryllium abundance is indicated by data which show that beryllium is characteristically more abundant in rhyolite and dacite in some areas than it is in others (Coats and others, 1962).

This article shows in tabular form the average beryllium content and chemical composition of several groups of igneous rocks. It also presents a detailed comparison of the beryllium content with the silica content of igneous rocks. In addition, attention is called to the apparent relation between the depth at which igneous rocks crystallized and the amount of beryllium in the rocks. In the light of the data presented, magmatic differentiation seems to be only one of several controls involved in the production of rocks relatively enriched in beryllium.

he analyses evaluated in this summary were collected largely by Verne C. Fryklund as part of another study of igneous rocks by the U.S. Geological Survey. The analyzed rocks were distinguished as "alkalic" or "normal" according to classifications assigned by the original authors. Among the normal igneous rocks, plutonic rocks with >60 percent silica and hypabyssal and volcanic rocks with >61 percent silica were classified arbitrarily as "silicic," and those below as "mafic".

The abundances of beryllium are based mostly on spectrographic analyses, and the accuracy of such analyses is not easily appraised. Ahrens and Fleischer (1960, p. 87) made a similar collection of analyses of granite G–1; the beryllium content commonly accepted as correct for this rock is 3.3 parts per million, but the reported values ranged from <1 to 4 ppm. This analytical uncertainty is smaller than most of the differences regarded as significant in this discussion, but it accounts for much of the scatter of the points in figure 1.

Table 1 gives the range and average beryllium content of 422 igneous rocks compiled in the present study. Mafic rocks contain an average of <1 ppm beryllium; silicic rocks, 6.5 ppm; and alkalic rocks, 11.4 ppm. The only mafic rocks that contain detectable beryllium are 6 volcanic and 4 plutonic rocks ranging in silica content from 48.6 to 60.6 percent; these 10 rocks are

TABLE 1.—*Range and average beryllium content of igneous rocks*

Rock type	Number of samples	Silica range (weight percent)	Beryllium content (parts per million)	
			Range	Average
All mafic rocks	152	33. 2–60. 7	0–8	<1
Mafic volcanic rocks	86	33. 2–60. 7	0–8	<1
Mafic hypabyssal rocks	10	41. 9–52. 5		0
Mafic plutonic rocks	56	34. 8–59. 9	0–5	<1
All silicic rocks	220	60. 1–77. 8	0–200	6. 5
Silicic volcanic rocks	81	61. 5–77. 8	0–20	4. 1
Silicic hypabyssal rocks	15	61. 8–77. 8	0–50	6. 8
Non-granophyre rocks	13	61. 8–77. 8	0–15	3. 5
Granophyre rocks	2	71. 9–74. 0	10–50	30
Silicic plutonic rocks	124	60. 1–77. 5	0–200	8. 2
Non-pegmatite rocks	112	60. 1–77. 5	0–30	3. 8
Pegmatite rocks	12	72. 0–75. 4	4–200	49
All alkalic rocks	50	34. 8–70. 1	0–50	11. 4
Alkalic volcanic rocks	17	34. 8–62. 0	0–20	4. 7
Alkalic hypabyssal rocks	11	44. 6–64. 0	0–30	9. 6
Alkalic plutonic rocks	22	35. 5–70. 1	0–50	13. 8

compared in tabe 2 with rocks of the same silica range that contain no detectable beryllium.

TABLE 2.—*Comparison of beryllium-bearing and non-beryllium-bearing mafic igneous rocks having similar ranges of silica content*

[Constituents given in weight percent except as noted; numbers in parentheses are number of samples]

	Plutonic rocks (12)		Volcanic rocks (40)			
	Without Be	With Be	Without Be	With Be	Without Be	With Be
Silica range [1]	53. 7–56. 5	53. 3–56. 9	48. 6–54. 5	48. 6–54. 4	59. 6–60. 7	60. 0–60. 6
Number of samples	8	4	29	4	5	2
Constituents:						
SiO_2	56. 1	56. 3	52. 4	51. 8	60. 6	62. 7
Al_2O_3	17. 3	15. 0	16. 0	14. 1	17. 0	16. 4
Fe_2O_3	. 8	2. 5	3. 7	4. 0	3. 7	3. 6
FeO	6. 1	8. 8	6. 3	8. 7	2. 5	4. 7
MgO	5. 1	3. 2	6. 3	4. 9	3. 0	1. 0
CaO	7. 1	6. 8	9. 6	6. 7	7. 0	3. 8
Na_2O	3. 6	3. 2	3. 0	3. 4	3. 7	3. 4
K_2O	2. 3	1. 7	1. 0	2. 4	1. 5	3. 2
TiO_2	1. 1	2. 0	1. 2	2. 4	. 6	. 8
P_2O_5	. 3	. 3	. 3	1. 4	. 3	. 3
MnO	. 2	. 2	. 2	. 2	. 1	. 1
Be (ppm)	0	3. 4	0	4. 0	0	3. 3

[1] Silica range based on silica reported in chemical analyses; analyses reported water free.

In table 3, the chemical composition and beryllium content of 258 of the alkalic and silicic rocks of table 1 are summarized. They are divided into categories, first on the basis of whether the rocks are alkalic or silicic, and secondly on the basis of whether they are plutonic, hypabyssal, or volcanic. Within each category, analyses were grouped according to silica content; the compositions shown are averages for the groups (recalculated to 100 percent without water and minor constituents). The silica ranges were chosen so that a statistically significant number of samples was included in most categories.

In figure 1, the beryllium content is plotted against the silica content of individual samples of silicic and alkalic plutonic, hypabyssal, and volcanic rocks. From these scatter diagrams it is clear that the maximum beryllium concentration is characteristically found in rocks containing somewhat less than the maximum silica concentration.

Table 1 shows that among rocks with alkalic and silicic compositions, volcanic rocks contain less beryllium than do hypabyssal rocks, and these less than plutonic. This tendency is particulary emphasized by the fact that there is no group among volcanic rocks that contains as much beryllium as granophyres and pegmatites, rocks that are commonly interpreted as late-stage volatile-rich types. The effect of apparent depth of crystallization on the distribution of beryllium is further illustrated by the data of table 4, in which rocks from different environments but with similar silica content are compared.

The tendency for a decrease in beryllium content from plutonic to hypabyssal to volcanic rocks may be a result of loss of beryllium along with volatile materials at lower pressures. If this is so, we might expect to find concentrations of beryllium minerals in country rocks in the vicinity of some near-surface intrusions, where volatile materials moved from the intrusions along favorable structural paths into the country rock, and there concentrated beryllium. The possibility should not be overlooked, however, that the difference in beryllium content of igneous rocks formed in different depth zones simply indicates a lack of genetic relationship among the rocks.

The data compiled in this article cannot alone indicate what igneous processes cause concentration of beryllium. We think, however, that the data do not wholly support the theory of beryllium concentration by magmatic differentiation, because (1) in most suites, the beryllium-concentrating processes reach their maximum effectiveness at silica ranges somewhat below those apparently achieved by continued differentiation, and (2) factors not clearly related to such differentiation—the depth of final crystallization, and the alkalic versus silicic character of the bulk composition—do appear related to the beryllium concentration. Other processes that may account for the distribution of beryllium in igneous rocks are (1) loss of beryllium in a volatile fraction during late magmatic stages; (2) alteration of rocks with accompanying loss of beryllium in late or post-igneous stages; and (3) silicification of igneous rocks, which diminishes beryllium content by dilution.

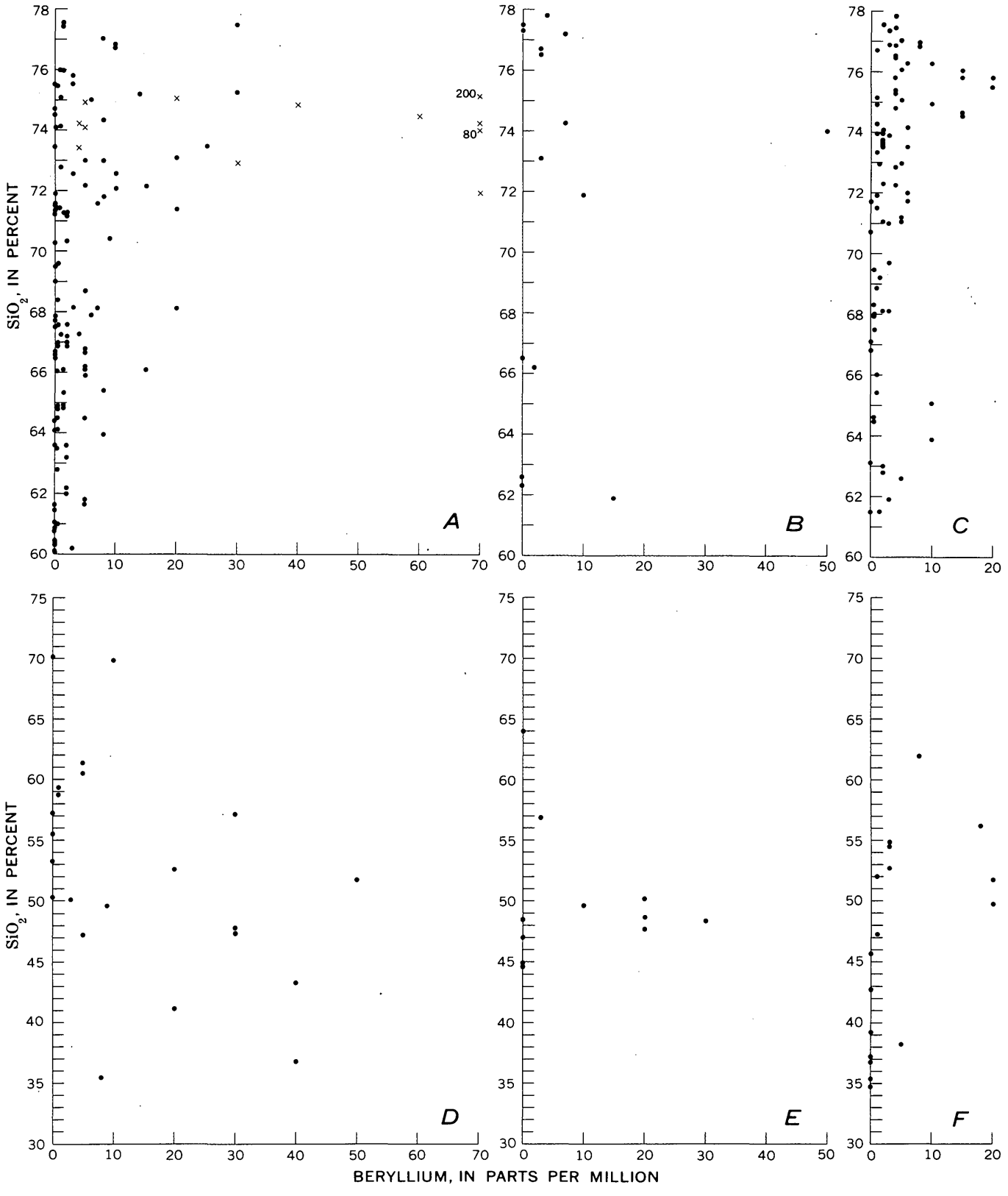

FIGURE 1.—Beryllium content plotted against silica content of igneous rocks. *A*, silicic plutonic rocks: dots, nonpegmatite (112 samples); ×'s, pegmatite (12 samples). *B*, silicic hypabyssal rocks (15 samples). *C*, silicic volcanic rocks (81 samples). *D*, alkalic plutonic rocks (22 samples). *E*, alkalic hypabyssal rocks (11 samples). *F*, alkalic volcanic rocks (17 samples).

TABLE 3.—*Average chemical composition and beryllium content of igneous rocks*

[Constituents given in weight percent except as noted; numbers in parentheses are number of samples]

		Silicic plutonic rocks (112)									Silicic hypabyssal rocks (15)			Silicic volcanic rocks (81)								
	Silica range [1]	60.1–61.8	62.0–64.0	64.1–66.0	66.0–67.9	68.2–69.6	70.3–72.0	72.1–73.5	74.1–76.0	76.0–77.5	61.8–66.5	71.9–74.3	76.5–77.8	61.5–61.9	62.6–63.9	64.5–66.0	66.8–67.9	68.1–69.7	70.7–71.9	72.0–74.0	74.0–75.8	76.0–77.8	
1	Number of samples	14	8	12	23	8	15	11	14	7	5	4	6	3	5	5	5	7	9	14	17	16	1
	Constituents:																						
2	SiO_2	62.6	64.3	66.3	68.6	70.1	72.1	73.5	75.7	77.5	65.0	74.6	77.6	62.4	64.5	67.2	69.1	71.7	73.5	76.0	76.6	77.4	2
3	Al_2O_3	16.4	15.8	15.9	15.1	15.2	14.9	13.7	12.9	12.3	16.5	13.4	12.4	17.3	16.7	16.0	15.6	14.7	14.0	12.9	12.6	12.5	3
4	Fe_2O_3	1.9	2.6	1.7	1.7	1.1	1.0	0.9	0.6	0.5	2.1	1.2	0.5	2.8	3.2	2.3	1.5	1.4	1.4	1.0	0.8	0.9	4
5	FeO	3.7	2.8	3.0	2.5	2.5	1.2	1.5	1.0	0.6	2.7	1.1	0.4	2.7	2.0	1.8	1.4	1.2	0.6	0.5	0.5	0.2	5
6	MgO	3.1	2.4	1.8	1.5	0.8	0.8	0.5	0.3	0.1	1.9	0.4	0.1	2.5	1.6	1.1	1.3	0.6	0.3	0.2	0.1	0.1	6
7	CaO	4.8	4.1	3.3	2.6	1.9	1.7	1.2	1.0	0.7	3.7	1.2	0.5	5.3	4.1	2.8	3.3	2.1	1.3	0.8	0.6	0.3	7
8	Na_2O	3.5	3.3	3.5	3.2	2.7	3.3	3.2	3.2	3.3	3.8	3.5	3.5	3.8	3.9	4.0	3.9	3.3	3.9	3.2	3.7	3.9	8
9	K_2O	2.8	3.6	3.6	3.9	5.2	4.5	5.1	5.0	4.9	3.2	4.4	4.9	2.1	3.0	4.1	3.2	4.4	4.5	5.2	4.8	4.6	9
10	TiO_2	0.8	0.7	0.6	0.6	0.4	0.4	0.3	0.2	0.1	0.6	0.1	0.1	0.7	0.7	0.5	0.4	0.4	0.3	0.2	0.1	0.1	10
11	P_2O_5	0.3	0.3	0.2	0.2	0.1	0.1	0.1	0.1	0.0	0.4	0.1	0.0	0.3	0.2	0.1	0.2	0.1	0.1	0.0	0.1	0.0	11
12	MnO	0.1	0.1	0.1	0.1	0.0	0.0	0.0	0.0	0.0	0.1	0.0	0.0	0.1	0.1	0.1	0.1	0.1	0.1	0.0	0.1	0.0	12
13	Be (ppm)	0.9	2.0	1.9	2.4	4.4	3.5	9.2	4.9	8.8	3.1	17.5	2.8	1.5	3.8	2.6	0.4	1.6	2.7	3.0	7.6	5.4	13

		Alkalic plutonic rocks (22)					Alkalic hypabyssal rocks (11)			Alkalic volcanic rocks (17)				
	Silica range [1]	35.5–43.4	47.3–51.8	52.6–57.3	58.8–61.4	69.9–70.1	44.6–47.0	47.7–50.2	56.9–64.0	34.8–39.1	42.9–49.8	51.9–56.3	62.0	
1	Number of samples	4	7	5	4	2	3	6	2	6	4	6	1	1
	Constituents:													
2	SiO_2	41.8	50.6	56.9	61.6	70.3	48.6	51.2	61.5	38.0	48.1	55.9	62.7	2
3	Al_2O_3	17.8	12.2	17.1	16.0	16.9	16.1	12.9	21.7	12.6	15.9	18.0	18.9	3
4	Fe_2O_3	6.2	3.1	3.4	2.1	0.1	3.3	3.9	1.0	5.6	1.8	3.0	4.3	4
5	FeO	2.6	5.3	3.1	2.6	0.8	7.9	5.0	0.6	6.0	8.4	2.6	0.1	5
6	MgO	4.3	9.5	2.0	2.0	0.4	7.2	7.2	0.3	10.8	2.8	2.8	0.4	6
7	CaO	14.2	7.0	4.2	4.1	0.9	8.4	7.9	1.2	12.2	8.9	5.0	0.9	7
8	Na_2O	6.8	2.1	4.5	4.4	6.5	4.2	2.6	3.2	2.9	5.6	5.3	7.0	8
9	K_2O	3.3	7.9	7.2	5.8	3.6	1.8	6.9	10.0	5.9	5.4	6.3	5.0	9
10	TiO_2	2.1	1.2	1.0	0.8	0.1	2.1	1.2	0.4	4.9	2.3	0.6	0.3	10
11	P_2O_5	0.6	1.0	0.4	0.5	0.4	0.3	1.0	0.1	0.9	0.6	0.3	0.2	11
12	MnO	0.3	0.1	0.2	0.1	0.0	0.1	0.2	0.0	0.2	0.2	0.2	0.2	12
13	Be (ppm)	27	18	10	2.5	5	0	17	1.5	0.8	5.2	8.0	8.0	13

[1] Silica range based on silica reported in chemical analyses; analyses reported water free.

TABLE 4.—*Comparison of beryllium content of silicic rocks crystallized at different depths but having similar ranges of silica content*

[Constituents given in weight percent except as noted]

	Pegmatite	Plutonic rocks	Hypabyssal rocks	Volcanic rocks
Silica range [1]	72. 0–75. 4	72. 1–76. 0	71. 9–74. 3	70. 7–74. 0
No. of samples	12	25	[2] 4	23
Constituents:				
SiO_2	74. 9	74. 8	74. 6	75. 3
Al_2O_3	15. 3	13. 3	13. 4	13. 3
Fe_2O_3	0. 3	0. 7	1. 2	1. 0
FeO	0. 4	1. 2	1. 1	0. 5
MgO	0. 1	0. 4	0. 4	0. 2
CaO	0. 3	1. 1	1. 2	1. 0
Na_2O	4. 8	3. 2	3. 5	3. 5
K_2O	3. 5	5. 0	4. 4	5. 0
TiO_2	0. 0	0. 2	0. 1	0. 2
P_2O_5	0. 3	0. 1	0. 1	0. 0
MnO	0. 1	0. 0	0. 0	0. 0
Be(ppm)	49	6. 8	17. 5	2. 9

[1] Silica range based on silica reported in chemical analyses; analyses reported water free.
[2] Includes two granophyres that appreciably raise average beryllium content.

REFERENCES

Ahrens, L. H., and Fleischer, Michael, 1960, Report on trace constituents in granite G–1 and diabase W–1, *in* Stevens, R. E., and others, Second report on a cooperative investigation of the composition of two silicate rocks: U.S. Geol. Survey Bull. 1113, p. 83–111.

Beus, A. A., 1956, Geochemistry of beryllium: Geochemistry (a translation of Geokhimiya), no. 5, p. 511–531 [1960].

Coats, R. R., Barnett, P. R., and Conklin, N. M., 1962, Distribution of beryllium in unaltered silicic volcanic rocks of the western conterminous United States: Econ. Geology, v. 57, p. 963–968.

Goldschmidt, V. M., and Peters, C. L., 1932, Zur geochemie des berylliums: Gesell. Wiss. Göttingen Math.-phys. Kl., Nachr., Heft 4, p. 360–376.

Griffitts, W. R., Larrabee, D. M., and Norton, J. J., 1962, Beryllium in the United States: U.S. Geol. Survey Min. Inv. Map MR–35.

Norton, J. J., Griffitts, W. R., and Wilmarth, V. R., 1958, Geology and resources of beryllium in the United States, *in* United Nations, Survey of raw material resources: Internat. Conf. Peaceful Uses Atomic Energy, 2d, Geneva, Sept. 1958, Proc., v. 2, p. 21–34.

Sandell, E. B., 1952, The beryllium content of igneous rocks: Geochim. et Cosmochim. Acta, v. 2, p. 211–216.

Turekian, K. K., and Wedepohl, K. H., 1961, Distribution of the elements in some major units of the Earth's crust: Geol. Soc. America Bull., v. 72, p. 175–192.

Warner, L. A., Holser, W. T., Wilmarth, V. R., and Cameron, E. N., 1959, Occurrence of nonpegmatite beryllium in the United States: U.S. Geol. Survey Prof. Paper 318, 198 p.

T–PHASE OF MAY 11, 1962, RECORDED IN HAWAII

By HAROLD L. KRIVOY and ROBERT A. EPPLEY, [1]
Hawaiian Volcano Observatory, Hawaii, Honolulu Observatory, Hawaii

Abstract.—An underwater nuclear explosion on May 11, 1962, generated a T-phase which was felt by coastal residents of Hawaii. It was also recorded throughout the State by 12 short-period seismometers. From the times of the T-phase maxima at seismographs on Hawaii, Maui, and Oahu the azimuth from the Hawaiian Islands to the source of the T-phase could be roughly calculated.

A portion of the energy released in a large and (or) shallow submarine seismic event is propagated through the overlying water as sonic waves (the T-phase) with a velocity of about 1.5 kilometers per second. Hydrophones have proved effective in the detection of these water-borne sound waves and have also shown that this phase is propagated to great distances with only slight attenuation through the deep ocean "low-velocity channel." This phenomenon is discussed by Northrup (1962) and Milne (1959).

To seismologists in Hawaii, T-phases are of considerable interest because they are most effectively generated by earthquakes of submarine or near-shore origin, which include those most likely to send destructive tsunamis out across the Pacific. T-phases are quite common on records of the short-period seismometers in use in Hawaii since 1957, which have magnifications between 10,000 and 40,000 in the period range of recorded T-phases (0.2 to 0.6 sec). Indeed, T-phases are produced by many small circum-Pacific earthquakes that yield no other phases on our records.

The relative ground amplitude produced by a T-phase at different stations in the Hawaii network appears to depend on many factors including direction of approach and period of the waves, distance of the recording station from the submarine slopes where the water-borne sonic waves are converted to their rock-borne equivalent, and configuration of the submarine slopes where the conversion occurs. Mere proximity of a station to

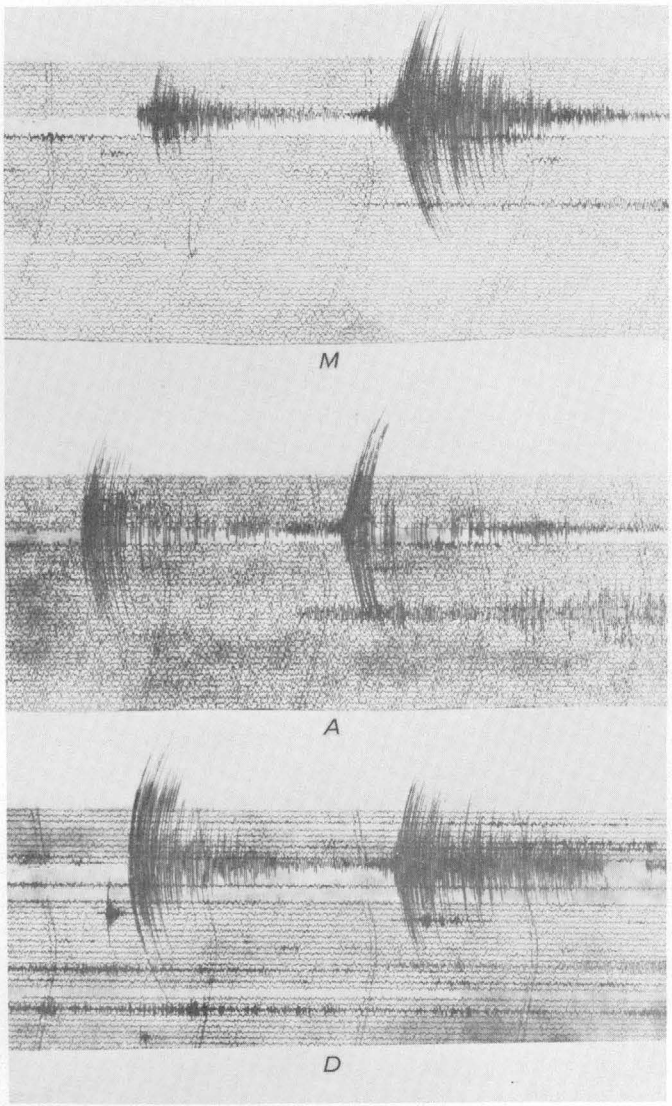

FIGURE 1.—Copies of portions of the short-period smoked-paper recordings made at the Hawaiian Volcano Observatory by instruments at sites Mauna Loa (M), Ahua (A), and Desert (D). The recordings show the sharp arrival of phases of a local quake followed in about 1 minute by the large spindle-shaped arrival of a T-phase. Drum speed is 60 mm/minute.

[1] Seismologist, U.S. Coast and Geodetic Survey.

the water's edge does not insure that it will record large-amplitude T-phases. On the other hand, the three T-phases felt in Hawaii (May 14, 1955, from a submarine nuclear explosion;[2] July 10, 1958, from the Lituya Bay, Alaska, earthquake;[2] and the one here reported) were felt only by people near the shore on the side of the island facing the source of the T-phase.

At about 10:40 (Hawaiian standard time) on the morning of May 11, 1962, we observed that unusual records were being written by the four telemetered seismographs in the library of the Hawaiian Volcano Observatory. Three of these records are shown on figure 1. Almost at once two reports were received that residents along Hawaii Island's northeast coast at Hilo and Ookala had felt a quake. Later, another report of a quake was received from Hilo. As can be seen on figure 1, a local quake began to be recorded about 1 minute prior to the recording of the T-phase. In order to decide which of these two events had been felt by the residents it was necessary to compare these and other records. Optical records from other Hawaii stations are represented on figure 3. The optical record made in the vault of the Hawaiian Volcano Observatory (fig. 2, *7*), together with the data from the processed records shown on figure 1, indicated that the local quake that occurred just prior to the T-phase originated in the region just south of point *A* in figure 2. Moreover, the local quake was only of magnitude 2.2 and was not felt in populated areas near the epicenter; thus it could not have been felt in the northeastern part of the island.

Data of May 11 from the Hawaiian Volcano Observatory were compared with those of the Honolulu Observatory on Oahu (fig. 2, *1*, *2*). These data for the time of arrival of the maximum part of the T-phase led to the conclusion that the T-phase approached the Hawaiian Islands from the northeast, as shown on figure 2. This solution was arrived at by graphical means on the assumptions that (1) a distant source was involved and the wave front would be linear as it passed through the Hawaiian chain, (2) the average T-phase velocity was 1.5 km/sec in water, and (3) travel time across the terminal "land" portion of each path was negligible. The three graphical solutions agree within 1°.

On figure 1 it can be seen that records from Mauna Loa, Ahua, and Desert (fig. 2, *M*, *A*, and *D*) are sufficiently similar in character to permit relative timing of the T-phase maxima with an error no larger than 1 or 2 seconds. On figure 3, however, it is seen that while records from the Hawaiian Volcano Observatory and Maui retain this character, those from Naalehu (*6*), Pahoa (*5*), Hilo (*4*), and the Honolulu Observatory (*2*) do not have such quality and character as to permit more than a rough estimate of the arrival time of T-maxima. The calculated azimuth of approach of the waves may be in error by several degrees.

This T-phase was detected in the absence of P, S, R, or other features of a distant earthquake. Furthermore, no earthquake was reported near southern California, the only active seismic near-shore area in the direction of the source. It was therefore assumed to be of artificial origin. Hawaiian newspapers of May 12 carried a short story indicating that a nuclear device had been fired beneath the Pacific.

The eventual listing of U.S. Atomic Energy Commision press releases from the Project Dominic series (U.S. Atomic Energy Commision, 1962) indicated a shot on "May 11th at 4:P.M., EDT, Eastern Pacific Ocean several hundred miles from the closest land area, low yield." With the above origin time, a 40-minute T-wave travel time is indicated.

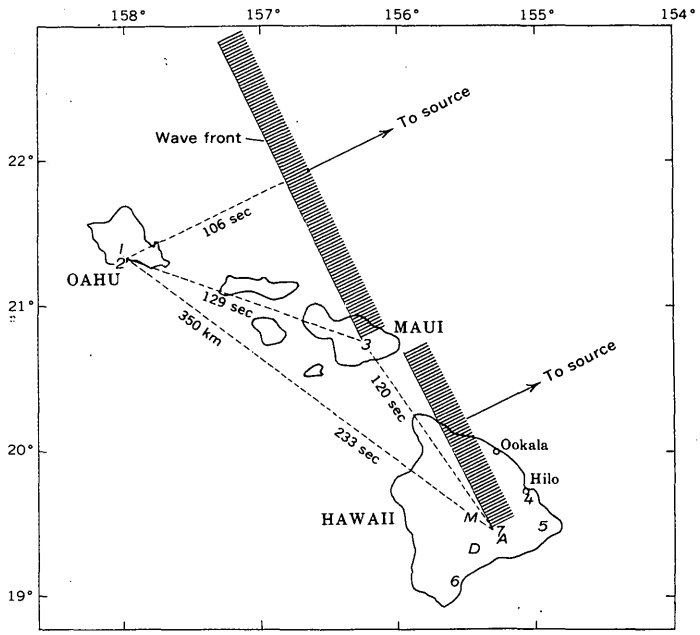

FIGURE 2.—Wave fronts and azimuth of the T-phase of May 11, 1962, computed from the time of arrival of the T-phase maximum at various seismograph stations in the Hawaiian Islands. Short-period seismographs are at Mauna Loa (*M*), Ahua (*A*), and Desert (*D*). Others are at Honolulu Observatory (*1*, *2*) Maui (*3*), Hilo (*4*), Pahoa (*5*), Naalehu (*6*), and Hawaiian Volcano Observatory (*7*).

[2] Based on unpublished data furnished by J. P. Eaton, U.S. Geological Survey.

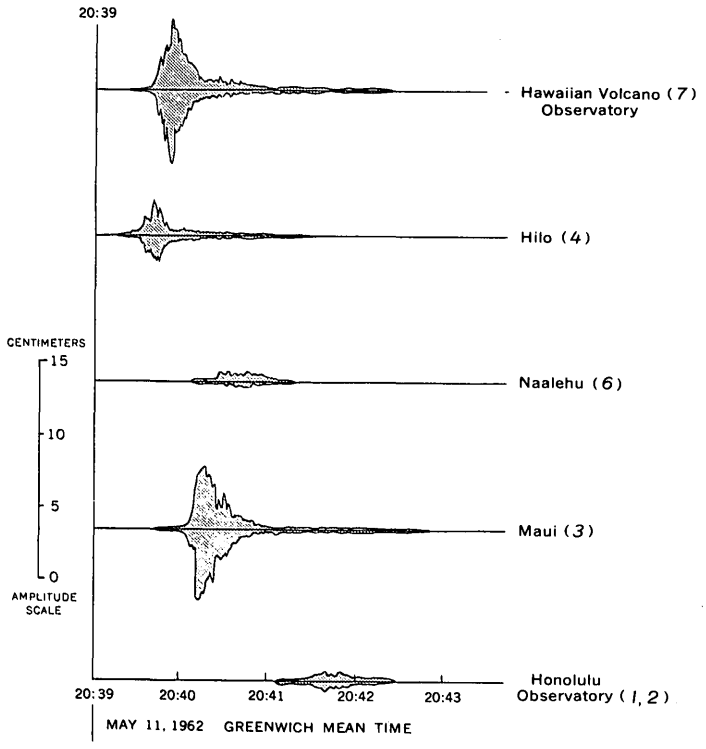

FIGURE 3.—T-phase envelopes traced from the optical records of five short-period vertical seismometers, Numbers in parentheses refer to locations shown on figure 2.

Minor tsunamis have originated from earthquakes smaller than magnitude 7.0 for which no T-phase was recorded. On the other hand, we have observed T-phases from large earthquakes which sent no tsunami to Hawaii, as for example, the Lituya Bay, Alaska, earthquake of 1958 that was felt by residents along the northeast coasts of Hawaii and Kauai. It does not seem likely that study of the T-phase will supply a simple technique for predicting tsunamis, because tsunami-producing quakes do not necessarily produce T-phase on seismograms in Hawaii. It is to be expected, however, that the growing knowledge of these phenomena will improve our assessment of other parameters of a seismic event, such as focal depth, magnitude, fault motion, and ocean-floor displacement.

REFERENCES

Eaton, J. P., Richter, D. H., and Ault, W. U., 1961, The tsunami of May 23, 1960, on the Island of Hawaii: Seismol. Soc. American Bull., v. 51, no. 2, p. 135–157.

Milne, A. R., 1959, Comparison of spectra of an earthquake T-phase with similar signals from nuclear explosions: Seismol. Soc. America Bull., v. 49, no. 4, p. 317–329.

Northrup, John, 1962, Evidence of dispersion in earthquake T-phases: Jour. Geophys. Research, v. 67, no. 7, p. 2823–2830.

U.S. Atomic Energy Commission, 1962, AEC press releases, *in* Seismological notes: Seismol. Soc. America Bull., v. 52, no. 4, p. 974.

725–328 O—64——8

EFFECTS OF THE GNOME NUCLEAR EXPLOSION UPON ROCK SALT AS MEASURED BY ACOUSTICAL METHODS

By D. D. DICKEY, Denver, Colo.

Work done in cooperation with the U.S. Atomic Energy Commission

Abstract.—An attempt was made to measure, by acoustical methods, changes in physical properties of rock salt at the GNOME site, New Mexico, which were caused by the detonation of a nuclear device. Longitudinal and shear velocities of rock in place were measured before and after the explosion. Postexplosion velocities were slower, owing to fracturing of the rock, for a distance of more than 200 feet from the shot point. Various elastic constants were calculated for the rock salt before and after the blast, using the measured velocities.

A nuclear device of about 3 kilotons equivalent TNT used in project GNOME was detonated December 10, 1961, in rock salt of the Salado Formation of Late Permian age. The device was 1,200 feet below the surface of the earth at a location about 25 miles southeast of Carlsbad, N. Mex.

The preexplosion dynamic elastic properties of the rock salt were calculated from measurements of the compressional and shear velocities of acoustic waves made in the tunnel that was excavated preparatory to emplacement of the device (line *Y–Z*, fig. 1). Postexplosion measurements were made on June 15 and 16, 1962, in the reentry tunnel. Figure 1 shows the spatial relationships of the shot point, the preexplosion and postexplosion tunnels, and the lines along which the velocities were measured. The accompanying table lists the results obtained from these measurements. All measurements were made in the same manner and with the same equipment.

The rock salt is not pure; some units contain as much as 30 percent clay. Polyhalite beds are present in the salt sequence, one of which is less than 10 feet above the explosion center and another of which is less than 10 feet below it. Further details of the geology are given by Gard (1963).

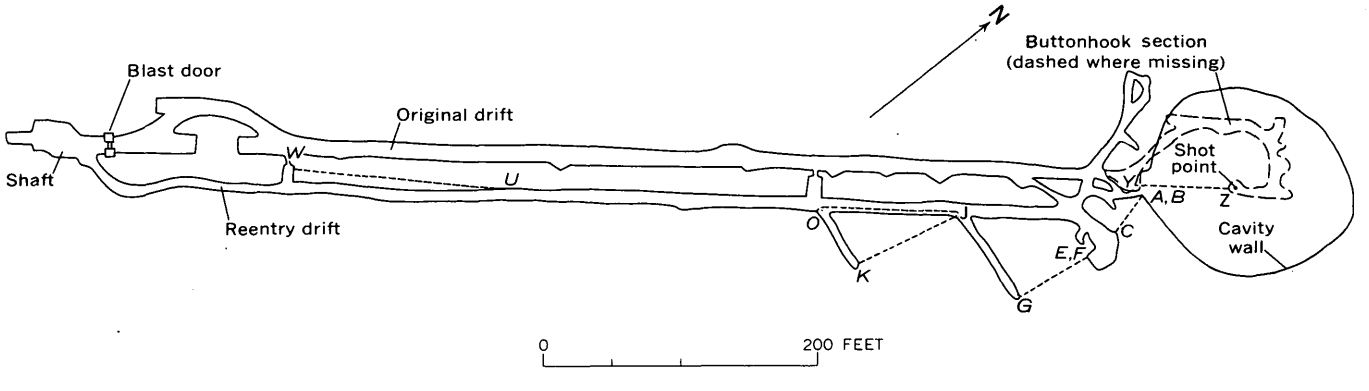

FIGURE 1.—Map of GNOME underground workings and cavity, showing sonic-velocity stations (italic letters). Lines of measurement shown by short dashes.

U.S. GEOL. SURVEY PROF. PAPER 501-B, PAGES B108-B111

Measured velocities and calculated elastic moduli for rock salt near the position of the GNOME explosion

[All arrival times determined from comparison of two or more records from each line of measurement except those for line *J–O*. Only one acceptable record was obtained from line *J–O*. Line *Y–Z*, the preexplosion line of measurement, is 5½ feet higher stratigraphically than the other lines. Measurements by D. D. Dickey and D. R. Cunningham]

Line of measurement	Distance from explosion point (feet)	Length of line (feet)	Travel time of first arrival (milliseconds)		Velocity (fps)		Poisson's ratio	Young's modulus (10^6 psi)	Shear modulus (10^6 psi)	Bulk modulus (10^6 psi)
			Compressional	Shear	Compressional	Shear				
Postexplosion measurements										
A–C	80–110	34. 99	2. 9	6. 05	12, 100	5, 800	0. 35	2. 6	0. 95	2. 9
B–C	80–110	32. 15	2. 7	5. 6	11, 900	5, 750	. 35	2. 5	. 93	2. 8
G–E	140–205	66. 80	5. 6	10. 4	11, 900	6, 400	. 30	3. 0	1. 1	2. 5
G–F	140–205	67. 09	5. 7	10. 4	11, 800	6, 450	. 29	3. 0	1. 2	2. 4
J–O	235–350	114. 74	8. 8	14. 9	13, 000	7, 700	. 23	4. 1	1. 7	2. 6
J–K	235–325	90. 52	7. 0	13. 1	12, 900	6, 900	. 30	3. 5	1. 4	2. 9
U–W	600–785	186. 22	13. 4	24. 4	13, 900	7, 650	. 29	4. 2	1. 6	3. 3
Preexplosion measurement										
Y–Z	5–85	81. 37	6. 05	11. 5	13, 500	7, 100	. 31	3. 5	1. 4	3. 1

EQUIPMENT

The equipment used in this study consisted of a Tektronix-535 oscilloscope, a Polaroid Land camera mounted on the oscilloscope, a time-mark generator, a preamplifier, accelerometers, steel plates bolted to the tunnel wall, and a hammer wired as part of the trigger circuit.

PROCEDURE

At the GNOME site, steel plates were bolted solidly to the tunnel wall at the sending and receiving stations, and the distances between them were surveyed. At each receiving station, an accelerometer was fastened to the steel plate. Output from the accelerometer was fed through the preamplifier to the oscilloscope, which was adjusted to sweep once when triggered by an external circuit. The trigger circuit used in these tests was a 6-volt dry cell in series with the oscilloscope; the hammer and the steel plate at the sending station acted as the switch. The time-mark generator was used on the second channel of a dual-trace oscilloscope to provide timing marks. It was also used to calibrate the grid on the oscilloscope screen, which in turn was used for measuring time. This is virtually the same procedure as used by Warrick and Jackson (1961) to measure velocities in salt and potash ore.

The actual observations were made as follows: After the shutter on the camera was opened the sending plate was struck sharply with the hammer, thus closing the circuit and starting the trace on the oscilloscope to sweep. The acoustic waves generated by the hammer blow were imposed on the sweeping trace. The camera shutter was closed and the photograph immediately developed. The process was repeated until two satisfactory photographs had been taken. Figure 2, one of the photographs taken for the *G–F* line of measurement (fig. 1), is a typical example. In this photograph the time required by the oscilloscope beam to move one vertical grid line to the next was 2 milliseconds. The trace was started on a grid line, and the time was easily measured from starting time to the first arrival of the compressional wave. The photograph was enlarged by projection in order to more accurately pick this time. The first arrival of the shear wave was picked with a little less certainty, but when two or more pictures were used, this value was quite accurate. On figure 2 the times for the compressional and shear arrivals were picked at 5.7 and 10.4 milliseconds, respectively. It should also be noted that variation in the manner of striking the sending plate produced variation in the relative amounts of compressional and shear energy. Deliberate attempts at producing more shear energy by striking the sending plates on the side or top sometimes sharpened the shear arrival and reduced the relative compressional energy.

The elastic moduli–Poisson's ratio (ratio of the transverse strain to the longitudinal strain of a body under longitudinal stress), Young's modulus (force per unit area multiplied by the length of a body, divided by the change in length), shear modulus (stress-strain ratio for simple shear, or the force per unit area divided by the ratio of the change in length to the original length of a body in shear), and bulk modulus (decrease in volume with increase in density of a body under pressure) of the rock salt were calculated from the following formulas (Howell, 1959, p. 152, 158, 204, 207; Jaeger, 1956, p. 56–58):

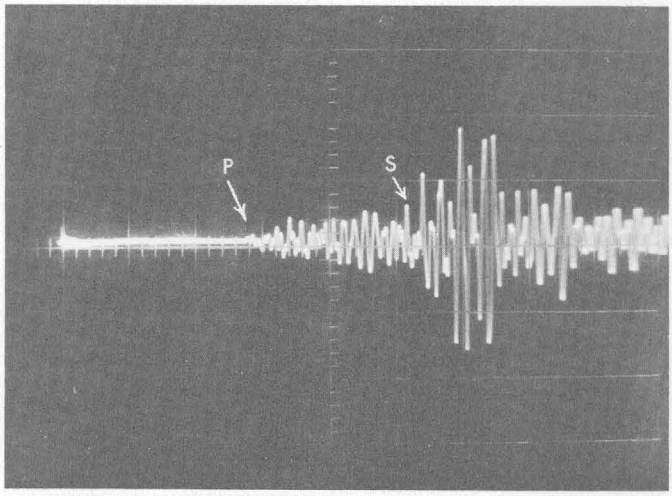

FIGURE 2.—Photograph of oscilloscope trace measuring travel times of compressional and shear waves for line of measurement *G–F* shown on figure 1. Vertical grid lines represent a time interval of 2 milliseconds. Oscilloscope started to sweep when circuit was closed and sound wave was initiated (left side of picture). First arrival of compressional wave **P** was at 5.7 milliseconds and first arrival of shear wave **S** was at 10.4 milliseconds.

$$\text{Poisson's ratio, } \sigma=\frac{\frac{1}{2}\left(\frac{V_p}{V_s}\right)^2-1}{\left(\frac{V_p}{V_s}\right)^2-1},$$

where V_p is compressional velocity in feet per second, and V_s is shear velocity in feet per second.

$$\text{Young's modulus, } E=\frac{\rho V_p^2(1+\sigma)(1-2\sigma)}{144g(1-\sigma)}=\frac{\rho V_s^2(1+\sigma)}{72g},$$

where E is in pounds per square inch, ρ is density of the rock in pounds per cubic foot, and g is the acceleration due to gravity, or 32.2 feet per second squared. And

$$\text{shear modulus, } \mu=\frac{E}{2(1+\sigma)}$$

$$\text{bulk modulus, } K=\frac{E}{3(1-2\sigma)},$$

where μ and K are in pounds per square inch. The density of a representative sample of the rock as determined in the U.S. Geological Survey laboratory is 131 pounds per cubic foot.

Particular care was given to placing all the sending and receiving plates in the same salt stratum. Two plates were mounted at each station where feasible—one was placed 1 foot above the polyhalite bed (unit 15 of Gard, 1963), and the other 2 feet above it. Where this was not possible, the single plate was placed either 1 foot or 2 feet above the polyhalite bed. The one exception to this in the postexplosion lines was the placing of plates *A* and *B*; at this station the polyhalite bed was below the tunnel floor and was not visible. Both plates, therefore, were put at an elevation estimated to be 3½ feet above the polyhalite bed.

The plates for the preexplosion line, *Y–Z*, were placed 6½ feet above the polyhalite bed.

RESULTS

Measurements along line *Y–Z* (fig. 1) were made prior to the explosion, and measurements along line *U–W* were made after the explosion but at a distance far enough from it that little change was expected. The calculated elastic moduli of the rock along these paths, with the exception of Poisson's ratio, were higher for line *U–W* (see table). The velocity also was slightly higher. These differences may be attributable either to the difference in the position of the paths with regard to the geology, line *Y–Z* being about 5½ feet higher stratigraphically, or possibly to the closeness of line *U–W* to the line of the tunnel.

Lines *J–O* and *J–K* extend from a common point and are about the same distance from the explosion point. The compressional velocities along these lines are the same, but the shear velocities are different. This difference cannot be confidently assumed to indicate a difference in elastic properties of the rock along these lines, because there was only one record for line *J–O* and the time fo the first shear-wave arrival may not have been picked accurately.

Using the values calculated for line *J–K*, we see that Poisson's ratio at this distance from the explosion is not substantially different from that calculated for line *U–W*, farther from the explosion. The values for the three other computed elastic moduli (Young's modulus, shear modulus, and bulk modulus) and the velocities are a little lower for line *J–K*.

Likewise, the velocities and the calculated elastic moduli, except Poisson's ratio, for rock along lines *G–E* and *G–F* are lower than those for rock farther from the explosion point.

The elastic moduli calculated for rock along lines *A–C* and *B–C*, the lines closest to the explosion point, are quite different from those calculated for the other lines. Poisson's ratio is higher and Young's modulus and the shear modulus are lower than for any other line of measurement. The bulk modulus is higher than for lines *G–E* and *G–F*.

The compressional velocities are lower for lines *A–C* and *B–C* than all other measured compressional velocities except those for lines *G–E* and *G–F*, which are about the same. The shear velocities, however, are much

lower than even those for lines *G–E* and *G–F*. The proposed reason for this is as follows:

Much faulting and fracturing in the rock from the cavity wall to a distance of 120 feet from the shot point have been shown by mapping (L. M. Gard, 1963). This fracturing is believed to be responsible for the reduction in velocities. If some of the fractures were open and made an air gap between the sending and receiving plates—and there is reason to believe that this is true—the shear wave could not have travelled by the most direct path and would have been slowed even more than the compressional wave. Unmappable small fractures may be present at distances beyond 120 feet from the explosion and would explain the decreased velocities out to a distance of more than 200 feet.

The values of the elastic constants calculated for these travel paths closest to the explosion point, therefore, are believed to be in error. The rock is probably so badly fractured that it does not act as an elastic medium and the calculated values do not apply.

Excepting the values calculated for the lines *A–C* and *B–C* we see that the postexplosion values of Poisson's ratio of the rock showed no appreciable change as the shot chamber was approached, but that the bulk modulus consistently decreased in value. Young's modulus and the shear modulus also showed a steady decrease in value as the chamber was approached, even along lines *A–C* and *B–C*. The one factor included in all measurements except Poisson's ratio is density, which we have assumed to be the same for all the rock. This assumption was based on only a few samples taken before the explosion and a few taken after it, and not in great enough numbers to insure the validity of the assumption. Therefore, one might suspect that compaction or a change in density would be responsible for the systematic change in the elastic moduli. This has to be discounted, however, on the grounds that a density change of more than 25 percent would be required to produce changes so large in the elastic moduli, and this density change would be easily detectable. A possible explanation for the change in the elastic moduli is that it is due to the changes in the stress of the rocks surrounding the explosion.

It might be noted here that elastic-moduli results obtained from samples of similar rock removed from the ground are different from those measured with the rock in place (Warrick and Jackson, 1961) and that the amount of change is at present not predictable.

CONCLUSIONS

Predicted effects of the explosion on the rock included fracturing and compaction, both of which theoretically would be detectable by acoustic methods. Compaction should change the elastic moduli of the rock, and fracturing should change the velocities. However, the results of this study showed that (1) although fracturing of this rock is detectable by the acoustic method used, compaction is not, and (2) the elastic moduli are changed for reasons other than compaction. Furthermore, the amount of fracturing is semiquantitatively estimable by acoustic means. Compaction is not shown by the changes in elastic moduli caused by the explosion, because of the larger changes in elastic moduli not related to compaction. These changes, however, may indicate the amount and position of changes in stress of the rock surrounding an explosion.

REFERENCES

Gard, L.M., 1963, Nuclear explosion; some geologic effects of the Gnome shot: Science, v. 139, no. 3558, p. 911–914.

Howell, B. F., Jr., 1959, Introduction to geophysics: New York, McGraw-Hill Book Co.

Jaeger, J. C., 1956, Elasticity, fracture, and flow: New York, John Wiley.

Warrick, R. E., and Jackson, W. H., 1961, Poisson's ratio of rock salt and potash ore: Art. 102 *in* U.S. Geol. Survey Prof. Paper 424–B, p. B241–B242.

HABIT OF THE ROCKY VALLEY THRUST FAULT IN THE WEST NEW MARKET AREA, MASCOT-JEFFERSON CITY ZINC DISTRICT, TENNESSEE

By J. G. BUMGARNER,[1] P. K. HOUSTON,[2] J. E. RICKETTS,[3] and HELMUTH WEDOW, JR.,[4] Bartow, Fla., New York, N.Y., Mascot, Tenn., and Knoxville, Tenn.

Work done in cooperation with the American Zinc Co. of Tennessee and Tri-State Zinc, Inc.

Abstract.—Post-thrust folding and high-angle reverse faulting of the Rocky Valley thrust fault occurred in the West New Market area when continued or renewed compressive forces deformed the upper and lower plates of the fault as a unit.

The trace of the Rocky Valley thrust fault (Bays Mountain fault of Bridge, 1945) extends northeastward across the Mascot-Jefferson City zinc district, Tennessee (fig. 1) as mapped by Bridge (1956, pl. 1).

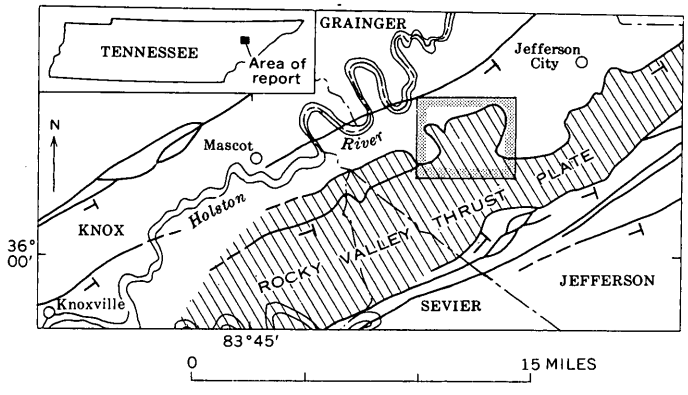

FIGURE 1.—Index map of the Mascot-Jefferson City zinc district, Tennessee, showing relation of West New Market area (shaded outline) to the upper plate of Rocky Valley thrust fault (diagonally ruled). T indicates upper plate of thrust faults. Position of faults after Rodgers (1953).

The fault has a gentle dip to the southeast, but this is modified locally by minor folds and faults. The low-angle nature of the Rocky Valley fault was early recognized by Keith (1901). Rodgers (1953, p. 134 and pl. 2) believed that this fault might be the northeastward extension of the Knoxville fault, but later, more detailed mapping by J. M. Cattermole, in the John Sevier quadrangle, has shown that the throw of the Knoxville fault is taken up completely in an asymmetrical anticline just a few miles northeast of the Holston River.

Exploration drilling in the West New Market area (figs. 1 and 2) by the American Zinc Co. of Tennessee began in 1950. It was completed during the period 1954–56, with the financial and technical assistance of the Defense Minerals Exploration Administration, U.S. Department of the Interior. This exploration was one of the most successful large-scale semidetailed reconnaissance drilling programs supported by DMEA in the United States. The DMEA work resulted in the discovery of 35 million tons of zinc ore (Oder, 1958).

In 1960, Tri-State Zinc, Inc., did additional drilling that led to the joint venture, New Market Zinc, Inc., between Tri-State and American Zinc to develop part of the West New Market reserves. Diamond drilling in the combined programs of the two companies totalled close to a half a million feet in nearly 400 holes. For the most part these holes were arranged in a wide-spaced grid pattern with followup drilling at the centers and along the sides of the grid squares. As the collars of many of the holes were in the overthrust plate of the

[1] Geologist, International Minerals and Chemical Co., formerly with American Zinc Co. of Tennessee.
[2] Geologist, Guggenheim Exploration Co., formerly mining geologist with Tri-State Zinc, Inc.
[3] Head geologist, American Zinc Co. of Tennessee.
[4] Geologist, U.S. Geological Survey.

Rocky Valley fault, and because the target zone is below the fault, numerous intersections of the thrust surface were obtained. Geologic sections and structure-contour mapping from the drill-core data have provided one of the most complete pictures yet available on the habit of a major sector of the Rocky Valley fault and on the structural events involved in the development of its configuration. A brief statement on the general habit of the Rocky Valley fault was included by Oder (1958) in his article on the results of the American Zinc-DMEA drilling program in the West New Market area.

In the West New Market area the Rocky Valley fault superimposes Cambrian and Lower Ordovician rocks on Middle Ordovician strata. The maximum stratigraphic displacement of the fault is more than 4,000 feet. The horizontal displacement must locally exceed 2 miles and probably is as much as 4 miles. Although most of the horizontal displacement is dip-slip, an appreciable but as yet unknown amount of strike-slip movement also occurred.

The low dip of the Rocky Valley fault in the West New Market area has been proved conclusively by the drilling. The upper plate of the thrust fault is but the thin erosional remnant of the Rocky Valley anticline that was thrust north-northwestward over dark

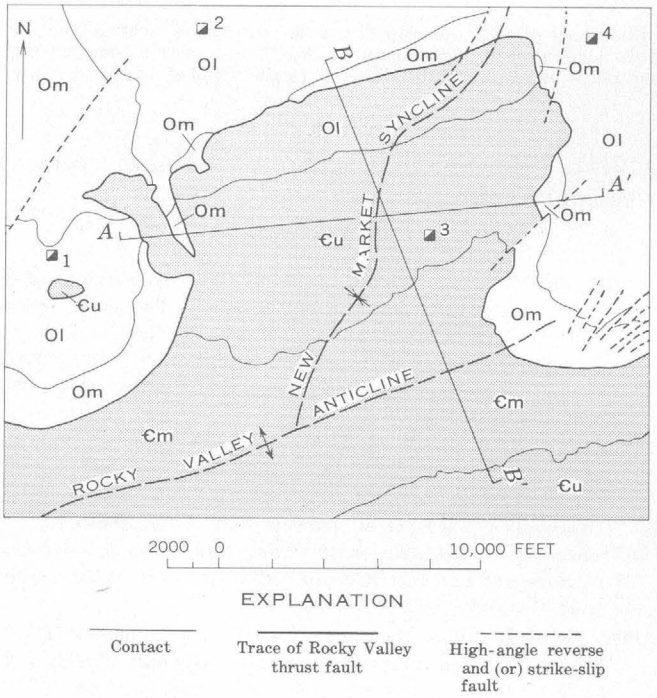

FIGURE 2.—Geologic sketch map of the West New Market area. 1, Young mine; 2, Friends Station mine; 3, New Market mine; 4, Grasselli mine. *A–A′* and *B–B′*, lines of structure sections shown on figure 3. Cm, Middle Cambrian; Cu, Upper Cambrian; Ol, Lower Ordovician; Om, Middle Ordovician. Stippled area, upper plate of Rocky Valley thrust fault. Geology adapted from Bridge (1945).

shaly zones in the Middle Ordovician Lenoir Limestone (figs. 2 and 3). It is of interest to note that Bridge's interpretation (1956, pl. 1, sec. M–M′) of the structure along section *B–B′* (figs. 2 and 3) varies only in minor detail from the interpretation based on the drilling data. The only significant differences brought out by the drilling are the somewhat greater depth to the fault surface, the broad synclinal folding of the fault surface, and the general tendency of the fault to remain at the same horizon in the Middle Ordovician rocks rather than to crosscut minor folds under the fault. It is the post-thrust downwarp along the axis of the New Market syncline that helped preserve the upper plate in the West New Market sector when the rocks on anticlinal warps to the east and west were eroded.

A brief outline of the structural history of the West New Market area directly related to the formation of the Rocky Valley fault follows:

(1) Compressive forces acting generally from the southeast formed a pair of asymmetrical folds, that is, a synclinal-anticlinal couple with the common limb near vertical or overturned to the northwest.

(2) Further pressures ruptured the paired folds along the common limb, thrusting the anticline north-northwestward over and beyond the syncline.

(3) Continued or renewed compression, acting on both the upper and lower plates of the fault as a unit, caused further folding along the axis of the Rocky Valley anticline and developed the crosswarp called the New Market syncline. This post-thrust folding is well illustrated by the geologic sections (fig. 3) and by structure contours on the thrust surface (*A*, fig. 4). The general parallelism of the folded thrust surface and the folds in stratigraphic horizons as much as 700 to 900 feet lower is well shown in the structure sections (fig. 3), and by the structure contours on the Lower-Middle Ordovician unconformity, the "chert-matrix" sandstone at the base of the Mascot Dolomite, and the "Minus-C" oolite in the Kingsport Formation (*B*, *C*, and *D*, respectively, fig. 4). Contours on several other horizons beneath the thrust surface show similar configurations.

(4) A fourth and final stage is represented by zones of high-angle reverse faults that dip southeast. This later faulting also acted on both the upper and lower plates of the Rocky Valley fault as a unit, offsetting the thrust surface as well as lower stratigraphic horizons. Although this faulting is classified as high-angle reverse on the basis of stratigraphic displacement, some of the faults may have strong strike-slip components. Surface evidence of this later faulting is well illus-

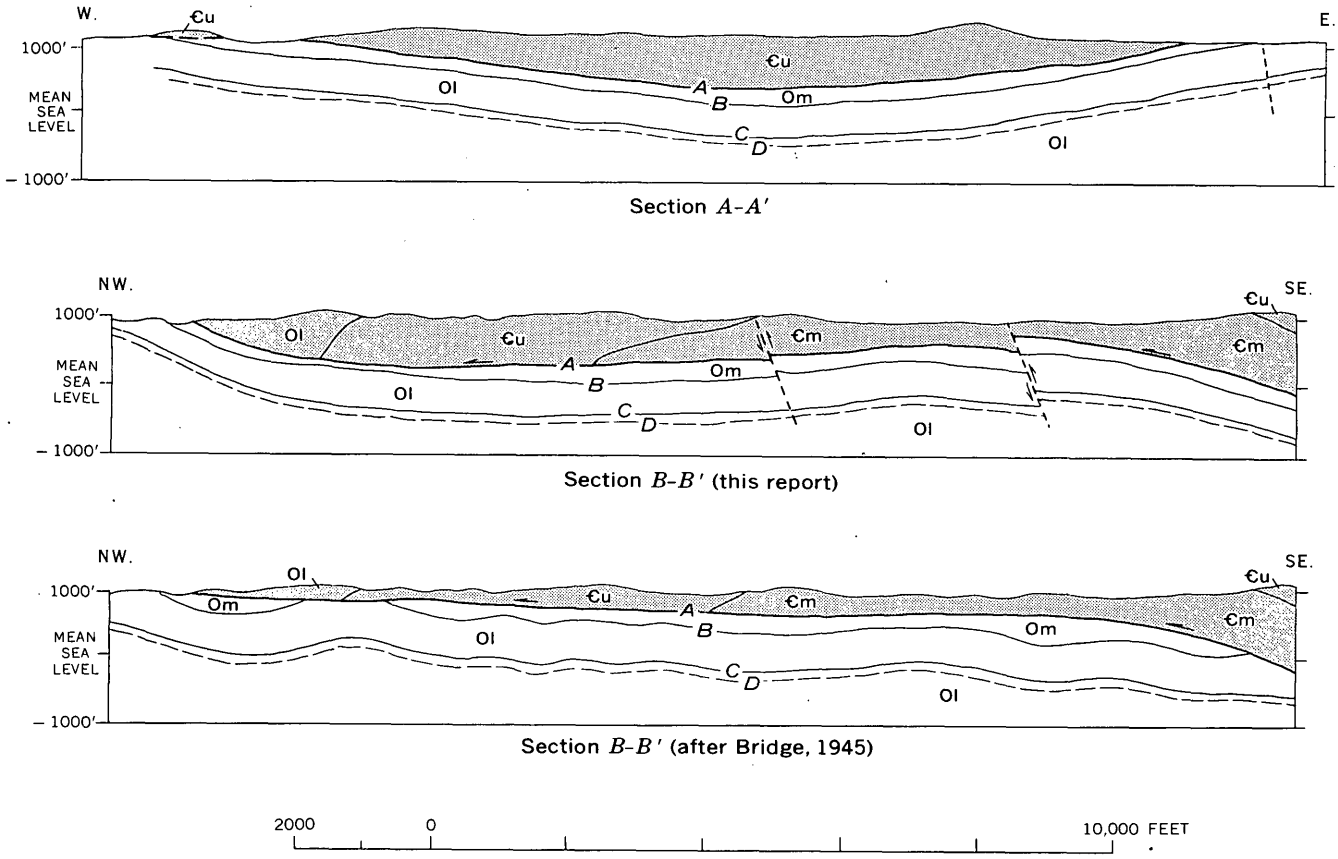

FIGURE 3.—Structure sections in the West New Market area. For lines of sections see figure 2. Horizons (contoured on figure 4): *A*, Rocky Valley thrust surface; *B*, Lower-Middle Ordovician unconformity; *C*, "chert-matrix" sandstone (base of Mascot Dolomite); and *D*, "Minus-C" oolite. Upper plate of Rocky Valley thrust fault stippled; arrows show directions of relative movement on faults.

trated by the conspicuous offset in the trace of the Rocky Valley fault in the eastern part of the area (figs. 2 and 4). This specific zone of late-stage faulting has been traced by drilling for more than a mile to the southwest along the crestal area of the Rocky Valley anticline (figs. 2, 3, and 4). The hash of faults at the extreme eastern margin of the area mapped by Bridge (1945, 1956) and reproduced in figures 2 and 4 may also be a part of the zone of later movement along the crestal area of the Rocky Valley anticline.

The prominent local depression on the east limb of the New Market syncline, shown on the structure-contour map of the Lower-Middle Ordovician unconformity (*B*, fig. 4), is a fossil sinkhole or channel. At this site the drilling penetrated an abnormally thick section of Middle Ordovician beds. These beds fill a channel or hole several hundred feet deep cut into the Mascot Dolomite by pre-Middle Ordovician erosion. Similarly filled depressions on this paleo-erosion surface have been recognized elsewhere in East Tennessee by Keith (1901, p. 2), Rodgers (1943), Laurence (1944), Bridge (1955), and S. W. Maher (personal communication).

REFERENCES

Bridge, Josiah, 1945, Geologic map and structure sections of the Mascot-Jefferson City mining district, Tennessee (scale 1:31,680): Tennessee Dept. Conserv., Div. Geol.

——— 1955, Disconformity between Lower and Middle Ordovician series at Douglas Lake, Tennessee: Geol. Soc. America Bull., v. 66, p. 725–730.

———1956, Stratigraphy of the Mascot-Jefferson City zinc district, Tennessee: U.S. Geol. Survey Prof. Paper 277.

Keith, Arthur, 1901, Description of the Maynardville quadrangle (Tennessee): U.S. Geol. Survey Geol. Atlas, Folio 70.

Laurence, R. A., 1944, An early Ordovician sinkhole deposit of volcanic ash and fossiliferous sediments in East Tennessee: Jour. Geology, v. 52, p. 235–249.

Oder, C. R. L., 1958, How American Zinc's Tennessee DMEA program proved 35,000,000 tons ore: Mining World, v. 20, no. 7, p. 50–53.

Rodgers, John, 1943, Geologic map of Copper Ridge district, Hancock and Grainger Counties, Tennessee: U.S. Geol. Survey, Strategic Mins. Inv., prelim. map.

——— 1953, Geologic map of East Tennessee with explanatory text: Tennessee Dept. Conserv., Div. Geol. Bull. 58, pt. 2.

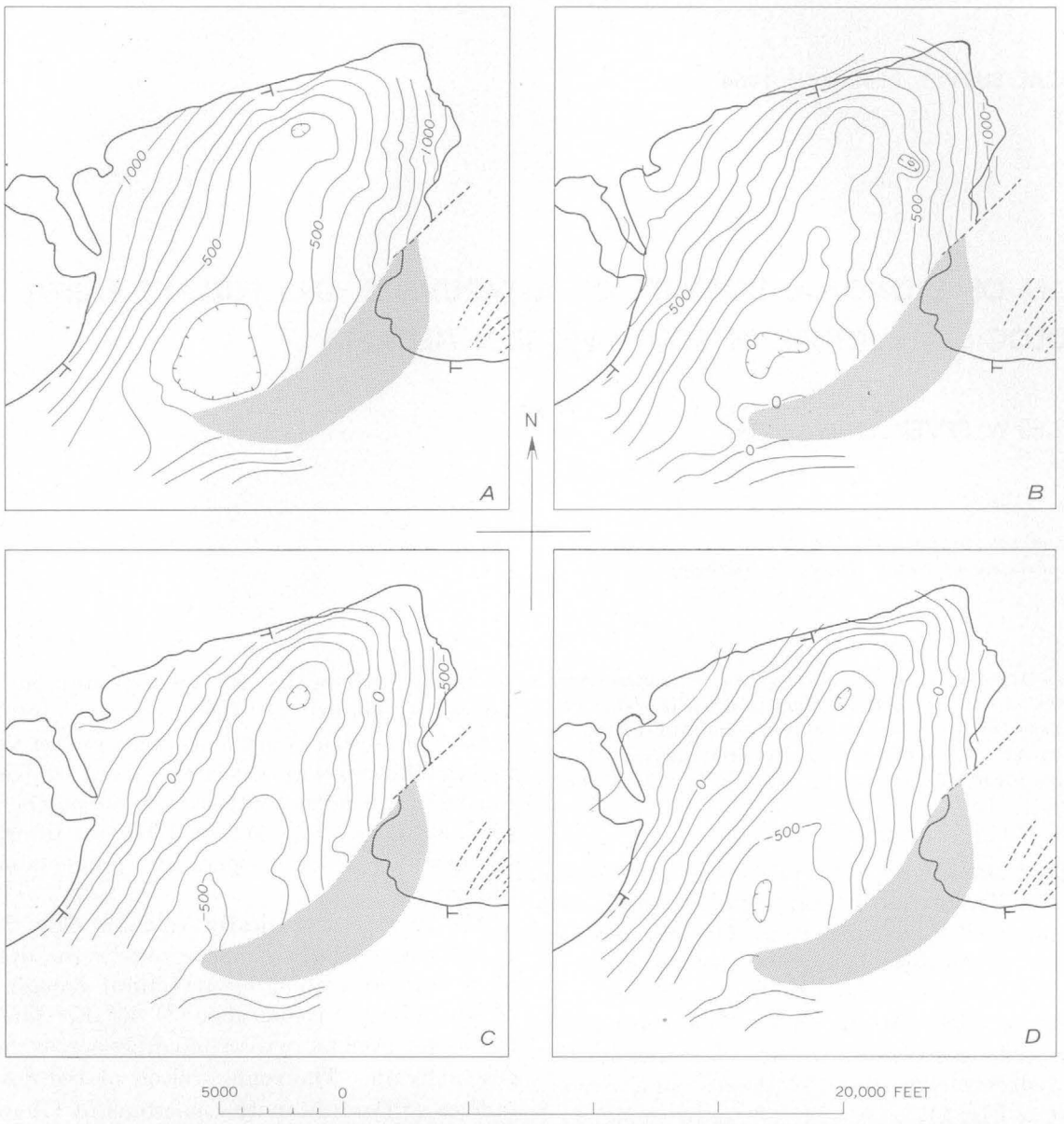

FIGURE 4.—Structure-contour maps of *A*, Rocky Valley thrust surface; *B*, Lower-Middle Ordovician unconformity; *C*, "chert-matrix" sandstone or base of Mascot Dolomite; and *D*, "Minus-C" oolite, in the West New Market area. Datum mean sea level; contour interval 100 feet. Stippled area is zone of high-angle reverse and strike-slip faults. Other symbols as in figures 1 and 2.

RELATION OF ECONOMIC DEPOSITS OF ATTAPULGITE AND FULLER'S EARTH TO GEOLOGIC STRUCTURE IN SOUTHWESTERN GEORGIA

By CHARLES W. SEVER, Quitman, Ga.

Work done in cooperation with the Georgia Department of Mines, Mining, and Geology

Abstract.—Mapping of geologic structure in southwestern Georgia revealed that all existing mines in deposits of attapulgite and fuller's earth are near the axis of a southwest-plunging structural trough. Recognition of this relationship should aid in prospecting for other economically valuable deposits of these clays.

Deposits of attapulgite and a mixture of attapulgite and montmorillonite, locally called fuller's earth, are mined at many sites in southwestern Georgia and the adjacent part of Florida. These clay deposits occur in the upper part of the Hawthorn Formation of the Alum Bluff Group of middle Miocene age. The relationship of these deposits to geologic structure was noted during a recent hydrogeologic study of Decatur and Grady Counties, Ga. (fig. 1).

The clays are gray to light green, finely laminated, nonplastic, highly absorptive, and have a low specific gravity. Reportedly, they occur at three distinct horizons between altitudes of 100 and 220 feet (fig. 2) and are discontinuous in each horizon. Mining is by open-pit method where the clay deposits crop out along the sides of stream valleys. Beds as thin as 3 feet are mined if the overburden is not more than 15 feet thick. The greatest known clay thickness, about 30 feet, is in a mine about 2 miles southeast of Meigs, Ga. Drilling mud, cleaning compound, oil filter, cat litter, and dust for insecticides are the principal products made from the clay.

All known economically valuable clay deposits in Decatur and Grady Counties overlie the deepest part of a southwest-plunging structural trough, the axis of which locally trends about N. 45° E. The structure has been traced more than 160 miles across the Georgia coastal plain. The configuration of the downwarped surface of the Suwannee Limestone of Oligocene age, which underlies the Tampa Limestone of early Miocene age, is shown by structural contours on figure 1. The contours are based on the control points shown, which were determined from logs of wells for which the land-surface altitude was known.

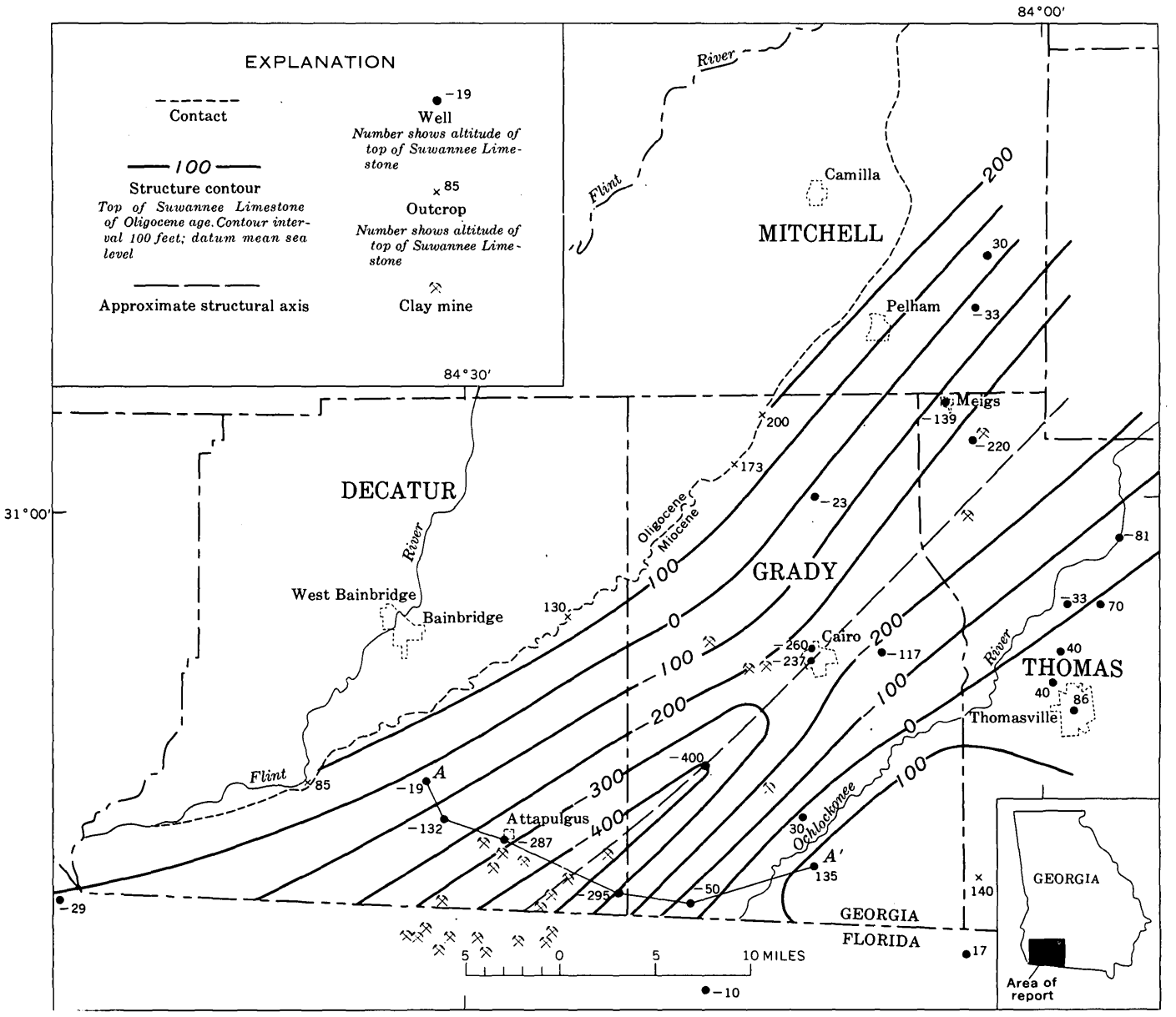

FIGURE 1.—Structural-contour map of the top of the Suwannee Limestone of Oligocene age, showing location of clay mines in southwestern Georgia and northern Florida.

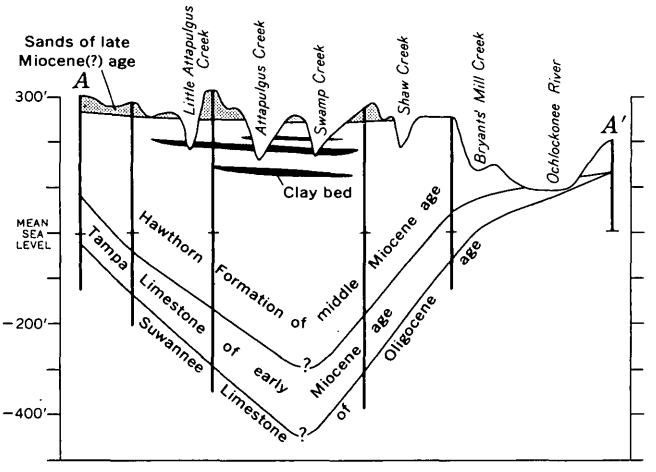

FIGURE 2.—Geologic section *A–A'* across structural trough in Decatur and Gray Counties, Ga. Location is shown on figure 1.

As neither the clay beds within the Hawthorn nor the overlying sands of late Miocene(?) age (fig. 2) are similarly downwarped, it is postulated that the structural movement occurred after the Suwannee and Tampa were deposited but before the clay beds of the Hawthorn were laid down.

Because all the existing clay mines are within the limits of the structural trough and most are near its axis, it seems quite likely that the deposition of the clay was controlled either by continuation of the downwarping that produced the trough or by compaction of the underlying unconsolidated deposits in the deeper part of the trough. In the past, prospecting for clay has proceeded in a rather haphazard fashion, but on the basis of the findings described in this article, it is suggested that future prospecting be concentrated along the axis of the buried structural trough.

PROFILES OF RIVERS OF UNIFORM DISCHARGE

By W. B. LANGBEIN, Washington, D.C.

Abstract.—The concavity of the profile of rivers of uniform discharge increases with length and decreases with rate of discharge. This observed concavity is in accord with random-walk models, which indicate that profile shape is independent of base level and is determined by length, fall, and discharge.

The ubiquitous concavity of the profile of rivers has been ascribed to several causes—as, for example, increasing discharge, decreasing size of bed material in the downstream direction, or more complex causes. It will be instructive, therefore, to examine under what conditions the profiles of rivers of uniform discharge are concave.

The problem was explored in a previous paper (Leopold and Langbein, 1962) by the use of random-walk models. A profile so defined without reference to an increasing downstream discharge is concave, and approaches base level asymptotically. Throughout the present article the term "profile" means the energy grade line, not the backwater curve.

An asymptotic profile is infinite in length, and so to apply the model to more realistic examples, a constraint of length was introduced into the random-walk model. These computations showed that (1) the constraint of length reduces the concavity, and for some short lengths, the profile is linear, and (2) a change in base level along such a profile alters length in such a way as not to modify the profile. Thus, base level as such has no effect on the upstream profile. This finding supports Rubey (1952).

However, the random-walk model does not consider the effect of a downstream increase in discharge, a significant factor in the hydraulic geometry of most rivers. Slope as well as velocity, depth, width, and frictional resistance are mutually adjusted so as to minimize total work and to distribute work uniformly. Field data show that slopes of rivers in humid regions generally tend to decrease at about the 0.6 to 0.8 power of the bankfull discharge. Thus, the concavity of a profile varies significantly with the rate at which discharge changes. As a corollary, a reach of river in which discharge is uniform would have a uniform slope.

This finding seems to differ from that derived from the random-walk profiles, which were, as stated, independent of discharge. The two results can be shown to be quite consistent. Data are given to show that rivers of uniform discharge may be concave, provided they are sufficiently long, but that increasing discharge is indeed the cause of major concavity.

RANDOM-WALK PROFILES

A random-walk model works as follows: Consider an initial point on the landscape, above base level. The flow of a stream from this point, as drawn on a graph, is plotted in unit steps to the right with two choices at each step. There is the probability p that it will move downward one unit of elevation or the probability q that it will continue at the same level. Since there are only these two alternatives, $p+q$ must equal unity. These steps may be considered as infinitesimal approximations to a profile.

In the first model used in this study, a condition that the rate of energy expenditure is proportional to the height above base level was included in the model by varying the probability p of a downward step so that it was proportional to the height above base level, decreasing to zero when a random walk reached base level.

In an alternative model, the random walks were constructed without reference to a base level; that is, the probabilities of downward steps remained unchanged. Then after the random walks were constructed, an average elevation of the walks at successive distances from the origin was computed considering base level as an absorbing medium; that is, random walks were terminated upon reaching base level. The average elevation at any distance from the origin includes only those walks that survive or remain above base level. The averages defined by this model also produce a profile that approaches base level asymptotically.

Natural streams, however, have a finite length and intersect base level at a finite angle. A random-walk model can also be used to define the effect of length on the profile. In this case, in computing the average path, one selects only those random walks that reach base level at or before reaching a given limiting distance. Profiles constructed in this way show that the shorter the profile, the less the concavity; short streams of uniform discharge would exhibit no sensible concavity.

CONCAVITY OF LONG RIVERS OF UNIFORM DISCHARGE

Data on profiles of long rivers of uniform discharge can be obtained from streams which drain mountain headwaters and then flow over long desert reaches receiving no major affluents on the way to the stream-mouth.

However, in comparing profiles of the lower reaches of different rivers, one needs a measure of length, because according to the theory, concavity increases with length. The measure of length should be dimensionless because the concavity is dimensionless. Lengths should be expressed in ratio to the length of a unit horizontal step in the random-walk model. It shall be assumed that the length of a unit step is proportional to the square root of the mean discharge of the river. The justification for this assumption rests upon evidence that planimetric dimensions of rivers, such as river widths and meander lengths, vary with the square root of the discharge. The ratio of length in miles to the square root of the mean discharge in cubic feet per second is therefore used as a length ratio.

The accompanying table contains pertinent data for several rivers of the kind described above. Lengths shown are river mileages from the points listed to the mouth. The dimension H is the total fall over the length indicated, and A is the difference in altitude between the profile at mid-distance and the straight line connecting the ends of the profile. Concavity equals the ratio $2A/H$.

The discharges listed are estimated "virgin" flows—average natural flows before depletion for irrigation. The discharges probably decrease due to evaporation and transpiration losses over the lower reaches as the streams traverse arid regions, a fact that would tend to introduce a measure of convexity into the profiles. This phenomenon appears to have affected the profile of the Nile below Aswan, as a result of several millenia of irrigation.

A plot of the concavity in relation to the stream-length factor, $L/\sqrt{Q}$ is shown in figure 1. The data clearly define an increasing concavity with increasing length factor. Scatter is less than expected, considering the variations in lithology along a single river and from one river to another. The graph includes streams in areas of greatly differing geology, and although particular profiles may be greatly affected by a particular

Length, discharge, and concavity of profile of rivers with uniform discharge

[Symbols defined in text]

River	Upstream point or elevation at which profile begins	River length (mi)	Discharge Q (cfs)	$L/\sqrt{Q}$	A (ft)	H (ft)	Concavity	Source of data
Indus (Pakistan)	15 mi below Panjand Paka.	500	200,000	1.1	14	300	0.09	Hydrology Directorate, West Pakistan Public Works Dept.
Nile (Sudan, Egypt).	Atbara River	1,650	100,000	5.2	225	1,140	.35	"Sudan Irrigation," Ministry of Irrigation and Hydroelectric Power, Khartoum, Sudan, 1957, and Nile Control General Inspectorate, Cairo, Egypt.
Amu-Dar'ya (U.S.S.R).	Elev. 250 m	650	47,000	3.0	50	640	.16	1:1,000,000 Maps of the World, AMS 1301.
Syr-Dar'ya (U.S.S.R.).	Tashkent	690	20,000	4.8	90	700	.26	1:1,000,000 Maps of the World, AMS 1301; discharge data from Stevens (1949).
Colorado (U.S., Mexico).	Virgin River	470	20,000	3.3	70	740	.19	La Rue (1925, pl. 3).
Murray (Australia)	Wentworth, New South Wales.	515	12,000	4.7	18	106	.34	W. M. Anderson, Deputy Engineer-in-Chief, Engineering and Water-Supply Dept., State of South Australia.
Rio Grande (U.S., Mexico).	Pecos River	450	8,000	5.1	85	450	.38	U.S. Geological Survey topographic maps and water-supply papers.
Gila (Arizona)	Salt River	170	2,000	3.8	90	900	.20	Do.
Truckee (Nevada)	Sparks, Nev	50	1,100	1.4	0	560	0	Do.
Walker (Nevada)	Junction of west and east Walker Rivers.	52	500	2.3	13	360	.07	Do.
Sevier (Utah)	Elev. 4,700 ft	75	450	3.5	25	180	.28	Do.
Laboratory flume		.04	10	.01	0		0	Simons and others (1961).

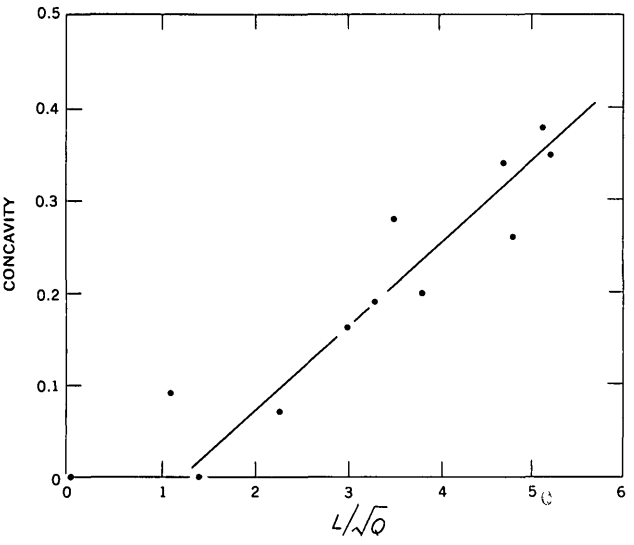

FIGURE 1.—Relation of concavity to stream length (L) and discharge (Q).

geologic condition, it would be very surprising if the various conditions by chance produced effects that agreed so well with differences in length and discharge. Geologic controls might introduce a concavity greater than that indicated, but apparently rivers do not have less concavity.

Note that concavity is zero for a length factor of about 1.2. This corresponds to a very great length. The lower Nile, below Aswan, is about 700 miles long, yet relative to its discharge it is short; its length factor is about 2.2. This profile has no concavity. Nor, for example, does concavity develop in short laboratory flumes on alluvial beds. If one wished to model a channel to test whether concavity in a movable channel could be developed experimentally, one would need a channel more than 1.2 miles long with complete liberty to adjust its slope for a flow of 1 cubic foot per second, and at least 4 miles long for a flow of 10 cfs. No estimate can be made of the length of time required for the channel to adjust to a most probable profile. It might also be observed that in a humid region the lengths of river between major junctions of the drainage network are such that $L/\sqrt{Q}$ is of the order of 1 or less, so that appreciable concavity in such short reaches is not expected.

The degrees of concavity found for rivers of uniform discharge are quite small when compared with degrees for rivers of the same length in which discharge increases in a downstream direction. The concavity of rivers of increasing discharge is nearly always more than 0.5, whereas those reported in the accompanying table are each less than 0.5 Increasing discharge is thus a major source of concavity.

RANDOM-WALK PROFILES IN TERMS OF LENGTH AND RELIEF

In order to compare profile shapes, several random-walk profiles constructed on a nondimensional basis, as explained previously, are shown in figure 2. It must be noted that lengths and elevations on this diagram are in terms of unit steps of the random walks in the model described. A vertical step need not be of the same length as a step in the horizontal direction.

These graphs also indicate that the greater the ratio of length to relief (L/H), the greater the concavity.

EFFECT OF BASE LEVEL ON PROFILE

Although each random-walk profile was constructed in a way that included the position of base level in its definition, a change in "base level" alters the total relief and stream length in such a way that the change has no effect on such a stream profile.

This result is explained as follows: On figure 3, curve AB represents the random-walk profile of a stream with a total fall of 5 vertical units and a length of 10 horizontal units. This curve is consistent with that for L/H=2.0 on figure 2. Assume that base level on figure 3 is raised to elevation 1.22, which intersects the profile AB at point C, at 6 horizontal units.

The problem now is to fit a random-walk profile between points A and C with elevation 1.22 as the new "base level." The ratio L/H is now 6/3.78=1.59. Constructing a random-walk profile between points A and C by interpolating between the nondimensional curves on figure 2 yields the points shown as circles on figure 3, in agreement with the original. Calculations made for other combinations yield the same agreement.

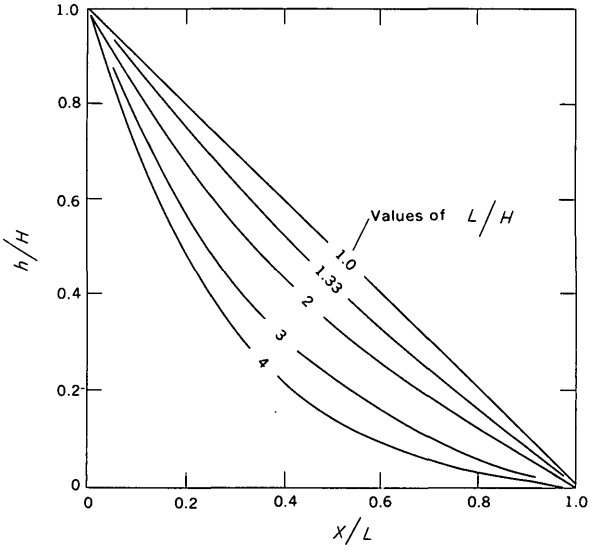

FIGURE 2.—Dimensionless diagram of random-walk profiles. H. total fall in length L; h, fall corresponding to distance X.

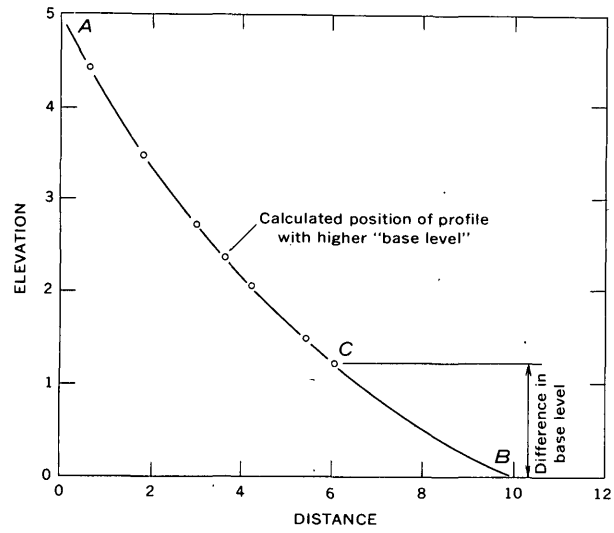

FIGURE 3.—Random-walk profile, showing the effect of raising base level on position of profile. Letters mark points referred to in text.

Thus, a rise in "base level" appears to exert no effect on the profile. The effect of a decline in base level, on the other hand, would depend on the profile of the newly exposed land, a condition extraneous to the argument. The general conclusion is that the profile shape is determined by length, fall, and discharge.

REFERENCES

LaRue, E. C., 1925, Water power and flood control of Colorado River below Green River, Utah: U.S. Geol. Survey Water-Supply Paper 556.

Leopold, L. B., and Langbein, W. B., 1962, The concept of entropy in landscape evolution: U.S. Geol. Survey Prof. Paper 500–A.

Rubey, W. W., 1952, Geology and mineral resources of the Hardin and Brussels quadrangles (in Illinois): U.S. Geol. Survey Prof. Paper 218, 175 p.

Simons, D. B., Richardson, E. V., and Albertson, M. L., 1961, Flume studies using medium sand: U.S. Geol. Survey Water-Supply Paper 1498–A. 76 p.

Stevens, G. C., 1949, Flow, temperature, and quality of water in principal rivers of the interior part of the U.S.S.R.: U.S. Geol. Survey open-file report.

LARGE RETROGRESSIVE LANDSLIDES IN NORTH-CENTRAL PUERTO RICO

By WATSON H. MONROE, San Juan, P.R.

Work done in cooperation with the Department of Industrial Research, Puerto Rico Economic Development Administration

Abstract.—Retrogressive landslides are present in Puerto Rico at the sides of rivers where thick limestone formations are underlain by clay. The landslides grow headward as masses of limestone break away from cliffs, but the slides are comparatively stable except near cliffs and in the banks of rivers.

North-central Puerto Rico between the Río Grande de Manatí and the Río de la Plata is a rugged area in which a few rivers flow in deep valleys that separate areas of karst topography characterized by sinkholes and internal drainage systems. The cliffs at the sides of the through valleys range from about 50 to more than 200 meters in height.

The oldest rocks exposed in the area are largely volcanic and intrusive rocks of Cretaceous and early Eocene age; these are overlain unconformably by a sequence of predominantly limestone formations of late Oligocene and early Miocene age.

Large apparently nearly stable landslides are common in two belts (fig. 1) in the limestone region at places where massive limestone rests on marl or clay. In the southern belt, massive to thin-bedded Lares Limestone (Oligocene) rests on clay, sand, and gravel of the San Sebastián Formation (Oligocene); in the northern belt, alternating beds of hard limestone and soft marly and clayey limestone of the Aguada Limestone (early Miocene) rest on very clayey chalk of the Cibao Formation (Oligocene and Miocene). In both areas large masses of limestone have broken away from cliffs (fig. 4) and have slid a short distance downhill on the surface of the underlying clay. The landslides at the contact of the San Sebastián and the Lares are generally larger than those at the contact of the Cibao and the Aguada.

The slides are bounded on one side by a nearly vertical cliff of limestone and on the other by a river. The surfaces of the slides from the cliff to the river have a moderate slope that ranges from about 10 to 25 percent. The slide surfaces are hummocky; depressions uphill from the hummocks are common, particularly close to the cliffs that bound the uphill side of the slides.

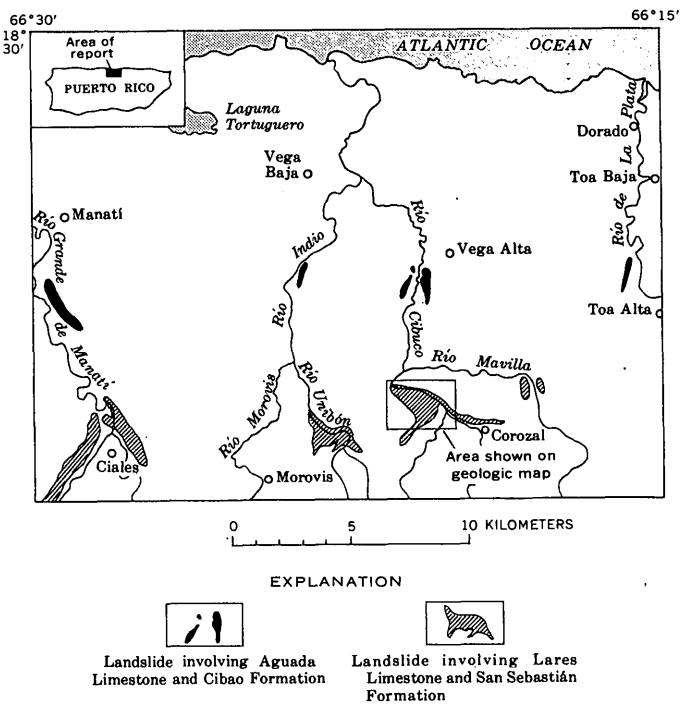

FIGURE 1.—Map of part of north-central Puerto Rico, showing larger areas of retrogressive landslides.

LANDSLIDE AREA 3 KILOMETERS WEST OF COROZAL

One of the largest landslides (figs. 2 and 3) is 3 kilometers west of Corozal. The main part of the slide,

725-328 O—64——9

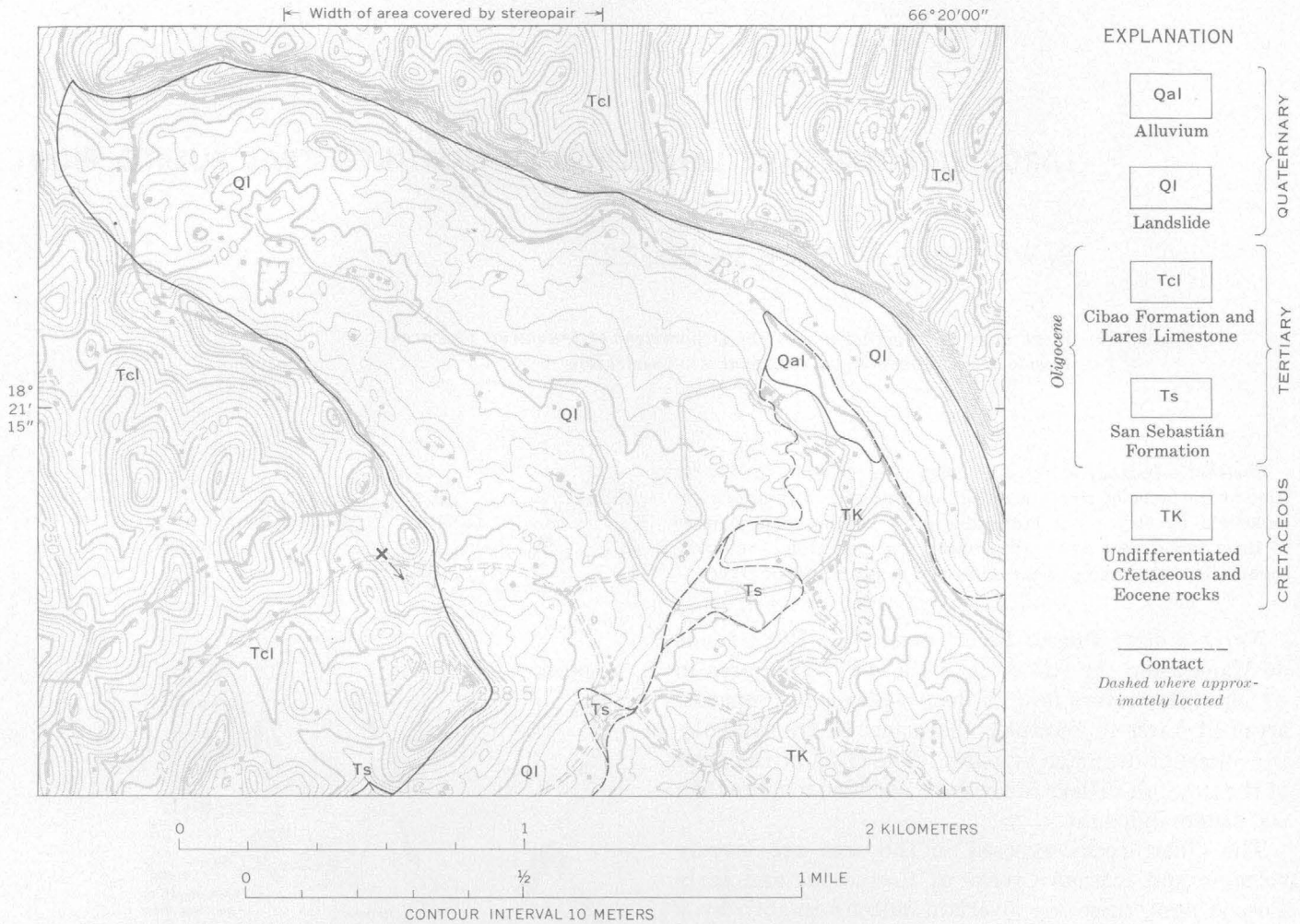

FIGURE 2.—Geologic map of landslide area on both sides of the Río Cibuco, about 3 km west of Corozal. Base from topographic map of the Corozal quadrangle. X and arrow in the south-central part of the map show the place and direction in which the photograph in figure 4 was taken.

from cliff to river, forms a triangle 2,200 m long and 1,300 m wide. Several gullies cut into the slide more than 20 m without reaching the bottom. On the assumption that the slide material is more than 30 m thick, the volume of the slide is greater than 43 million cubic meters, equivalent to about 100 million tons of rock. The breakaway slopes on the southwest and on the north are both steep cliffs of Lares Limestone; limestone of the Cibao Formation caps some of the higher knobs on the cliff north of the river. The surface of the landslide is hummocky and is covered by tilted blocks of limestone.

The stereopair of the same area (fig. 3) shows undisturbed tower-karst on both sides of the river. The notch where a part of the cliff is breaking away is well exposed near the southern ledge of the overlap area of the pair. A ground view of this notch is shown in figure 4. Elongated northwest-trending ridges and swales on the slide are remnants of older slumps. Each small ridge is made up of tumbled blocks of limestone, most of which dip at steep angles. Small depressions are common on the landslide surface. Near the northwestern corner of the stereopair is a high ridge that appears to be a slump block from the northern cliff; if so, the river now flows in the trench between this block and the parent cliff.

Stratified clay, sand, and marl of the San Sebastián Formation are well exposed at a few places in the outcrop belt between the Lares Limestone and the Cretaceous-Eocene rocks; clay and sand can also be seen in

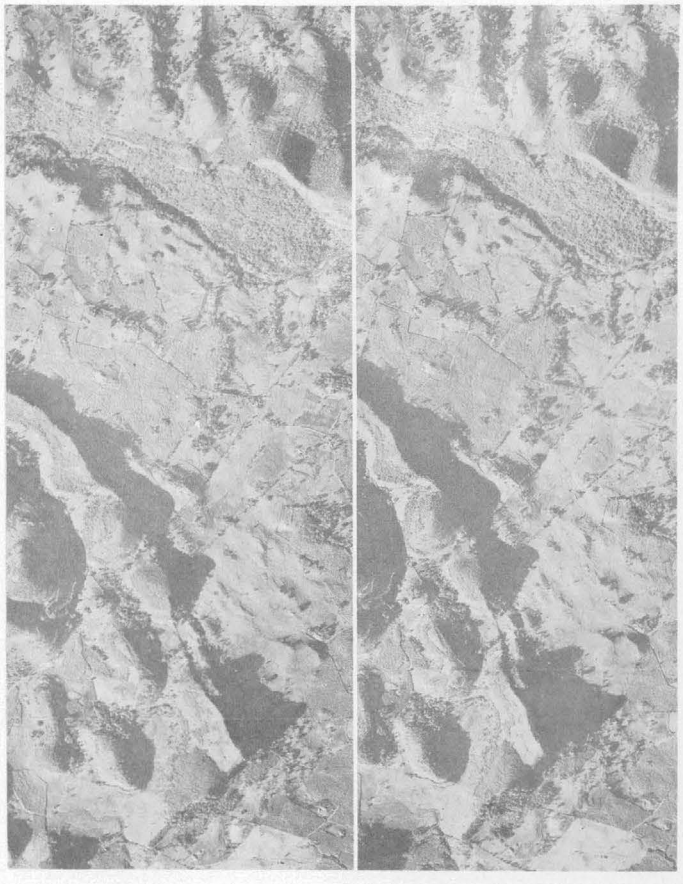

FIGURE 3.—Stereopair of aerial photographs showing the valley of the Río Cibuco about 3 km west of Corozal. Area covered is the central part of figure 2. Scale approximately same as figure 2.

the lower slopes of the narrow slide north of the river, but the bedding is contorted and is obviously involved in the sliding.

The slide material on the north side of the Río Cibuco forms a steep slope. The active lateral erosion of the river would tend to make this slope much less stable than the gentler slope southwest of the river, and the slide material probably moves actively during rainy seasons, for few houses and no roads are built on the north side of the river.

When the clay beds in the San Sebastián Formation and the Cibao Formation become wet during rainy

FIGURE 4.—A segment of a cliff of Lares Limestone that is breaking away at the head of a landslide. (The photograph was taken at point X on figure 2, looking southeast). Note that the block just to the left (north) of the notch has settled a few meters. A knob in the left-central part of the photograph is all that remains of a former slip block. At the extreme left of the photograph the ground surface begins to rise to a third slice, which contains broken blocks of limestone.

periods, the weight of the overlying rock apparently causes the clay to squeeze out under the limestone. Unsupported blocks of the overlying limestone, many as large as 15,000 cu m, tend to break away from the main mass, possibly along joints, and to move downhill. With continued wetting of the clay and further movement downhill, the blocks of limestone break up into smaller blocks. Apparently after movement of a short distance downhill the mass of limestone blocks and clay, sand, and marl reaches a state of equilibrium, and further movement downhill is exceedingly slow, amounting only to a slow feeding of the material to the riverbeds at the foot of each landslide mass. This type of landslide movement has been characterized as retrogressive by Kjellman (Varnes, 1958, p. 31) because the slide grows headward—in the direction opposite to the movement.

REFERENCE

Varnes, D. J., 1958, Landslide types and processes, *in* Landslides and engineering practice: Natl. Research Council, Highway Research Board Spec. Rept. 29, p. 31.

THE ZANJÓN, A SOLUTION FEATURE OF KARST TOPOGRAPHY IN PUERTO RICO

By WATSON H. MONROE, San Juan, P.R.

Work done in cooperation with the Puerto Rico Economic Development Administration

Abstract.—Zanjones are solution trenches that form sets of parallel scars in thin-bedded limestone. They range from a few centimeters to about 3 meters in width and from about 1 to 4 meters in depth. Apparently they form by the widening and deepening of joints by solution.

Several groups of parallel trenches resulting from solution of limestone have been observed in two areas in the outcrop belt of the late Oligocene Lares Limestone in northern Puerto Rico (fig. 1). As trenches of this type have apparently not hitherto been described, I propose the name "zanjón" (pronounced sanhóne), adopted from the Spanish word for large drainage ditch or trench.

Zanjones are trenches as long as 100 meters or more, with vertical sides ranging in width from a few centimeters to about 3 m and in depth from about 1 to 4 m. They occur as parallel trenches oriented generally in the same direction, as shown in figure 2. In the area of figure 2 most of the trenches trend N. 25° to 40° E., but a few shorter ones trend N. 80° to 90° W. Both the trenches and the intervening ridges vary somewhat in width. Because one commonly must cross as many as 8 parallel zanjones in a distance of 100 m., few trails traverse the valleys containing zanjones. Such valleys are so overgrown with vegetation that they are a veritable jungle, as shown in figure 3.

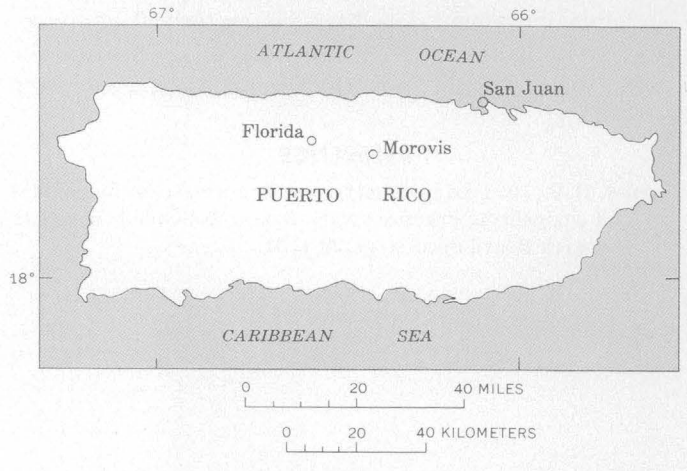

FIGURE 1.—Index map of Puerto Rico showing areas referred to in text.

Figure 3 shows a typical zanjón in the Florida area. This zanjón, most of which is impassable because of heavy jungle growth, is 1½ to 3 m wide, 3 to 4 m deep, and at least 50 m long. The walls are nearly vertical and fairly straight, and the tops of the ridges on each side of the trench are nearly flat. The floor is covered with forest litter and irregular blocks of limestone which appear to have fallen from the walls. Irregular deep cracks in the floor make footing somewhat precarious. This zanjón, located at a on figure 2, trends N. 40° E., nearly at right angles to the trend of the valley.

In another valley in the same area a group of zanjones, located at b on figure 2, lie parallel to the trend of the valley, N. 25° E., but are so narrow and deep that they make the valley impenetrable except at considerable risk. These zanjones are from 30 cm to 1 m wide and 2 to 3 m deep; they form a series of parallel trenches separated by ridges less than a meter wide.

In the Florida area the zanjones have formed in a part of the Lares Limestone that is 20 to 40 m above the base of the formation. This interval of the Lares consists of beds of fairly pure tightly cemented limestone in beds 10 to 30 cm thick. This sequence is underlain by thinner bedded less pure limestone and is overlain by massive purer limestone, neither of which contains zanjones. The base of the massive limestone that overlies the zanjón-bearing unit shows plainly on figure 2.

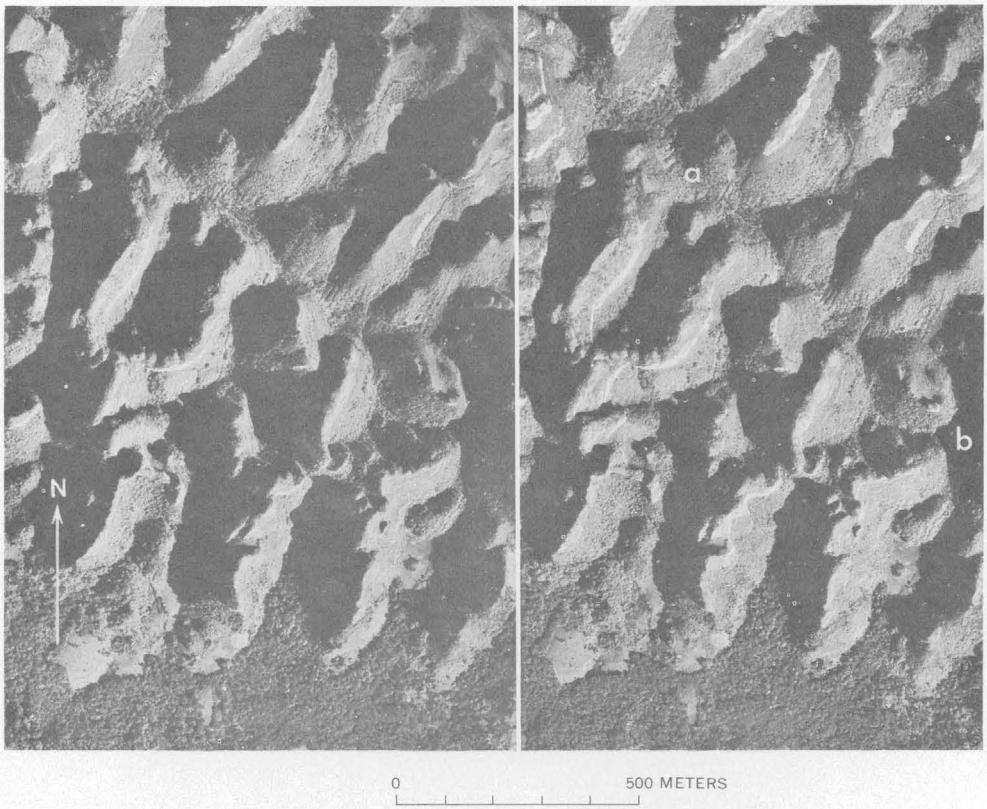

FIGURE 2.—Stereopair of photographs showing karst-valley area 6 km southeast of Florida, P.R. The zanjones are sub-parallel grooves, resembling striations, confined to a thin-bedded limestone until in the bottom of the karst valleys. The base of overlying massive limestone is sharply defined by the upper limit of the zanjones. a, location of zanjón shown on figure 3; b, location of another group of zanjones, referred to in text.

FIGURE 3.—Zanjón in karst valley about 6 km S. 30° E. of Florida, P.R. (coordinates 53,890 m N., 141,300 m E., Florida quadrangle). Aluminum map case rests on blocks of limestone on the floor of the zanjón.

A much larger but less spectacular area of zanjones is about 10 km farther east, in the Ciales quadrangle, 1 to 4 km northwest of Morovis. Here the entire Lares Limestone consists of thin-bedded limestone, and zanjones have coalesced to form a wide band of narrow valleys made up of narrow trenches trending N. 25° to 40° E. (fig. 4). In this area, in contrast to the Florida area, the forest has been cleared to make pasture and most trenches are partly filled with residual soil on which grass is growing. The ridges resemble outcropping ledges of steeply dipping limestone, but actually the limestone is nearly horizontal, as shown on figure 5, in which the strata dip 5° directly toward the camera. Although the topography of the area of zanjones near Morovis generally is more subdued than that of the Florida area, individual zanjones are deep and rugged in both areas.

As previously stated, the zanjones in the Morovis area are restricted to places where the Lares consists of beds of limestone 10 to 30 cm thick. Both toward the east and west the thin-bedded limestone changes to massive limestone, and at these places the zanjones terminate. This is demonstrated 4 km west-northwest of Morovis

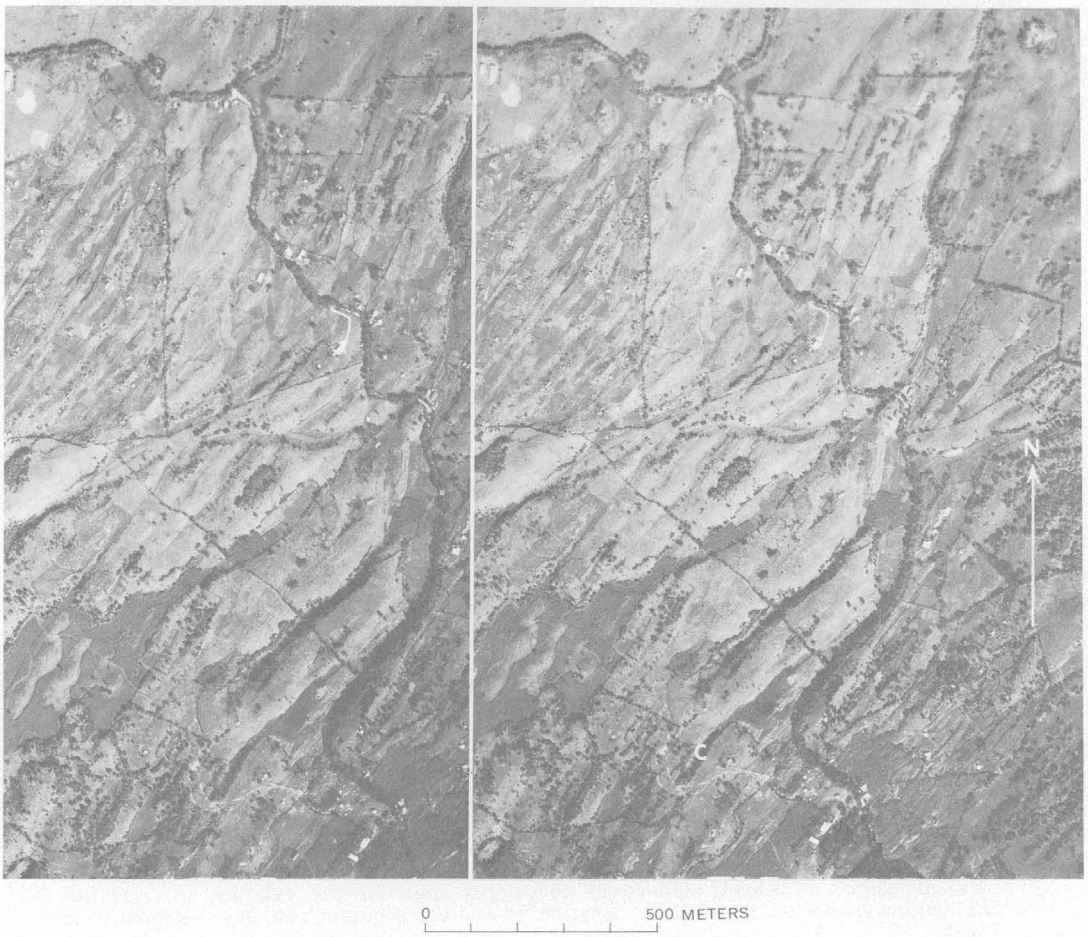

FIGURE 4.—Stereopair of photographs showing an area about 3 km northwest of Morovis, P.R. Zanjones are continuous in valleys and on hills; valleys are compound zanjones. C, location of zanjón shown on figure 5.

FIGURE 5.—Zanjón trending southwestward between hills about 3 km northwest of Morovis, P.R. Location of the zanjón is shown as C on figure 4.

(coordinates 56,010 m N., 151,100 m E., Ciales quadrangle), where pronounced southwest-trending zanjones are found northeast of a ridge of massive limestone but not farther southwest.

Zanjones are related in some way to jointing, for they show notable preferred directions. Examination of the ends of individual zanjones, however, shows only unjointed limestone. The floors of most zanjones have open joints. In the Florida area, the strong N. 25° to 40° E. alinement is evident as shown in figure 2; short zanjones in this area have a trend of N. 80° to 90° W.

Zanjones resemble slightly the lapiés or karren described by Cvijić (1893, p. 221–225; 1924, p. 26–49), but lapiés forms only on pure, generally massive limestone, and the grooves of lapiés are generally much narrower and deeper than zanjones. Furthermore, Cvijić states (1924, p. 40) that lapiés are found on bare rock, seldom at places where rock is overlain by soil. In contrast, zanjones have been observed only in bedded limestone, and the trenches generally contain a layer of soil or forest litter.

In some ways zanjones resemble the cutters described by Whitlatch and Smith (1940, p. 46, 47), but cutters are formed only under fairly thick soil cover, whereas many zanjones are formed with only a very thin soil cover, mainly in the bottom of the trenches.

Zanjones seem to represent a persistent deepening and widening of joint cracks by action of acidic waters derived largely from decay of forest vegetation. Apparently, in northern Puerto Rico the sets of parallel joints form only in rather thin-bedded limestone and do not extend into massive or thick-bedded limestone. Widening of the trenches seems to take place by spalling off of limestone from the sides. As can be seen in figure 2, many of the larger limestone ridges and karst valleys are roughly parallel to the zanjones, and it seems reasonable to assume that they, too, are controlled by the same joint systems as the zanjones. These larger features, however, are not so uniformly parallel or so sharply defined.

REFERENCES

Cvijić, Jovan, 1893, Der Karstphänomen: Geographische Abhandlungen von Albrecht Penck in Wien, v. V, no. 3, p. 221–329

——— 1924, The evolution of lapiés, a study in karst physiography: Geog. Rev., v. 14, p. 26–49.

Whitlatch, G. I., and Smith, R. W., 1940, The phosphate resources of Tennessee: Tennessee Dept. Conserv., Div. Geol. Bull. 48, 444 p.

THE CHARLESTON, MISSOURI, ALLUVIAL FAN

By LOUIS L. RAY, Washington, D.C.

Abstract.—The alluvial fan at Charleston, Mo., just west of the confluence of the Ohio and Mississippi Rivers, was developed by torrential floodwaters coursing down the Mississippi valley and through Thebes Gap. It represents the last geomorphic event in the complex history of the broad alluvial lowlands at the head of the Mississippi Embayment prior to the development of the present flood plain of the combined Mississippi and Ohio Rivers.

An irregular remnant of a once more extensive topographic feature, the Charleston fan, in the center of the Charleston lowland (fig. 1),[1] has an area of approximately 100 square miles, a maximum north-south length of approximately 18 miles, and a maximum east-west width of 10½ miles. Its west margin, along a flood channel of the Mississippi River, now protected from floodwaters by artificial levees, is generally low and in places almost imperceptible. Its irregular east margin, scalloped by the meandering river, is in large part well defined by meander scars, especially to the north where the fan has its maximum elevation above the flood plain. With a steeper gradient than the adjacent flood plain, the maximum slope of the fan surface is southward to the level of the flood plain. From its south tip a low natural levee of younger flood-plain alluvium extends almost to the river in a broad arc along the outside of a now abandoned meander.

Relief is so low that the surface of the fan appears flat, although on aerial photographs shallow channels are discernible (fig. 2). Its general surface, relatively unmodified by erosion since its development, is shown by restored contour lines (fig. 1) that indicate an average slope to the south of almost 2 feet per mile. So low is the local relief that drainage ditches follow the general southward slope of the surface but do not necessarily follow the shallow channels of the original surface.

The fan is mantled by brownish, very fine to medium-fine sandy soils. Normally well drained, they are in marked contrast to the darker, finer textured, and less well-drained soils of the surrounding flood plain. In general, surficial soils of the north part of the fan are somewhat coarser and more porous than those to the south. This, combined with the higher position of the soils to the north above the general flood-plain level and ground-water table, has permitted better internal drainage which has resulted in a more advanced development of the profile of weathering. Auger holes, a few shallow road cuts, and a fresh borrow-pit exposure indicate a distinctly zonal profile. In the borrow pit, 2 miles north of Charleston on Mississippi County Highway N, a characteristic 5-foot profile is exposed. There the surficial A zone consists of 10 to 15 inches of light buff, fine silty sand with a fine platy structure. The B zone below, 14 to 18 inches thick, is a compact, dark-yellow-brown, clayey silty fine sand that breaks into irregular fragments as much as half an inch in diameter. The underlying C zone is relatively unmodified, unconsolidated, grayish-brown silty sand. The section is noncalcareous. A few small pebbles of chert and crystalline rock are widely scattered throughout.

To the south, where drainage is poorer and the soil somewhat finer in texture, soils tend to be lighter in color, mottled, and in places the subsoil contains rusty-brown concretions of iron and manganese oxides. Soil zonation here is generally less well developed, although the sediments are contemporaneous in age with those to the north.

The topography and soils of the Charleston fan distinguish it from the adjacent flood plain and nearby terrace remnants. Its topographic character and regional relationships are best revealed by study of the Bayouville, Cairo, Charleston, Sikeston, Thebes, and Wickliffe topographic quadrangle maps.

RELATION OF THE CHARLESTON FAN TO NEARBY ALLUVIAL TERRACES

Two distinct alluvial terraces, the Blodgett (here named for the village of Blodgett on the terrace surface) and the well-known Sikeston Ridge, rise in step-

[1] The Charleston Lowland of Marbut (1902), virtually synonymous with the Cairo Lowland of Fisk (1944), is used because of its priority.

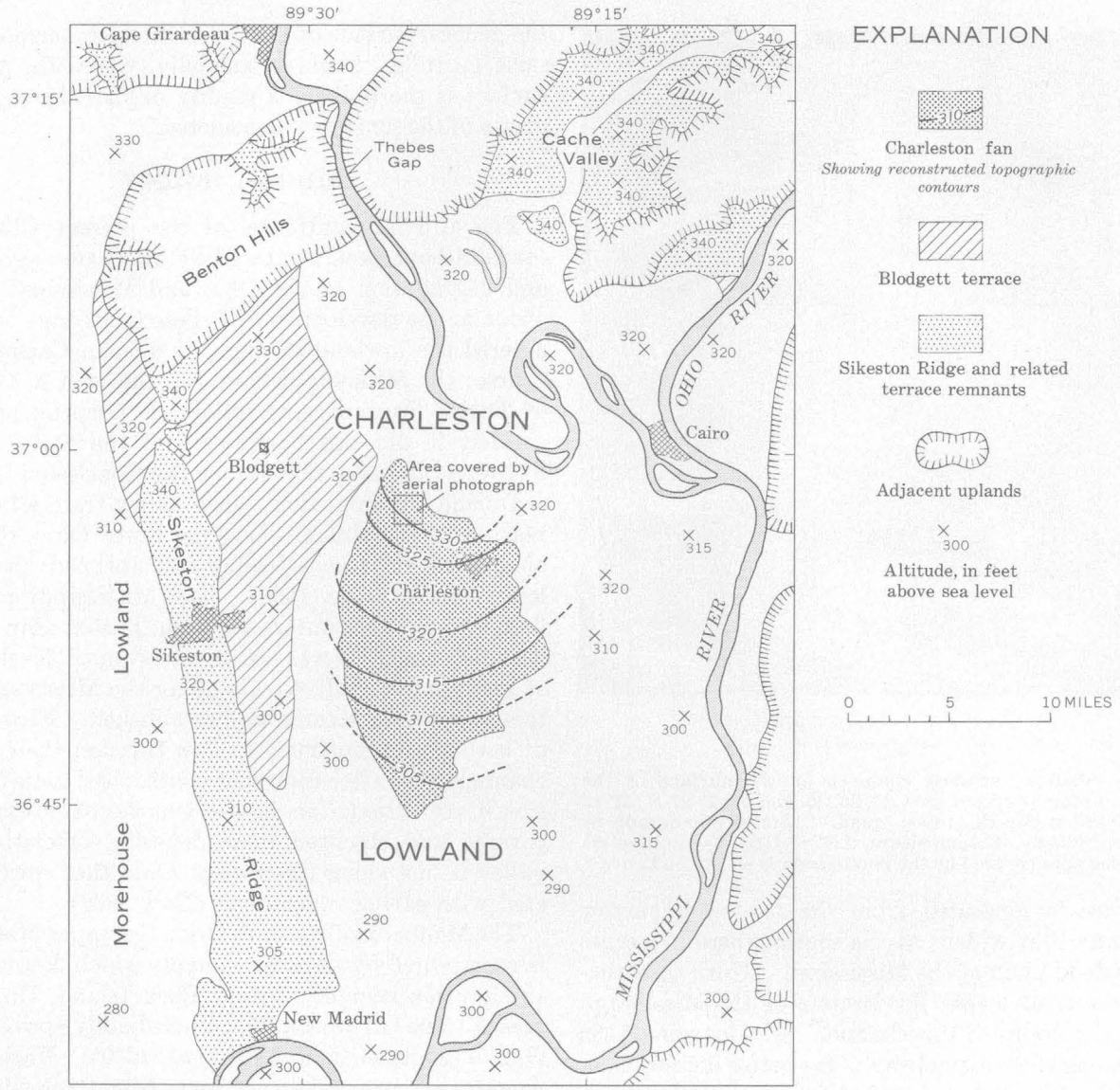

FIGURE 1.—Geomorphic features of the Charleston lowland and environs.

like succession west of the Charleston fan (fig. 1). Sikeston Ridge separates the Charleston lowland from the Morehouse lowland to the west. The character of the two terrace surfaces and their relations to the alluvial history of the region are in marked contrast to that of the Charleston fan.

Sikeston Ridge, ranging from 2 to more than 5 miles in width, extends as a continuous surface, except for two pronounced channels that cut across its north part, for about 35 miles from the Benton Hills to the Mississippi River at New Madrid (fig. 1). The average slope of its surface is to the south, from about 340 to 300 feet, or slightly more than 1.1 foot per mile. This is less than that of either the Charleston fan or the Blodgett terrace.

The sandy surface of the north part of Sikeston Ridge is roughened by flood channels and sand dunes, one of which rises to 377 feet above sea level. The surface of the south part is relatively smooth, with broad shallow depressions marking the braided channels of the aggrading river to which the surface of the ridge owes its origin. Relatively straight, stream-eroded escarpments, in places 20 feet or more high, bound the ridge on both its east and west sides. Small ravines are cutting headward into the sandy alluvium along the marginal escarpments, and the sandy soils of its surface are drifting in places.

Remnants of the somewhat lower Blodgett terrace are present on both sides of Sikeston Ridge (fig. 1), across which they are connected by two ancient floodwater channels. The north part of the east margin of the Blodgett terrace is an escarpment 10 to 30 feet in height, cut by the Mississippi at the margin of its present flood plain. At the north tip of the Charleston fan,

FIGURE 2.—Shallow, braided channels on the surface of the Charleston fan (parts of secs. 22, 23, 26, and 27, T. 27 N., R. 15 E., Charleston, Mo-Ill., topog. quad.). Aerial photograph by U.S. Department of Agriculture, ASCS, UB–4F–26, June 30, 1950. The area covered by the photograph is shown on figure 1.

the terrace is separated from the fan by a narrow channelway that widens to the south, where it merges with the flood plain of the Mississippi. Until construction of artificial levees, floodwaters of the Mississippi occasionally occupied this channel. The margin of the terrace along this channelway is far better defined than that of the Charleston fan, indicating that the floodwaters which cut into the terrace were those of a stream older than the modern floodwaters and were contemporaneous with the building of the fan.

The sandy surface of the Blodgett terrace is covered by a closely spaced network of braided stream channels. Interbraids are peppered with mounds of sand believed to be dunes. These are in part contemporaneous with the terrace alluvium and in part the result of later eolian shifting of the sandy alluvium. Most of the dunes are less than 15 feet high; many are steepsided, and one (sec. 6, T. 27 N., R. 15 E., Thebes quad.) rises sharply to 365 feet—some 40 feet above the general terrace surface.

The southward slope of the Blodgett terrace is approximately 1.4 feet per mile, which is somewhat greater than that of the Sikeston Ridge and distinctly less than that of the Charleston fan. The highest part of the Charleston fan is more than 10 feet higher than the general surface of the older Blodgett terrace in the same latitude. Such an anomaly, where the younger surface is the higher, is readily explainable when the origin of the surfaces is considered.

ALLUVIAL HISTORY

The alluvial landforms of the present Charleston lowland have been produced by alternate aggradation and degradation of the Ohio and Mississippi Rivers. Prior to the development of these landforms the Ohio entered the lowland through its ancient Cache Valley course; the Mississippi flowed to the west at the head of Thebes Gap gorge, to follow an independent course so that it did not participate in the early alluvial history of the area that is now the Charleston lowland.

During Tazewell time, when valley-train alluviation reached its maximum along the lower Ohio, the Ohio abandoned the Cache Valley and assumed its present lower course (Ray, 1963). The Mississippi probably first sent its floodwaters through Thebes Gap during late Cary time. It was not, however, until development of the Mankato valley train along the Mississippi that this new course became well established. Floodwaters of both rivers continued to flow through their ancient channels long after their new courses had come into use. Post-Cary alluviation in the Charleston lowland has covered and obscured those deposits correlative with valley trains along the ancient Ohio that were associated with earlier glaciations (Ray, 1963).

The Mankato valley train along the upper Mississippi is represented by terrace remnants which descend from an elevation near 600 feet at Rock Island, Ill., to 365 feet at Cape Girardeau, Mo., immediately above Thebes Gap (Leighton and Willman, 1949). Valley-train deposition continued downstream from Cape Girardeau through Thebes Gap into the area of the present Charleston lowland, and also to the west, along the ancient Mississippi into the area of the Morehouse lowland (fig. 1). From these two sources a continuous apron of glacial outwash was spread from Crowleys Ridge, west of the Morehouse lowland, to the hilly uplands marking the east margin of the Charleston lowland. Across this aggrading surface the waters flowed in a maze of shallow, braided channels now discernible on two well-preserved terrace remnants—Sikeston Ridge, and the Malden plain to the west and south of the present Morehouse lowland (see Fisk, 1944, pl. 15, sheet 1).

No valley train of Mankato age is recognized in the lower Ohio valley. Aggradation by the Mississippi at this time in the area of the Charleston lowland, however, ponded the lower course of the Ohio and that of

its abandoned channel, the Cache Valley, producing widespread deposition of slack-water silts and fine sands to an elevation comparable to the height of alluviation by the Mississippi. Remnants of these slack-water alluvial flats now comprise the floor of the Cache Valley (fig. 1) and the horizontal terrace surface that extends up the Ohio valley to the area of Paducah, Ky. (Ray, 1963).

With waning of the Mankato ice sheet, aggradation was supplanted by degradation along both the Ohio and Mississippi Rivers. With continued waning of the ice sheet and perhaps its disappearance from the drainage basin of the Mississippi, degradation was retarded. Just how far below the present alluvial surface the erosion at this time was active is not known. Presumably, however, by the close of this period of river degradation the lowlands on either side of Sikeston Ridge had been outlined.

Advance of the succeeding ice sheet of Valders age into the drainage basin of the Mississippi reversed the river regimen to produce aggradation similar to that of Mankato time, but on a smaller scale. The Mississippi River, split at the head of Thebes Gap, flowed into both the Morehouse and Charleston lowlands where aggradation developed the surface now represented by the Blodgett terrace. The widespread apron of outwash supported a maze of shallow braided channels; low dunes were developed from the sandy alluvium on the interbraids.

Aggradation in the Charleston lowland ponded the lower Ohio, producing slack-water alluvial deposits, the remnants of which are now discernible as a terrace some 10 to 15 feet below that of Mankato age. The correlative of the Valders terrace is especially well developed along the margin of the Ohio flood plain north of Oscar, Ky. (Cairo, Ill.-Ky., topog. quad.). As the older and higher deposits of Mankato age had not been removed by erosion from the Cache Valley, that valley was not ponded during the aggradation of Valders age in the Charleston lowland.

Waning of the Valders ice sheet once again reversed the regimen of the Mississippi so that it became a degrading stream. Degradation had not been long established, however, when the Mississippi is believed to have been subjected to an unusual event, a sudden catastrophic torrent that swept down its valley. The specific cause of the torrent cannot be determined in this area, but it may have originated, as suggested by Leighton and Willman (1949), by a sudden release of the impounded waters of Lake Agassiz. It is proposed that the position of the constricted gorge, Thebes Gap, at the head of the embayment lowlands, and the unusual and perhaps relatively long-continued flooding resulted in the development of the Charleston fan.

At the head of Thebes Gap the torrential floodwaters were divided, some flowing to the west through the ancient Mississippi channel into the Morehouse lowland and some flowing to the south through Thebes Gap. Floodwaters entering the Morehouse lowland spread across the broad alluviated flats. Waters pouring through Thebes Gap gorge, on the other hand, had a greater velocity as a result of the slope through the bedrock constriction. When released, either at the northern edge of the present Charleston lowland or from a channel in the then more extensive Blodgett terrace, the floodwaters not only swept along the sediments they were already transporting but those that were excavated by the floodwaters from the alluvium of the lowland immediately below the point of issue from the constricted channel. Presumably the capacity of the floodwaters to erode was so increased by the constriction that excavation of the lowland alluvium was possible.

Reduction of stream velocity with increasing distance from the influence of the constricted channel and below the point of stream incision of the lowland alluvium resulted in deposition by the overloaded stream in the channel axis, thereby creating the Charleston fan. Lateral drainage channels, occupied jointly by the Ohio drainage and Mississippi floodwaters on the east and by the Mississippi floodwaters on the west, prevented extensive lateral alluviation. Once initiated, the obstruction caused by the fan in the main channel continued to grow by floodwater depositional accretion. Alluvium swept on to the fan surface by floodwaters was deposited by the braided surficial stream; that carried to the lateral channels was swept on downstream.

It is not possible now to specifically date the torrent to which the fan owes its origin. Neither can one reconstruct the upstream extent of the fan nor its elevation above the adjacent Blodgett terrace, but both are believed to have been relatively small. Height of the apex of the fan above the bed of the main river channel may have been, however, relatively greater than expectable, for the river presumably excavated deeply into the lowland alluvium as it debouched from the mouth of the constriction before piling the displaced material on to the fan surface.

With cessation of the catastrophic torrent on the Mississippi, development of the present flood plain began. Meandering widely, the rivers have shaped by lateral planation the flood-plain margins by cutting into both the Blodgett terrace and the Charleston fan.

Abandoned meanders and natural levees on the flood plain have produced a topography of greater relief than that of the Charleston fan surface.

REFERENCES

Fisk, H. N., 1944, Geological investigation of the alluvial valley of the lower Mississippi River: Vicksburg, Miss., Mississippi River Commission, 78 p.

Leighton, M. M., and Willman, H. B., 1949, Itinerary of [2nd Pleistocene] field conference: Urbana, Ill., auspices of the State Geologists, 86 p.

Marbut, C. F., 1902, The evolution of the northern part of the lowlands of southeastern Missouri: Missouri Univ. Studies, v. 1, no. 3, 63 p.

Ray, L. L., 1963, Quaternary events along the unglaciated lower Ohio valley: Art. 33 in U.S. Geol. Survey Prof. Paper 475–B, p. B125–B128.

PLEISTOCENE GLACIATIONS OF THE SOUTHWESTERN OLYMPIC PENINSULA, WASHINGTON

By DWIGHT R. CRANDELL, Denver, Colo.

Abstract.—Valleys heading on the southwestern side of the Olympic Mountains were occupied by glaciers three times during Wisconsin (=post-Sangamon) time, and at least once in pre-Wisconsin time. Some of these glaciers extended westward beyond the mountain front as broad lobes and reached the present Pacific shoreline.

The Olympic Peninsula is bounded by the Pacific Ocean, the Strait of Juan de Fuca, and the Puget Sound lowland. Most of the peninsula is occupied by the Olympic Mountains, which include an area of nearly 4,000 square miles. Most of the range is below 5,000 feet altitude, but some peaks reach 7,000 to 8,000 feet. The windward side of the mountains receives very heavy precipitation from moisture-bearing westerly winds from the Pacific; annual precipitation at localities only a few hundred feet above sea level along the western and southwestern margins of the mountains ranges from 115 to 150 inches (U.S. Weather Bureau 1962).

The Olympic Mountains are drained by rivers that flow eastward into Hood Canal, northward into the Strait of Juan de Fuca, westward into the Pacific Ocean, and southward into the Chehalis River, which flows westward into the Pacific. Except for a broad lowland lying mostly below 600 feet altitude in the southwestern part of the peninsula, only narrow strips of land separate the mountains from adjacent bodies of marine water (fig. 1). The western and southwestern sides of the Olympic Mountains are indented by glaciated valleys that extend headward into the high core of the range from which ice flowed out into the lowland during Pleistocene time.

The extent and sequence of glaciations in the southwestern part of the Olympic Peninsula are especially significant because these relations are obscure in other parts of the peninsula where alpine glaciers evidently merged with lobes of Cordilleran ice that occupied the Puget Sound lowland and the Strait of Juan de Fuca. Detailed studies of glacial deposits in the southwestern part of the peninsula have not yet been made, owing perhaps in part to the poor accessibility and limited outcrops in this densely forested region.

The purpose of this article is to summarize tentative conclusions reached from brief reconnaissance studies made during the summers of 1961–63, and to indicate the inferred extent of glaciers from the Olympic Mountains and their relation to the Puget lobe of the Cordilleran ice sheet.

The writer expresses his appreciation to R. K. Fahnestock (oral communication, 1962), University of Texas, for information regarding location of till outcrops on the Olympic Peninsula.

DRIFT OF GLACIERS FROM THE OLYMPIC MOUNTAINS

During the Pleistocene, the southwestern part of the Olympic Mountains was glaciated at least four times. The youngest three drifts are here interpreted as being of Wisconsin (=post-Sangamon) age; the older deposits represent one or more glaciations in pre-Wisconsin time. Distinction between drifts of the various glaciations is based chiefly on differences in depth and degree of weathering, and on differences in physiographic features of the deposits.

The three youngest drifts are here designated as older, intermediate, and younger Wisconsin. These terms refer only to the order of succession, for there is no direct evidence regarding when the drifts were deposited, in absolute years. The three drifts are regarded as being of probable post-Sangamon age because their weathering features do not seem to be extensive enough to account for post-Illinoian time, which has been estimated to include the past 150,000 years (Broecker and others, 1958). Current estimates place the end of Sangamon time about 70,000 years ago (Broecker and others, 1958; Frye and Willman, 1960,

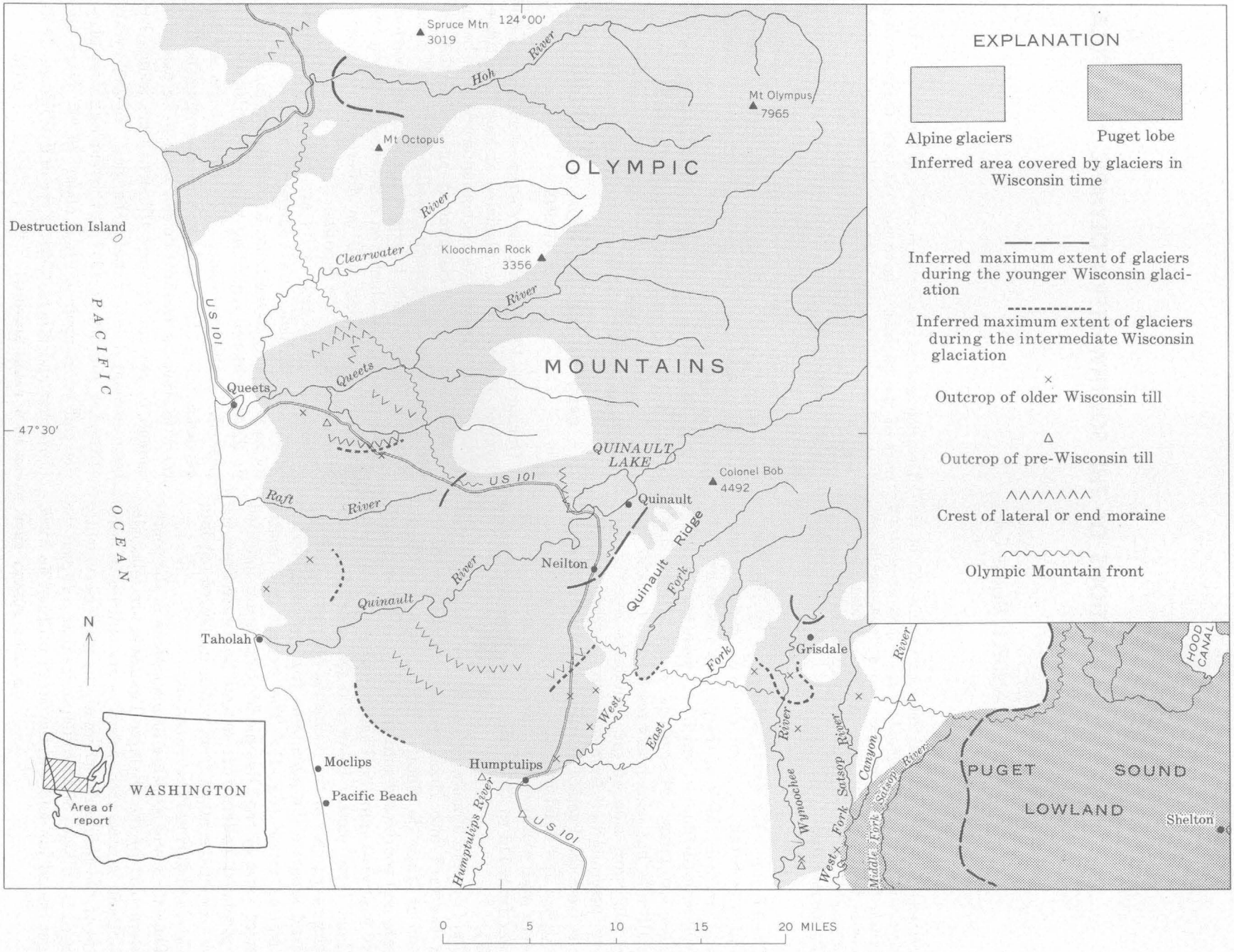

FIGURE 1.—Extent of glaciers on the southwestern side of the Olympic Mountains in Wisconsin time.

1963; Flint, 1963); presumably the older Wisconsin glaciation in the Olympic Mountains occurred some time after this date. Comparison of weathering features between tills of the older and intermediate Wisconsin glaciations, and between tills of the intermediate and younger Wisconsin glaciations suggests that intervals of weathering that separated deposition of these tills were not of sufficient duration to represent Sangamon time.

PRE-WISCONSIN DEPOSITS

Surficial deposits in areas just beyond the limits of Wisconsin glacial deposits are characterized by clayey reddish-brown to reddish-yellow soil profiles. Stones in the upper 5 or 10 feet of these deposits are so weathered that they can easily be cut through with a shovel or a knife. Most of these deposits are fluvial gravels that are oxidized throughout, but till has been observed at a few localities. For example, an extensively weathered till crops out in a roadcut in the Wynoochee River valley in the SW¼ sec. 36, T. 20 N., R. 8 W. (see measured section). It has a clayey red profile of weathering that is overlain by a much less weathered till of the older Wisconsin glaciation. An even more deeply weathered till crops out in a roadcut along U.S. Highway 101 in the NW¼SW¼ sec. 20, T. 20 N., R. 10 W., about 2 miles south of Humptulips. Here, stones in the till are decomposed to a depth of at least 6 feet and the upper 4½ feet of the till has a clayey red profile of weathering; a less-weathered gravel deposit overlies the till.

Measured section at roadcut in SW¼ sec. 36, T. 20 N., R. 8 W., on east side of Wynoochee Valley

	Feet
4. Till, grayish-brown, very compact; oxidized to dark reddish-brown to depth of about 9 feet (older Wisconsin)	12
3. Till, oxidized throughout to dark reddish brown; clayey red profile of weathering 1½ feet thick at top (pre-Wisconsin)	29
2. Sand and gravel; contains irregular masses of compact stony till; oxidized throughout	25
1. Siltstone (bedrock)	

Evidence has not been found that any pre-Wisconsin glacier was substantially larger than the most extensive glacier of Wisconsin time. The outcrop of till south of Humptulips (fig. 1) is only about 2 miles beyond the inferred maximum extent of the older Wisconsin glaciation in the Humptulips River valley. In most of the Olympic Peninsula, the only surficial deposit of probable glacial origin beyond the outermost till of Wisconsin age is fluvial gravel.

OLDER WISCONSIN DRIFT

Till of the older Wisconsin glaciation in the southwestern part of the Olympic Peninsula contains stones in the upper few feet of the soil profile that have weathered rinds 3 to 6 mm thick. These rinds are best developed on fine-grained basic igneous rocks; they are poorly developed on the more abundant graywacke stones. The oxidized till is dark reddish brown and generally extends to a depth of 10 to 15 feet. Surface drainage on the till is integrated, and although morainal topography is subdued, major relief features of the till sheets are still discernible.

This till was seen only in drainage basins of the Satsop, Wynoochee, Quinault, and Queets Rivers. Its distribution indicates that a broad piedmont ice lobe was formed on the lowland beyond the southwest mountain front and was nourished largely by glaciers in the drainage basins of the Quinault and Queets Rivers. Part of this lobe may have reached as far west as the present shoreline of the Pacific Ocean along the Queets valley. Although a comparably large glacier may have occupied the Hoh valley during the older Wisconsin glaciation, its drift was not recognized.

INTERMEDIATE WISCONSIN DRIFT

Till of the intermediate Wisconsin glaciation has a profile of weathering characterized by oxidation to a depth of 3 to 6 feet and by weathered rinds 1 to 2 mm thick on stones of fine-grained basic rocks near the till surface. Constructional topography is generally well preserved, and closed depressions still exist in areas of end moraine.

The most extensive glacier of the intermediate Wisconsin glaciation was a piedmont lobe in the Quinault drainage basin that possibly reached the present Pacific shoreline near Taholah. Two large end moraines were built during the recession of this lobe, each 1 to 2 miles wide, in addition to many smaller arcuate ridges that probably also are end moraines.

In the Hoh valley the glacier evidently was considerably narrower than in the Quinault. Outcrops of till a few miles upstream from the mouth of the Hoh River indicate that this glacier probably reached as far west as the present shoreline of the Pacific. According to Reagan (1909, p. 147), a Hoh valley glacier reached Destruction Island, about 3 miles offshore in the Pacific; however, this information was not verified by the writer.

YOUNGER WISCONSIN DRIFT

The youngest till recognized in the southwestern part of the Olympic Peninsula is oxidized to a depth of

only about 2 feet and lacks even thin weathered rinds on stones in the soil profile. Moraines have sharply defined constructional features, and drainage on them is poorly integrated or unintegrated.

The probable maximum downvalley extent of alpine ice during the younger Wisconsin glaciation has been located, thus far, only in the Hoh, Quinault, and Wynoochee River valleys. Lupton (1915) recognized that Quinault Lake is impounded by a moraine, and Harvey [1] subsequently suggested that the moraine is of the same age as the youngest drift (Vashon) in the Puget Sound lowland. The writer concurs in these conclusions, but the moraine at Quinault Lake apparently does not mark the greatest extent of the younger Wisconsin ice. Drift with identical profiles of weathering is exposed along U.S. Highway 101 as far south as Neilton, and as far west as a point about 5½ miles west of Quinault Lake. The extent of the younger Wisconsin drift was not determined along the central part of the Quinault valley and along several other valleys owing to inaccessibility.

ALTITUDE OF SNOWLINE IN SOUTHWESTERN OLYMPIC MOUNTAINS IN WISCONSIN TIME

The altitude of the snowline during the older and intermediate Wisconsin glaciations can be inferred from cirques on the west side of Quinault Ridge east of Quinault Lake. Here, 6 northwest-trending U-shaped valleys head in cirques whose floors are at an altitude of 1,400 to 1,600 feet. At their mouths, the valley floors hang about 1,000 feet above the floor of Quinault Valley and Quinault Lake. The hanging valleys drain parts of Quinault Ridge that reach maximum altitudes of 2,500 to 4,000 feet. Farther south, northwest-draining valleys that head in lower parts of the ridge are V-shaped in cross profile and apparently have not been glaciated.

Thicknesses of profiles of weathering in surficial deposits in Wright Canyon, 2 miles northeast of the community of Quinault, indicate that the canyon was not glaciated during the younger Wisconsin glaciation, but probably was last glaciated during the older or intermediate glaciation. If so, the local snowline was then probably at an altitude between 1,500 and 2,000 feet. In contrast, cirque floors in the Quinualt River drainage basin that probably were formed during the younger glaciation range in altitude from 3,000 to 3,500 feet.

[1] J. L. Harvey, 1959, Ageologic reconnaissance in the southwest Olympic Peninsula: Washington Univ. [Seattle], unpub. M.S. thesis.

EXTENT OF THE PUGET LOBE

During the last major glaciation (Vashon) of the Puget Sound lowland, the Puget lobe of the Cordilleran ice sheet pushed southwestward to a point about 20 miles west of Shelton (fig. 1). Till deposited by this lobe is oxidized to a depth of about 2 feet, and stones in the soil profile lack weathered rinds. Radiocarbon dates from organic materials below and above the Vashon Drift indicate that the drift was deposited between about 20,000 and 13,000 or 14,000 years ago in the Puget Sound lowland.

Till, somewhat more weathered than the Vashon but of similar provenance, crops out beyond the limit of Vashon Drift west of Shelton. This pre-Vashon till extends as far west as the divide between the Middle and West Forks of the Satsop River, and this divide is breached in at least eight places by short melt-water channels formed along the front of the Puget lobe.

Profiles of weathering on this pre-Vashon drift indicate that it is correlative with the older or intermediate tills of the Olympic Peninsula or both. Its somewhat greater westward extent than the Vashon Drift is consistent with size relations of the Wisconsin glaciers from the Olympic Mountains, as indicated by the drift sheets of the glaciers.

SUMMARY

Distribution of drift of the younger and intermediate Wisconsin glaciations, as well as that of one or more pre-Wisconsin glaciations, indicates that vast amounts of ice formed in the Olympic Mountains during the Pleistocene. The ice flowed outward along major valleys, and locally formed broad piedmont glaciers beyond the mountain front at altitudes only a few hundred feet above present sea level. During these glaciations, the interior of the mountains probably was mantled by extensive icefields, if not by a continuous icecap above which only the highest ridges and peaks protruded.

The younger Wisconsin glaciers were substantially smaller, and may have been fed almost wholly by cirques and small icefields. The present sharp and rugged topography in the high Olympic Mountains may be largely a product of alpine glaciation and an increased rate of mechanical weathering processes in late Wisconsin time.

REFERENCES

Broecker, W. S., Turekian, K. K., and Heezen, B. C., 1958, The relation of deep sea sedimentation rates to variations in climate: Am. Jour. Sci., v. 256, p. 507–517.

Flint, R. F., 1963, Status of the Pleistocene Wisconsin Stage in central North America: Science, v. 139, p. 402–404.

Frye, J. C., and Willman, H. B., 1960, Classification of the Wisconsinan Stage in the Lake Michigan glacial lobe: Illinois Geol. Survey Circ. 285.

Frye, J. C., 1963, Development of Wisconsinan classification in Illinois related to radiocarbon chronology: Geol. Soc. America Bull., v. 74, p. 501–506.

Lupton, C. T., 1915, Oil and gas in the western part of the Olympic Peninsula, Washington: U.S. Geol. Survey Bull. 581.

Reagan, A. B., 1909, Some notes on the Olympic Peninsula, Washington: Kansas Acad. Sci. Trans., v. 22, p. 131–238.

U.S. Weather Bureau, 1962, Climatological data, Washington, annual summary 1961: Climatological data for the United States, by sections, v. 65.

725–828 O—64——10

PRELIMINARY REPORT ON BED FORMS AND FLOW PHENOMENA IN THE RIO GRANDE NEAR EL PASO, TEXAS

By ROBERT K. FAHNESTOCK [1] and THOMAS MADDOCK, JR.,
Austin, Tex., Tucson, Ariz.

Work done in cooperation with the U.S. Section, International Boundary and Water Commission

Abstract.—Studies in two 1,600-foot-long reaches of the Rio Grande near El Paso, Tex., showed that the bed forms ranged from dunes to a plane bed in the 100-foot-wide reach; dunes and prominent bars were always present in the 200-foot-wide reach. Changes in water temperature between March and August caused changes in bed form and hydraulic characteristics.

One of the major difficulties experienced by researchers studying sediment transport in movable bed channels is that a change in one variable changes most of the other variables. It is virtually impossible to hold all but two variables constant so as to see the effect of one variable on another, independent of the interactions of the others.

A good example of this complexity is provided by the record of flow conditions in straightened, rock-revetted reaches of the Rio Grande near El Paso, Tex., during the 1962 irrigation season. These observations emphasized that two parameters—width-depth ratio and water temperature—are more important than many investigators have recognized in the past in determining sediment transport, bed form, and flow conditions.

The studies were made near Vinton, about 20 miles above El Paso, Tex., in two 1,600-foot-long straight reaches with long straight approaches. The upstream reach of the pair, referred to here as the Vinton 200, is about 200 feet wide; the downstream reach, the Vinton 100, is about 100 feet. They are about a mile apart and carried similar discharges of sediment and water.

Water-surface slope was computed from frequent staff-gage readings taken while other measurements were being made. These staff gages were installed by the U.S. Section, International Boundary and Water Commission, for use in this study. Sediment concentrations were measured by methods which integrated the variations over the cross section of the stream. Velocities were measured by standard current-meter techniques. Sediment and discharge data were collected and analyzed by personnel of the Quality of Water Branch of the U.S. Geological Survey. The gross configuration of the bed was mapped at frequent intervals with a plane table and alidade.

Figure 1 (after Simons and Richardson, 1961) outlines the bed forms found in laboratory flume studies of

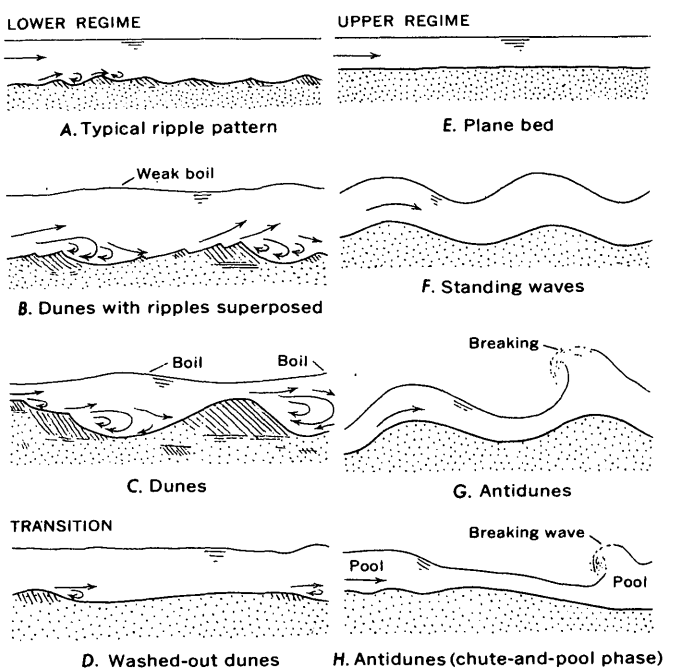

FIGURE 1.—Forms of bed roughness in sand channels (after Simons and Richardson, 1961).

[1] University of Texas.

U.S. GEOL. SURVEY PROF. PAPER 501-B, PAGES B140-B142

sediment transport. These forms in order of increasing flow, starting from a plane bed without motion, are ripples, dunes, transition from dunes to plane bed, plane bed, standing waves, and antidunes. Modifications and combinations of these forms and larger sand waves or bars were found along the Rio Grande.

All the forms found in the laboratory by Simons and Richardson (fig. 1), with the exception of *H*, the chute-and-pool phase of antidunes, were observed in the Rio Grande in this investigation. The larger bars and sand waves were successively attached to opposite banks of the stream. These alternating bars (alined in direction of flow) were observed only at high width-depth ratios. Striking differences in bed-form and flow phenomena were noted between the Vinton-100 and Vinton-200 reaches at all discharges. Marked differences were noted also between March and August flows in the same reach.

Figure 2 shows a series of cross sections taken at similar discharges within the two reaches but at radically different water temperatures. Water temperatures were in the 40's (degrees fahrenheit) during the March measurements and were in the high 70's and low 80's during the August measurement. March flows had higher velocities, were shallower, and had smaller flow resistances than the flows of August. The sinuosity of divergence of the main flow from a direction parallel to the banks (indicated by arrows) is markedly greater in the Vinton-200 reach in August than in March. The asymmetry of the cross sections was greater in August than in March. In the Vinton-100 reach, at these discharges, the flow was more nearly two-dimensional; that is, it diverged little from a direction parallel to the banks.

In the Vinton-100 reach, the bed was largely plane during March but shifted to large dunes in August. In both reaches the flow resistances did not differ materially from those found in flume studies for similar bed forms with similar bed materials.

Figure 3 shows isovels (lines of equal velocity) for March and August flows in the Vinton-100 reach. The changes in velocity, depth, and flow resistance discussed previously are apparent in this figure. The lack of uniformity of the August isovels as compared to those of March may indicate the presence of large-scale turbulence associated with large dunes.

This narrow reach is stable, with a rock revetment on one bank and an earthen bank with willow trees on the other. It efficiently carries all the sediment and water delivered to it by the broader channel upstream. The slope of the Vinton-100 reach averaged 0.00054 foot per foot as compared to a slope of 0.00069 foot per foot in the Vinton-200 reach.

Figure 4 shows the velocity distributions in the Vinton-200 reach. Again there were differences between the March and August observations. The tendency of these sand-bed channels to be higher in the middle and lower along the sides is clearly shown in this figure. Although the August discharge shown in figure 4 is considerably larger than that of March, the mean velocity was less and the velocity distribution much more irregular.

What was the cause of the striking differences between the flows of March and August? Temperature is the most obvious independent variable in the system.

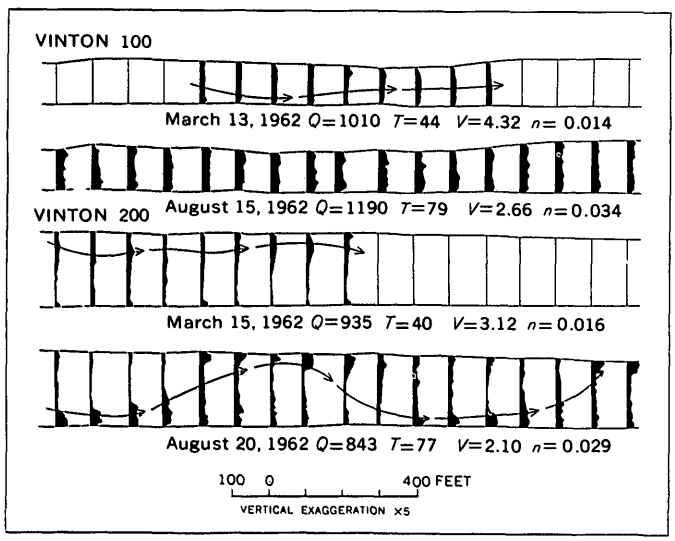

FIGURE 2.—Plan view of two reaches (Vinton 100 and Vinton 200) of the Rio Grande near Vinton, Tex., with cross sections at 100-foot intervals, showing depth of the channel. Cross sections (in black) are rotated to the horizontal. *Q*, discharge, in cubic feet per second; *T*, temperature, in degrees Fahrenheit; *V*, average velocity, in feet per second; *n*, Manning coefficient; arrows indicate main current.

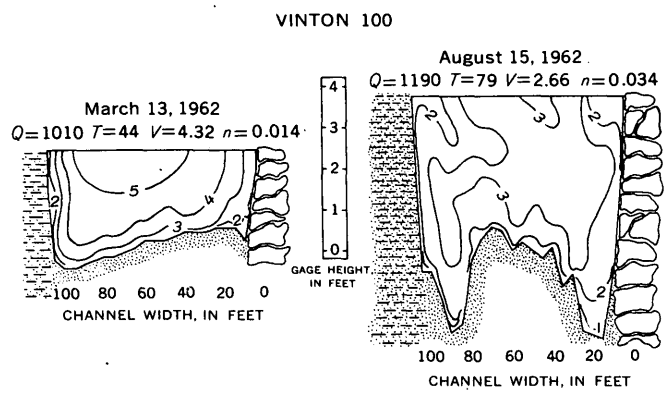

FIGURE 3.—Cross section of the 100-foot-wide (Vinton-100) reach of the Rio Grande near Vinton, Tex., showing isovels, in feet per second. The right bank is a rock revetment, the left an earthen bank with willow trees. *Q*, *T*, *V*, and *n* are defined in the caption of figure 2.

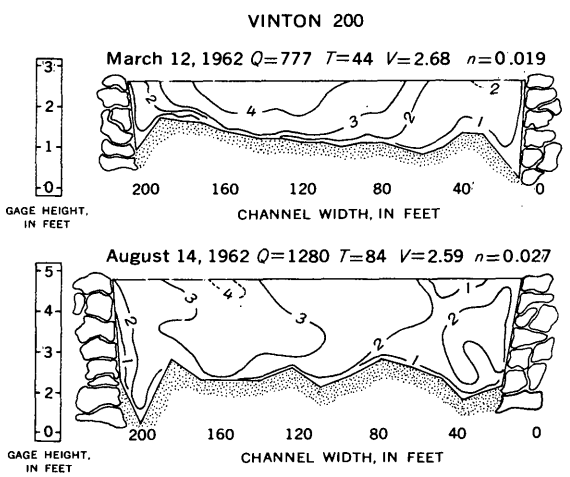

FIGURE 4—Cross section of the 200-foot-wide (Vinton-200) reach of the Rio Grande near Vinton, Tex., showing isovels, in feet per second. Both banks are rock revetments. Q, T, V, and n are defined in the caption of figure 2.

Various writers have expressed pronounced, but sometimes opposite, opinions about the effects of temperature on sediment transport.

Hubbel and Ali (1961) found that changes in temperature were always accompanied by changes in sediment transport and resistance to flow. They suggested that the change in viscosity produced by changes in water temperature, from 40° to 80°F in nature, caused a change in fall velocity and effective size of the sediment. Associated with this change in fall velocity were changes in bed form, in flow resistance, and in velocity and depth. In their flume experiments, the direction and amount of the changes in flow parameters depended in part on the bed form when the temperature was changed. This explained the somewhat anomalous results of some earlier experiments. Colby (1961) has noted that increasing temperature decreased the sediment transport at a constant depth and velocity.

Field evidence shows that the availability of sediment for transport may vary throughout the flow season. Since bed form is associated with sediment load, a stream may be able to carry different sediment loads at a given discharge. The direction and amount of the effects of variation in sediment availability would depend on the bed forms present, just as in temperature variation.

Flume experiments by Simons and others (1963) have shown that clay in suspension affects viscosity, bed form, and flow resistance similar to the way in which temperature does. These changes depend on the mineralogy of the clay as well as the concentrations present.

The complications of the interrelations among depth of flow, velocity, and sediment load were noted by Colby (1961). He stated that with a given size of sediment an increase in velocity can provide an increase, no change, or a decrease in sediment transport, depending on what happens to the depth of flow while the velocity is changing.

In summary, the bed configuration and flow phenomena on the Rio Grande near El Paso were at least in part determined by channel width and water temperature and the amount of sediment load available. As none of these elements leaves a distinct record in a sedimentary deposit, the task of determining environment precisely from sedimentary structures may be more difficult than many observers have suspected. The difficulty of stable channel design is also compounded by having to account for these effects. Much more work is necessary before either the study of the origin of sedimentary structures or the design of stable channels can be put on a firm quantitative basis from which reliable predictions of environment or bed-form occurrence can be made.

REFERENCES

Colby, B. R., 1961, Effect of depth of flow on discharge of bed material: U.S. Geol. Survey Water-Supply Paper 1498–D, p. D1–D12.

Hubbell, D. W., and Ali, K. A-S., 1961, Qualitative effects of temperature on flow phenomena in alluvial channels: Art. 301 *in* U.S. Geol. Survey Prof. Paper 424–D, p. D21–D23.

Simons, D. B., and Richardson, E. V., 1961, Forms of bed roughness in alluvial channels: Am. Soc. Civil Engineers Proc., v. 87, no. HY 3, p. 87–105.

Simons, D. B., Richardson, E. V., and Haushild, W. L., 1963, Some effects of fine sediment on flow phenomena: U.S. Geol. Survey Water-Supply Paper 1498–G.

RAPID METHOD OF ESTIMATING LITHOLOGY OF GLACIAL DRIFT OF THE ADIRONDACK MOUNTAINS, NEW YORK

By CHARLES S. DENNY and A. WILLIAMS POSTEL,
Washington, D.C.

Abstract.—The proportion and size of stones of various rock types in drift are estimated by study of 100 pebbles selected at intervals along a measuring tape laid on the surface of an outcrop. Surface samples selected in this manner and bulk samples of the same deposit yield similar results.

A rapid method of estimating the proportion and size of stones of various rock types in the coarse fraction of the drift in the northern Adirondack Mountains yields results comparable to the slower method of identifying fragments sieved from bulk samples. The method of sampling is adapted from Wolman's (1954) procedure for sampling coarse riverbed material with certain modifications by Hack (1957). Under favorable circumstances a sample of 100 pebbles can be selected and analyzed in about a half hour.

A measuring tape is laid on the surface of an outcrop of glacial drift. Starting at some convenient point, any stone larger than about half an inch in diameter that lies beneath an inch mark on the tape is selected until a subsample of 25 specimens has been collected. The procedure is repeated along adjacent segments of the tape until 3 more subsamples of 25 specimens each have been selected. The sample is thus divided into four parts to assure that any changes in the composition of the deposit along the line of the tape will be detected. The length sampled—the total length of tape used in selecting a sample—varies with the abundance of stones on the outcrop. The results are not, of course, typical of a whole deposit, but only of the coarse fraction, which in the areas studied makes up only a few percent of the total volume. If there is need for estimates of the mean size of the stones in the whole sample or in each lithologic group, such estimates can be made by placing each particle in a size class. From the percentage of stones in each size class an estimated mean size can be determined.

Till.—A body of gray calcareous sandy loam till, exposed on the floor of a borrow pit in the Saranac River valley at Picketts Corners, N.Y., was sampled by this method. The bare floor of the pit measured about 100 feet by 50 feet and was 3 to 6 feet below the original position of the top of the deposit. Bedrock in the immediate vicinity is concealed by surficial deposits. Low mountains to the north and west are underlain chiefly by granite gneiss with minor amounts of amphibolite and metasedimentary rock. Paleozoic sedimentary rocks floor lowlands to the east and form hills to the south (Postel, 1951; Fisher and others, 1962). In table 1, 2 groups of surface samples selected by the tape method (samples A–E) are compared with a group of samples sieved from four 10-quart pails of till dug at 4 different points from beneath the floor of the pit (samples F–I). Groups 1 and 3 are subdivided into smaller units (samples and subsamples) that show something of the range within each group.

Table 1 shows no great difference in lithology between stones selected by the tape method and those sieved from bulk samples. For example, the proportion of fragments of the common sandstone in surface samples averages 54 percent and ranges from 47 to 59 percent, whereas in bulk samples this sandstone averages 48 percent with a range of 42 to 55 percent. Most of the other lithologic types follow the same pattern. The greatest differences between surface and bulk samples are for limestone and dolomite and for granite gneiss. Total limestone and dolomite (fresh plus weathered specimens) constitute 7 percent of the surface samples and 19 percent of the bulk samples. Granite gneiss averages 6 percent and ranges from 5 to 7 percent in the surface samples, and forms 2 percent of the bulk samples. If these differences are real and not inherent in the two sampling methods, perhaps they reflect both weathering of stones prior to excavation of pit and differential wear of stones during excavation.

TABLE 1.—*Lithology of stones in till at Picketts Corners, N.Y.*

[Samples from area about 50 feet by 100 feet on floor of borrow pit northwest of Saranac Central School, Dannemora quadrangle. Stones ½ inch or larger]

Lithology	Surface samples																				Bulk samples						Surface and bulk samples combined	
	Group 1																		Group 2		Groups 1 and 2		Group 3							
	Sample A				Sample B				Sample C				Sample D				Total number of stones	Percentage of total [1]	Sample E		Total number of stones	Percentage of total	Sample F	Sample G	Sample H	Sample I	Total number of stones	Percentage of total	Total number of stones	Percentage of total
	1	2	3	4	1	2	3	4	1	2	3	4	1	2	3	4			Number of stones	Percentage of total			Percent							
	Number of stones																													
Paleozoic sedimentary rocks:																														
Sandstone, white, yellow, brown, gray	10	14	13	13	11	16	14	14	12	14	8	14	11	18	15	10	207	52 (47–56)	102	59	309	54	53	42	55	43	385	48	694	51
Sandstone, red	1	0	2	2	0	0	4	2	2	0	1	0	2	2	2	2	22	6 (3–8)	5	3	27	5	4	4	2	11	42	5	69	5
Sandstone, arkosic	6	4	2	3	6	5	5	3	5	6	5	2	4	1	6	1	64	16 (13–19)	20	12	84	15	17	19	19	15	136	17	220	16
Conglomerate	0	0	0	1	1	0	0	0	0	0	0	0	0	0	0	0	2	1 (0–1)	0	-------	2	Tr.	1	1	0	Tr.	5	1	7	Tr.
Conglomerate, arkosic	2	2	1	3	0	2	0	1	1	1	1	1	0	1	1	3	20	5 (3–8)	6	3	26	5	3	1	2	4	20	3	46	3
Limestone and dolomite, fresh	2	2	4	1	2	0	0	2	1	2	6	3	2	0	0	2	29	7 (4–12)	8	5	37	6	9	13	11	18	101	13	138	10
Limestone and dolomite, weathered	0	1	0	0	0	0	0	0	0	0	0	1	0	0	0	2	4	1 (0–2)	4	2	8	1	6	12	2	5	50	6	58	4
Siltstone	1	2	0	0	1	1	1	1	1	1	1	0	2	0	0	2	14	3 (3–4)	8	5	22	4	2	3	2	Tr.	14	2	36	4
Precambrian rocks:																														
Granite gneiss	2	0	2	1	3	0	1	1	2	0	1	2	1	2	1	3	22	5 (5–7)	11	6	33	6	2	2	2	2	15	2	48	4
Amphibolite	0	0	0	0	0	0	0	0	0	0	0	0	0	0	0	0	0	-------	0	-------	0	-------	0	0	0	Tr.	1	Tr.	1	Tr.
Pegmatite	0	0	0	1	1	0	0	0	1	0	0	0	0	0	0	0	3	1 (0–1)	0	-------	3	1	Tr.	0	1	1	4	Tr.	7	Tr.
Metadiabase	0	0	0	0	0	0	0	0	0	0	1	1	0	0	0	0	2	1 (0–2)	0	-------	2	Tr.	Tr.	0	1	0	2	Tr.	4	Tr.
Metasedimentary rocks	0	0	0	0	0	0	0	0	0	0	1	1	1	0	0	0	3	1 (0–2)	1	1	4	1	2	3	2	0	14	2	18	1
Miscellaneous	1	0	0	0	0	1	0	1	0	1	1	1	0	0	0	0	6	1 (0–3)	7	4	13	2	1	Tr.	1	1	8	1	21	2
Total	25	25	24	25	25	25	25	25	25	25	26	26	23	24	25	25	398	100	172	100	570	100	100	100	100	100	797	100	1,367	100

[1] Values in parentheses are variations between samples A, B, C, and D.

TABLE 2.—*Lithology of stones in ice-contact stratified drift near Schuyler Falls, N. Y.*

[Samples of pebble gravel and sand exposed in borrow pit about 100 feet in diameter, located about 1½ miles northwest of Schuyler falls, Dannemora quadrangle. Stones ½ inch or larger]

Lithology	Surface samples																		Bulk samples					Surface and bulk samples combined	
	Group 1																		Group 2						
	Sample A				Sample B				Sample C				Sample D				Total number of stones	Percentage of total[1]	Sample E	Sample F	Sample G	Total number of stones	Percentage of total	Total number of stones	Percentage of total
	1	2	3	4	1	2	3	4	1	2	3	4	1	2	3	4									
	Number of stones																		Percent						
Sandstone, white, yellow, brown, gray	16	17	16	17	17	19	13	10	17	18	18	16	16	14	11	15	250	63 (56–69)	67	63	67	344	66	594	64
Sandstone, red	0	1	0	2	0	0	0	2	0	2	2	1	1	0	0	0	11	3 (1–5)	4	5	3	20	4	31	3
Sandstone, arkosic	2	5	4	2	4	3	5	6	5	2	3	2	0	3	4	4	54	14 (11–18)	7	9	9	45	9	99	11
Conglomerate	0	0	0	0	0	0	0	0	0	0	0	0	0	0	1	0	1	Tr. (0–1)	0	0	0	0	0	1	Tr.
Conglomerate, arkosic	0	0	0	0	0	0	0	0	0	0	0	0	0	0	0	1	1	Tr. (0–1)	0	0	0	0	0	1	Tr.
Limestone and dolomite, fresh	0	0	0	1	0	0	0	2	0	0	0	0	0	0	1	1	5	1 (0–2)	0	0	0	0	0	5	1
Limestone and dolomite, weathered	0	0	0	0	0	1	0	0	1	0	2	0	0	3	0	1	8	2 (0–4)	3	0	1	7	1	15	2
Siltstone	4	0	1	1	2	1	2	4	1	3	0	2	2	2	3	1	29	7 (6–9)	11	11	11	58	11	87	9
Precambrian rocks	1	1	2	2	2	1	3	1	0	0	0	2	5	1	2	1	24	6 (2–9)	6	7	6	31	6	55	6
Miscellaneous	2	1	2	0	0	0	2	0	1	0	0	2	1	2	3	1	17	4 (2–7)	2	5	3	16	3	33	4
Total	25	25	25	25	25	25	25	25	25	25	25	25	25	25	25	25	400	100	100	100	100	521	100	921	100

[1] Values in parentheses are variations between samples A, B, C, and D.

Sand and gravel.—A deposit of outwash sand and gravel exposed in a small borrow pit near Schuyler Falls, N.Y., on the west edge of the Champlain Valley, was sampled in the same way as the till at Picketts Corners. The floor of the pit was about 6 feet below the top of the deposit. The local bedrock is Potsdam Sandstone. Beekmantown Dolomite underlies lowlands to the east, and Potsdam Sandstone and Lyon Mountain Granite Gneiss form highlands to the west (Postel, 1951). Table 2 shows that for water-laid drift, as for till, surface samples of stones selected by the tape method approximate bulk samples dug from the bank. Here, too, a sample of 100 stones selected with a tape proved adequate to characterize the stones on or in this deposit.

We conclude that a surface sample of 100 fragments characterizes the stones on the surface of an area sampled by the tape method provided the 4 subsamples are reasonably similar to one another. Our data suggest that within an area a few hundred feet in diameter the proportions of the various rock types in a surface sample approximate those of the stones in the underlying deposit.

REFERENCES

Fisher, D. W., and others, 1962, Adirondack sheet, *in* Broughton, J. G., and others, Geologic map of New York, 1961: New York State Mus. Bull. and Sci. Service, Geol. Survey, Map and Chart Series 5.

Hack, J. T., 1957, Studies of longitudinal stream profiles in Virginia and Maryland: U.S. Geol. Survey Prof. Paper 294–B, p. 45–97.

Postel, A. W., 1951, Geology of the Dannemora quadrangle, New York: U.S. Geol. Survey Geol. Quad. Map GQ–14.

Wolman, M. G., 1954, A method of sampling coarse river-bed material: Am. Geophys. Union Trans., v. 35, p. 951–956.

DETERMINATION OF HAFNIUM CONTENT AND Hf/Zr RATIOS IN ZIRCON WITH THE DIRECT-READING EMISSON SPECTROMETER

By CLAUDE L. WARING, Washington, D.C.

Abstract.—Hafnium content and Hf/Zr ratios in zircons were determined with the direct-reading emission spectrometer using a 1-mg sample in a d–c arc with a controlled atmosphere. The precision for the determination of hafnium and of the ratios is excellent, and the ratios agree well with similar determinations by X-ray fluorescence.

Use of the direct-reading spectrometer in conjunction with a controlled atmosphere, d–c arc, and small samples has proved very effective for the determination of hafnium percentages and Hf/Zr ratios in zircons.

A 1-mg sample, ground to an impalpable powder, is mixed with 5 milligrams of graphite and arced for 3 minutes, along with suitable standards, in an atmosphere of 80 percent argon and 20 percent oxygen. A d–c arc of 20 amperes and open-circuit potential of 250 volts is used. The jet controlling the argon-oxygen mixture is described by Helz (1964). The exit slits are set at 2681.7A for zirconium and 2738.7A for hafnium, positions which previous experience has proved reliable (Waring and Worthing, 1956). These positions are suitable for the exit-slit installations without interfering with the slits used for other elements. The spectrograph is the plane-grating type (15,000 lines per in.) with 5A/mm reciprocal linear dispersion. The source is focused on the collimator mirror, and the grating is masked to exclude the electrode images. The entrance slit is 50μ and the exit slits are 100μ.

To help reduce the background, a No. 9863 Corning ultraviolet transmitting filter is used in the optical path. With this filter in place, the background produced by the blank (graphite alone in the electrode) is still fairly high, but the reproducibility is high enough to maintain accuracy.

The intensities of the zirconium, which is also used as the internal standard, and the hafnium are read from the dials, and working curves for hafnium and for the ratios are prepared. Pure oxides of zirconium, hafnium, and silicon are ground together in the proper proportions to make the standards. As a control, a known zircon sample is included in each test run.

As a check on the precision of the method, 30 arcings of a zircon containing 0.66 percent hafnium and an Hf/Zr ratio of 0.013 were completed. The standard deviation for hafnium was 0.0055, and for the Hf/Zr ratio, 0.00063. Limited data on the accuracy of the method are shown in the accompanying table. The

Comparison of results obtained by three methods of analysis for hafnium content and Hf/Zr *ratios in zircon*

Sample No.	Location (county in Ontario, Canada)	Rock	Direct-reading emission spectrometry [1]		Conventional spectrography [2] Hf/Zr	X-ray spectrometry [3] Hf/Zr
			Hafnium (percent)	Hf/Zr		
Z–5511	Haliburton	Granite pegmatite	1. 28	0. 026		0. 027
Z–557	Hastings	do	2. 51	. 050		. 044
Z–558	Nipissing	do	3. 40	. 068		. 072
Z–551	Haliburton	Meta-pyroxenite	. 85	. 017		. 016
Z–553	Renfrew	Syenite pegmatite	. 55	. 011		. 012
Z–554	Haliburton	do	. 66	. 013	0. 012, 0. 013	. 012
Z–555	Hastings	Nepheline pegmatite	. 89	. 018		. 018
Z–559	Haliburton	Syenite pegmatite	1. 01	. 020		. 020

[1] Average of duplicates.
[2] Dutra (1961).
[3] Isidore Adler, analyst.

agreement between the data for the ratios by this method and by X-ray fluorescence is very good, but there are no data with which the present results for the hafnium content can be compared. The direct-reading method is 1½ times faster than spectrographic procedures based on photography, densitometry, and plate calibration.

The use of a 1-mg sample is advantageous both to the mineralogist and to the spectrographer. Earlier work showed that low values and erratic results are obtained with samples weighing more than 1 mg, because of incomplete burning caused by the highly refractory nature of zirconium. The zircon content of most of the rocks is low, requiring at least 25 pounds of crushed rock to yield enough purified zircon for the analysis. The use of small, 1-mg samples saves time and labor in completing the purification process. However, care should be taken to insure that the zircon sample separated is large enough to be representative. The spectrographic and the direct-reading techniques are not applied to the original crushed rock because of the lack of sensitivity of the equipment to the hafnium and zirconium and because of the undesirable effects produced by other elements in the rock.

REFERENCES

Dutra, C. V., 1961, Spectrochemical studies on some Brazilian zircons: Bol. Soc. Brasilian Geol., v. 10, no. 1, p. 25–37.

Helz, A. W., 1964, A gas jet for d–c arc spectroscopy: Art. 159 *in* U.S. Geol. Survey Prof. Paper 475–D, p. D176–D178.

Waring, C. L., and Worthing, H. W., 1956, A spectrographic method for determining the hafnium-zirconium ratio in zircon: U.S. Geol. Survey Bull. 1036–F, p. 81–90.

A SPECTROGRAPHIC METHOD FOR THE DETERMINATION OF CESIUM, RUBIDIUM, AND LITHIUM IN TEKTITES

By CHARLES ANNELL, Washington, D.C.

Abstract.—Spectrographic determinations of cesium, rubidium, and lithium in tektites, in concentrations as low as 1 ppm, are made with a K_2CO_3=sample mixture and a 15-amp d–c arc. Selective filtering at the focal plane permits measurable line intensities for the two exposure conditions required.

A method for the detection of cesium in concentrations of < 10 parts per million in tektites was required in order to study its abundance relative to that of other alkali elements. Several methods have been reported for trace-alkali determinations in rock and ore samples (Ahrens and Taylor, 1961, p. 194–201), and one procedure has been described for the determination of cesium, rubidium, and lithium in Australian tektites (Taylor, 1960).

A 1-ppm analytical limit for cesium was obtained using a 3-meter concave-grating spectrograph, a cylindrical quartz lens focusing the arc source on the grating, Eastman I–N emulsion, a 15-ampere d–c arc, and anode excitation of a mixture of a 10-milligram sample and 20 mg of K_2CO_3 which acted as a buffer for the sample. The method was primarily designed to determine the cesium content of tektites, with adaptation to rubidium and lithium determinations. The most sensitive analytical lines were used for all three elements: cesium, 8521.1; rubidium, 7800.2; and, lithium, 6707.8. A special filter at the focal plane of the spectrograph was necessary to obtain measurable intensities of the lithium-6707.8 line relative to the other lines.

EXPERIMENTAL PROCEDURE

In order to minimize errors arising from spectral interferences, an "average" tektite matrix was prepared from high-purity compounds, based upon several analyses reported previously (Cuttitta and others, 1961). Eight common oxides (or carbonates) were thoroughly mixed in the proportions shown in table 1. The mixture was sintered at 800°C in a muffle furnace for 30 minutes. The cooled material was then ground for 10 minutes in an agate mortar.

A standard lepidolite, NBS 183, containing 0.3 percent Cs_2O, 3.5 percent Rb_2O and 4.1 percent Li_2O was diluted with the tektite matrix to give a graded series of alkali concentrations. For each dilution, some of the previously prepared standard and a portion of the tektite matrix were ground for 30 minutes in an agate mortar. This gave an adequate range of alkali standards (in parts per million):

Standard 1: Cs, 100; Rb, 1,140; Li, 680
2: Cs, 46; Rb, 529; Li, 320
8: Cs, 0.5; Rb, 5.3; Li, 3.2

The silicate-rock standards G–1 and W–1 were also included as standards in this work, using the following recommended values (in parts per million) (Stevens, and others, 1960):

	Cs	Rb	Li
G–1	1.5	220	24
W–1	1.1	22	12

Exposures of four or five of these standards were made along with the tektite samples for each analytical plate prepared.

TABLE 1.—*Composition of a synthetic tektite matrix*

Compound	Percentage	Compound	Percentage
SiO_2	76	CaO	2
Al_2O_3	14	MgO	1
Fe_2O_3	3	Na_2O (Na_2CO_3)	1
K_2O (K_2CO_3)	2.5	TiO_2	0.5

Alkali buffers are frequently used to enhance the intensity of many low-energy spectral lines (Ahrens and Taylor, 1961; and Rusanov and others, 1959, for example). Potassium salts are more effective than sodium salts for the enhancement of cesium. This is due to the lower ionization potential of potassium (4.32 ev), compared to that of sodium (5.12 ev), which in-

creases the probability of populating the upper energy level (1.45 ev) of the cesium atom that is responsible for the 8,521 line. The same reasoning applies to the enhancement of the rubidium-7800 (1.58 ev) and lithium-6707.8 (1.84 ev) lines. The three lines of the alkali elements all involve ground-state transitions (energy levels are taken from Moore, 1945).

Johnson, Matthey and Co., Ltd., "Specpure" K_2CO_3 was used because it contained no detectable cesium and had a very low rubidium and lithium blank. After a series of tests, a mixture of 10 mg of sample and 20 mg K_2CO_3 was found to provide the required cesium detectability and precision. Similar results were obtained for rubidium and lithium, although the period of lithium excitation generally extended slightly beyond the main "K arc".

A 10-mg finely ground sample or standard is mixed with 20 mg of powdered K_2CO_3. The mixing is conveniently done in an aluminum weighing pan with a plastic or wooden toothpick. The mixture is tamped with a small glass rod into the crater of a high-purity graphite electrode. In a humid environment the K_2CO_3 will absorb water and become difficult to handle. A "dry box" or a similar low-humidity system is necessary under these conditions. All electrodes are stored in a dessicator when loaded. Approximately an hour before arcing, the electrodes must be dried in an oven set at 110°C to drive off excess moisture. Failure to dry the samples will result in popping and frothing after the arc is struck.

The lower or sample electrode (anode) is made from high-purity ¼-inch graphite rod. The electrode is machined to give a cup 0.24-inch deep having an inner diameter of 0.144 inch and outer diameter of 0.174 inch. The outside is machined to a shoulder 0.40 inch below the cup opening. The upper electrode is a straight ⅛-inch-diameter high-purity graphite rod (cathode). The electrodes are maintained at a 4-mm gap during arcing.

The preheated electrodes are arced within 10 minutes after removing from the oven. An initial current of 5 amps d–c is used for 5 seconds to minimize any frothing or sample loss. The current is then increased to 15 amps for the remainder of the period. The output current remains remarkably steady at 15 amps throughout the arcing period, until the potassium has volatilized. Then a slight drop in the output current is noted along with a more erratic behavior.

The exposure conditions for cesium are slightly different from those for lithium. Since the spectrograph used for these determinations covers a spectral range of about 1,300 A in the first order, it is necessary to take separate exposures. The first exposure can include cesium 8521.1 and rubidium 7800.2, and the second exposure includes rubidium 7800.2 and lithium 6707.8. The cesium-8521 line has a slight interference from a carbon band which can be ignored, provided the exposure is stopped when the potassium is gone. The loss of potassium from the electrode is marked by a change from a bluish-gray to a bright-blue color in the arc, as well as by the variation in the output current. The time required for this change in a 15-amp arc is approximately 90 seconds.

The exposure for lithium and rubidium determinations is extended approximately 120 seconds, until there is complete sample consumption. No interferences are noted for lithium 6707.8 or rubidium 7800.2.

A 450-mm cylindrical quartz lens focuses the source on the grating, which is masked to exclude background radiation from the electrode tips. A 25-micron slit is used. On the optical bench between the collimating lens and the slit, at the Sirk's focal point, a filter holder is fixed.

For the cesium and rubidium determinations a filter is selected so that the cesium-8521.1 line in W–1 (1.1 ppm) gives an intensity value at least twice that of the standard deviation (table 2). This will give a cesium working range of 1–20 ppm when using I–N emulsion. The rubidium-7800.2-line intensity must be further attenuated to provide a measurable density in the 20–220-rubidium range. This is accomplished by using a 7-percent neutral filter mounted in a special holder which can be affixed at the focal plane in the casette (fig. 1).

The lithium-rubidium determinations are made using about a 5-percent transmission filter in front of the slit and an additional 50-percent filter at the focal plane for the lithium-6707.8 line, permitting a workable lithium range of 4–150 ppm.

In addition to neutral filters, an ultraviolet and blue-green absorbing filter is used to eliminate second-order spectra. The plates contain exposures of 5 or 6 standards and 5 or 6 samples, in duplicate. A calibration spectrum of a G–1/W–1, 1 : 1 mixture, using a 50/100-percent transmission-step filter, is exposed between the duplicate sets of standards and samples.

The visible-red-sensitive I–N emulsion (Eastman) is used for all determinations. The plate is processed in D–19 developer for 4 minutes at 18°C, placed in an acetic acid short stop 30 seconds, and acid fixed for 5 minutes. The plate is dried with a warm-air blower.

Plate calibration is based on the two-step method (Churchill, 1944). A few lines in the 7300–8500–A region are selected for measurement with a densitometer.

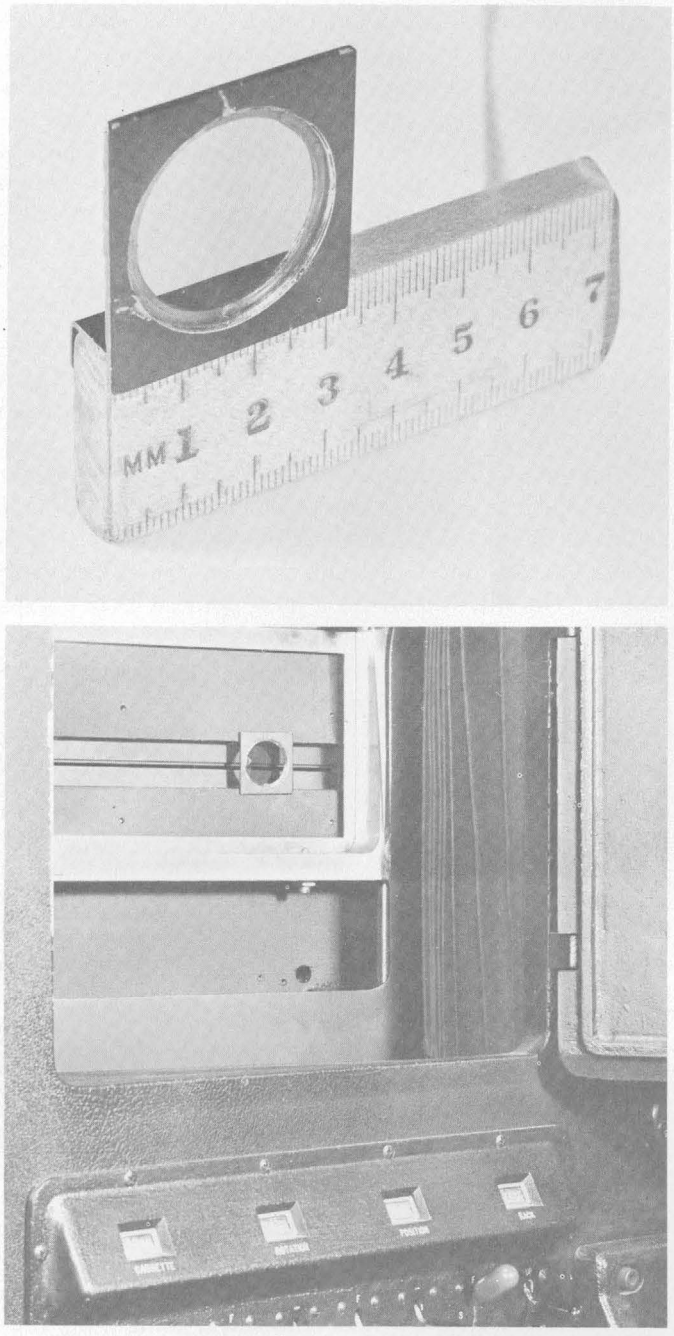

FIGURE 1.—Closeup view of neutral filter mounted in a special brass holder (above); and view of spectrograph, showing position of filter and holder at the focal plane in the spectrograph (below).

The cesium-line intensities are corrected for adjacent background. The selection of pure chemicals for the tektite matrix avoids any cesium contamination in the blank, but any further correction of the cesium blank results in an overcorrection of the analytical curve. The rubidium and lithium lines require no background correction when using the conditions described. Typical analytical curves for the alkali elements are shown in figure 2. The lithium and rubidium lines show reversal at the higher concentrations.

No internal-standard lines could be found in the 6500–9000A region which were suitable for densitometry under these conditions. However, by means of voltage regulation at the source input coupled with the potassium buffering in the arc, satisfactory precision is obtained.

A measure of the precision of the determinations is shown in table 2. Tektites having closely similar concentrations of trace alkalis are grouped together. One group of tektites from an area centered around Lee County, Tex., and commonly referred to as "bediasites", have relatively low trace-alkali concentrations. The other group includes tektites from southeast Asia and Indonesia. The deviations of duplicate determinations obtained from the same spectrographic plates were used to calculate the standard deviations and coefficients of variation (Youden, 1951, p. 16–17; American Society for Testing Materials, 1960, p. 95).

No accuracy tests were made because of a lack of analyzed samples. However, the level of trace-alkali concentrations in these groups of tektites is in agreement with the results reported by Taylor (1960, p. 89) for the australites.

TABLE 2.—*Trace-alkali precision in analyses of two groups of tektites*

Element	*Group*	$\bar{x}$ *(avg. concentration, in ppm)*	*S.D.*	*C.V.*	*n*
Cesium	Bediasite (Texas)	2. 04	0. 22	10. 7	13
	Tektite (southeast Asia and Indonesia).	5. 3	0. 35	6. 7	11
Rubidium	Bediasite (Texas)	66. 5	3. 95	5. 9	8
	Tektite (southeast Asia and Indonesia).	106	4. 92	4. 6	16
Lithium [1]	Tektite (southeast Asia and Indonesia).	46. 6	2. 76	5. 9	12

d=difference between duplicate values.
n=number of duplicate determinations.
$\bar{x}$=average of all determinations in a group.

$$S.D.=\sqrt{\frac{\Sigma d^2}{2n}}=\text{standard deviation.}$$

$$C.V.=100\frac{S.D.}{\bar{x}}=\text{coefficient of variation.}$$

[1] Lithium in bediasites was determined by another spectrographic method.

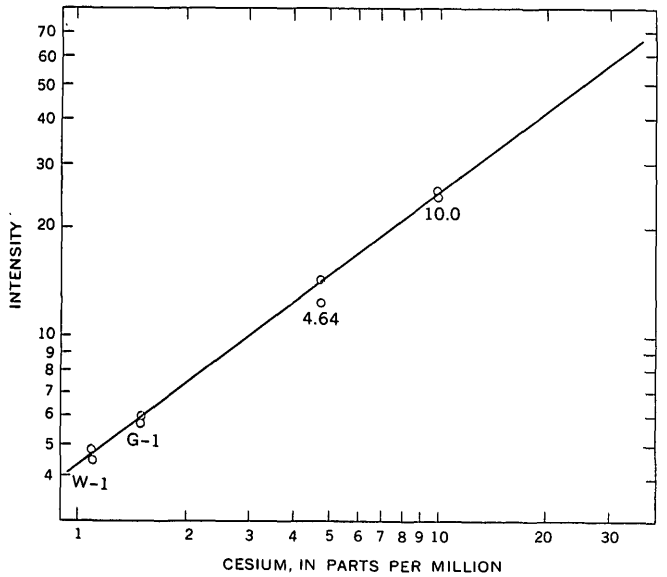

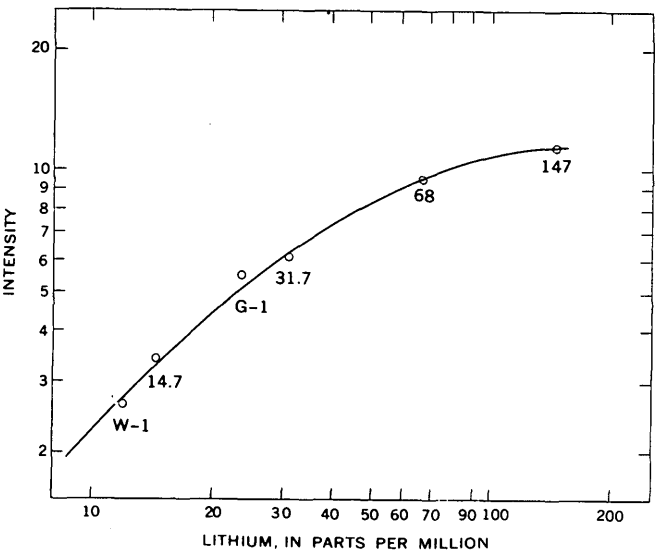

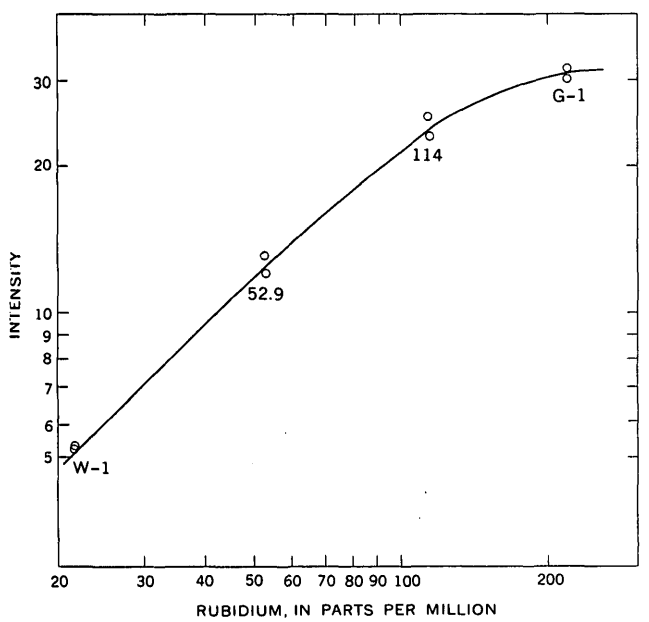

FIGURE 2.—Analytical curves for the determination of cesium, lithium, and rubidium in tektites, based on G–1, W–1, and synthetic-tektite standards.

REFERENCES

Ahrens, L. H., and Taylor, S. R., 1961, Spectrochemical analysis, 2nd. ed: Reading, Mass., Addison-Wesley Pub. Co., Inc., 454 p.

American Society for Testing Materials, 1960, Methods for emission spectrochemical analysis, 3rd ed: Philadelphia, p. 685.

Churchill, J. R., 1944, Techniques of quantitative spectrographic analysis: Indust. and Eng. Chem., anal. ed., v. 16, p. 653.

Cuttitta, Frank, Carron, M. K., Fletcher, J. D., and Chao, E. C. T., 1961, Chemical composition of bediasites and philippinites, *in* U.S. Geological Survey astrogeologic studies semiannnual progress report to NASA, February 25, 1961 to August 25, 1961: p. 15–47.

Moore, C. E., 1945, A multiplet table of astrophysical interest, rev. ed: Princeton, N.J., Princeton Univ. Observatory, 96 p.

Rusanov, A. K., Khitrov, V. G., and Botova, N. T., 1959, Use of low temperature carbon arc as a source for excitation of Rb, Cs, Tl and In spectra in the spectrographic analysis of silicates: Zhur. Anal. Khim., v. 14, p. 534–541 [in Russian].

Stevens, R. E., and others, 1960, Second report on a cooperative investigation of the composition of two silicate rocks: U.S. Geol. Survey Bull. 1113, 126 p.

Taylor, S. R., 1960, Abundance and distribution of alkali elements in australites: Geochim. et Cosmochim. Acta, v. 20, p. 85–100.

Youden, W. J., 1951, Statistical methods for chemists: New York, John Wiley and Sons, Inc., 126 p.

STAINING OF PLAGIOCLASE FELDSPAR AND OTHER MINERALS WITH F. D. AND C. RED NO. 2

By RUPERTO V. LANIZ,[1] ROLLIN E. STEVENS, and MEADE B. NORMAN,
Palo Alto, Calif.; Menlo Park, Calif.

Abstract.—Procedures are given for sequentially staining plagioclase red with F. D. and C. Red No. 2 (amaranth) and K-feldspar yellow with cobaltinitrite in rock slabs, thin-sections, and mounted sands. Although amaranth staining is not specific for plagioclase, it is frequently useful because other minerals can be distinguished by the hue and depth of the stain. Addition of a calcium chloride dip is necessary to stain Na-rich plagioclase.

Bailey and Stevens (1960) proposed the staining of plagioclase feldspar red by treatment of the rock surface, etched with hydrofluoric acid, first with a solution of barium chloride and then with one of potassium rhodizonate. Barium ion is preferentially adsorbed on the etched plagioclase and forms insoluble barium rhodizonate, staining the plagioclase brick red. This staining technique for plagioclase was combined with yellow staining of K-feldspar with cobaltinitrite.

Success with other dyes for staining plagioclase has also been reported. Robert F. Gantnier and James A. Thomas (written communication, 1961) used several pH-indicator dyes. Reeder and McAllister (1957) used hematein, and Graham (1955) malachite oxalate for staining plagioclase.

This article describes the staining of plagioclase with the fruit dye F. D. and C. Red No. 2, after the mineral has been etched with hydrofluoric acid and dipped in barium chloride solution. This method can be combined with the well-known staining of K-feldspar with cobaltinitrite (Gabriel and Cox, 1929; Keith, 1939a, b; Chayes, 1952; and Rosenblum, 1956) to stain K-feldspar yellow and plagioclase red in rock slabs, in mounted sand grains, and in thin sections. Unlike the potassium rhodizonate the fruit dye is inexpensive and can be obtained from many dyestuff distributors.

F. D. and C. Red No. 2 (amaranth) is listed as C. I. 16185 in the Colour Index of the American Association of Textile Chemists and Colorists (1957, p. 3084). It was formerly called amaranth, and was listed in older Colour Indexes as C. I. 184. The dye has the formula

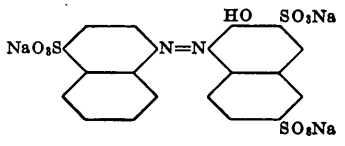

This dye and similar compounds are reactive toward metallic ions, which form ring structures by replacing the H in the OH group and joining to one of the N atoms with a coordinate link.

Deep-red staining of the plagioclase is obtained by first adsorbing barium ion on the etched plagioclase surface, as in the rhodizonate staining technique, and then dipping the specimen in the amaranth dye. The resulting barium salt is slightly soluble and is retained on the etched plagioclase if the specimen is washed only briefly. Although the barium-dye compound is much more soluble than barium rhodizonate, washing techniques for the dye were developed which color all plagioclase surfaces in the rock slabs a brilliant purple-red that contrasts sharply with the color of K-feldspar (stained yellow by cobaltinitrite), unstained quartz, and dark ferromagnesian minerals. Pure albite fails to stain with either this dye or rhodizonate, but it can be stained by first dipping the etched specimen in calcium chloride solution. Other minerals containing alkaline earths or lead can be stained distinctive shades with the dye.

DETAILED STAINING PROCEDURE

The step-by-step procedure for staining rock slabs is as follows:

1. Prepare a smooth flat surface with No. 400 to 800 grit on a lap. If the rock is porous, first fill the surface with molten Lakeside before grinding it smooth.

[1] Stanford University.

2. Etch the surface for 10 to 15 seconds in concentrated hydrofluoric acid (52-percent HF).
3. Dip the slab once in water.
4. Immerse the slab in a saturated solution of sodium cobaltinitrite for 1 minute.
5. Remove the excess cobaltinitrite by rinsing the slab gently in tap water.
6. Dry the slab under a heat lamp.
7. Immerse the slab for 15 seconds in 5-percent barium chloride solution (W/V).
8. Dip the slab once quickly in water, and dry gently with compressed air.
9. Immerse the slab for 15 seconds in amaranth solution (1 oz. F., D. and C. Red No. 2, 92 percent pure coal-tar dye, in 2 liters of water).
10. Dip the slab once quickly in water.
11. Direct a gentle stream of compressed air onto the stained surface to sweep off the remaining excess of amaranth solution.
12. Where milky white areas suggestive of albite remain after the above treatment, repolish, repeat steps 1 to 3, dip in calcium chloride solution, dry, then proceed as in steps 4 to 11.

For staining sand grains, mount them in melted Lakeside containing lamp black to make it opaque; cool; grind a surface smooth to expose the sand grains; and etch and stain as directed for rock slabs.

For staining thin sections the procedure is as follows:

1. Etch the uncovered rock section for 15 seconds in hydrofluoric acid vapor.
2. Immerse in the cobaltinitrite solution for 15 seconds.
3. Rinse briefly in tap water.
4. Immerse for a few seconds in the barium chloride solution.
5. Dip in distilled water.
6. Immerse for 1 minute in the amaranth solution.
7. Dip once in water.
8. Sweep away the excess amaranth solution, still left on the slide, with a gentle stream of compressed air.

AMARANTH STAINING OF OTHER MINERALS

The etched plagioclase feldspars are not the only minerals stained by the amaranth. Various other minerals containing akaline earths or lead may also be stained, the depth of color depending upon the content of these elements in the mineral reacting with the dye, and upon the extent to which the mineral is etched with hydrofluoric acid. Silicate minerals containing alkaline earths or lead are readily stained because a significant etch residue is left on the mineral.

Deep-red stains were obtained, after etching, on the following minerals: benitoite, celsian, cordierite, dolomite, hydrogarnet, pectolite, vesuvianite, witherite, wollastonite. Very faint or insignificant stains were obtained on anglesite, anhydrite, barite, calcite, and celestite because these minerals do not leave an etch residue to retain the stain.

That the amaranth stain is not specific for plagioclase is frequently an advantage in that certain other minerals may be delineated in the specimen because the depth of red produced on them contrasts with the shade of red of the stained plagioclase. For example, in a stained rock slab the deep red of stained cordierite contrasted well with the less intense red of the stained plagioclase, and the structural relationships in the rock could be plainly seen, showing a complex assemblage of deep-red-stained cordierite, less-red plagioclase, yellow-stained K-feldspar, uncolored quartz, and dark ferromagnesian minerals.

Dolomite is stained a deep red with amaranth, and calcite a faint pink. These results have been repeated on a number of samples and the test was found to be diagnostic for distinguishing calcite from dolomite. In samples with intergrowths of calcite and dolomite the deep red of the stained dolomite contrasted clearly with the faint pink of the calcite.

REFERENCES

American Association of Textile Chemists and Colorists, 1957, Colour index, v. 3, 2nd ed., 1956: Lowell, Mass., Lowell Technol. Inst.

Bailey, E. H., and Stevens, R. E., 1960, Selective staining of K-feldspar and plagioclase on rock slabs and thin sections: Am. Mineralogist, v. 45, p. 1020–1025.

Chayes, Felix, 1952, Notes on the staining of potash feldspar with sodium cobaltinitrite in thin sections: Am. Mineralogist, v. 37, p. 337–340.

Gabriel, Alton, and Cox, E. P., 1929, A staining method for the quantitative determination of certain rock minerals: Am. Mineralogist, v. 14, p. 290–292.

Graham, E. R., 1955, Rapid determination of quartz, potash minerals, and plagioclase feldspars: Chemist-Analyst, v. 44(2), p. 37–38.

Keith, M. K., 1939a, Selective staining to facilitate Rosiwal analyses: Am. Mineralogist, v. 24, p. 561–565.

———1939b, Petrology of the alkaline intrusive at Blue Mountain, Ontario: Geol. Soc. American Bull., v. 50, p. 1795–1826.

Reeder, S. W., and McAllister, A. L., 1957, A staining method for the quantitative determination of feldspars in rocks and sands from soils: Canadian Jour. Soil Sci., v. 37, p. 57–59.

Rosenblum, Samuel, 1956, Improved technique for staining potash feldspars: Am. Mineralogist, v. 41, p. 662–664.

SUCCESSFUL SEPARATION OF SILT-SIZE MINERALS IN HEAVY LIQUIDS

By ROBERT SCHOEN and DONALD E. LEE, Menlo Park, Calif.

Abstract.—Routine separations of particles as small as 10 microns are possible by centrifuging fine fractions in heavy liquids. Rapid application of centrifugal force allows separation of particles to precede flocculation.

One of the major stumbling blocks in the application of theoretical geochemical principles in earth science is the inability to determine the precise chemical composition of natural coexisting phases. Many rocks are so fine grained that their mineral phases cannot be purified for chemical analysis. Fine-grained igneous rocks, hydrothermally altered rocks, and many sedimentary rocks are subject to this problem. The geochemical analysis of some of the most interesting natural systems often founders because an approximate or ideal composition for one or more of the phases must be assumed.

The usual sink-float techniques of mineral separation in heavy liquids fail, when applied to small particles, for two reasons. First, the rate of sedimentation of very small particles is slow in liquids whose specific gravity is close to that of the particles. Second, and more important, the relatively large surface area in relation to weight of small particles leads to their aggregation into flocs whose individual grains can no longer sink or float independently.

Two recent papers (Loughnan, 1957; Kittrick, 1961) describe methods by which expansible clay minerals may be purified by sink-float techniques. Both methods depend upon the ability of particular clays to change their specific gravity appreciably when they adsorb certain liquids. Unfortunately, the methods are limited to expansible clay minerals and possibly to zeolites, and are restricted to relatively large particle sizes, because of the tendency of the grains to flocculate.

As part of a geochemical study of hydrothermal alteration, a method was developed to make routine heavy-liquid separations of particles as small as 10 microns in diameter. Particles smaller than 10 microns can be separated if large density differences exist among the phases, as for instance in pyrite and quartz.

The success of this method depends upon its ability to overcome the two previously mentioned obstacles common to ordinary sink-float techniques. A centrifuge capable of producing 1,500-gravities acceleration must be used in order to speed up the sinking or floating of the mineral grains (Hutton, 1943). Repeated short high-speed centrifugations, with intermittent stirring, are necessary to allow separation to occur before flocculation. Familiarity with the general principles of heavy-liquid techniques (Twenhofel and Tyler, 1941, p. 67–84; Hutton, 1950) is assumed in the following discussion and description. Particular care must be used to avoid inhalation of vapors from any of the organic liquids, many of which are highly toxic.

EQUIPMENT

The following special equipment is useful in making clean separations and minimizing loss of sample:

1. Heavy-wall centrifuge tubes of special shape (fig. 1) are necessary to avoid breaking of tubes and to minimize contamination of concentrates (Hutton, 1943, p. 76). This shape allows the light fraction to be poured off and the top of the tube rinsed without contamination of the heavy fraction. Such tubes may be obtained on special order from a glassblower. In conjunction with this tube, a stopper (fig. 1) must be used to seal off the lower bulb of the tube. The stopper may be made by attaching to a metal rod a plug of hard rubber that has been shaped to fit the constriction in the centrifuge tube, or a plug may be made by shaping molten polyethylene inside a wet centrifuge tube to fit the constriction.
2. A three-element filter of the millipore type is superior to an ordinary funnel for filtration of heavy liquids. The millipore filter has the advantage of rapid filtration because of its large area for filtration. There is no danger of the filter paper breaking as it is supported on a fritted glass disc. The cellulose filters supplied for normal use in a millipore filter must not be used, as they are soluble in organic solvents. Instead, a smooth hardened filter paper such as Whatman 50 is trimmed to fit on top of the glass disc. This results in a 300-percent saving in filter-paper cost.

3. An inexpensive water aspirator is preferable to a vacuum pump for producing suction in the vacuum flask. The poisonous and corrosive vapors produced by heavy liquids are difficult to trap, and their accumulation in a vacuum pump requires flushing and refilling with expensive oil. An aspirator, on the other hand, flushes these vapors away and there is no disposal problem. Although an aspirator produces less vacuum than a pump, the large filtration area of a millipore filter results in rapid filtration. The aspirator also causes less evaporation of heavy liquids.
4. Although a rubber stopper can be used to support the millipore-filter assembly, a rubber filter support and closure marketed under the trade name "Filtervac" will greatly speed up transfer of the filter assembly from flask to flask. The usual arrangement of the pieces of filtration equipment is diagrammed in figure 2.

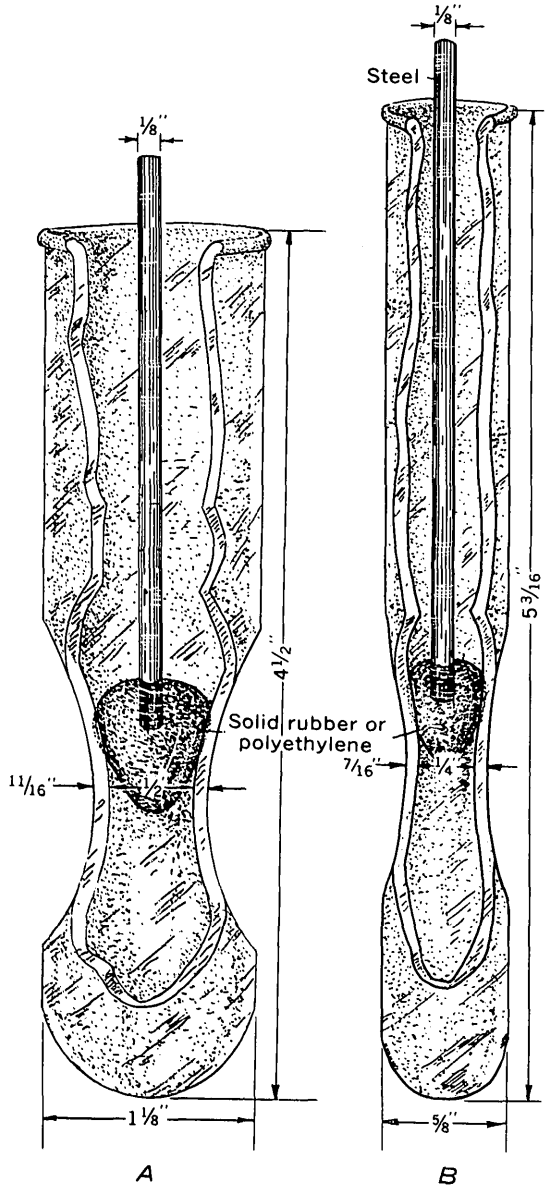

FIGURE 1.—Specially shaped centrifuge tubes (*A*, 40-ml and *B*, 10-ml capacity) with stoppers, for the separation of minerals in heavy liquids.

725-828 O—64——11

PROCEDURE

1. Crush the sample to pass through a 200-mesh sieve and then size it as follows: Let the sample settle in a water-filled 10-cm-high vessel for 2 minutes; decant the suspension. Let the suspension settle for 10 minutes and decant again. This procedure gives three solid fractions whose approximate size limits are: 30–75 μ, after 2 minutes; 10–30 μ after 10 minutes; and less than 10 μ in the remaining suspension. Dry the two coarse fractions under a heat lamp. A final washing with anhydrous acetone gives a powdery sample free from lumps.
2. Pour the size fraction whose largest grains are monomineralic onto a creased glazed weighing paper. Crush any lumps to form a free-flowing powder.
3. Pour the sample into the special centrifuge tubes. The 40-ml tube will hold 2 g or less and the 10-ml tube will hold ½ g or less.
4. Fill each tube to the same level with a heavy-liquid mixture of the proper specific gravity. If a complete separation of a rock is attempted, it is best to start with the heaviest liquid and work successively with lighter liquids. In this way, the bulk of the sample is always floating at the top of the tube where it can be stirred to free more heavy minerals.
5. Stopper the mouth of each tube, preferably with a neoprene or a plastic stopper, to prevent evaporation of the liquid and a consequent change in specific gravity.
6. Gently invert each tube several times to disperse the sample throughout the liquid. Quickly place the tubes into a centrifuge and rapidly accelerate it to 1,500 to 2,000 gravities.
7. Stop the centrifuge slowly after about 1 minute. Prolonged centrifugation only hardens the floating cake of mineral grains, making further separation difficult.
8. Stir the floating cake to redisperse it completely, but avoid mixing in the heavy fraction. After stirring, quickly put the tubes into the centrifuge and again rapidly accelerate it to high speed.
9. Three centrifugations are usually enough, but centrifuging should be repeated until no further addition to the heavy fraction is noted. Even if no heavy minerals separate during the first run, it is best to stir and centrifuge again. If the amount of heavy minerals separated seems disappointingly small, filter the liquid anyway as several hundred milligrams will appear insignificant if divided among several tubes.
10. Gently twist the specially-shaped stopper through the floating cake. This loosens the cake so that it can be poured off yet does not cause mixing of the light (solids) and heavy fractions. Seal off the lower bulb of the tube and pour the light fraction into the millipore filter. With the stopper held tightly against the constriction of the tube, rinse the upper portion with a jet of heavy liquid from a squeeze bottle until all the light fraction is on the millipore filter. Repeat step 10 for each tube.
11. After filtering the heavy liquid into a vacuum flask, break the vacuum, remove the vacuum flask containing heavy liquid, and insert a clean vacuum flask beneath the millipore filter. Wash the light fraction and the sides of the funnel with a jet of anhydrous acetone from a squeeze bottle. Filter off the acetone washings.

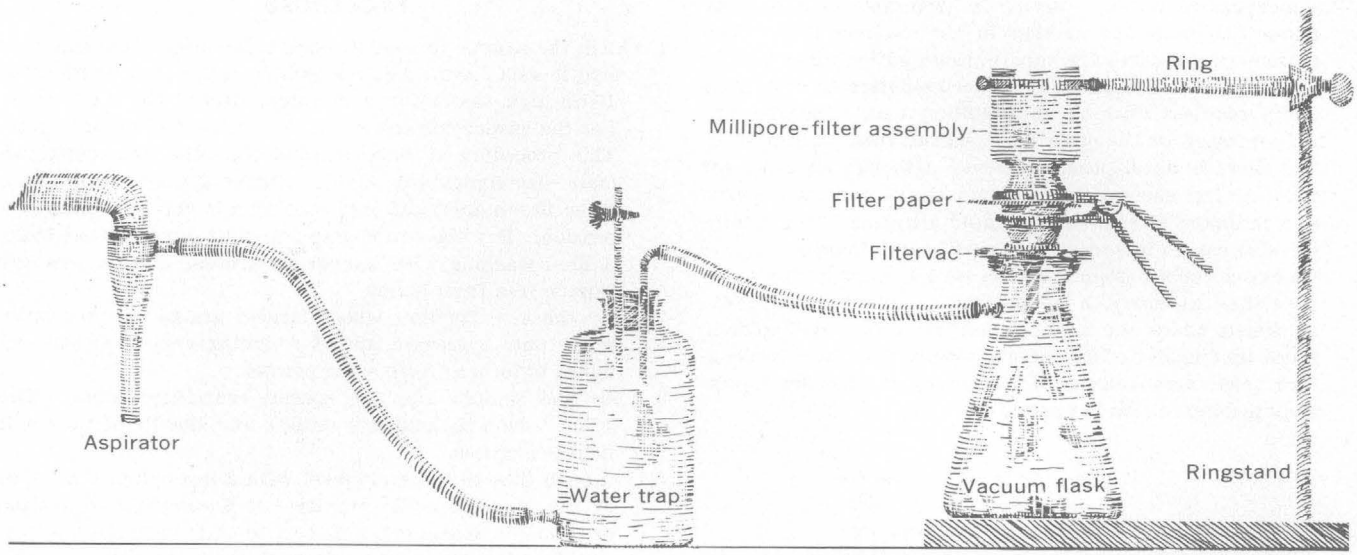

FIGURE 2.—Arrangement of equipment for the filtration of heavy liquids under vacuum.

12. Carefully open the millipore filter holder and remove the filter paper. Scrape the grains sticking to the funnel onto the filter paper and dry under a heat lamp. Rinse the funnel with acetone and dry. Install a new filter paper and reassemble the filter. Pour off the heavy fraction from each tube. Rinse the tube with heavy liquid. Change the vacuum flask and wash with acetone as before.
13. The heavy-liquid filtrate can be reused after its specific gravity is checked and adjusted if necessary. The acetone washings should be saved in a large brown bottle for eventual recovery of pure heavy liquid by standard methods.

An example of the purification routinely possible by this method is presented on figure 3. The rock, a hydrothermally altered basaltic andesite, consisted of K-feldspar, celadonite, and lesser amounts of pyrite and anatase. The 10–30 μ fraction, *A*, consisted of individual grains of K-feldspar, celadonite, and pyrite with very small inclusions of anatase in otherwise pure mineral grains. Separated fractions of K-feldspar, *B*, and celadonite, *C*, each with included anatase, are being chemically analyzed. The analyses will be corrected for anatase by subtracting TiO_2 (anatase) from each analysis. If more sample had been available, the concentrates illustrated on figure 3 could have been purified further.

The careful application of this method will lead to cleaner separations and, therefore, to more meaningful chemical analyses. When a sufficient amount of sample is available, the purity of the fractions will depend largely on the patience of the investigator.

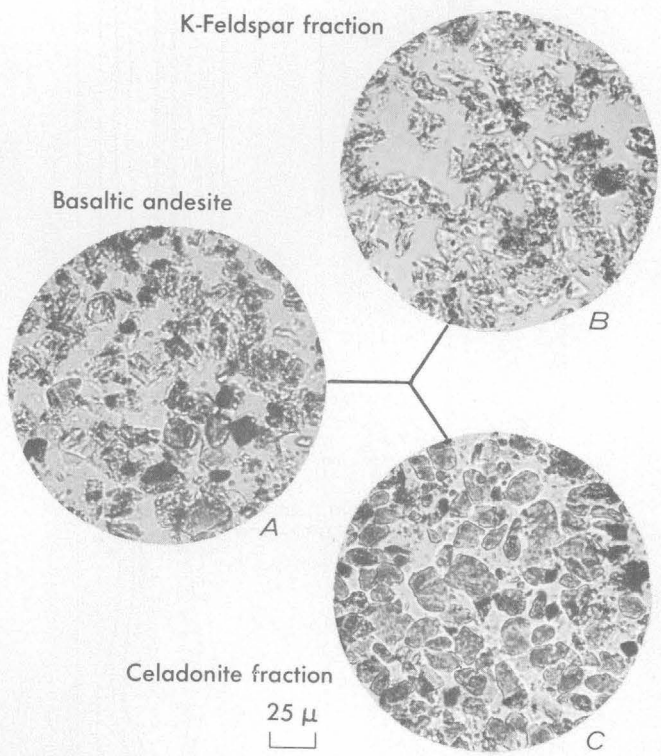

FIGURE 3.—Photomicrographs of fine-grained mineral fractions purified with heavy liquids. *A*, the 10–30 μ fraction of crushed basaltic andesite; *B*, separated K-feldspar fraction; *C*, separated celadonite fraction. The mineral grains are mounted in an oil, refractive index 1.535, that enhances the tiny anatase inclusions. Although apparently contaminated, the K-feldspar fraction, *B*, contains only 0.60 percent titanium.

REFERENCES

Hutton, C. O., 1943, Some features of heavy mineral separations: Royal Soc. New Zealand Trans. and Proc., v. 73, p. 76–83.

——— 1950, Studies of heavy detrital minerals: Geol. Soc. America Bull., v. 61, p. 635–716.

Kittrick, J. A., 1961, The density separation of clay minerals in thallous formate solutions: Am. Mineralogist, v. 46, p. 744–747.

Loughnan, F. C., 1957, A technique for the isolation of montmorillonite and halloysite: Am. Mineralogist, v. 42, p. 393–397.

Twenhofel, W. H., and Tyler, S. A., 1941, Methods of study of sediments: New York, McGraw-Hill, 183 p.

EFFECT OF SEICHES AND SETUP ON THE ELEVATION OF ELEPHANT BUTTE RESERVOIR, NEW MEXICO

By GEORGE L. HAYNES, JR., Santa Fe, N. Mex.

Abstract.—Recorded deviations from the normal water-surface elevation of Elephant Butte Reservoir occur as setup and seiche and are caused by wind and barometric pressure changes and by flash-flood waves from reservoir tributaries. Single-station weather data provide only a general indication of setup production and seiche excitation.

Transitory surges of the water surface in reservoirs can introduce significant error in the computation of capacity. However, such errors can be reduced by careful selection of sites for gages and by correcting for known anomalies. Surges caused by wind, barometric-pressure changes, and flash-flood waves at Elephant Butte Reservoir on the Rio Grande in south-central New Mexico were studied to aid in establishing guidelines for locating reservoir and lake gages. Elephant Butte Reservoir is a long narrow lake whose major axis has a general north-south orientation; at maximum elevation, 4,231.5 feet, the reservoir has a capacity of 2,195,000 acre-feet and comprises two main bodies of water separated by a constriction called the Narrows.

Deviations from the normal water surface recorded by the reservoir gage at the dam occur as static and dynamic surges or as a combination of the two. These surges are caused by wind and air-pressure changes and by flood waves from tributaries that discharge into the reservoir. Water-surface fluctuations are compared with weather observations at the Truth or Consequences, N. Mex., airport, 7½ miles northeast of Elephant Butte Dam.

Static surges classified as setup are caused primarily by strong winds of extended duration, but pressure difference over the water surface can augment or suppress the effect of wind. The U.S. Army Corps of Engineers (1955) found that pressure differences had to be accounted for in relating setup to hurricane parameters on Lake Okeechobee in Florida. Irish and Platzman (1962) investigated the possibility of resonant coupling resulting from movement of the stress band accompanying frontal passages of cyclonic systems across Lake Erie. They concluded that resonance is almost entirely suppressed when the stress-band width is greater than the length of the lake; this is the case for Lake Erie, which has a length of about 200 miles—much less than the scale of cyclonic systems.

Figure 1 shows the relation between the north or south component of wind velocity and setup or setdown as recorded by the reservoir gage. A more precise procedure would be to relate setup to wind force, $(\rho_a V^2)$,

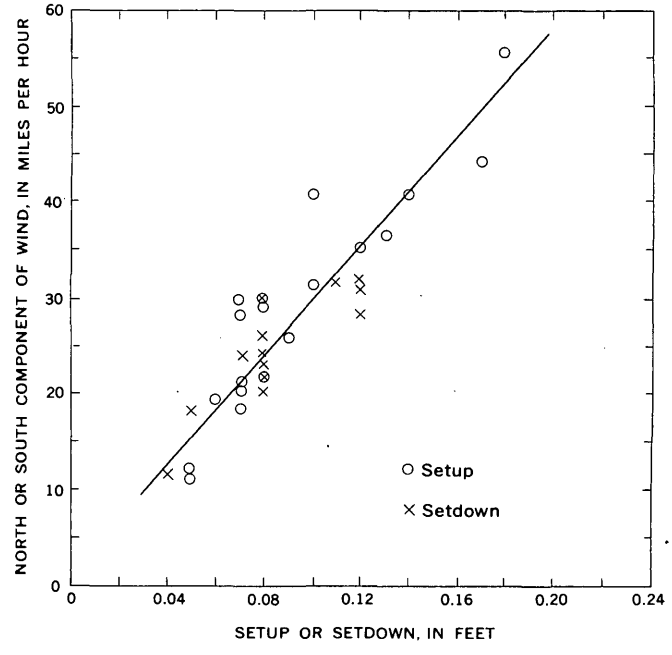

FIGURE 1.—Relation between wind velocity and setup and setdown for Elephant Butte Reservoir during the period 1950–61.

where ρ_a is the air density and V is the wind velocity, and to adjust for pressure difference over the water surface. This procedure, however, would require weather data and water temperature at several points over the reservoir surface. The computation of setup requires data on fetch, depth, shear stress, and in some situations, barometric pressure and planform (shape of water body in plan view). The determination of shear stress is extremely complicated.

Dynamic surges, or seiches, are oscillatory long-period standing waves whose periods are intermediate between those of lunar tidal waves and storm waves. The resonant oscillation of seiches is analogous to similar behavior of mechanical, acoustical, and electrical systems and may be expressed one-dimensionally by the differential equation for a linear-damped oscillating system with forced vibrations. Seiches may be excited by any force acting on the water surface, including wind, atmospheric pressure, flood waves, landslides, earthquakes, and rainfall. These forces may act singly or in combination to produce oscillations or to damp oscillations previously excited.

Seiche periods for irregular basins may be computed by Du Boys' (1891) equation

$$T=\frac{2}{k}\int_0^L \frac{dx}{\sqrt{gd}},$$

in which d is the depth corresponding to an increment of length, dx, g is acceleration of gravity, L is total length, and k is the number of nodes. Observed periods of oscillation on Elephant Butte Reservoir were compared with theoretical periods computed by Du Boys' equation, using the method described by Shen (1961). The comparison, shown in figure 2, is influenced by several factors. Friction losses in shallow water cause observed wave celerities to be less than computed values. Seddon (1900), in his studies on

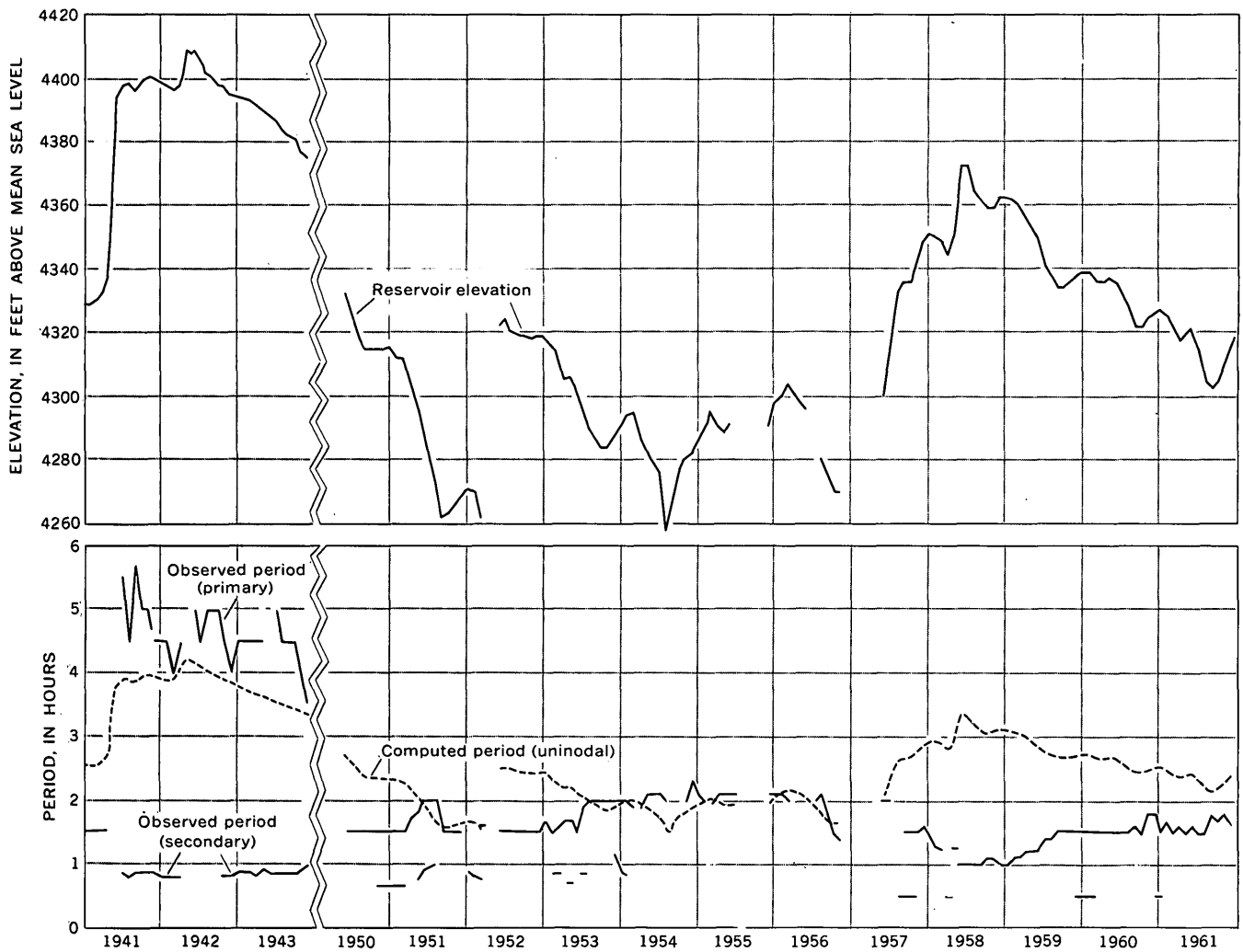

FIGURE 2.—Observed and computed periods of seiche oscillation on Elephant Butte Reservoir during the periods 1941–43 and 1950–61.

the Mississippi River, found the celerity in a reach to be dependent on the mean width of channel; this factor would probably affect long narrow reservoirs such as Elephant Butte in similar fashion. Extensive sedimentation, particularly in the upper reaches of the reservoir, also may affect the comparison. Computed periods are based on depths from the 1961 survey below the Narrows and the 1957 survey above the Narrows.

The best agreement of observed and computed periods is for the period 1950–56, when the water surface was confined to the area below the Narrows. During the period 1957–59, the water surface occupied part of the area above the Narrows. The rise in elevation through the Narrows was accompanied by a gradual decrease in the observed period of primary oscillation from 1½ hours to 1 hour. As the water-surface elevation through the Narrows later dropped, the observed period increased to 1½ hours. Shen (written communication, 1963) suggests that the Narrows influences the seiche characteristics such that uninodal oscillation for elevations below the Narrows changed to trinodal above the Narrows and that during the transition the behavior was similar to that of an open-end basin. Figure 3 indicates the general classification of seiche mode with respect to reservoir elevation, and figure 4 illustrates how oscillations may have occurred under these conditions.

With the reservoir at high stage in 1941–43 (fig. 2), trinodal oscillations apparently were replaced by uninodal primary oscillations accompanied by secondary oscillations of about the fourth or fifth harmonic. The uninode probably was located in the Narrows as indicated by figure 4. For the secondary oscillations, the reservoir may have behaved as two distinct open-end or closed basins separated by the Narrows.

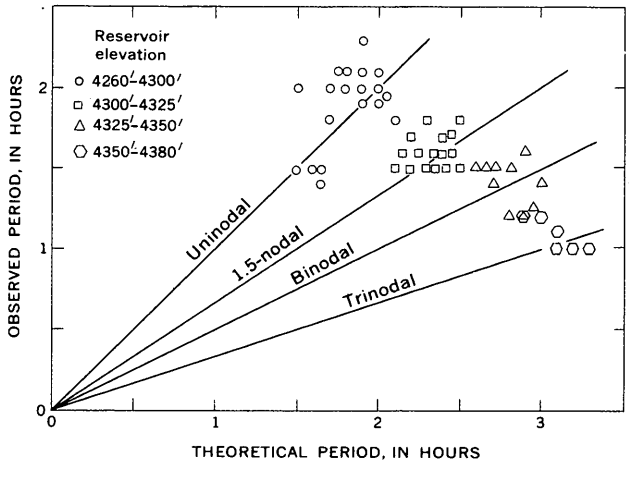

FIGURE 3.—General classification of seiche mode on Elephant Butte Reservoir with respect to water-surface elevation during the period 1950–61.

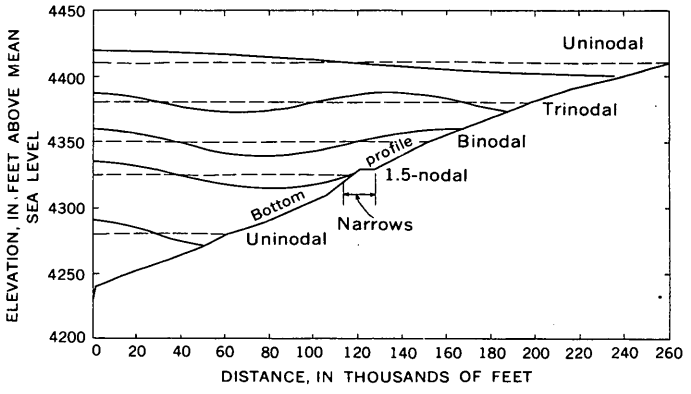

FIGURE 4.—Sketch showing probable mode of primary seiche oscillation on Elephant Butte Reservoir for different water-surface elevations.

This study indicates that seiches on Elephant Butte Reservoir may be excited by wind and barometric-pressure fluctuations and by flood waves from tribu-

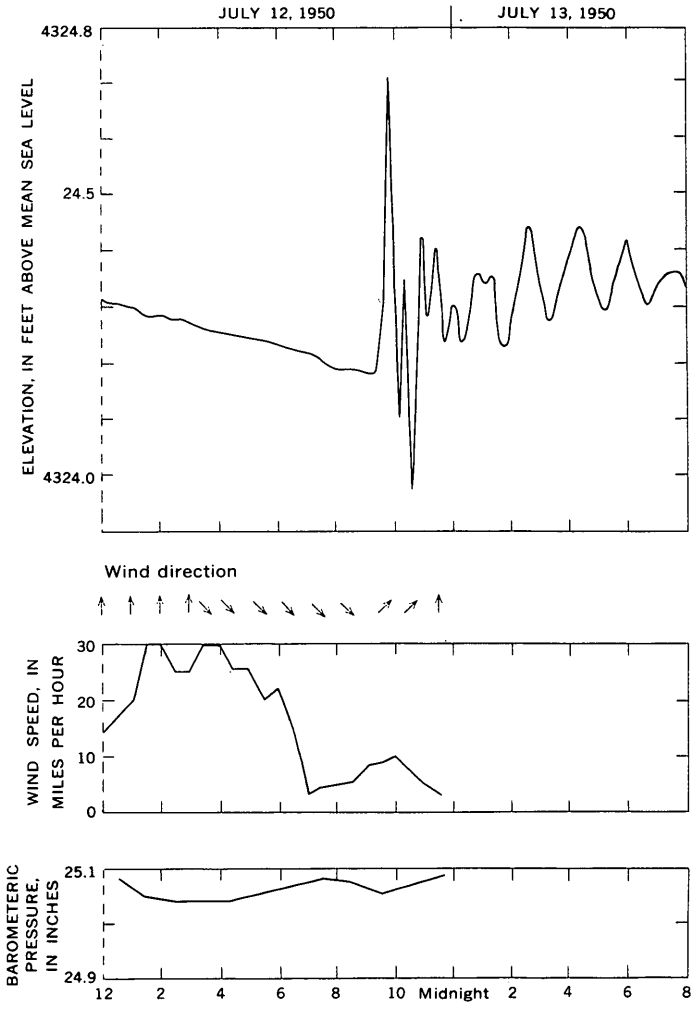

FIGURE 5.—Record of a seiche probably resulting from flash floods, and the relation of the seiche to associated weather conditions, July 12, 13, 1950, Elephant Butte Reservoir. For wind-direction symbols, north is toward top of page.

taries to the reservoir. However, data observed at the single weather station provide only a general indication of the specific conditions responsible for seiche excitation. The largest seiche amplitudes recorded during the study period were apparently produced by flash-flood waves from tributaries to the reservoir. Figure 5 shows a seiche probably resulting from a flash flood of about 1,000 cubic feet per second out of Ash Canyon, noted on the chart by an observer at the reservoir. The associated weather conditions shown support this likelihood.

A seiche probably excited by the sudden subsidence of strong winds is shown on figure 6. Weather conditions associated with other seiches studied indicated that excitation commonly resulted from sharp pressure changes and wind reversal. The excitation of some seiches studied was particularly obscure, emphasizing the limited applicability of single-station data in quantitative seiche analysis.

Two classes of weather systems have been identified as producing setup and in exciting seiches. Cyclonic systems produce most occurrences of setup; thunderstorm systems excite most seiches. Frequency of occurrence of setup and seiche during 1941–43 and 1950–61 is shown in figure 7; the number of occurrences of pure setup is small compared to the number of seiches. Thunderstorm systems are responsible for the greatest number of deviations from the normal water-surface elevation. Because of the small scale of thunderstorm systems, a comprehensive quantitative analysis of seiche excitation would require complete weather observations at a number of locations over the reservoir surface; fewer observations would be required for cyclonic systems because of their larger scale. A properly instrumented study might show that the phenomenon of resonant coupling resulting from thunderstorm systems is an important factor in exciting seiches or in augmenting seiche amplitude.

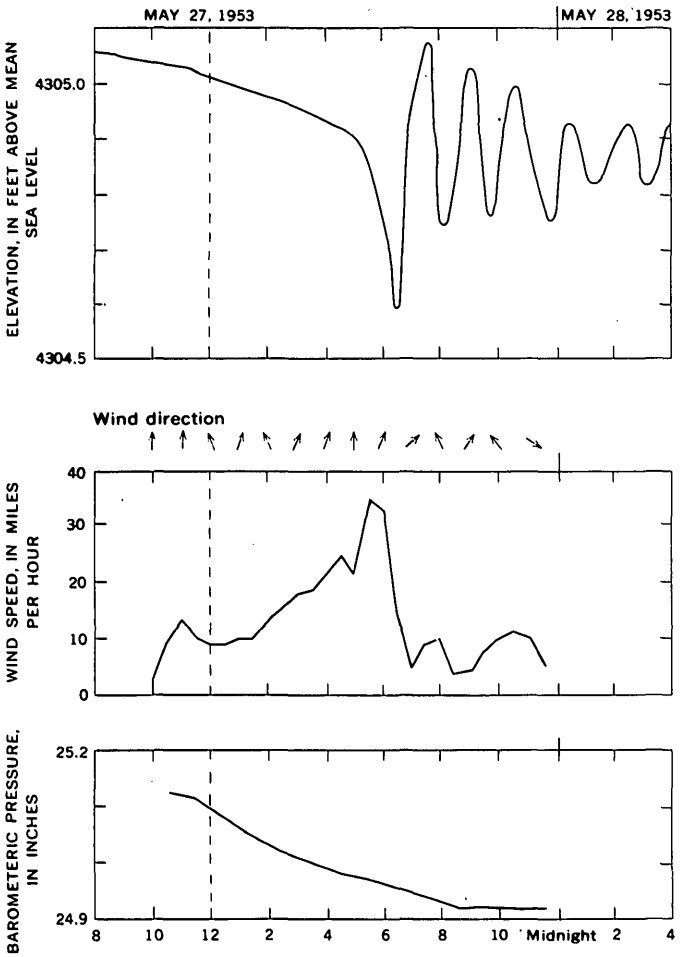

FIGURE 6.—Record of a seiche resulting from sudden subsidence of strong winds, and the relation of the seiche to associated weather conditions, May 27, 1953, Elephant Butte Reservoir. For wind-direction symbols, north is toward top of page.

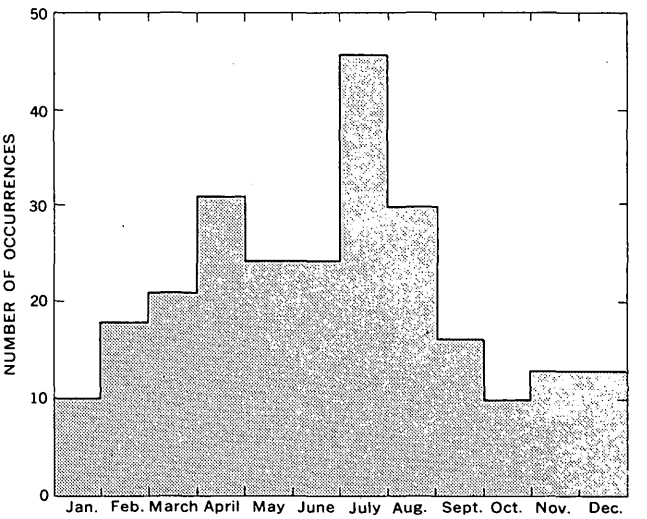

FIGURE 7.—Monthly distribution of 256 occurrences of setup and seiches exceeding 0.10-foot amplitude on Elephant Butte Reservoir during 1941–43 and 1950–61.

A knowledge of the characteristics, and an understanding of the principles, of setup and seiche occurrence are necessary for the proper interpretation and accurate computation of reservoir and lake-stage records and for the optimum placement of gages to minimize or delineate seiche and setup effects. Formidable problems in gage location would be posed by the complexity of these characteristics when applied to reservoirs having irregular planforms and subject to large ranges in stage.

REFERENCES

Du Boys, P., 1891, Essai théorique sur les seiches: Archives des Sciences Physiques et Naturelles, Genève, p. 628.

Irish, S. M., and Platzman, G. W., 1962, An investigation of the meteorological conditions associated with extreme wind tides on Lake Erie: Monthly Weather Rev., U.S. Dept. of Commerce, Weather Bur., v. 90, no. 2, p. 39–47.

Seddon, J., 1900, River hydraulics: Am. Soc. Civil Engineers Trans., v. 43, p. 217–229.

Shen, John., 1961, Characteristics of seiches on Oneida Lake, New York: U.S. Geol. Survey Prof. Paper 424–B, p. B80–B81.

U.S. Army, Corps of Engineers, 1955, Waves and wind tides in shallow lakes and reservoirs: Office of the District Engineer, Jacksonville, Fla., Summary Report, 46 p.

FLOOD INUNDATION MAPPING, SAN DIEGO COUNTY, CALIFORNIA

By L. E. YOUNG and H. A. RAY, Menlo Park, Calif.

Work done in cooperation with the California Department of Water Resources

Abstract. A flood-hydrology study of San Diego County streams indicates that flood magnitude-frequency relations can be estimated from drainage-area size and a dimensionless basin-shape factor. Floods of 50- and 100-year magnitude were estimated for selected sites and, by means of a simple reservoir-storage routing method, the peak discharges were adjusted, where necessary, for the attenuation that would result from storage in existing reservoirs. Areas of potential inundation are shown on topographic maps.

In an investigation of flood hazard in San Diego County, Calif., a new approach was used to determine, from floods of 50- and 100-year recurrence intervals, the areas of potential inundation along five major rivers. A dimensionless flood hydrograph was used in adjusting regionalized flood-frequency results to allow for the attenuating effect of existing reserviors. This investigation consists of two major parts, (1) a flood-hydrology study of streams draining the western slopes of the Peninsular Range in San Diego County, and (2) determination of areas of potential inundation along the flood plains of the five major rivers, for annual floods of 50- and 100-year recurrence intervals.

The regional concept of flood-frequency analysis was used in the flood-hydrology study because the flood series for an individual stream-gaging station is a random sample that may not be representative of the long-term average distribution of floods at that gaging station. The regional concept combines the experience at a number of gaging stations in a homogeneous area, thus providing more reliable flood magnitude-frequency relations. This method of analysis is described in detail in a recent U.S. Geological Survey report (Benson, 1962).

Statistical multiple-correlation techniques were used to relate floods of selected recurrence intervals to hydrologic and physiographic characteristics of gaged streams in the area. The equations relating the annual peak discharge of T-year recurrence interval, Q_T, to various basin hydrologic and physiographic parameters have the general form

$$Q_T = a\,B^b C^c D^d,$$

where

B, C, and D = basin parameters (independent variables), and

a, b, c, and d = constants of the regression equation.

The most significant parameters for use in estimating the 50- and 100-year floods were found to be drainage area and a dimensionless basin-shape factor. This shape factor, Sh, is defined as

$$Sh = d/l,$$

where

d = diameter, in miles, of a circle with an area equal to the basin area, and

l = length, in miles, of the drainage basin measured parallel to the principal stream channel.

The effects of mean annual precipitation, mean annual basin loss (precipitation minus runoff), main channel slope, and channel storage, on annual peak discharges were also investigated, but were found not to be significant for use in estimating the 50- and 100-year floods.

To determine the area of potential inundation, the generalized equations from the flood-hydrology study were used to estimate magnitude of 50- and 100-year floods for selected locations along the San Luis Rey and San Dieguito River flood plains. These peak discharges were then adjusted, where necessary, for the attenuation that would result from reservoir storage. The degree of attenuation was determined by a simple reservoir-storage routing method whereby the storage and outflow discharge are assumed to be uniquely related (Carter and Godfrey, 1960). A composite dimensionless flood hydrograph, developed for the study

area, was used in conjunction with the estimated peak discharges to construct hydrographs of hypothetical reservoir inflow. The dimensionless flood hydrograph, which relates percent of peak discharge to time elapsed since the beginning of storm runoff, was developed from the few available recorded flood hydrographs for the major rivers in the area.

The standard step method of backwater analysis (Chow, 1959) was used to compute water-surface profiles for the adjusted peak discharges. This method uses the Manning equation for computing tranquil gradually varied flow.

The hydraulic properties of the reaches of river channel under study were determined from field surveys and from large-scale topographic maps, These data, along with the appropriate peak discharges, were then applied in the equation, and by trial-and-error computation the water-surface profiles were determined. These profiles were adjusted for backwater effect from bridge constrictions, and the adjusted profiles were used to delineate the areas of potential inundation along the streams.

The areas of potential inundation on the San Luis Rey and San Dieguito River flood plains for 50- and 100-year floods were shown on 7½-minute topographic maps. Two sets of maps (not shown) were prepared; one set shows the area that would be inundated if the floods occurred when reservoirs were initially half full, and the second set shows the inundated area if the floods occurred when reservoirs were initially full.

REFERENCES

Benson, M. A., 1962, Evolution of methods for evaluating the occurrence of floods: U.S. Geol. Survey Water-Supply Paper 1580–A, 30 p.

Carter, R. W., and Godfrey, R. G., 1960, Storage and flood routing: U.S. Geol. Survey Water-Supply Paper 1543–B, 104 p.

Chow, V. T., 1959, Open-channel hydraulics: New York, McGraw Hill, 680 p.

THE RELATION OF DISCHARGE TO DRAINAGE AREA IN THE RAPPAHANNOCK RIVER BASIN, VIRGINIA

By H. C. RIGGS, Washington, D.C.

Abstract.—A family of curves relating discharge to drainage area, for discharges ranging from flood peaks to low flows, has been derived from gaging-station records in the Rappahannock River basin. The extrapolation of these curves to small drainage areas within the basin is verified by 4 series of 30 low-flow measurements in a portion of the basin. The curves may be used to estimate the magnitudes of low flows at selected frequencies.

Stream discharge is commonly related to drainage area by the model

$$Q=CA^n,$$

where Q is some selected discharge such as the 20-year flood, mean discharge, or drought discharge; and A is drainage area. The constants C and n will vary with the selected discharge. Thus, for a drainage basin, a family of curves is needed to cover the range in discharge. Such a family of curves is defined from gaging-station records in the Rappahannock River basin above Fredericksburg, Va. These curves may be extrapolated to small drainage areas within the basin, but without additional information the reliability of the extrapolated portion is unknown. Discharge measurements made on small streams at times of relatively steady flow verify the curve extrapolations in a portion of this basin. After defining the curve family and verifying the extrapolation to small drainage areas, one can estimate drought discharges from the measured small streams.

The family of curves is developed from records for eight gaging stations in the basin. The basin and the gaging-station locations are shown on figure 1.

The relation with mean discharge is defined by records for 7 stations, and an estimate for 1, for the period 1944–50. The plot shows considerable scatter. The amount of rainfall increases from north to south in this part of Virginia; consequently, the mean discharge per square mile from the southern drainage areas is greater than from the northern ones. This information can be used by adding to the relation a variable of latitude. Figure 2 shows mean discharge, both unadjusted and adjusted for latitude, plotted against drainage area. The equation of the relation is

$$\log Q_m=0.356+0.956 \log A-0.0052 L,$$

where Q_m is mean discharge, 1944–50, in cubic feet per second; A is drainage area in square miles; and L, which ranges from 21 to 47, is latitude in minutes north of 38° N lat.

Short records do not permit accurate definition of streamflow at specific probability levels. Therefore,

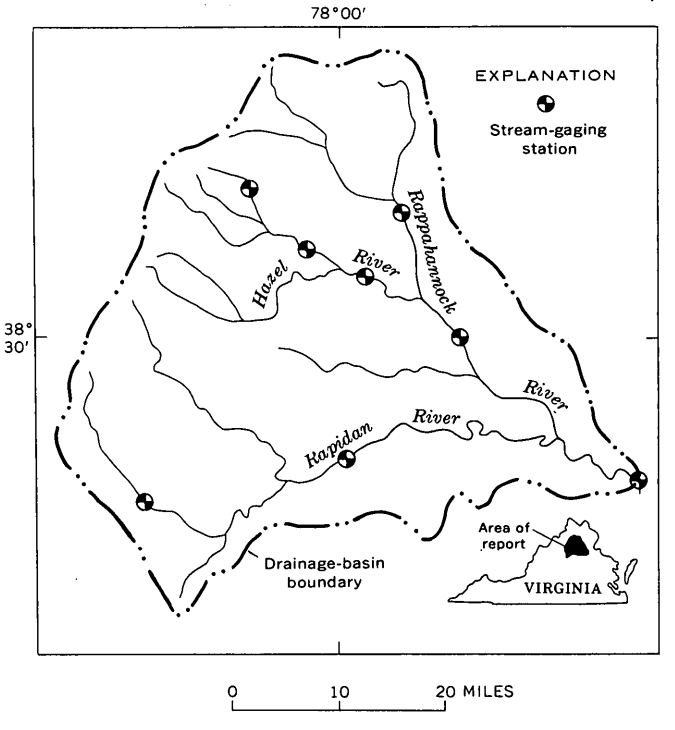

FIGURE 1.—Map of the Rappahannock River basin above Fredericksburg, Va. Circles indicate gaging stations used in this analysis.

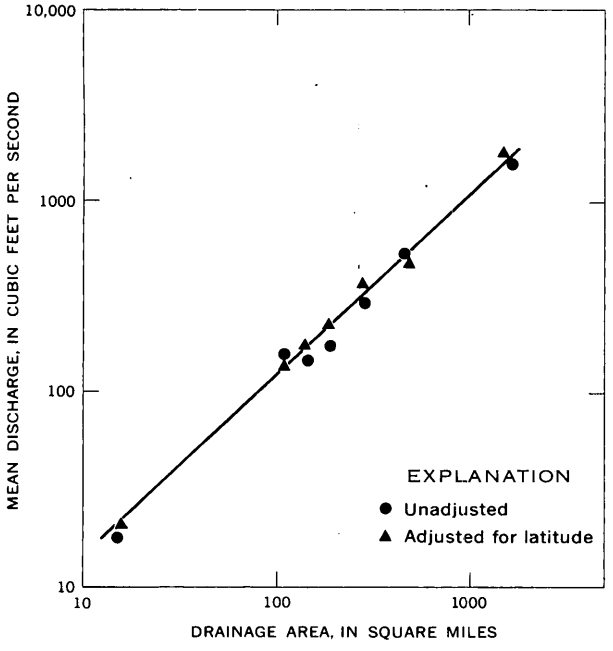

FIGURE 2.—Relation of drainage area to mean discharge, 1944–50, in the Rappahannock River basin.

concurrent discharges are used to develop other relations with drainage area throughout the discharge range.

Peak discharges for the annual floods of 1942, 1955, and 1956 at the several gaging stations and at some miscellaneous stream-measurement sites are plotted against drainage area in figure 3 (curves 1, 2, and 3 respectively). Although not all the peaks for a particular flood have the same recurrence interval, the differences should not be great. Curve 4 (fig. 3) is the relation of drainage area to mean discharge, transferred from figure 2. Curves 5 through 9 are defined by minimum daily discharges for the following months of low flow: September 1955, September 1956, September 1954, October 1954, and October 1930. The ordinate scale is discharge plus 0.1 cfs so that a discharge of zero can be plotted.

The relation curves are defined by the gaging-station records for drainage areas as small as 15 square miles. Downward extrapolations of these curves for discharges

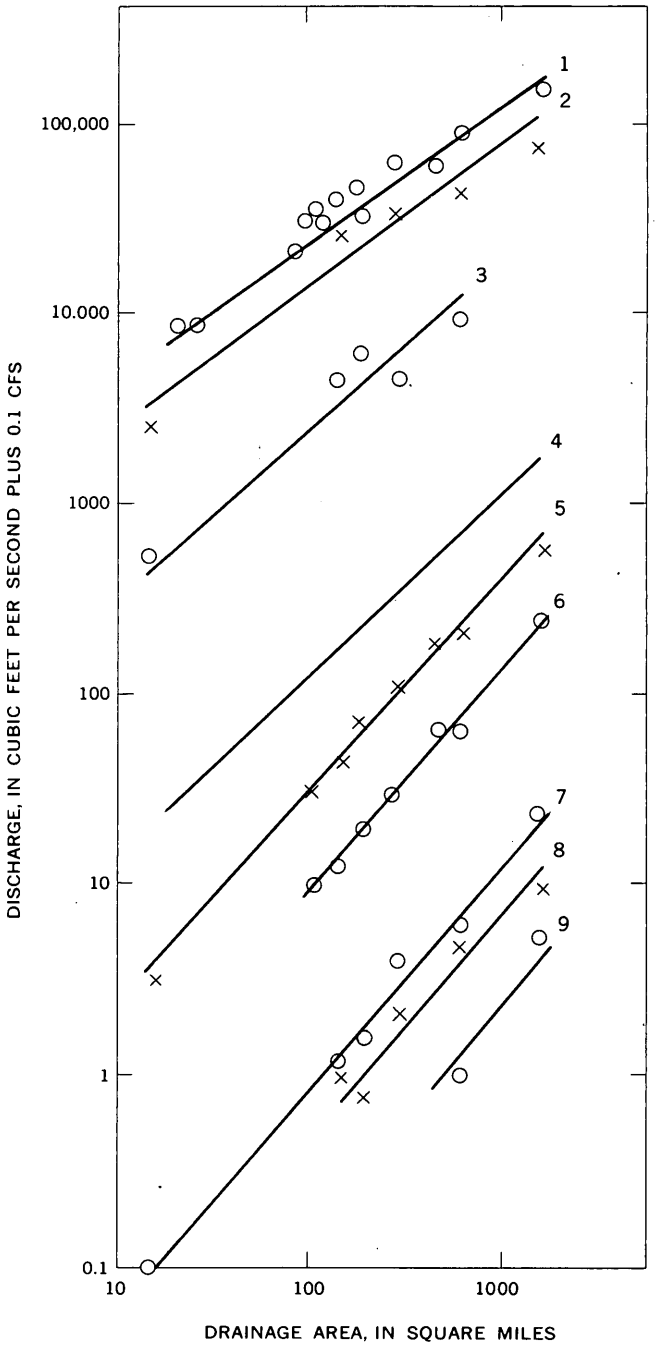

FIGURE 3.—Relation of selected discharge to drainage area in the Rappahannock River basin.

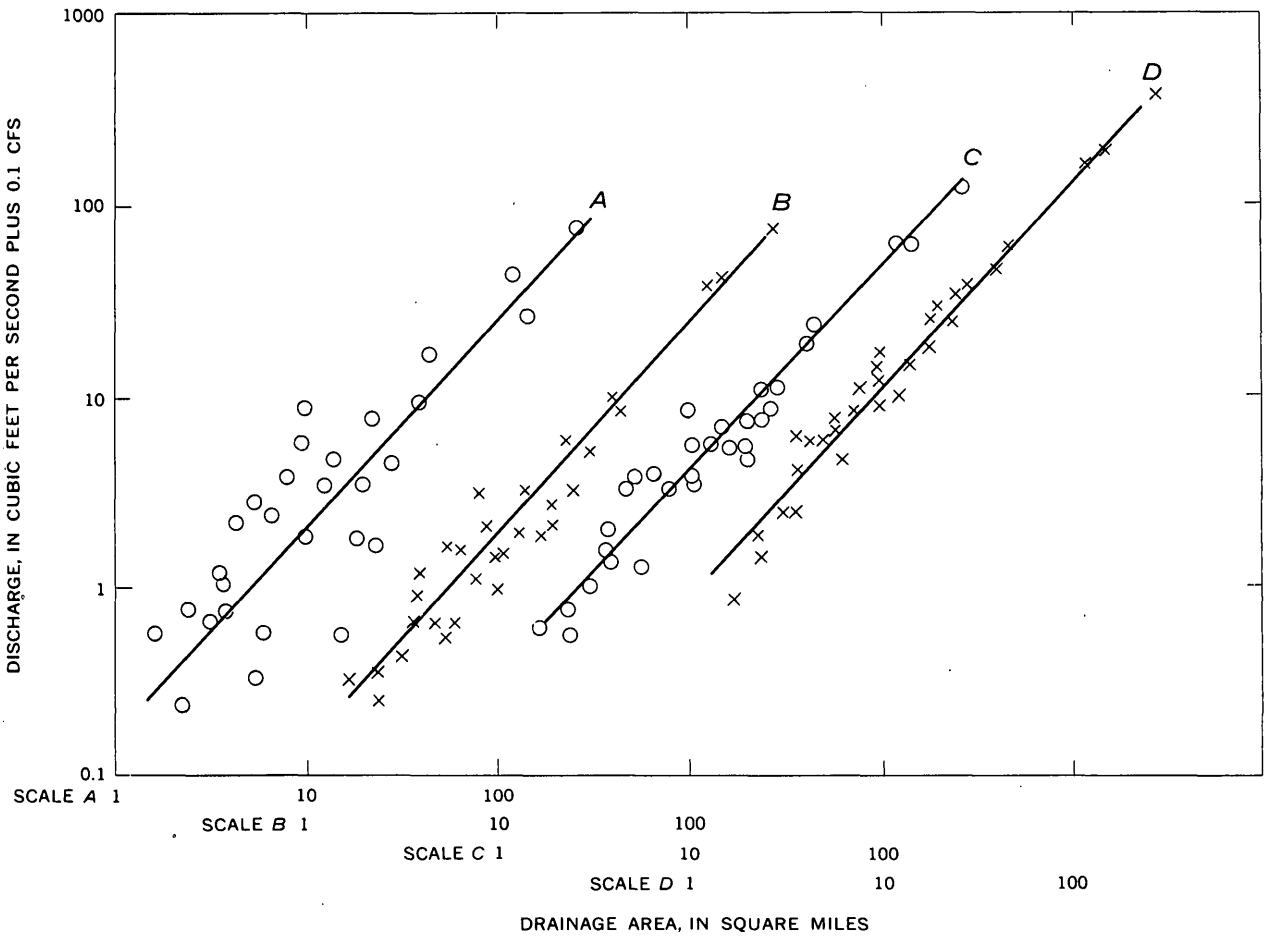

FIGURE 4.—Discharge–drainage-area relations in the Hazel River basin. *A*, October 30 and 31, 1961; *B*, September 24 and 25, 1962; *C*, May 15 and 16, 1963; and *D*, June 25 and 26, 1962.

less than the mean have been checked by discharge measurements.

Four sets of about 30 discharge measurements each, made in the Hazel River basin, a subbasin of the Rappahannock, are used to define the relations with drainage area shown in figure 4. The scatter of the points about the mean curves of figure 4 may be due to one or both of the following: (1) variation in base-flow yield, and (2) variation in recent precipitation experience among the basins. The curves describe the yield of an average subbasin of the Hazel River basin. If the measured discharges of a stream are consistently above or below the average lines, that deviation is assumed to indicate no unusual precipitation influence and, therefore, a yield greater or less than the average. Some of the measurements in the Hazel River basin indicate an occasional influence of nonuniform precipitation over the basin, and others indicate definite differences in yield of certain subbasins.

The curves of figure 4 have about the same slopes as the comparable curves of figure 3, indicating the hydrologic homogeneity of the Hazel River basin and

the general applicability of the curves of figure 3, when extrapolated, to small drainage areas in that basin. The extrapolated curves permit inferences as to the probable discharges of small streams in the Hazel River basin during droughts. For instance, extrapolations of curves 6 and 9 in figure 3 reach zero discharge at about 2 and 70 square miles, respectively, indicating that most streams draining smaller areas probably were not flowing at those times. The frequencies of these events can be estimated from gaging-station records. For streams on which measurements have been made, the respective drought discharges obtained from the average curves should be modified on the basis of measured discharges. Unless a base-flow measurement is available somewhere on a stream, the results from the average curves should be considered as first approximations.

Differences in yield of subbasins are more pronounced at extremely low discharges. An additional set of discharge measurements made under drought conditions in August 1963 (fig. 5) shows this to be true. Thus, the generalized curves are least reliable under extreme drought conditions.

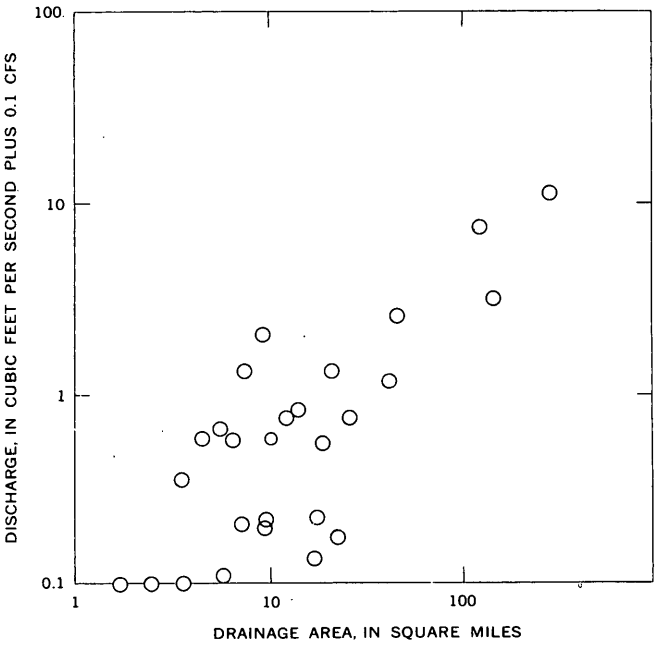

FIGURE 5.—Discharge–drainage-area relations under drought conditions, August 6 and 7, 1963, in the Hazel River basin.

THE ARTESIAN AQUIFER OF THE TIERRA DEL FUEGO AREA, CHILE

By WILLIAM W. DOYEL and OCTAVIO CASTILLO U.,
Washington, D.C., Santiago, Chile

Work done in cooperation with the Instituto de Investigaciones Geológicas, Santiago, Chile, and under the auspices of the Agency for International Development, U.S. Department of State

Abstract.—Water flows from wells tapping the Los Olivos and Bellavista Members of the Palomares Formation of Tertiary age. Although the areal extent and hydrologic characteristics of these artesian aquifers are not known fully, considerable additional development of water supplies from them seems feasible.

During the exploration for, and exploitation of, petroleum by the Empresa Nacional del Petróleo de Chile (ENAP) in the Tierra del Fuego area,[1] artesian water was found in wells in the northern part of the Isla Grande de Tierra del Fuego and on the mainland north of the island (fig. 1). Some of the wells have as much as 70 meters of artesian head above land surface. Various ENAP geologists (Mordojovich, 1950; Alvarez, 1953; Duhart, 1955; and Marino and Mordojovich, 1955) have made brief studies of the occurrence of the ground water, and González and Cortés (1953) have correlated the subsurface data with the surface geology. In 1962 the water was being utilized for public supply and industrial use at ENAP installations in the northern part of the Isla Grande de Tierra del Fuego. Additional study and subsequent exploitation of the artesian supply will help alleviate the shortage of water, which is handicapping further economic development of the area.

[1] For the purposes of this report the Tierra del Fuego area is defined as the area shown in figure 1.

The artesian system consists of two aquifers, the Los Olivos and Bellavista Members, which are separated by the Companario Member, all in the lower part of the Palomares Formation of late Tertiary age. The Tertiary units occupy a structural basin that is bounded on the south and west by the partly submerged Cordillera de los Andes. Rocks of Paleozoic and Mesozoic age crop out on the northeast flank of the Cordillera and dip toward the north and east. Tertiary rocks overlie and crop out in a band northeast of the Mesozoic rocks (fig. 1) and in the Río Gallegos area of Argentina. The deepest part of the basin seems to coincide approximately with the Estrecho de Magallanes (Straits of Magellan) where it borders the north side of the Isla Grande de Tierra del Fuego.

The description of the Palomares Formation given in the accompanying table is based on the work of González and Cortés (1953) and applies only to the northern part of the Isla Grande and the southern part of the mainland north of the Estrecho de Magallanes. Although detailed studies of the late Tertiary sequence have not been made, the Palomares Formation is believed to be continuous throughout the Punta Arenas–Puerto Natales–Río Gallegos area (fig. 1). Underlying the Palomares Formation is a lower Tertiary marine clay which has been identified only in wells (see table).

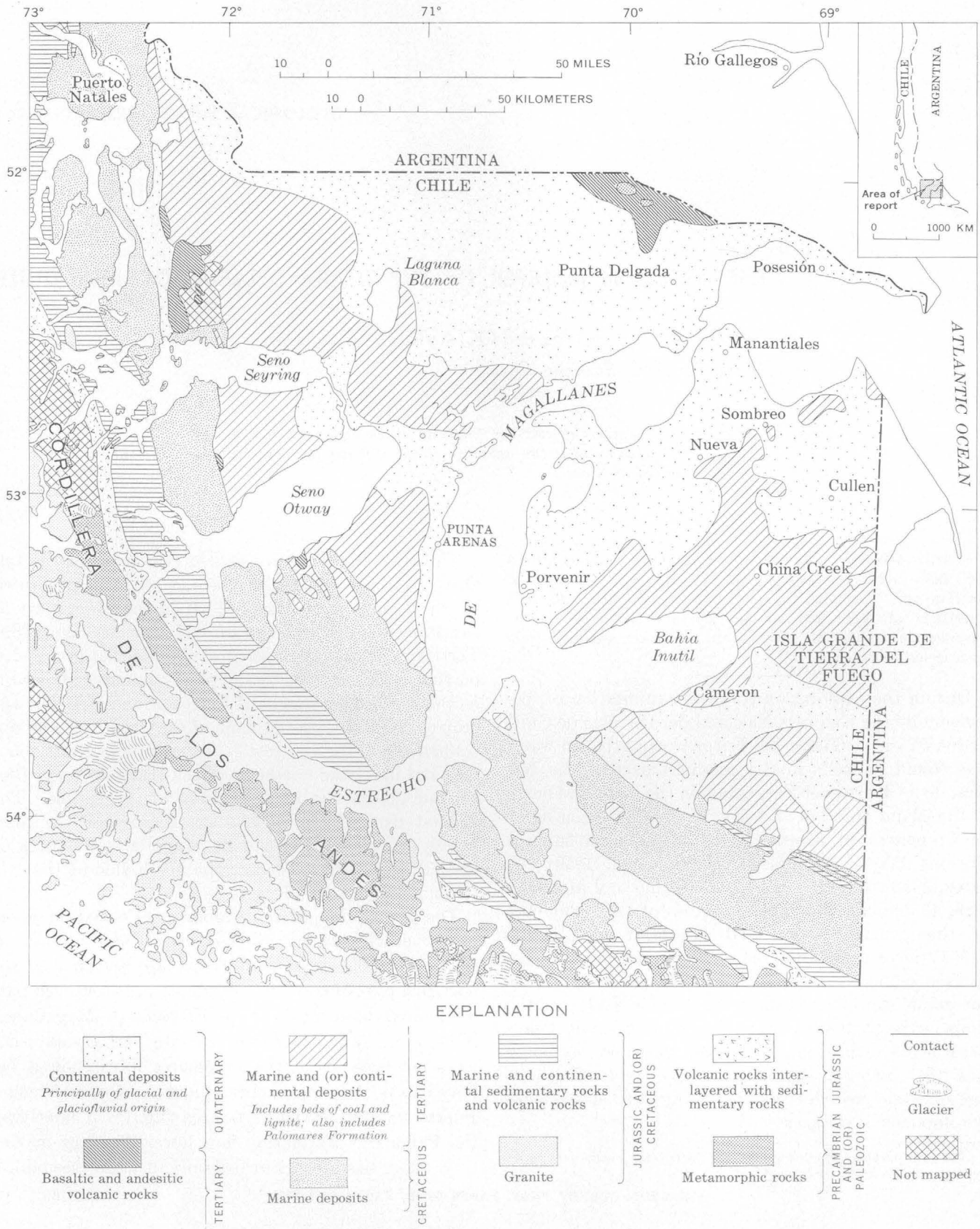

FIGURE 1.—Geologic map of the Tierra del Fuego area. After geologic map of Chile by Instituto de Investigaciones Geológicas, 1960.

Stratigraphy of the post-Cretaceous deposits of the Tierra del Fuego area

[After González and Cortes, 1953]

System	Formation	Member	Description	Thickness (meters)
Quaternary			Principally poorly sorted glaciofluvial and morainal deposits filling valleys and covering flatland areas.	----------
Tertiary	Palomares	Palomares Superior	Tuff, white to yellow, fine- to coarse-grained, poorly sorted, irregularly stratified. Contains some plant stems.	±70
		Primavera	Sandstone and conglomerate, blue, poorly sorted, partially to well cemented; interbedded with white to yellowish-gray tuff. High content of basalt and pumice. The tuff contains some plant impressions.	±80
		Bellavista	Sandstone and conglomerate, blue, poorly sorted, partially cemented, crossbedded; blue color due to staining on basalt grains. Contains pebbles and cobbles of basalt and pumice. Highly permeable; contains water under artesian pressure.	±30
		Campanario	Clay, gray to yellowish-gray; bentonitic in the upper part. Contains red tuffaceous clay near the base, stringers of lignite, and, in the lower part, many plant fossils.	±30
		Los Olivos	Sandstone, gray to grayish-blue, fine- to coarse-grained, poorly sorted, partially cemented, crossbedded; bluish color due to staining on basalt grains. Includes a high percentage of basalt grains. Highly permeable; contains water under artesian pressure.	±30
	Unconformity		Not identified in outcrop, but in the subsurface, marine clay underlies the Los Olivos and is underlain by a thick section of marine Tertiary sedimentary deposits.	500–1000
Cretaceous			Marine sedimentary deposits.	----------

During the Pleistocene, the Tierra del Fuego area, and most of southern Chile, was subjected to glaciation. The Estrecho de Magallanes then probably was above sea level and was occupied by a tongue of glacial ice. Now, much of the lower lying part of the area is mantled with glaciofluvial and morainal deposits as much as 25 m thick. Conspicuous volcanoes distributed along an east-west line near the Chilean border with Argentina (52° south latitude) are post-Tertiary and may be of late Pleistocene or Recent age.

The outcrops of the highly permeable Los Olivos and Bellavista Members of the Palomares Formation in the north-central part of Isla Grande de Tierra del Fuego probably are the principal recharge area of the artesian aquifer system. The altitude of the land surface in the outcrop area ranges from about 100 to 110 m. Down the hydraulic gradient from the outcrop, the unnamed marine clay underlying the Los Olivos, the Campanario Member between the Los Olivos and Bellavista, and the Primavera Member overlying the Bellavista confine the water in the Los Olivos and the Bellavista Members. A piezometric map constructed by Duhart (1955) shows that wells tapping the Los Olivos and Bellavista in the northern part of the Isla Grande flow where the land-surface altitude is less than 100 m. The piezometric surfaces here slope northward. Available data are insufficient to determine the direction of the slope in the area north of the Estrecho de Magallanes, but the geologic structure and stratigraphy suggest strongly that it is generally eastward. The aquifer system probably discharges along the coastline of the Atlantic Ocean and contiguous tidal-water bodies and possibly through submarine springs and by leakage upward through confining beds.

The quality of the water is considered satisfactory for domestic and industrial use by the ENAP, the only user of the water in 1962. The results of chemical analyses made in the ENAP chemical laboratory show that the dissolved-solids content ranges from 300 parts per million in a well at Cullen to 901 ppm in a well in Posesión.

No quantitative studies have been made, and hence the hydrologic characteristics of the artesian aquifer system are imperfectly known. In 1962, wells were producing sufficient water to supply the requirements of ENAP installations, with little or no evidence of decline in artesian head. The nature of the sedimentary rocks composing the aquifer system, the nearness of the recharge area to actual or potential points of withdrawal, the moderate rainfall well distributed throughout the year,[2] and the yields of the wells indicate that the artesian aquifer system is capable of producing con-

[2] The city of Punta Arenas has an average annual rainfall of 438 mm for the period 1901–56 (United Nations, 1960, p. 15).

siderably larger quantities of water than now are being withdrawn. A marked decline in artesian head near tidal-water bodies, however, could result in the intrusion of salt water into the aquifers.

The Quaternary deposits contain a shallow water-table aquifer throughout the basin area, and this aquifer is tapped by shallow wells for stock and domestic supplies. Because there are wide local variations in the horizontal and vertical permeabilities of the shallow aquifers, the possibilities for large-scale withdrawals are limited except in areas of exceptionally favorable conditions for the percolation of water both from the surface and laterally through the deposits.

Water for domestic, municipal, and industrial use, and also for supplemental irrigation, can be obtained from the artesian system throughout the northern part of the Isla Grande and the area north of the Estrecho de Magallanes. Additional geologic studies and quantitative and qualitative hydrologic studies, however, should be made before large-scale withdrawals.

REFERENCES

Alvarez, Jorge, 1953, Cuenca artesiana de la parte norte de Tierra del Fuego: Empresa Nacional del Petró leo de Chile open-file report.

Duhart, Javier, 1955, Cuenca artesiana en la parte N.E. de Tierra del Fuego: Empresa Nacional del Petróleo de Chile open-file report.

González, Eduardo, and Cortés, Raul, 1953, Levantamiento geológico en la parte noreste de Tierra del Fuego: Empresa Nacional del Petróleo de Chile open-file report.

Marino, Mario, and Mordojovich, Carlos, 1955, Posibilidades de agua subterránea en Flamenco y Cullen: Empresa Nacional del Petróleo de Chile open-file report.

Mordojovich, Carlos, 1950, Cuenca artesiana en la península Espora: Empresa Nacional del Petróleo de Chile open-file report.

United Nations, 1960, Los recursos Hidráulicos de Chile: Mexico City, Mex.

A METHOD FOR EVALUATING OIL-FIELD-BRINE POLLUTION OF THE WALNUT RIVER IN KANSAS

By ROBERT B. LEONARD, Topeka, Kans.

Work done in cooperation with the Kansas State Department of Health

Abstract.—Ratios of the concentration of major ionic constituents to the concentration of chloride in oil-field brine are used to determine the percentage of the dissolved-solids load that oil-field brine contributes to the Walnut River, Kans.

Oil-field brine is a major source of dissolved solids in the Walnut River basin, Kansas (fig. 1), although marked improvement of the quality of both surface and ground water has resulted from an extensive pollution-abatement program of the Kansas State Department of Health. This article describes a method used to determine the approximate magnitude of oil-field-brine pollution from analyses of samples of river water and from published oil-field data. The method is based upon the premise that the concentration of chloride ion carried by the river can be used as a quantitative index of the degree of oil-field-brine pollution. It was developed as part of an extensive cooperative investigation of the quality of the water resources of the basin and is illustrated here by preliminary data obtained in a salinity survey made in 1962.

In Kansas oil-field brines, the ratios of the concentration of calcium, magnesium, and sodium (as reported here the concentration of sodium includes concentration of potassium) to the concentration of chloride are virtually constant despite wide differences in dissolved-solids concentrations (Jeffords, 1948). Mean and weighted-mean ratios of the concentrations of selected constituents to the concentration of chloride in oil-field brine are listed in table 1. The ratios were calculated from analyses of 45 samples of brine from oil wells, separators, and brine-disposal ponds in the Walnut River basin (Schoewe, 1943; Rall and Wright, 1953). The samples represent nearly random geographic (figs. 1 and 2), stratigraphic, and compositional distribution.

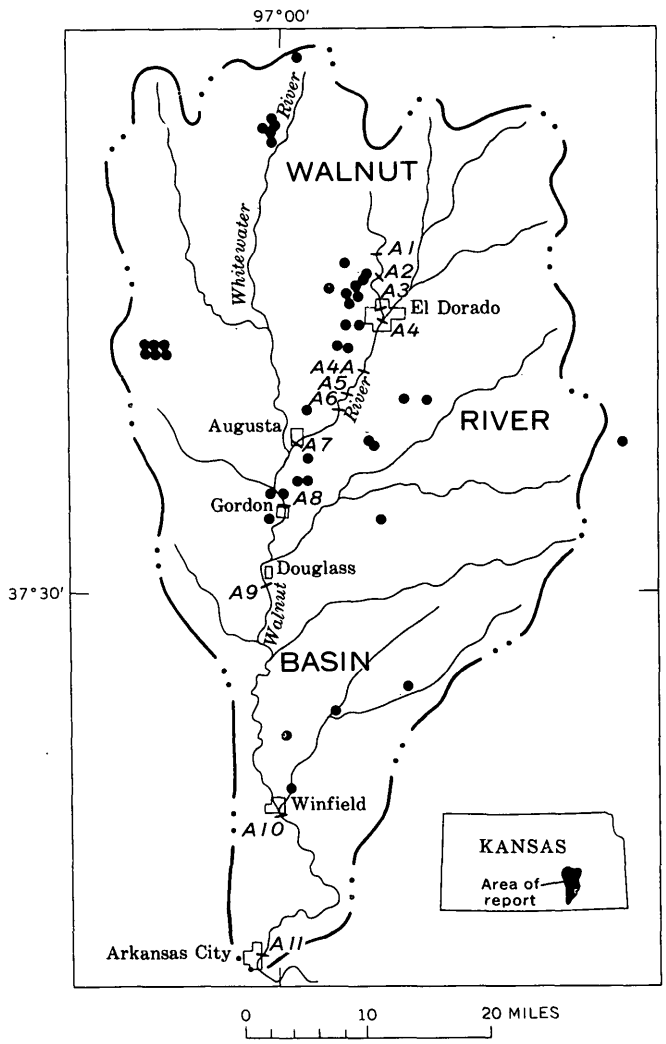

FIGURE 1.—Map of the Walnut River basin in southern Kansas. Numbers refer to river sampling stations for which data are given on figure 2. Dots show brine-sampling sites.

TABLE 1.—*Mean and weighted-mean ratios of the concentration of selected constituents to the concentration of chloride in oil-field brine in the Walnut River basin*

	All samples		Samples with <90,000 ppm chloride	Samples with >90,000 ppm chloride
No. of analyses	45		29	16
Σchloride (ppm)	2, 491, 778		707, 796	1, 783, 982
	Mean ratio	Weighted-mean ratio	Mean ratio	
Sodium/chloride	0. 522	0. 5105	0. 5328	0. 5017
Calcium/chloride	. 074	.0769	. 0710	. 0793
Magnesium/chloride	. 022	. 0229	. 0220	. 0234
Sulfate/chloride	. 026	. 0115	. 0396	. 004

The concentrations of chloride in the 45 samples ranged from about 10,000 to 140,000 parts per million. As the concentration of chloride increased, the concentrations of the major constituents other than sulfate increased, the calcium/chloride and the magnesium/chloride ratios increased slightly, and the sodium/chloride ratio decreased (table 1). The sulfate/chloride ratio was less than 0.001 in many samples of concentrated brine, but it was as much as 0.14 in one sample. Because the total pollutive effect of equal volumes of brine varies almost directly with concentration of chloride, ratios weighted with respect to chloride are most applicable to this study of oil-field-brine pollution where neither the concentrations nor the exact locations of multiple sources are known.

The method of computing the weighted-mean ratios (table 1) is illustrated by the computation of the weighted mean for the sodium/chloride ratio. The mean sodium/chloride ratio for each group (<90,000 ppm chloride, and >90,000 ppm chloride) was multiplied by the ratio of the sum of the chloride concentrations in that group to the sum of the chloride concentrations in both groups. The weighted-mean ratio is the sum of these products. The numerical computation is as follows:

$$(0.5328)\left(\frac{707{,}796}{2{,}491{,}778}\right)+(0.5017)\left(\frac{1{,}783{,}982}{2{,}491{,}778}\right)$$

$$=\text{weighted mean}\ \frac{\text{sodium}}{\text{chloride}}\ \text{ratio}=0.5105$$

If the calculated ratios are valid, an approximate anion-cation balance in equivalents per million should exist in a brine reconstituted by multiplying the ratios by an arbitrary concentration of chloride. The equation representing the concentrations of the major constituents of a typical oilfield brine is

$$Na^{+1}+Ca^{+2}+Mg^{+2}=SO_4^{-2}+Cl^{-1}$$

The concentrations, in parts per million, of the various constituents, can be expressed as the products of an arbitrary chloride concentration and the appropriate ratios:

Cations (ppm)	*Anions (ppm)*
$Na^{+1}=0.5105\ Cl^{-1}$	$SO_4^{-2}=0.0115\ Cl^{-1}$
$Ca^{+2}=0.0769\ Cl^{-1}$	$Cl^{-1}=Cl^{-1}$
$Mg^{+2}=0.0229\ Cl^{-1}$	

The concentrations can then be converted to equivalents per million (epm) and arranged as an equation:

$$\underset{\text{Cations}}{0.0222\ Cl^{-1}+0.0038\ Cl^{-1}+0.0019\ Cl^{-1}}=\underset{\text{Anions}}{0.0002\ Cl^{-1}+0.0282\ Cl^{-1}},$$

which reduces to

$$\underset{\text{Cations}}{0.0279\ Cl^{-1}}=\underset{\text{Anions}}{0.0284\ Cl^{-1}}$$

The percentage of error is approximately 1.

Although low concentrations of bicarbonate and of other ions are commonly present in the oilfield brine, they apparently have no direct relation to the concentration of chloride. The small percentage of error substantiates the hypothesis that exclusion of these ions does not appreciably affect the accuracy of the method as applied in this area.

The proportion of dissolved solids attributable to brine carried by the Walnut River during base flow can be calculated from the concentration of chloride in the river water. The amount of chloride introduced by oilfield operations, past and present, is approximately the difference between the natural and present chloride loads at a sampling station. The natural chloride load is determined from quality-of-water data obtained before 1914, the year that oil was discovered in the basin (Parker, 1911; Kansas State Board of Health, 1960), and from recent water-quality studies of tributaries draining geologically similar areas unaffected by oilfield activity. The concentrations of the other constituents derived from the brine can be determined by multiplying the concentration of chloride derived from brine by the appropriate R value shown in table 2.

TABLE 2.—*Computation of the contribution of oil-field brine to the dissolved solids content of the Walnut River at station A8, November 1, 1962*

[Concentration in parts per million, except as noted; discharge of river 165 cfs]

	Total concentration	Concentration attributed to oil-field brine	Concentration attributed to natural sources	R[1]
Calcium	161	[2] 20	141	0. 077
Magnesium	35	[2] 6	29	. 023
Sodium	150	[2] 135	15	. 511
Bicarbonate	332	0	332	------
Chloride	286	266	20	------
Sulfate	172	[2] 3	169	. 012
Dissolved solids (residue at 180°C)	1, 010	430	580	------
Dissolved solids (tons per day)	450	192	258	------

[1] Weighted-mean ratio of concentration of indicated constituent to concentration of chloride, in oil-field brine; taken from last column of table 1.
[2] $R \times 266$ (concentration of chloride attributed to oil-field brine).

Although calcium and magnesium are derived partly from oil-field brine, they are derived principally from the dissolution of limestone, gypsiferous shale, and gypsum of Permian age. Limestone crops out along and is present as float in all major stream courses, and gypsiferous strata are at or near the surface throughout much of the western part of the basin. Hardness (as $CaCO_3$) of water in the lower reaches of the main stem at low flow is characteristically greater than 300 ppm.

Sodium is derived principally from oil-field brine, although minor amounts are naturally present. The sodium/chloride ratio of waters containing oil-field brine is normally less than 0.60. The concentration of sodium-plus-potassium in unpolluted surface water in the Walnut River basin commonly is <20 ppm, although concentrations ranging from 100 to 150 ppm are now common in the main stem. The concentration of potassium is uniformly low (5 to 6 ppm) at all sampling sites. Some sodium and potassium may be attributed to municipal sewage and to the use of fertilizers.

Sulfate is derived principally from gypsum and gypsiferous shale of Permian age. Natural sulfate concentrations in some tributaries of the Walnut River normally exceed 200 ppm. Only a minor part of the total sulfate load is derived from oil-field brine and from oxidation of sulfurous materials associated with some oils. The sulfate/chloride ratio of natural water in the basin is commonly greater than one. In periods of low flow during the study, ratios were as high as 11 in tributaries draining the western part of the basin but as low as 0.03 in those draining oil fields.

Chloride concentrations greater than 200 ppm are not uncommon during periods of low flow in the Walnut River. Under similar conditions, water unpolluted by brine from the eastern part of the basin commonly

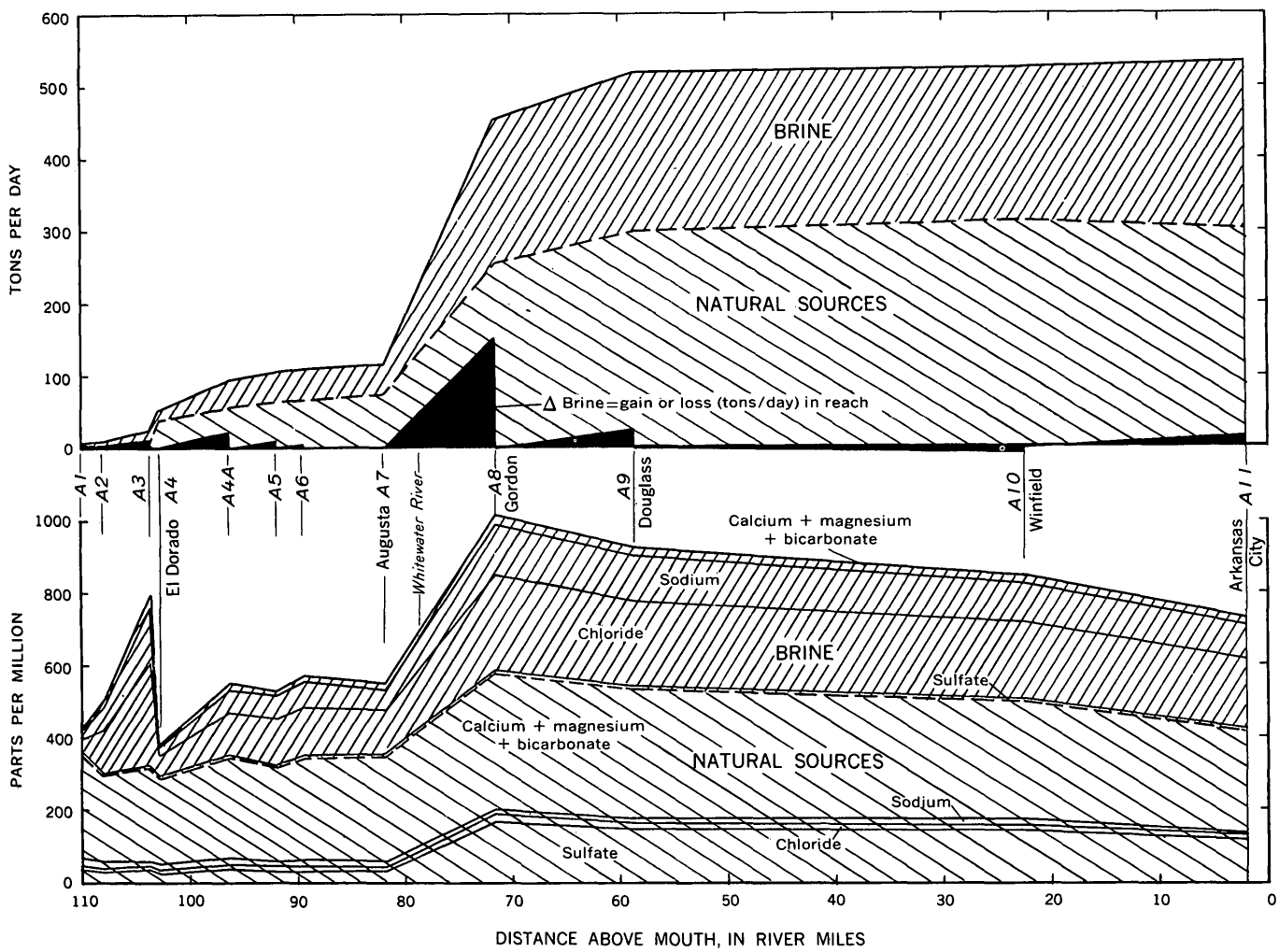

FIGURE 2.—Chemical-quality profile of the Walnut River on November 1, 1962, showing the part of the dissolved-solids load derived from natural sources and the part due to pollution by oil-field brine.

contains less than 12 ppm of chloride, and water from the western part seldom contains more than 30 ppm. On the basis of concentration-discharge relations and data obtained prior to the discovery of oil, the natural chloride concentration is assumed to be 12 ppm in the part of the Walnut River upstream from Augusta (*A1–A7*, figs. 1 and 2) and 20 ppm in the part downstream from the confluence with the Whitewater River (*A8–A11*). The assumed values are sufficiently accurate for illustration of the method; however, they may be changed slightly as a result of studies now in progress. Application of the method to data collected on November 1, 1962, at sampling station A8 in the water-quality study is presented in table 2; the results of similar computations for all river sampling stations are illustrated on figure 2.

The utility of the method described is based on the assumption that the chemical analyses, sampling procedures, and discharge measurements adequately describe actual field conditions. Discharge measurements and chemical analyses are considered to be accurate within 5 percent, but other variables are difficult to evaluate as precisely. Slight errors in any of the variables could cause apparent inconsistencies in the results. For example, the computed loss of about 1 percent of the tonnage of total dissolved solids ascribed to brine in the reach between Douglass and Winfield (fig. 1) is well within the limits of accuracy for the method.

The ratios of the constituents of brine polluting a particular reach or tributary may not conform to the computed ratios because of isolated and practically indeterminate anomalies in the distribution and characteristics of the sources of brine. However, expected variations from the weighted mean are commonly minor. For example, the standard error of the sodium/chloride ratio (0.5105) determined from the 45 available analyses is only 0.008.

Inaccuracies in the assigned value of natural chloride concentration may affect adversely the results for sites in the basin where the natural concentration of chloride constitutes a large proportion of a low concentration of chloride. However, under these conditions such error is insignificant because the tonnage attributable to oil-field brine carried by the stream would also be low.

Bicarbonate and minor constituents of the brine are disregarded in determining the magnitude of the brine component in the samples of the Walnut River water. The concentration of bicarbonate derived from brine is probably insignificant when compared with that derived from contact with calcareous rocks, the soil, and the atmosphere. Generally the concentration of the other disregarded constituents of brine is extremely low.

This study shows how analyses of water samples can be used to determine the percentage of the dissolved-solids load that oil-field brine contributes to the Walnut River, Kans. On the basis of preliminary data, oil-field brine accounted for about 40 percent of the dissolved-solids load downstream from the confluence of the Walnut and Whitewater Rivers at the time of the survey described in this article.

REFERENCES

Jeffords, R. M., 1948, Graphic representation of oil-field brines in Kansas: Kansas Geol. Survey Bull. 76, pt. 1, 12 p.

Kansas State Board of Health, 1960, Chemical quality of surface waters in the Walnut River basin, 1906–1960: Topeka, Kans., Div. Sanitation, 57 p.

Parker, H. N., 1911, Quality of the water supplies of Kansas: U.S. Geol. Survey Water Supply Paper 273, 375 p.

Rall, C. G., and Wright, Jack, 1953, Analyses of formation brines in Kansas: U.S. Bur. Mines Rept. Inv. 4974, 40 p.

Schoewe, W. H., 1943, Kansas oil-field brines and their magnesium content, pt. 2 of Reports of studies: Kansas Geol. Survey Bull. 47, p. 37–76.

COMPUTING STREAM-INDUCED GROUND-WATER FLUCTUATION

By M. S. BEDINGER and J. E. REED, Little Rock, Ark.

Work done in cooperation with the U.S. Army, Corps of Engineers

Abstract.—Changes in ground-water level induced by a fluctuating surface-water boundary can be analyzed by separating the surface-water stage hydrograph into a sequence of steady stages separated by instantaneous changes. Each change in ground-water level is considered to be the net effect of antecedent changes in surface-water stage weighted according to the drain function.

In places where surface water is hydraulically continuous with ground water, changes in the stage of a surface-water body commonly are the principal cause of water-level fluctuations in nearby wells. Ferris (1951), drawing from analogous expressions for heat flow, developed mathematical equations relating the amplitude of sinusoidal stage changes in a surface-water body to the amplitude of the corresponding water-level changes in the adjacent ground-water reservoir.

Except for surface-water bodies affected by tidal forces, sinusoidally fluctuating bodies of water are rare. A method is presented here for analysis of ground-water fluctuations induced by either sinusoidal or irregular surface-water fluctuations. In this method the surface-water hydrograph is generalized as a sequence of instantaneous changes separating steady stages of equal duration. The effect of each unit duration of surface-water stage on the ground-water level at a specific location is analyzed separately. The changes in ground-water level are then considered to be the algebraic sum of the effects of independently acting antecedent changes in surface-water stage. The latter summation is based upon the principle of superposition which, in turn, is valid only if ground-water flow is described by linear differential equations. The procedure used is taken from the method developed by Langbein (1949) for the computation of soil temperatures.

Consider an extensive uniform aquifer bounded by a stream. If a change in the amount of water stored in the aquifer is proportional to and instantaneous with the corresponding change in ground-water level, the change in ground-water level induced by a change in the stage of a surface-water body from one steady stage to another is described by the following equation (Stallman, *in* Ferris and others, 1962, p. 126):

$$s=s_0\left[1-\frac{2}{\sqrt{\pi}}\int_0^{\frac{x}{2\sqrt{Tt/S}}} e^{-u^2}du\right]=s_0D(u)_h, \qquad (1)$$

where $u^2=x^2S/4Tt$ or, in U.S. Geological Survey units, $u^2=1.87x^2S/Tt$; x is the distance from the surface-water body to the point at which the amount of head change, s, is to be determined; s_0 is the abrupt change in surface-water stage at $t=0$; t is the time since the change in surface-water stage; and T and S are the coefficient of transmissibility and storage, respectively, of the aquifer. $D(u)_h$ replaces the quantity in brackets and represents the drain function of u for the constant-head situation.

For leaky artesian aquifers, the following expression, developed by Hantush (1961, p. 79) with symbols changed to conform with Survey usage, applies instead of equation 1:

$$s=\frac{s_0}{2}\left[e^{-x\sqrt{P'/Tm'}}\ \mathrm{carf}\left(u-\frac{\left(\frac{x}{2}\right)\sqrt{P'/Tm'}}{u}\right)+e^{x\sqrt{P'/Tm'}}\ \mathrm{cerf}\left(u+\frac{(x/2)\sqrt{P'/Tm'}}{u}\right)\right], \qquad (2)$$

where P' and m' are the permeability and thickness respectively, of the leaky confining bed, cerf represents the complementary error function which is the same as the drain function of u for the constant-head situation $[D(u)_h]$, and the other symbols are as defined previously.

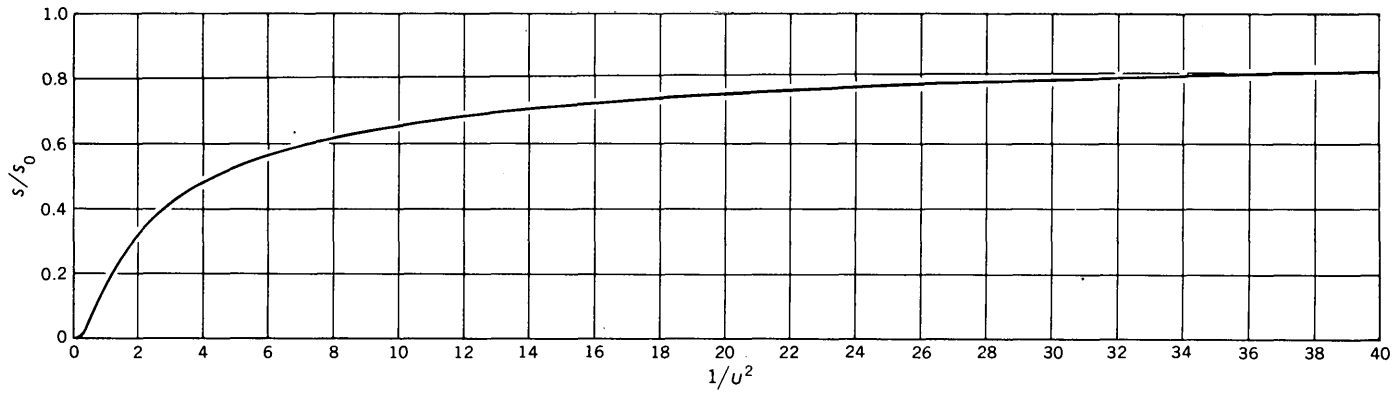

FIGURE 1.—Graph of equation 1, showing change in ground-water level in response to an instantaneous change in river level. Symbols are defined in text.

The following procedures, although applied in this article only to equation 1, may be applied to equation 2.

A graph for the solution of equation 1 is given in figure 1, where the ratio s/s_0 is plotted as the ordinate and $1/u^2$ as the abscissa. Because s/s_0 is a function of time, the graph illustrates the fluctuation in ground-water level in response to a permanent change in surface-water stage.

To implement the method presented in this article, we must know the separate effects of a change of one time unit during subsequent units of time. Consider a point 2,500 feet from a river in an aquifer with a ratio of transmissibility to storage of 5.84×10^6 gallons per day per foot. Arbitrarily choosing 1 day as the time unit we find this corresponds to $1/u^2=5.84\times10^6/1.87\times6.25\times10^6=0.5$. Values of $1/u^2$ and $D(u)_h$, for the first 12 units of time, are listed in columns 2 and 3, respectively, of table 1, and identical values of $D(u)_h$, each offset by 1 time unit, are listed in column 4. The differences between the fourth and third columns, listed in column 5, are the coefficients of the distributive effect of a change of 1-day duration. For example, a rise in river stage of 10 feet at time 0 will effect a component of rise of $10\times0.046=0.46$ foot the first day, $10\times0.111=1.11$ feet the second day, $10\times0.091=0.91$ foot the third day, and so forth.

Next, consider the changes in ground-water level at well A–4, 1,700 feet from the Arkansas River in Jefferson County, Ark. The transmissibility of the aquifer at well A–4 was estimated from the lithologic log to be 108,000 gpd per foot. The coefficient of storage from pumping tests in the area averages about 0.02. The value of $1/u^2$ for 1 day equals 1.0. The drain function of u for the constant-head situation, $D(u)_h$, read at intervals of 1 day was used to determine the coefficients

TABLE 1.—*Coefficients of the distributive effect for changes of 1-unit duration*

[Symbols explained in text]

Time, in days (1)	$1/u^2$ (2)	$D(u)_h$ (3)	$D(u)_h$ offset by one time unit (4)	Coefficient of distributive effect (5)
1	0.5	0.046	0	0.046
2	1.0	.157	.046	.111
3	1.5	.248	.157	.091
4	2.0	.317	.248	.069
5	2.5	.371	.317	.054
6	3.0	.414	.371	.043
7	3.5	.449	.414	.035
8	4.0	.479	.449	.030
9	4.5	.505	.479	.026
10	5.0	.527	.505	.022
11	5.5	.547	.527	.020
12	6.0	.564	.547	.017

of the distributive effect shown in column 5 of table 2. The daily component of rise after the twelfth day of a change in river stage is small and was neglected. The daily change in water level at the given point was therefore computed as the net effect of the preceding 12 daily changes in river stage, each weighted according to the coefficients of the distributive effect.

Figure 2 shows hydrographs of the stage of the Arkansas River at Pine Bluff, Ark., and of the measured water-level fluctuation in well A–4, based on daily readings of continuous recorder charts at 7 a.m. Using the coefficients of distributive effects for well A–4, shown in table 2, and daily changes in river stage at Pine Bluff, daily water-level changes were computed for the location of well A–4. The computed daily changes, shown as circles in figure 2, agree closely with the measured fluctuations of the water level in well A–4. The differences probably represent variations in accretion to the aquifer and in hydraulic diffusivity.

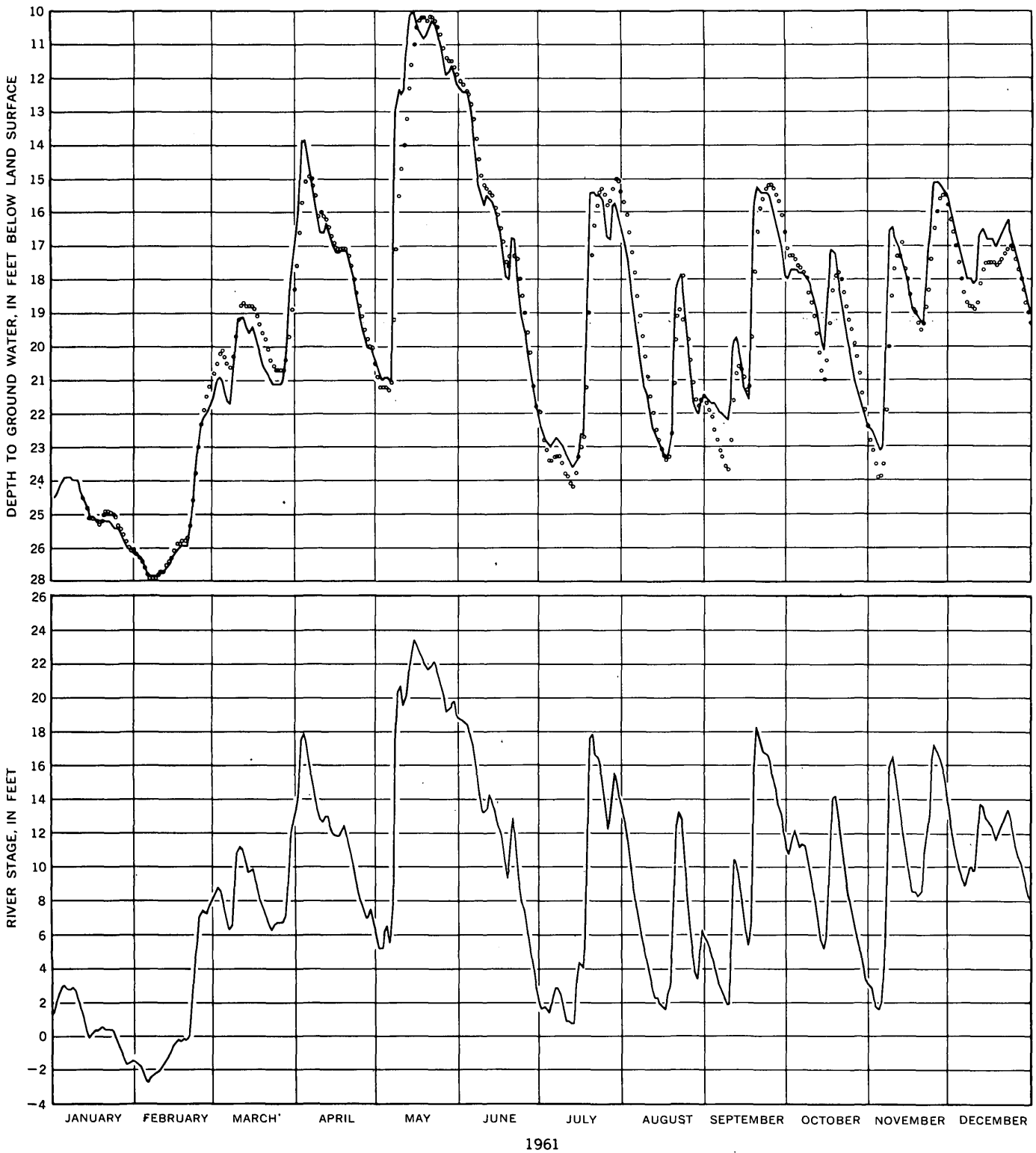

FIGURE 2.—Hydrographs of (1) the stage of the Arkansas River at Pine Bluff, Ark. (below), and (2) measured water-level fluctuations in well A–4 (solid line) and computed stream-induced water-level fluctuations (circles) at the location of well A–4 (above).

TABLE 2.—*Coefficients of the distributive effect at the location of well A–4*

[Symbols explained in text]

Time, in days (1)	$1/u^2$ (2)	$D(u)_A$ (3)	$D(u)_A$ offset by 1 time unit (4)	Coefficient of distributive effect (5)
1	1	0. 157	0	0. 157
2	2	. 317	. 157	. 160
3	3	. 414	. 317	. 097
4	4	. 479	. 414	. 065
5	5	. 527	. 479	. 048
6	6	. 564	. 527	. 037
7	7	. 593	. 564	. 029
8	8	. 617	. 593	. 024
9	9	. 637	. 617	. 020
10	10	. 655	. 637	. 018
11	11	. 670	. 655	. 015
12	12	. 683	. 670	. 013

The example demonstrated in figure 2 required the use of 12 enumerations for each daily change in water level. For points farther from the river or with a smaller coefficient of hydraulic diffusivity, river-induced fluctuations will be smaller in amplitude and will occur with greater time lag. At such points the coefficient of daily distributive effect will be smaller and the water-level changes will be significantly affected by a longer period of antecedent river stages. Where the daily distributive effect is small, the number of computations can be reduced by generalizing the surface-water hydrograph as averages of segments of several days' duration. As a guide to generalizing the surface-water hydrograph, it has been found that satisfactory results can be obtained if the effects of each change in surface-water stage are distributed over 12 to 15 successive time units whose coefficients total 0.65 to 0.70.

The method presented here, because it can be done manually, is of advantage where construction of an analog or programming for a digital computer is not practical. Although the computations are tedious, the method is not unduly time consuming if the surface-water hydrograph has been conveniently generalized. This method permits the estimation of the T/S ratio for aquifers where water-level fluctuations are caused mostly by changes in river stage. Also, if the hydraulic coefficients of an aquifer are already known, it can be an aid in the analysis of complex hydrographs where changes in river stage are one of several factors causing water-level fluctuations.

REFERENCES

Ferris, J. G., 1951, Cyclic fluctuations of water level as a basis for determining aquifer transmissibility: Internat. Union Geodesy and Geophysics, Assoc. Sci. Hydrology Assembly, Brussels, 1951, v. 2, p. 148–155.

Ferris, J. G., Knowles, D. B., Brown, R. H., and Stallman, R. W., 1962, Theory of aquifer tests: U.S. Geol. Survey Water-Supply Paper 1536–E, 174 p.

Hantush, M. S., 1961, Discussion of "Intercepting drainage wells in artesian aquifer," by D. F. Peterson: Am. Soc. Civil Engineers, Jour. Irrigation and Drainage Div., v. 87, no. IR4, pt. 1, p. 79–81.

Langbein, W. B., 1949, Computing soil temperatures: Am. Geophys. Union Trans., v. 30, no. 4, p. 543–547.

USE OF WATER-LEVEL RECESSION CURVES TO DETERMINE THE HYDRAULIC PROPERTIES OF GLACIAL OUTWASH IN PORTAGE COUNTY, WISCONSIN

By EDWIN P. WEEKS, Madison, Wis.

Work done in cooperation with the Wisconsin Geological and Natural History Survey

Abstract.—Mathematical solutions derived for hypothetical "ideal" aquifers were used in determining, from data on water-level recessions following cessation of recharge, values of T/S for water-bearing glacial outwash. The results agree fairly closely with those obtained from a pumping test.

Values for the hydraulic properties of aquifers, including the coefficients of transmissibility (T) and storage (S), are needed to determine the availability of ground water and to predict changes in the hydrologic system caused by water-resource development. One method of determining these properties for shallow unconfined aquifers entails an analysis of water-level recessions following a period of recharge. This method of analysis yields a value for T/S, from which T can be computed if S is known, or S can be computed if T is known.

The analysis of water-level recession curves is made possible by idealizing the aquifer configuration and recharge conditions to the extent that water-level recessions may be analyzed mathematically. For the analyses, it is assumed that the aquifer is homogeneous and isotropic and that the aquifer approximates a simple geometric shape, such as an infinite strip, a rectangle, or a wedge, that is bounded by streams or by streams and impermeable rocks. Recharge to the aquifer is assumed to be distributed uniformly throughout the area and to occur either instantaneously or at an equilibrium rate (recharge equal to discharge) that ceases instantaneously. Despite the apparent restrictiveness of these assumptions, many aquifer configurations and recharge conditions may be idealized to fit the assumed conditions to the necessary degree of accuracy.

This article describes the analysis of water-level recession curves to determine the ratio T/S of glacial outwash in the drainage basins of the Plover and Little Plover Rivers, in Portage County, central Wisconsin. The idealized aquifer configurations and recharge conditions assumed for the determinations include those for an infinite-strip aquifer recharged by an instantaneous slug, an infinite-strip aquifer recharged at an equilibrium rate ending instantaneously, and a wedge-shaped aquifer recharged by an instantaneous slug (fig. 1).

Water-level recessions in five wells were analyzed. The recessions followed water-level rises resulting from recharge by infiltrating snowmelt and spring rains in 1960 and 1961. The large volume of spring recharge in 1960 could be idealized as an instantaneous slug because it occurred over a relatively short time and was followed by a relatively long period of little recharge. Because in 1961 the water level rose more slowly than in 1960 and remained at a fairly constant high level for some time before receding, recharge for some time immediately prior to the water-level recession was idealized as occurring at a constant rate in equilibrium with discharge and then ceasing instantaneously.

The water-bearing glacial outwash south of the Little Plover River was idealized as an infinite-strip aquifer, whereas that between the Little Plover and the Plover Rivers was idealized as a wedge-shaped aquifer. The hydraulic boundaries of the infinite-strip aquifer are the Little Plover River on the north and the marshlands that parallel the Little Plover about 4 miles to the south. Those of the wedge-shaped aquifer are the Little Plover River on one limb, the Plover and a short stretch of the Wisconsin River on the other limb, and

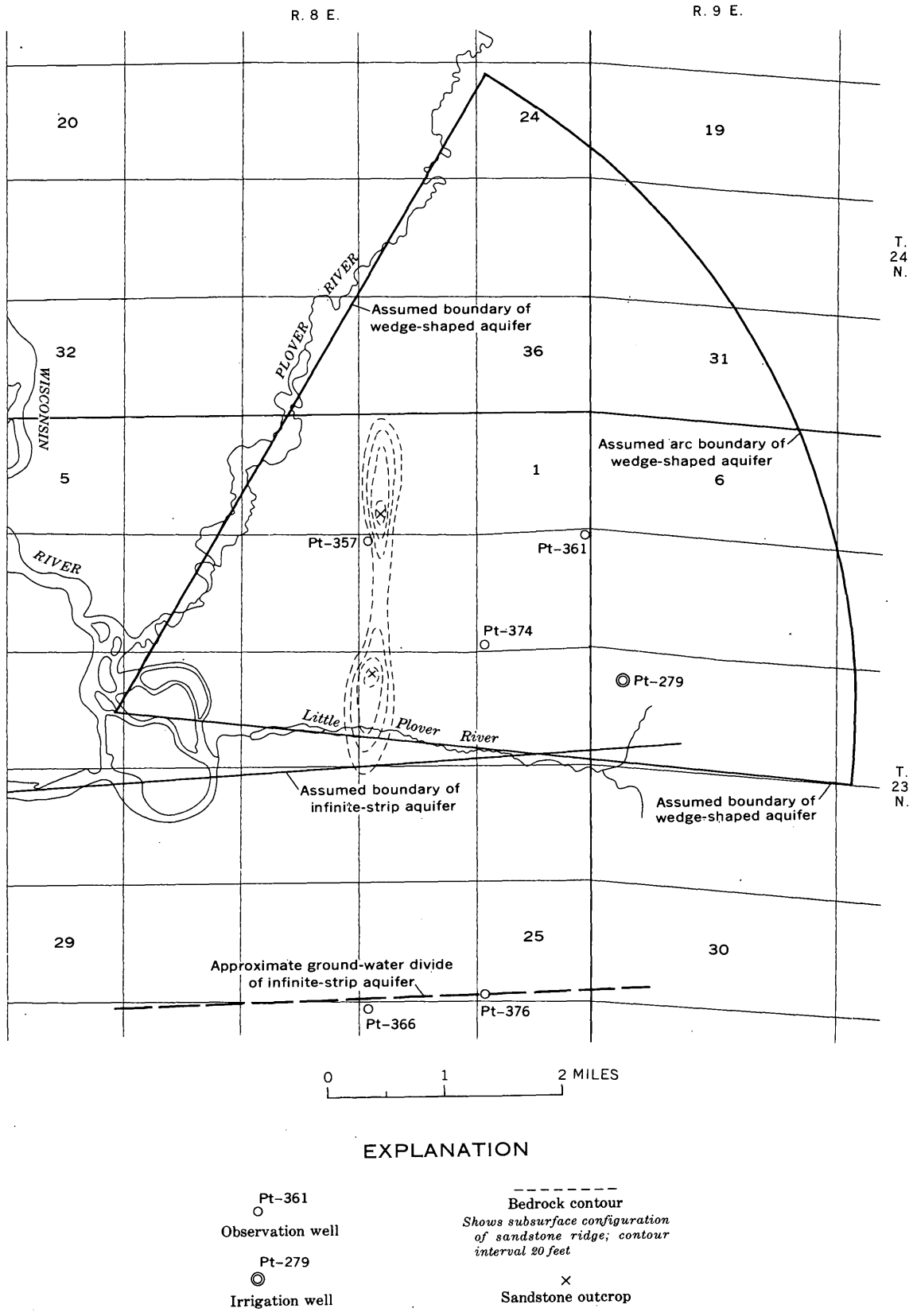

FIGURE 1.—Map showing location of streams and observation wells and the limits of the assumed ideal aquifers used in the recession-curve analyses.

an arbitrary arc of constant head assumed to be at a radius of 33,000 feet from the junction of the Little Plover and Wisconsin Rivers.

The following equation, derived by Brown (1963, p. C89), expresses the relation of (1) decline in head (water-level recession) at a given point in an infinitely long strip aquifer which has been recharged instantaneously to (2) the factors of time since recharge occurred, aquifer width, and the hydraulic properties of the aquifer:

$$\frac{h}{h_o}=\frac{4}{\pi}\sum_{n=1,3,5,\ldots}^{\infty}\frac{1}{n}\exp-\left(n^2\pi^2\frac{Tt}{4a^2S}\right)\sin\frac{n\pi x}{2a},$$

where h_o = change in head due to recharge,
h = residual change in head remaining at time t,
T = coefficient of transmissibility,
t = time since recharge occurred,
$2a$ = distance between streams,
S = coefficient of storage, and
x = distance from observation well to stream.

In analyzing the water-level recession that occurred in wells Pt–366 and Pt–376 (fig. 1) during the summer of 1960, type curves were prepared by plotting values of h/h_o versus $\log_{10} Tt/4a^2S$, the values of h/h_o being obtained by substituting assumed values for $Tt/4a^2S$ in the above equation.

Type curves for the same infinite-strip aquifer under the condition of recharge at an instantaneously ending equilibrium rate were prepared by plotting values of h/h_o versus $\log_{10}\frac{Tt}{4a^2S}$, the values of h/h_o being obtained by means of the equation (Jacob, 1943, p. 566)

$$\frac{h}{h_o}=\frac{\sum_{n=1,3,5,\ldots}^{\infty}\frac{1}{n^3}\exp-\left(\frac{n^2\pi^2Tt}{4a^2S}\right)\sin\frac{n\pi x}{2a}}{\sum_{n=1,3,5,\ldots}^{\infty}\frac{1}{n^3}\sin\frac{n\pi x}{2a}}.$$

These curves were used in analyzing the water-level recessions occurring during the summer of 1961 in wells Pt–366 and Pt–376.

The type curves prepared by Papadopulos (1963) from an integral equation derived by Jaeger (1942, p. 532) were used in analyzing the water-level recessions in wells Pt–357, Pt–361, and Pt–374. These wells are located in the wedge-shaped aquifer between the Little Plover and Plover Rivers (fig. 1).

The water-level data from each well in the study area were prepared for analysis by plotting values of h/h_o versus $\log_{10}t$. As indicated in the hydrograph for well Pt–366 (fig. 2) the increase in head due to recharge is equal to the actual rise in water level plus the water-level decline that would have occurred in the absence of recharge. The water-level trend without recharge was found by preparing a semilog plot of the antecedent water-level recession and extrapolating the straight line best fitting those data. Values of h_o and of h for various times were obtained by subtracting the extrapolated water level from the observed water level.

The data plots for wells Pt–366, Pt–376, and Pt–361 matched the type curves almost perfectly. The values for T/S obtained by analyzing the water-level recessions in these wells are given in the accompanying table. As the data plots for wells Pt–374 and Pt–357 did not match the type curves, reliable values for T/S could not be computed from them. It is likely that the buried ridge of sandstone that extends from sec. 2 to sec. 14, T. 23 N., R. 8 E., is so much less permeable than the glacial outwash that it affects water movement in the aquifer and, therefore, the shape of the water-level recession curves in these wells.

Values of T/S *determined from analysis of water-level recession*

Well No.	Ideal aquifer configuration	T/S (ft² per day)	Transmissibility T (gpd per ft if S=0.2)
Pt–366	Infinite strip, instantaneous recharge	1.8×10^5	270,000
	Infinite strip, equilibrium recharge	1.7×10^5	250,000
Pt–376	Infinite strip, instantaneous recharge	1.4×10^5	210,000
	Infinite strip, equilibrium recharge	1.3×10^5	200,000
Pt–361	Wedge, instantaneous recharge	2.0×10^5	300,000

The values of T/S were multipled by 0.2, the storage coefficient determined from specific-yield data, to obtain values for aquifer transmissibility in units of square feet per day and by 7.5 to change the units to gallons per day per foot. The values of transmissibility are somewhat greater than the transmissibility of 140,000 gpd per ft determined by a 3-day aquifer test made at well Pt–279, probably because of local differences in aquifer thickness. The thickness ranges from 0 at the sandstone outcrops to about 100 feet in the vicinity of wells Pt–376 and Pt–361 and is about 80 feet in the vicinity of well Pt–279. Differences in aquifer thickness probably also account for the range in transmissibility values determined for the several well sites. Transmissibility values determined from water-level recessions during 1960 in wells Pt–366 and Pt–376 agree quite closely with those from water-level recessions during 1961 in the same wells.

Values for hydraulic properties obtained by the recession-curve method of analysis are those characterizing an areally extensive homogeneous and isotropic aquifer in which the water-level recession would match

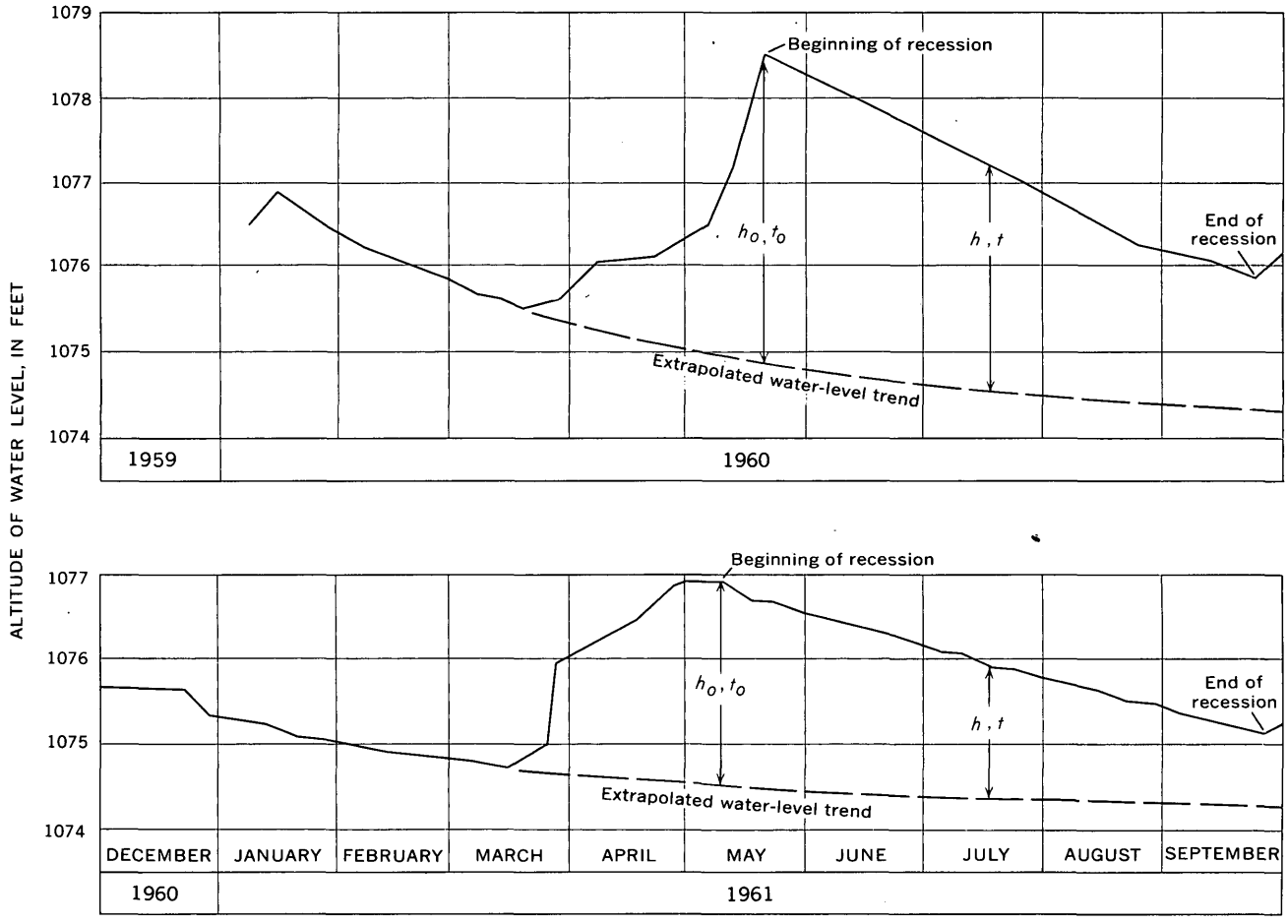

FIGURE 2.—Hydrograph of well Pt–366, showing the water-level recessions in the summers of 1960 and 1961 and the extrapolated water-level trends used to determine the head due to recharge. Datum is mean sea level.

that observed in the real aquifer. Because of this, local variations in transmissibility are masked and the results may be somewhat different from those of a pumping test at a given site in the aquifer. Values for the hydraulic coefficients determined by recession-curve analysis are more useful than pumping-test results in predicting areal effects of water-resource development, whereas pumping-test results are more useful in predicting local effects of pumping in the vicinity of the test site.

The methods described in this report could be used to determine the hydraulic properties of aquifers in many other areas. Much water-level information for aquifers throughout the county has been collected during basic-data programs and areal-reconnaissance studies, and many of these aquifers are bounded by streams or impermeable rocks in such a way that they can be idealized as wedges, infinite strips, or rectangles. Water-level recessions following recharge from snowmelt, torrential rains, or irrigation could be analyzed to determine the hydraulic properties of these aquifers.

REFERENCES

Brown, R. H., 1963, Ground-water movement in a rectangular aquifer bounded by four canals, *in* Bentall, Ray, compiler, Shortcuts and special problems in aquifer tests: U.S. Geol. Survey Water-Supply Paper 1545–C, p. C86–C100.

Jacob, C. E., 1943, Correlation of ground-water levels and precipitation on Long Island, New York; pt. 1, Theory: Am. Geophys. Union Trans., p. 564–573 [1944].

Jaeger, J. C., 1942, Heat conduction in a wedge, or an infinite cylinder whose cross-section is a circle or a sector of a circle: Philos. Mag. and Jour. Sci., v. 33, no. 222, p. 527–536.

Papadopulos, I. S., 1963, Preparation of type curves for calculating T/S of a wedge-shaped aquifer: Art. 54 *in* U.S. Geol. Survey Prof. Paper 475–B, p. B196–B198.

TREE GROWTH PROVES NONSENSITIVE INDICATOR OF PRECIPITATION IN CENTRAL NEW YORK

By WILLIAM J. SCHNEIDER and WILLIAM J. CONOVER, Washington, D.C.

Abstract.—Correlation of tree-ring widths, as measured on increment cores taken from coniferous trees, with precipitation demonstrates that although the two variables are not completely independent, measurements of ring width are of little value in determining past precipitation in the humid continental climate of central New York.

Previous studies (Fritts, 1962) have shown that in some areas, the rate of growth of trees can be related to hydrologic phenomena, particularly annual precipitation. A recent study by Schneider and Ayer (1962) has shown that a change in land use from abandoned farmland to coniferous woodland in 1933 reduced streamflow by 23 percent in the Shackham Brook watershed near Cortland, in central New York. Accordingly, an attempt was made to relate the rate of growth of trees in the Shackham Brook area to precipitation in order to understand more fully the interrelation between tree growth and hydrology.

More than 100 trees were systematically selected for sampling. Because the reforestation in 1933 was done by planting blocks of one or two species, sampling was also done by blocks and species. In each block, a group of five trees of a single species were selected arbitrarily. Twenty-three groups studied consisted of 7 groups of Norway spruce (*Picea abies*), 6 groups of European larch (*Larix decidua*), 6 groups of red pine (*Pinus resinosa*), and 4 groups of Scotch pine (*Pinus sylvestris*). Tree-ring widths, a measure of the annual growth of the tree, were measured on increment cores taken from each tree.

Ring widths were compared with the amount of precipitation recorded for the period of ring growth. The precipitation data used are an average of precipitation recorded at two sites in the 3.12-square-mile watershed. A May 1 to October 31 semiannual period, corresponding to the growing season, and a May 1 to April 30 annual period were used in this study.

Although reforestation was done in 1933, only data from 1940 on were used, thereby eliminating the early years of tree growth when ring widths tend to be disproportionately large. Only increase or decrease in ring size as compared to that of the preceding year was related to the increase or decrease in precipitation as compared to that of the previous year. In this manner, the test was kept as general as possible.

The sequential probability-ratio test of Wald (1947) was used with the following hypotheses:

H_0: An increase (or decrease) in ring width corresponds to an increase (or decrease) in the total amount of precipitation for the period of ring growth (12 months ending April 30) with a probability $p \geq 0.7$.

H_1: The probability p of a correspondence is <0.7.

The type-I error, that is, the probability of accepting H_0 when H_1 is true, was selected as 5 percent. The type-II error, that is, the probability of accepting H_1 when H_0 is true, was also selected as 5 percent. The zone of indifference—the values of p for which either H_0 or H_1 may be selected—is the interval from 0.65 to 0.75. In other words, if p, as defined by H_0, is between 0.65 and 0.75, we regard it as sufficiently close to 0.7 so that it does not matter which hypothesis we accept.

To use Wald's test graphically, the number of trials (v) is plotted as the abscissa, and the number of "successes" (d_v) as the ordinate. A "success" is defined as a comparison of ring size with precipitation in which both showed an increase over the previous year or half year, or in which both showed a decrease. A comparison in which one increases while the other decreases is a "failure." If either variable does not change in successive values, that trial is not counted.

The boundary lines, based on the selections of type-I error, type-II error, and zone of indifference, are as follows:

$$d_v = 6.17 + 0.706\, v$$
$$d_v = -6.17 + 0.706\, v$$

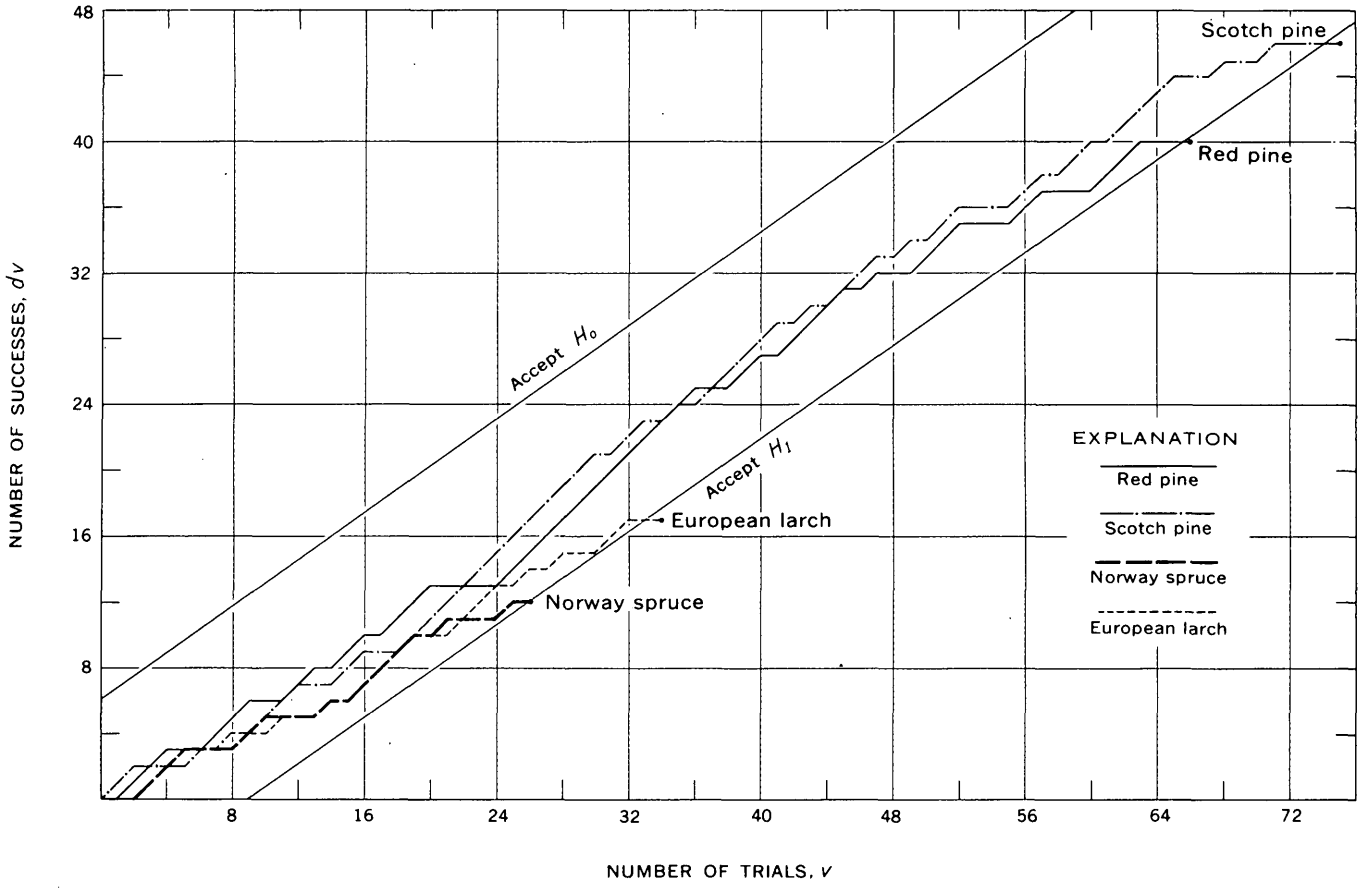

FIGURE 1.—Sequential analysis of relation between tree-ring growth and precipitation for May 1–April 30 periods.

The hypothesis H_0 is accepted when the graph crosses the upper boundary. When the graph crosses the lower boundary, the hypothesis H_1 is accepted. The experiment is continued until the graph crosses one of the boundaries.

The sequential order of the data for plotting was determined as follows: For each tree, the data were used chronologically. For each species, the order of the trees was selected by random process. The results of the study for the yearly period May 1 to April 30 are shown in figure 1. The graphs for all four species cross the lower boundary and we therefore accept the hypothesis H_1. Results for the study for the growing season of May 1 to October 31 are shown in figure 2. Again, the hypothesis H_1 is accepted.

This process was repeated four times for each of the study periods. In all cases, for each species and each period, the hypothesis H_1 was accepted.

Both figures 1 and 2 show that an increase (or decrease) in the amount of tree growth for the study periods will correspond to an increase (or decrease) in precipitation <70 percent of the time. If the rate of tree growth and amounts of precipitation were completely independent, the probability of correspondence would be 50 percent. The results, therefore, do not indicate complete independence of the variables. On the other hand, the results do not justify the use of tree-ring widths as sensitive hydrologic indicators in the humid continental climate of central New York.

REFERENCES

Fritts, H. C., 1962, An approach to dendroclimatology; screening by means of multiple regression techniques: Jour. Geophys. Research, v. 67, no. 4, p. 1413–1420.

Schneider, W. J., and Ayer, G. R., 1962, Effect of reforestation on streamflow in central New York: U.S. Geol. Survey Water-Supply Paper 1602, 61 p.

Wald, Abraham, 1947, Sequential analysis: New York, John Wiley and Sons.

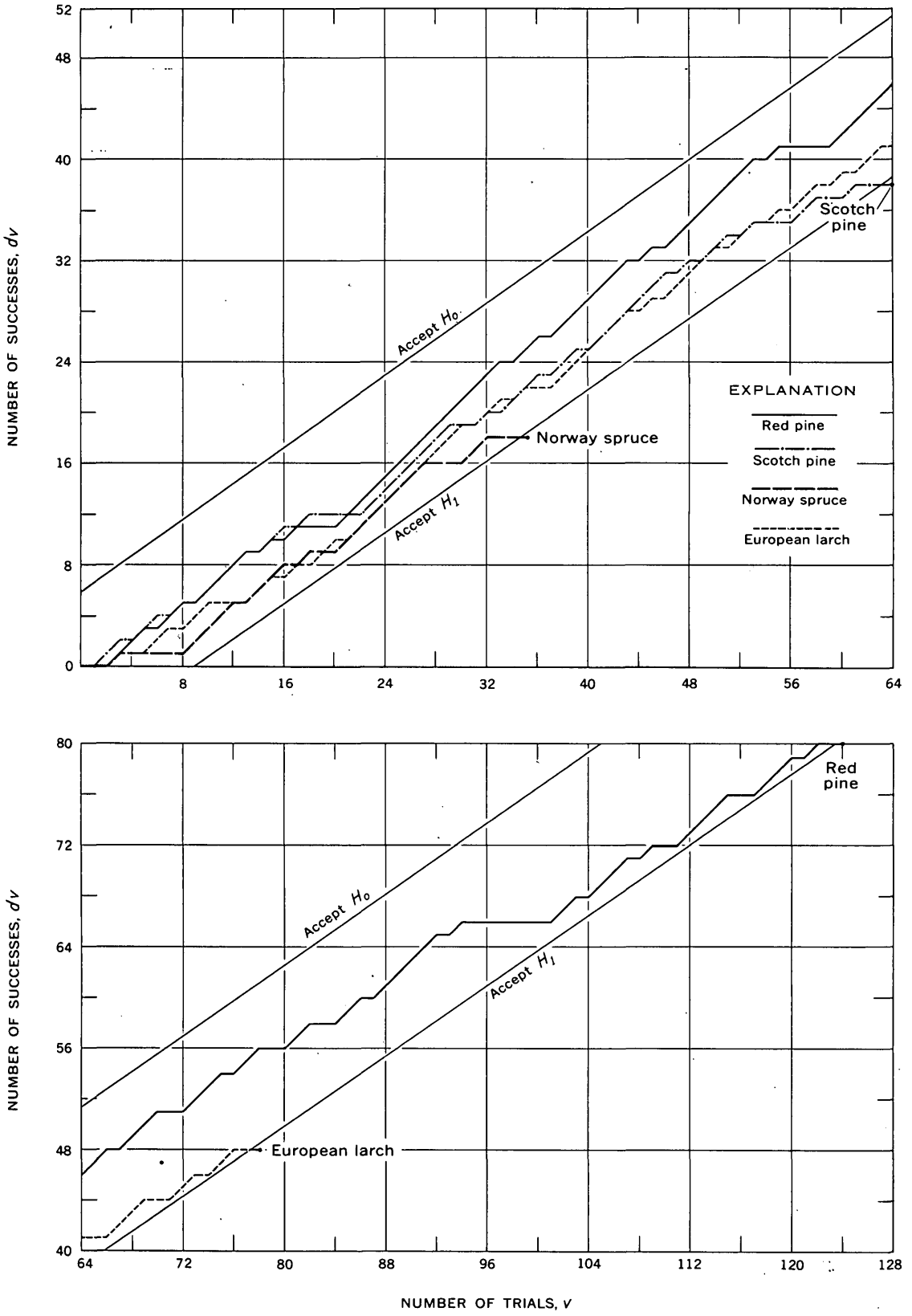

FIGURE 2.—Sequential analysis of relation between tree-ring growth and precipitation for May 1–October 31 growing seasons.

725-828 O—64——13

SUBJECT INDEX

[For major subject headings such as "Economic geology," "Geophysics," "Sedimentation," see under State names or refer to table of contents]

AUTHOR INDEX

U.S. GOVERNMENT PRINTING OFFICE: 1964 O—725-328